

Isotopic and microbiologic evidence of greenhouse gases transformation mechanisms in groundwater

A thesis submitted in partial fulfillment of the requirements for the degree of Doctor of Philosophy (Phd) in Engineering Science

by

Olha Nikolenko



Supervisor: Serge BROUYÈRE

Co-supervisor: Alberto V. BORGES

DOCTORAL COLLEGE IN ARCHITECTURE, ENGINEERING AND GEOLOGY

NOVEMBER 2020

Content

Abstract	3
Knowledge dissemination	5
Acknowledgements	7
List of symbols and acronyms.....	9
List of figures	14
List of tables	18
Introduction	20
Aquifers under agricultural areas as a source of greenhouse gases emission.....	20
Research objectives	23
Thesis outline.....	24
1. Isotopic composition of nitrogen species in groundwater under agricultural areas	26
1.1. Challenges in the interpretation of N dynamics in aquifers	26
1.2. Effects of sources, processes and factors on the isotopic signatures of nitrogen compounds in groundwater	32
1.3. Complementary investigations based on other stable isotopes	61
1.4. Conclusions	68
2. Dynamics of greenhouse gases in groundwater: hydrogeological and hydrogeochemical controls	71
2.1. Challenges in the interpretation of N dynamics in aquifers	71
2.3. Variability of hydrogeochemical parameters and isotopes across the chalk aquifer.....	81
2.4. Sources of N and C loading across the aquifer.....	85
2.5. Biogeochemistry of nitrous oxide, methane and carbon dioxide along lateral and vertical dimensions of the aquifer	88
2.6. Conclusions	101

3. Nitrification and denitrification capacity of the chalk aquifer and its effect on nitrous oxide (N ₂ O)	104
3.1. Vertical trends in the distribution of nitrogen compounds and their isotopes	105
3.2. Estimation of the rates of nitrification and denitrification processes	115
4. Microbiological evidence of nitrous oxide production/consumption processes	120
4.1. Functional gene expression as a key to understand nitrous oxide dynamics.....	120
4.2. Developing experimental design: essential concepts	125
4.3. General experimental setup	129
4.4. Actual nitrifier and denitrifier enzymatic pathways in the aquifer.....	141
Conclusions	147
Perspectives	152
References	154
Annex	187

Abstract

One of the major global challenges of this century is to find the balance between the intensive agricultural production and the environmental damage that it causes by contributing to climate change and deterioration of water resources and soils. Agriculture accounts for up to one third of anthropogenic emissions of greenhouse gases (GHGs) which exacerbate the climate change (increase in nitrous oxide (N_2O), methane (CH_4), and carbon dioxide (CO_2)) and lead to the depletion of stratospheric ozone layer (N_2O).

Recent studies have suggested that in agricultural areas groundwater systems might be the significant sources of GHGs emissions, especially N_2O , to the atmosphere due to intensive application of nitrogen containing inorganic and organic fertilizers used to increase soil fertility. However, the dynamics of N_2O , CH_4 and CO_2 in aquifers is still poorly characterized due to the insufficient insight into kinetics and controls of processes regulating their production, transport and consumption. That is why, it is important to obtain more information regarding functional zones controlling fate of GHGs in subsurface. This knowledge is important for constraining the GHGs budgets, understanding the mechanisms behind climate change and developing mitigation measures to stop the rise of concentrations of N_2O , CH_4 and CO_2 .

In this context this study focuses on evaluating the potential role of aquifers affected by the agricultural activities as a source of GHGs emission to the atmosphere and improving the understanding of the impact of the spatial heterogeneity of subsurface media on the dynamics of N_2O production and consumption processes. In this project advanced techniques and methods from hydrogeological, isotope and microbiological fields were used for investigation of the actual subsurface conditions and analysis of their impact on production and consumption of N_2O in groundwater.

The study was divided into two stages: 1) regional investigations and 2) local-scale explorations. The main aim of the regional survey was to examine the distribution and accumulation of GHGs in different parts of the studied aquifer across its lateral and vertical dimensions and to obtain better information regarding the hydrogeochemical

conditions of the subsurface. Meanwhile, the local scale investigations were focused on the occurrence of biochemical stratification in the same aquifer and analysis of its impact on N₂O dynamics. It aimed to identify and quantify the rates of N₂O production/consumption processes using data obtained from ambient groundwater and laboratory designed experiments. Since N₂O production and consumption processes can proceed through abiotic and biotic pathways, the measurements of the activity of the microorganisms that accomplish biotic N transformations were conducted to obtain more information about N₂O dynamics.

Knowledge dissemination

Journal article as first author

1. Nikolenko, O., Borges, A., Orban, P., & Brouyère, S. (2019). Analysing N sources and transformation processes in groundwater under agricultural areas (chalk aquifer, Belgium). CL: AIRE Library. <http://hdl.handle.net/2268/239471>
2. Nikolenko, O., Orban, P., Jurado, A., Morana, C., Jamin, P., Robert, T., ... & Brouyère, S. (2019). Dynamics of greenhouse gases in groundwater: hydrogeological and hydrogeochemical controls. *Applied Geochemistry*, 105, 31-44. <https://doi.org/10.1016/j.apgeochem.2019.04.009>
3. Nikolenko, O., Jurado, A., Borges, A. V., Knöller, K., & Brouyère, S. (2018). Isotopic composition of nitrogen species in groundwater under agricultural areas: A review. *Science of the Total Environment*, 621, 1415-1432. <https://doi.org/10.1016/j.scitotenv.2017.10.086>

Under review

1. Nikolenko, O., Brouyère, S., Goderniaux, P., Robert, T., & Morana, C. (2020). Dynamics of nitrous oxide with depth in groundwater: insights from ambient groundwater and laboratory incubation experiments (Hesbaye chalk aquifer, Belgium). *Journal of Contaminant Hydrology*. (under a review)

Journal article as coauthor

1. Jurado, A., Borges, A. V., Pujades, E., Briers, P., Nikolenko, O., Dassargues, A., & Brouyère, S. (2018). Dynamics of greenhouse gases in the river-groundwater interface in a gaining river stretch (Triffoy catchment, Belgium). *Hydrogeology Journal*, 26(8), 2739-2751. <https://doi.org/10.1007/s10040-018-1834-y>

Scientific conferences, congresses and symposia as first author

1. Nikolenko, O., Morana, C., Taminiu, B., Borges, A. V., Robert, T., Goderniaux, P., ... & Brouyere, S. (2020, May). Vertical interval dynamics of greenhouse gases in groundwater (Hesbaye chalk aquifer, Belgium). In EGU General Assembly Conference Abstracts (p. 4958). <http://hdl.handle.net/2268/227432>

2. Nikolenko, O., Orban, P., Morana, C., Borges, A. V., Jamin, P., B., Brouyere, S. (2019, September). Effects of the hydrogeochemical stratification on the distribution of greenhouse gases concentrations and their production/consumption processes in groundwater. 10th International Groundwater Quality Conference (GQ 2019). <http://hdl.handle.net/2268/252074>
3. Nikolenko, O., Orban, P., Jurado, A., Borges, A., Brouyère, S., Jamin, P., ... & Morana, C. (2018). Dynamics of nitrous oxide in groundwater under agricultural areas: insights from multi-isotopic studies (15N, 34S, 18O, 13C, 3H). <http://hdl.handle.net/2268/227432>
4. Nikolenko, O., Orban, P., Jamin, P., Jurado, A., Borges, A. V., & Brouyère, S. (2018). Biogeochemistry of greenhouse gases in groundwater under agricultural area (the Geer catchment, Belgium). *EGUGA*, 16102. <http://hdl.handle.net/2268/223849>

Scientific conferences, congresses and symposia as co-author

1. Jurado, A., Nikolenko, O., Orban, P., Borges, A., & Brouyère, S. (2018). Dynamics of greenhouse gases in the aquifers of two agricultural catchments of Belgium. <http://hdl.handle.net/2268/227977>

Acknowledgements

Mentioning certain people in these Acknowledgments shall not be interpreted as an objection or underestimation of the help of the unmentioned ones – I owe my gratitude to many people who helped me along the way towards the preparation of this thesis.

I acknowledge support from the European Union's Horizon 2020 research and innovation programme under the Marie Skłodowska-Curie grant agreement No 675120. I acknowledge support from the Department of the Applied Science of the University of Liège (Belgium).

This thesis was conducted under the supervision of Dr. Serge Brouyère and Dr. Alberto V. Borges. Dr. Serge Brouyère, this work would not have been possible without your mentoring and professional support. Thank you for all the scientific advice which you gave me throughout these years and the discussions that we had, they certainly contributed to my growth as a researcher. Dr. Alberto V. Borges, I am grateful for providing me the possibility to work at your laboratory as well as for your time and assistance throughout my work.

Dr. Anna Jurado, my first research steps within the PhD journey were accomplished under your guidance, and I am extremely grateful for teaching and advice which you provided. Thank you for sharing your knowledge and expertise. Prof. Kay Knöller and Dr. Bernard Taminiau, your enthusiasm and energy in scientific inquiries fuelled the fire of my love to science for the years ahead. Dr. Cedric Morana, the exhausting 3-weeks long 24/7 field and lab marathon would not have been possible without your presence and help. Dr. Philippe Orban, I would like to thank you for the participation in the field trips and in the discussions of the different aspects of this work.

I would like also to express my gratitude to Prof. Alain Dassargues and Prof. Pascal Goderniaux who devoted their time to evaluate this PhD thesis. In addition, I am grateful to Prof. Goderniaux for kindly providing the equipment for my field trials and all the following guidance and support from his side.

Thanks to my former and current colleagues from the Hydrogeology and Environmental Geology group: Tanguy, Joel, Ingrid, Roma, Claver, Max, Laura, Estanislao, Mathieu, Youcef B., Youcef H., Appoline, Pierre, Caroline, Richard, Agatha, Tom, Itzel, Gorge, for the support in the field, discussions and the time that we shared. Mathieu thank you for always taking the hardest work in the field.

The team of the INSPIRATION project, thank you for the good time we shared during our project meetings and for the scientifically interesting and personally inspirational conversations that we had. I sincerely wish all of you to be able to follow your dreams. Izabela and Wojtek, I will always remember great time that we shared during our common field campaigns in the Geer basin. Dr. Gabriella Kakonyi, thank you for being with me and supporting me even in the most difficult moment throughout these years.

I would like also to express my gratitude to the microbiology group of the University of Liège for welcoming me during the last year of my PhD studies. Christ, Elisa, Christina, Benjamine, Hiba, Sophie, Papa, thanks for your help during the demanding laboratory works and for the more relaxed moments we had in the time between. Thank you to TEAGASC research institute for giving me the opportunity to conduct my secondment at your facility. Owen, Karl, John, Dominika, Cathal, Golnaz, Fiona I appreciate your assistance and advice during my field and laboratory trials.

My deep gratitude goes to the secretariat staff Leila and Nadia for their availability, assistance and help throughout these years. Thanks to Stéphanie and Fabrice for their help in organizing the INSPIRATION corner as well as for support in various other matters.

Finally, I acknowledge an infinite wellspring of support from my family: my mom, Pavlina, who is the best friend and advisor that anyone can possibly have; my dad, Anatolii, from whom I inherited my love to nature and who encouraged my passion in science; and my brother Viktor, a person of versatile knowledge and contagious charisma.

List of symbols and acronyms

<i>AM</i>	animal manure	
<i>amoA</i>	ammonia monooxygenase	
<i>AOB</i>	ammonia-oxidizing bacteria	
α_w	the flow distortion coefficient	
<i>bdl</i>	below the detection level	
<i>C</i>	The concentration of a substance	(M/L ³)
<i>CA</i>	Confined aquifer	
<i>cDNA</i>	complementary deoxyribonucleic acid	
C_{inj}	the tracer concentration in the injected solution	(M/L ³)
<i>comA</i>	degenerate PCR primer pair targeting clade A <i>amoA</i> genes	
<i>comB</i>	degenerate PCR primer pair targeting clade B <i>amoA</i> genes	
C_w	the tracer concentration in the injection well at time t_0	(M/L ³)
$C_w(t)$	the variation of a tracer concentration in the injection well	(M/L ³)
<i>D</i>	denitrification	

δ	delta notation to report stable isotope data for all materials except interstellar dust	‰
<i>DI</i>	dilution	
<i>DIC</i>	dissolved inorganic carbon	
<i>DNA</i>	deoxyribonucleic acid	
<i>dNTPs</i>	nucleoside triphosphate	
<i>DNRA</i>	dissimilatory nitrate reduction to ammonium	
<i>DO</i>	dissolved oxygen	
<i>DOC</i>	dissolved organic carbon	
<i>Dom</i>	decomposition of organic matter	
ϵ	enrichment factor shows isotope enrichment of a reactions product relative to that of the substance	‰
<i>EC</i>	electrical conductivity	
e_{scr}	the well screen length	(L)
<i>FVPDM</i>	Finite Volume Point Dilution Method	
<i>GHGs</i>	greenhouse gases	
$\Delta H_{means}/L$	hydraulic gradient	
<i>IF</i>	inorganic fertilizers	
K_{est}	hydraulic conductivities	
<i>M</i>	mineralization	

<i>Mix</i>	mixing	
<i>mRNA</i>	messenger RNA	
n_e	effective porosity of the aquifer	
<i>nirK</i>	copper-containing nitrite reductase	
<i>nirS</i>	nitrite reductase / hydroxylamine reductase	
<i>NOB</i>	nitrite-oxidizing bacteria	
<i>norB</i>	quinol nitric oxide reductase	
<i>norC</i>	cytochrome c nitric oxide reductase	
<i>nosZ</i>	nitrous oxide reductase	
<i>OF</i>	organic fertilizers	
p	the probability to find the current result if the correlation coefficient were zero (null hypothesis)	
<i>PCR</i>	polymerase chain reaction	
q_{app}	apparent Darcy flux	(LT^{-1})
Q_{cr}	the critical flow rate	
$q_{D,app}$		
q_D	the effective Darcy flux in the aquifer	(LT^{-1})
Q_{inj}	the injection rate of a tracer	(L^3/T)

	solution	
Q_t	the rate of water intercepted at the screen level of the well (transit flow rate)	(L ³ /T)
r	Pearson's correlation coefficient – measure of the strength of the association between the two variables	
<i>RNA</i>	ribonucleic acid	
r_w	the radius of the well	(L)
<i>s.d.</i>	standard deviation	
<i>SL</i>	smart ladder	
<i>SOM</i>	self-organizing map	
<i>SP</i>	site preference	‰
S_w	the cross-sectional area of the well	(L ²)
<i>Taq</i>	<i>Thermus aquaticus</i>	
<i>UA</i>	unconfined aquifer	
<i>V</i>	volatilization	
V_{cov}	volume of covered aquifer material	(L ³)
$V_{d\ zone}$	volume of water in the “dead zone” of an aquifer	(L ³)
V_{inj}	injected volume of water	(L ³)
<i>VSMOW</i>	Vienna Standard Mean Ocean Water is an isotopic	

V_u	standard for water volatilization of urea	
V_w	the volume of water in the injection well	(L ³)
W_w	waste water	

List of figures

Figure 1. N sources and transformation processes that affect N species in the subsurface. The enrichment values ($^{15}\text{N-NO}_3^-$, $^{15}\text{N-NH}_4^+$) of such processes are also provided. [\rightarrow shows the transformation of the initial N compound; $---\blacktriangleright$ shows sources of different N species. References: 1 – Sharp, 2007; 2 – Kendall & Aravena, 2000; 3 – Mariotti et al., 1981; 4, 7 – Clark, 2015; 5 – Kendall., 1998; 6 – Well et al., 2012; 8 – Michener & Lajtha 2007; 9 – Bedard-Haughn et al., 2003; 10 – Hübner, 1986; 11 – Minamikawa et al., 2011; 12 – Brandes & Devol, 2002]. 28

Figure 2. NO_3^- isotopic signatures in groundwater: a summary of case studies in agricultural areas. 41

Figure 3. Sources, processes and factors that influence the $\delta^{15}\text{N-NO}_3^-$ values: summary (the following arrows connect processes with factors that have decisive effect on their dynamics and, consequently, on resulting fractionation effects: \rightarrow availability of electron donors; \rightarrow size of the substrate pool ; \rightarrow temperature; \rightarrow concentration of DO; \rightarrow hydrogeological structure; \rightarrow pH; \rightarrow land use). 45

Figure 4. Sources, processes and factors that influence the $\delta^{15}\text{N-NH}_4^+$ values: summary (the following arrows connect processes with factors that have the decisive effect on their dynamics and, consequently, on resulting fractionation effects: \rightarrow C/ NO_3^- - ratio; \rightarrow pH; \rightarrow temperature; \rightarrow size of the substrate pool). 54

Figure 5. Sources, processes and factors that influence the $\delta^{15}\text{N-N}_2\text{O}$ values: summary (the following arrows connect processes with factors that have decisive effect on their dynamics and, consequently, on resulting fractionation effects: \rightarrow water content in the subsoil; \rightarrow availability of substrate; \rightarrow residence time; \rightarrow concentration of DO; \rightarrow pH). 61

Figure 6. Map of the studied area in the Geer basin showing river network, isopieises, direction of groundwater flow and sampling points (wells and piezometers). Colors indicate different zones used to aggregate data. 75

Figure 7. $\delta^{15}\text{N}$ versus $\delta^{18}\text{O}$ values of NO_3^- (a) and $\delta^{15}\text{N}\text{-NO}_3^-$ versus $\delta^{11}\text{B}$ (b) of groundwater samples. The shape of the points shows affiliation to different zones presented in Figure 1. Colors indicate different concentrations of NO_3^- in groundwater samples. The isotopic compositions for NO_3^- and B sources are derived from Michener & Lajtha (2008), Xue et al. (2009) and Widory et al. (2004). Areas in the red circles are zoomed and displayed in Fig. 9 of Annex. 86

Figure 8. The results of Pearson correlation and linear regression analyses for the subset of data representing the unconfined part of the aquifer. 90

Figure 9. $\delta^{34}\text{S}$ versus $\delta^{18}\text{O}$ values of SO_4^{2-} for groundwater samples. The shape of the points shows affiliation to different zones presented in Figure 1. Colors indicate different concentrations of SO_4^{2-} in groundwater samples. The isotopic compositions for the SO_4^{2-} sources are derived from Krouse & Mayer (2000), Mayer (2005) and Knöller et al. (2005). 91

Figure 10. The component matrices derived from the application of SOM procedure. ... 92

Figure 11. Clustering of the groundwater samples using SOM algorithm. Group 1 – dark blue, group 2 – green, group 3 – blue and group 4 – yellow. The numbers of sampled locations are presented within each of the group. 93

Figure 12. $\Delta\delta^{15}\text{NNO}_3^- - \text{N}_2\text{O}$ versus SP (%) isotopomer map. The shape of the points shows affiliation to different zones presented in Figure 1. Colors indicate different concentrations of NO_3^- in groundwater samples. 95

Figure 13. $\Delta\delta^{15}\text{N} - \text{N}_2\text{O}$ (‰ v. AIR) versus $\delta^{18}\text{O} - \text{N}_2\text{O}$ (‰ v. VSMOW) isotopomer map. The shape of the points shows affiliation to different zones presented in Figure 1. Colors indicate different concentrations of NO_3^- in groundwater samples. 96

Figure 14. Piezometers and sampling depths at the Bovenistier (left) and SGB (right) sites. Sampling points are numbered from 1 to 10, as indicated in bold and italics on the left side of each piezometer. The groundwater level value is not indicated, since it was not stable between summer and winter campaigns. 105

Figure 15. NO₃⁻ and B isotope maps of groundwater samples collected at Bovenistier site. Graph A includes the data from summer and winter and graph B includes the data from summer only. The letter “w” next to the number of sampling location means that the sample was collected in the winter. Green circles of different size indicate different concentrations of NO₃⁻ in groundwater samples. The ranges of isotopic compositions for NO₃⁻ and B sources (boxes drawn in the graphs) are derived from Michener & Lajtha (2008), Xue et al. (2009) and Widory et al. (2004). Ratios of δ¹⁵N and δ¹⁸O of NO₃⁻ used to draw denitrification lines are taken from Koba et al., 2009. 107

Figure 16. NO₃⁻ and B isotope maps of groundwater samples collected at SGB site. Graph A includes the data from summer and winter and graph B includes the data from summer only. The letter “w” next to the number of sampling location means that the sample was collected in the winter. Green circles of different size indicate different concentrations of NO₃⁻ in groundwater samples. The ranges of isotopic compositions for NO₃⁻ and B sources (boxes drawn in the graphs) are derived from Michener & Lajtha (2008), Xue et al. (2009) and Widory et al. (2004). Ratios of δ¹⁵N and δ¹⁸O of NO₃⁻ used to draw denitrification lines are taken from Koba et al., 2009..... 109

Figure 17. Vertical distribution of N compounds, their isotopes and DO at SGB site during summer and winter periods. 111

Figure 18. Vertical distribution of N compounds, their isotopes and DO at the Bovenistier site during summer and winter periods..... 114

Figure 19. Enzymes used in denitrification and the genes encoding them..... 124

Figure 20. General scheme of ongoing PCR experiment (A) and visual presentation of its results (B): A – stages of PCR experiment; B – comparison of the location of three PCR products with a standard (Smart ladder (SL))..... 127

Figure 21. Structures of deoxyonucleotide and dideoxynucleotide, the substances required for DNA synthesis during Sanger sequencing reaction..... 128

Figure 22. Scheme of computer-generated chromatogram showing obtained sequence after all fragments pass the detector..... 129

Figure 23. Flow diagrams showing steps conducted to reveal gene expression of nitrifying and denitrifying bacteria in the groundwater samples collected from piezometers screening the chalk aquifer. 130

Figure 24. Results of 16S rDNA amplification in groundwater samples. From left to right: a standard (Smart Ladder (SL)), from 1 to 9 groundwater samples collected in summer, 1` to 10`groundwater samples collected in winter, a positive controls (P) and a negative control (N). 132

Figure 25. Results of the PCR analysis on three soil samples tested as positive controls. From left to right: a standard (Smart Ladder (SL)), soil cDNAs amplified with comA primer set (first three undiluted, followed by three diluted and negative control (N)), a standard (Smart Ladder (SL)), soil cDNAs amplified with comB primer set (first three undiluted, followed by three diluted and negative control (N)) and a standard (Smart Ladder (SL)). 138

Figure 26. Results of PCR analysis after the change in annealing temperature on three soil samples tested as positive controls using comB primer set. From left to right: a standard (Smart Ladder (SL)), soil cDNAs (first three undiluted, followed by three diluted) and negative control (N), a standard (Smart Ladder (SL)). 139

List of tables

Table 1. Analysis of NO_3^- isotopic signatures in groundwater: an overview of case studies (UA – unconfined aquifer, CA – confined aquifer, IF – inorganic fertilizers, OF – organic fertilizers, SON – soil organic N, AM – animal manure, Ww – wastewater, D – denitrification, N – nitrification, Dom – decomposition of organic matter, Mix – mixing, Dl – dilution).....	33
Table 2. Analysis of NH_4^+ isotopic signatures in groundwater: an overview of case studies (Vu – volatilization of urea, N – nitrification, V – volatilization, M – mineralization of organic N, s.d. – standard deviation, bdl – below detection level).....	47
Table 3. Analysis of N_2O isotopic signatures in groundwater: an overview of case studies	56
Table 4. Hydrogeochemical and isotopic composition (mean value \pm standard deviation) of groundwater in the chalk aquifer across spatial zones (see Fig. 1).	82
Table 5. Hydrogeochemical and isotopic composition of groundwater in the chalk aquifer at the Bovenistier, Overhaem and SGB sites (see Fig. 1).	84
Table 6. Mean hydrogeochemical parameters of the groundwater samples clusters produced by k-means clustering on SOM.....	94
Table 7. Quantities of RNA and DNA extracted from the biomass obtained from the groundwater samples collected from different depths at the Bovenistier and SGB sites during winter and summer campaigns.	131
Table 8. The most abundant nitrifying and denitrifying bacterial genus (species) revealed by means of 16S rRNA sequence analysis and targeted genes present in their genome (some bacteria carry several targeted genes, which explains the repeating records in the table).	134
Table 9. Primer sets used for PCR analysis. If primers are developed in this study, third column shows entries for nucleotide sequences in KEGG used to develop them.	136

Table 10. PCRs conditions used to detect the presence of nitrifying and denitrifying enzymes (T – temperature, t – time). 140

Table 11. Results of PCR and Sanger sequence analysis (SSA) conducted for groundwater samples collected during summer and winter campaigns at Bovenistier and SGB sites (yellow color highlights N₂O production pathway and green color – the presence of N₂O consumption mechanism). To distinguish between summer and winter samples winter ones are indicated with an apostrophe next to them. 142

Introduction

Aquifers under agricultural areas as a source of greenhouse gases emission

The observed rise of the global temperature is caused by intensive accumulation of greenhouse gases (GHGs) in the atmosphere since the mid-20th century. In comparison to the pre-industrial times atmospheric concentrations of three main GHGs: CO₂, N₂O and CH₄ – have increased by approximately 146 %, 122 % and 257 %, respectively, and now are at 410 ppm, 330 ppb and 1860 ppb concentration levels (World Meteorological Organization, 2018). In this context global community has started to discuss the issue of human-caused climate change and its dangerous consequences that are becoming evident throughout the world (IPCC, 2013). Nowadays, both public and academic debates pay particular attention to finding the ways to reverse or moderate the trend towards increase of the concentrations of GHGs in the atmosphere. In particular, the Paris Agreement on climate change anticipates a reduction, by 2030, of GHG emissions of at least 40% compared to 1990 emission levels. This is a challenging task, especially taking into account the necessity to provide for the needs of the growing global population.

In this context much attention has been devoted to quantification and monitoring of agricultural emissions which contribute approximately 12% to the global anthropogenic GHGs emissions (Smith et al., 2014). This type of emissions is characterized with wider uncertainty range ($\pm 30\%$) in comparison to the uncertainty level estimated for the largest source of GHGs emissions – the consumption of fossil fuel (approximately 10%) (IPCC, 2013; Tubiello et al., 2013). Agricultural activities (crop and livestock production) emit mainly non-CO₂ gases such as methane (CH₄) and nitrous oxide (N₂O), effectively contributing around 47% and 60% share to total anthropogenic emissions of these gases, respectively (Tian et al., 2019; Tubiello et al., 2015).

Agricultural emissions to the atmosphere can be divided into two groups: 1) direct emissions deriving from soils and animal production; 2) indirect emissions resulting from leaching and runoff of nitrogen (N) and carbon (C) compounds to adjacent water bodies (Jurado et al., 2017). While there exists an extensive body of research devoted to the

quantification and understanding of GHGs production/consumption mechanisms in soils, the GHGs budget of aquatic systems appears to be poorly constrained (McAleer et al., 2017; Beaulieu et al., 2011). In particular, two thirds of uncertainty within the total indirect agricultural emissions is attributed to the imprecise quantification of N₂O budget (Young et al., 2016).

In agricultural areas aquifers appear to be a significant indirect source of GHGs emissions, especially N₂O, to the atmosphere due to intensive application of inorganic and organic fertilizers used to increase soil fertility (Jurado et al., 2018; Mayer et al., 2018; Anderson et al., 2014; Reay et al., 2012). The GHGs produced in the aquifers can be further emitted to the atmosphere in the areas of groundwater discharge to surface waters or released because of pumping activities. Analysis of the dynamics of GHGs in groundwater remains a challenging task due to the possibility of simultaneous occurrence of both production and consumption processes in the spatially heterogeneous geochemical conditions of subsurface. The complexity of this task is further exacerbated by the difficulties of access to the aquifers, which makes the consistent monitoring of process dynamics in subsurface a challenging task. However, further explorations in this area are essential for improving the understanding of regional and global N and C cycles. In particular, it is important to obtain more information regarding the formation of hotspots of GHGs emissions (e.g. what are the geochemical conditions favorable for intensification of GHGs production; how the distribution of such hotspots varies in time and space). This knowledge is important for constraining the GHGs budgets, understanding the mechanisms behind climate change and developing mitigation measures to stop the rise of concentrations of N₂O, CH₄ and CO₂.

One of the promising approaches used to characterize and quantify the overlapping GHGs production and consumption processes is stable isotope and isotopomer analysis. Currently, there exists a range of studies exploiting the data about isotopic signatures of N and C species to disentangle different sources of their input into groundwater. Stable isotopes of N and C help in identification and quantification of transformation of N and C compounds in aquifers. However, the interpretation of obtained isotopic signals remains a challenging task, since it requires the profound

understanding of interactions between various spatially and temporally variable factors and processes and their effects on isotopic fractionations between different N and C species. Furthermore, the overlapping of isotopic signals produced by different sources and processes and complexity of hydrogeochemical conditions or the aquifers might make it impossible to distinguish between different processes of GHGs production and consumption.

In order to address this challenge, recent studies have started to explore the possibility of application of the analysis of N₂O isotopomers (molecules having the same number of each isotopic atom but differing in their position) for exploration of biogeochemical processes in the subsurface. It is expected that this method could provide more precise and unambiguous information about the N₂O dynamics in the subsurface, because the difference between central and peripheral ¹⁵N enrichment, which is called site preference (SP), is considered to be independent of the isotopic signature of the precursor. However, so far the majority of evidence about the influence of different microbiological processes on SP values comes from the pure culture experiments conducted at the lab. It is important to trace the distribution of ¹⁵N within N₂O molecule under different environmental conditions to understand which factors control its change and position.

Simultaneous application of other techniques, which can characterize subsurface microbial and physical-chemical heterogeneity, along with isotopomer approach will help to develop a detailed map of the interaction between various N transformation processes in aquifers. To understand better the nature of the processes in the subsurface, microbiological studies to detect the expression of genes used for formation of enzymes which are involved into biotic processes can be undertaken. The expression of genes means that the information carried by genes was used to create the proteins and proteins are enzymes that catalyze biotic reactions. It is measured by studying its mRNA pool. mRNA is a single-stranded molecule that is complementary to one of the DNA strands of a gene. Inside a cell it attracts to ribosomes the site where proteins are made. So far estimates of gene expression specific to denitrification and nitrification have been carried

out mainly during laboratory incubation and microcosm experiments. *In situ* field studies are less common and they are mainly focused on soils and sediments.

Therefore, a comprehensive consideration of subsurface abiotic and biotic components is required in order to devise smart and adaptive methodologies to elucidate N process dynamics in groundwater.

Research objectives

This research aims at obtaining better insight into the biogeochemistry of GHGs (N_2O , CH_4 and CO_2) in the groundwater under the agricultural areas focusing on N_2O , since this GHG gas is emitted to the atmosphere predominantly due to agricultural activities.

The objectives of this study are: 1) to estimate the variability of GHGs concentrations in groundwater under different hydrogeological, hydrochemical and land management conditions; 2) to identify and quantify the N_2O processes and reveal conditions that governs N_2O accumulation in groundwater; 3) to collect *in situ* evidence about the SP ranges of N_2O and activity of bacteria involved into N_2O production and consumption processes.

The research is divided into two stages: 1) regional investigations and 2) local-scale explorations. The main aim of regional survey is to examine the distribution and accumulation of GHGs in different parts of the chalk aquifer across its lateral and vertical dimensions and to obtain better information about the hydrogeochemical conditions of the subsurface. Local scale studies focus on the identification and quantification of the rates of N_2O production/consumption processes within the studied aquifer using data obtained from ambient groundwater and laboratory designed experiments. Since N_2O production and consumption processes can proceed through abiotic and biotic pathways, the measurements of the activity of bacteria that mediate biotic N transformations were conducted to obtain additional evidence about N_2O dynamics.

Thesis outline

The presented work consists of four chapters complemented by an introduction section and a final section presenting general conclusions and research perspectives.

The first chapter reviews available evidence about N isotope dynamics in aquifers affected by agricultural activities. Section 1.1 summarizes available evidence about $\delta^{15}\text{N}$ - NO_3 , $\delta^{15}\text{N}$ - NH_4 and $\delta^{15}\text{N}$ - N_2O ranges in groundwater from recent case studies (since 2000 year) conducted across the globe. Also, it compiles the evidence about isotopic signatures of principal anthropogenic sources of N compounds in subsurface. In addition, changes of ^{15}N composition of NO_3^- , NH_4^+ and N_2O under the influence of various biochemical and physicochemical processes and factors are characterized. Section 1.2 describes the possibilities to use other stable isotopes (^{18}O , ^{11}B , ^{13}C , ^{34}S , $^{87}\text{Sr}/^{86}\text{Sr}$ ratio) to clarify the uncertainties in overlapping of $\delta^{15}\text{N}$ isotopic signatures resulting from different sources and processes.

The second chapter presents the results of regional investigations which explored the variability in concentrations of GHGs (N_2O , CO_2 and CH_4) across lateral and vertical dimensions of the Hesbaye chalk aquifer located in the eastern part of Belgium. It starts with a discussion of the main challenges related to the characterization of GHGs fluxes in aquifers. Further, Section 2.2 describes the approach applied to the regional survey, and the following two sections present information about sources of N and C input to groundwater and processes that govern N_2O , CO_2 and CH_4 availability in the aquifer.

The next, third chapter, uncovers research work undertaken in order to specify the impact of nitrification and denitrification processes, occurrence of which was identified during the regional survey, on N_2O dynamics in groundwater. Section 3.1 examines variations in the distribution of N compounds and their isotopes with depth in the studied aquifer in order to identify zones (hotspots) where nitrification or denitrification processes dominate. The following section 3.2 focuses on the estimation of the magnitude of nitrification and denitrification processes in the top and bottom parts of the aquifer and discusses the challenges encountered during quantification of N transformation processes in the subsurface.

The final chapter 4 is devoted to the discussion of the findings of microbiological explorations conducted within the framework of this study in order to constrain zones of occurrence of nitrification and denitrification in the subsurface. In particular, the activity the activity of bacteria that accomplish these processes was estimated.

Chapter 1

This chapter is based on the following publication:

Nikolenko, O., Jurado, A., Borges, A. V., Knöller, K., & Brouyère, S. (2018). Isotopic composition of nitrogen species in groundwater under agricultural areas: A review.

Science of the Total Environment, 621, 1415-1432.

<https://doi.org/10.1016/j.scitotenv.2017.10.086>

1. Isotopic composition of nitrogen species in groundwater under agricultural areas

1.1. Challenges in the interpretation of N dynamics in aquifers

Cropland and pasture cover about 50% of the Earth's ice-free land surface (Ritchie & Roser, 2020). Intensive influx of nitrogen (N) compounds from agricultural areas into groundwater and surface water is an issue of worldwide concern, since it leads to disruption of multiple vital water-related environmental services (Robertson & Vitousek 2009; Sutton et al., 2011; Keuskamp et al., 2012). In particular, leaching of N-containing pollutants from arable lands into subsurface frequently has adverse effects on groundwater quality (Strebel et al., 1989; Directive, N., 1991; Di & Cameron, 2002, Ledoux et al., 2007). Moreover, it also considerably influences global N cycling because long groundwater residence time stimulates accumulation of N species and their biogeochemical transformations (Viers et al., 2012).

Pollution of aquifers in agricultural regions with reactive N poses multiple threats to sustainable development of global population. For instance, long-term exposure to high nitrate (NO_3^-) drinking water (>50 mg/l of NO_3^-) might increase human health risks associated with methemoglobinemia and cancer (WHO, 2008; Fewtrell, 2004, Xue et al., 2016). At the same time, N-polluted aquifers are the indirect sources of emission of nitrous oxide (N_2O) (Organization of Economic Co-operation and Development, 2009), produced by denitrification, nitrification or nitrifier denitrification processes. Since N_2O is a greenhouse gas (GHG) that possesses the capacity to trap large amount of heat and destroy the stratospheric ozone layer, such emissions contribute to global climate change (Knowles, 2000; Bernstein et al., 2008; Weymann et al., 2008).

Concentrations of different N species in groundwater could vary due to heterogeneity of N sources across the water bodies and shifting dynamics of N transport and transformation in the subsurface. In agricultural areas, aquifer pollution by N compounds might be attributed to various sources: intensive application of N-containing organic and inorganic fertilizers, inflow from animal manure and sewage discharge (Ostrom et al., 1998; Böhlke, 2002, Anderson et al., 2014). In subsurface environments, leached N compounds are further transformed by complex dynamics of different biochemical and chemical processes of the N cycle such as denitrification, dissimilatory nitrate reduction to ammonium (DNRA), nitrification, anammox (anaerobic ammonium oxidation), nitrifier denitrification, sorption and mineralization of organic matter (Fig. 1), which change their initial concentrations and produce new N species (Burgin & Hamilton, 2007; Jurado et al., 2017).

Denitrification is a microbial respiratory process where NO_3^- is used as a terminal electron acceptor and reduced to N_2 . It is considered to be the main process of NO_3^- attenuation which prevails under anaerobic conditions in groundwater systems. Intermediates in this reaction might include nitrite (NO_2^-), nitric oxide (NO) and N_2O (Tesoriero et al., 2000).



Similar to denitrification, DNRA is also an anaerobic reduction process that leads to consumption of NO_3^- . It is assumed that partitioning of NO_3^- consumption between denitrification and DNRA is controlled by availability of organic matter: denitrification dominates when carbon (electron donor) supplies are limiting and DNRA dominates when NO_3^- (electron acceptor) supplies are limiting (Korom, 1992; Kelso et al., 1997).

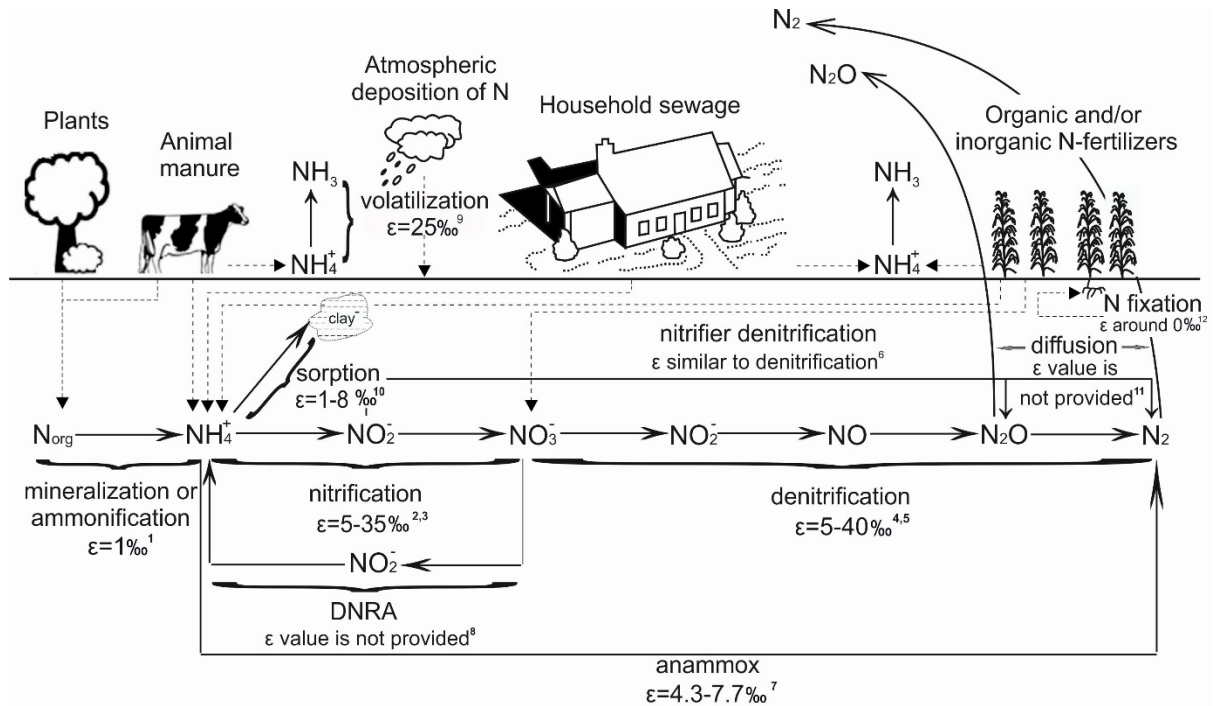
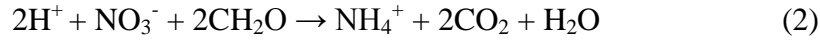
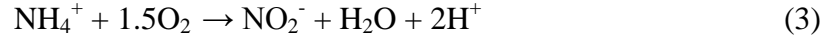


Figure 1. N sources and transformation processes that affect N species in the subsurface. The enrichment values ($^{15}\text{N}-\text{NO}_3^-$, $^{15}\text{N}-\text{NH}_4^+$) of such processes are also provided. [\rightarrow shows the transformation of the initial N compound; $-\text{---}\rightarrow$ shows sources of different N species. References: 1 – Sharp, 2007; 2 – Kendall & Aravena, 2000; 3 – Mariotti et al., 1981; 4, 7 – Clark, 2015; 5 – Kendall., 1998; 6 – Well et al., 2012; 8 – Michener & Lajtha 2007; 9 – Bedard-Haughn et al., 2003; 10 – Hübner, 1986; 11 – Minamikawa et al., 2011; 12 – Brandes & Devol, 2002].

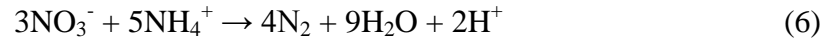
Biodegradation of ammonium (NH_4^+) occurs during the processes of nitrification, nitrifier denitrification and anammox.

Nitrification, which is a strictly anaerobic reaction, consists of two steps: 1) NH_4^+ oxidation to NO_2^- and 2) NO_2^- oxidation to NO_3^- (Buss et al., 2004).



Nitrifier denitrification is one of the nitrification pathways consisting of two following reactions: 1) NH_3 oxidation, which is attributed to nitrification, and 2) NO_2^- reduction via NO to N_2O or N_2 , which is regarded as denitrification (Zhu et al., 2013).

As for the anammox, it occurs in the presence of NO_2^- or NO_3^- , which play the role of electron acceptors, and leads to conversion of NH_4^+ to diatomic nitrogen (N_2) and water (Burgin & Hamilton, 2007; Kuenen, 2008):



Though there are several microbial reactions leading to attenuation of NH_4^+ , it is considered that the key reactive process controlling subsurface transport of NH_4^+ is sorption, which occurs as a result of cation exchange (Buss et al., 2004). Mineralization of organic matter, or ammonification, is the process that leads to conversion of organic N to NH_4^+ . It occurs under oxidizing conditions and is carried out by virtually all microorganisms involved in the decay of dead organic matter (Schimel & Bennett, 2004; Bernhard, 2012).

N-fixation is the process by which atmospheric nitrogen is converted into ammonia (NH_3) by N_2 -fixing organisms called diazotrophs. Some of them can fix N_2 in the free-living state, while others fix N_2 in association with plants (Brandes & Devol, 2002; Virginia & Delwiche, 1982).

In order to address the risks imposed by contamination of groundwater with N species, it is essential to develop comprehensive scientific understanding of N species transport and transformation in subsurface. However, this is a challenging task, since various aquifers could be simultaneously exposed to multiple contamination sources and characterized with occurrence of different N-cycle processes along groundwater flow paths. Moreover, analysis of subsurface N fluxes in agricultural areas could appear even more complicated due to predominance of diffusive N pollution, which makes it difficult to calculate the total pollutant input into the aquifers. Under such circumstances, understanding of pollution transfer between different parts of aquifer and across environmental compartments of the given catchment, such as atmosphere, soil, sediment, groundwater, surface water and biota, might become especially difficult.

To obtain information regarding origin, transport and transformation of N compounds in groundwater, many environmental researchers apply stable isotope analysis. This method helps to understand migration and mixing of N derived from multiple sources, to identify various chemical and biochemical processes involving N species and to explore the dynamics and effects of occurring reactions (Kaushal et al., 2011; Robinson, 2001). Throughout several decades analysis of N isotopes in groundwater has been employed in denitrification studies in order to identify the origin of N pollution and estimate its attenuation. Nowadays, with the rising interest towards climate change, N stable isotope analysis method also becomes more frequently applied to studies of transport and production/consumption of N₂O in subsurface. It is expected that applications of this approach in such domain should help to understand mechanisms controlling indirect N₂O emissions via groundwater pathway, improve quantification of N₂O fluxes and reveal the sites which are prone to such emissions, thus contributing to better constraint and more realistic detalization of N budget and GHG emission both on regional and global level.

While analysis of variations in stable N isotope ratios (¹⁵N/¹⁴N) can potentially provide valuable information regarding the N fluxes in agro-ecosystems, interpretation of the obtained experimental evidence is challenging. Besides the continuous simultaneous mixing of N species derived from various N pools such as atmospheric precipitation, soil

organic matter, synthetic fertilizers and manure characterized with different isotope compositions (Kendall C., 1998), the observed patterns of isotopic enrichment factor (enrichment/depletion of a reaction product relative to that of the substrate) of N species are considerably influenced by shifting dynamics of various microbiological (denitrification, nitrification, DNRA, anammox, etc.) and physicochemical processes (upward diffusion, sorption, volatilization, etc.) resulting in isotopic fractionation – enrichment of one isotope relative to another in an element during a chemical or physical process. Consequently, for proper interpretation of isotope signatures variability it is crucial to: 1) understand the factors and processes that may cause it, 2) consider the probable magnitude of the potential alterations; 3) verify the results of observations across a range of ecosystems with contrasting environmental settings; 4) support the interpretation of observed $\delta^{15}\text{N}$ values with results obtained using other experimental methods: analyses of other stable isotopes, concentration studies, microbiological analyses.

So far, considerable research effort has been devoted in order to accomplish these goals and improve the reliability of conclusions derived using experimental data provided by stable isotope analysis. Up to now few studies summarize the evidence regarding the NO_3^- isotopic signatures of different contamination sources (Choi et al., 2003), the variability of $\delta^{15}\text{N}\text{-NO}_3^-$ through landscapes (Bedard-Haughn et al., 2003) and the isotopic values of biologically produced N_2O in different environments, including groundwater (Yoshida & Toyoda, 2015). However, there is a lack of comprehensive review which would concentrate on the use of stable isotopes for studies of N species transport and transformation in groundwater under agricultural lands and summarize the evidence regarding factors determining the isotopic composition of NO_3^- , NH_4^+ and N_2O in subsurface in such environmental settings. The objectives of this chapter are: 1) summarizing the available data about the effects of sources, processes and factors on the $\delta^{15}\text{N}\text{-NO}_3^-$, $\delta^{15}\text{N}\text{-NH}_4^+$ and $\delta^{15}\text{N}\text{-N}_2\text{O}$ values in groundwater; 2) discussing the application of additional stable isotopes (^{11}B , ^{18}O , ^{13}C , ^{34}S , $^{87}\text{Sr}/^{86}\text{Sr}$) analyses to support the data obtained from the ^{15}N studies.

1.2. Effects of sources, processes and factors on the isotopic signatures of nitrogen compounds in groundwater

According to previous studies conducted under various environmental settings across the globe, the isotopic signatures of N species (NO_3^- , N_2O , NH_4^+) in groundwater under agricultural lands exhibit different ranges depending on variability of N sources, transformation processes and migration pathways (Hosono et al., 2013, Well et al 2012, Liu et al., 2012). In the cases when observed isotopic signatures of NO_3^- , N_2O , NH_4^+ in groundwater are simultaneously influenced by multiple sources and occurrence of several N-cycle processes, interpretation of $\delta^{15}\text{N}$ values demands thorough attention. While identification of the origin of N compounds in most cases still remains a relatively straightforward task, it might be more challenging to distinguish precisely the subsurface processes that cause different fractionations of N isotopes. The following section discusses the variability of isotope signals in groundwater, with particular emphasis on the agricultural areas, taking into account diversity of N sources, variety of N cycle processes and impact of multiple environmental parameters.

1.2.1. Variability of $\delta^{15}\text{N}\text{-NO}_3^-$ in groundwater

According to previous studies, the isotopic signature of $\delta^{15}\text{N}\text{-NO}_3^-$ in groundwater under agricultural areas show a considerably wide range from -8.3‰ to $+65.5\text{‰}$ (Table 1), depending on the heterogeneity of N sources, geochemical conditions and groundwater flow patterns as well as on the peculiarities of agricultural practices in the explored regions.

Table 1. Analysis of NO₃⁻ isotopic signatures in groundwater: an overview of case studies (UA – unconfined aquifer, CA – confined aquifer, IF – inorganic fertilizers, OF – organic fertilizers, SON – soil organic N, AM – animal manure, Ww – wastewater, D – denitrification, N – nitrification, Dom – decomposition of organic matter, Mix – mixing, DI – dilution).

Site	δ ¹⁵ N (‰)	δ ¹⁸ O (‰)	Aquifer type	Aquifer material	Potential NO ₃ ⁻ source	DO (mg/l)	NO ₃ ⁻ (mg/l)	pH	Processes altering the δ ¹⁵ N and δ ¹⁸ O of NO ₃ ⁻
the Chalk aquifer (France) (Mariotti et al., 1988)	+3 – +7 (s.d. 1.6)		UA	limestone	IF		3 – 10		–
	+5 – +20		boundary between UA&CA				0.37 – 12.2		D
	+0.9 – +5.8		CA				0.01 – 0.05 (s.d. 0.06)		Dom
the Arguenon watershed (Brittany, France) (Widory et al., 2005)	+2.7 – +21 (s.d. 0.2)			granitic gneiss and mica schist	AM, Ww		3.2 – 245 (mean value 106 (s.d. 78))	4.8 – 7.8	D, Mix (DI)
the “Roussillon” aquifer (Pyrénées, France) (Widory et al., 2005)	+5.4 – +23.9			deep alluvial formation; three aquifer levels due to the presence of clay layers	Ww, IF		10 – 139 (mean value 51 (s.d. 39))	6.5 – 7.9	Mix
the “Ile du Chambon” Catchment (the Allier Valley, France) (Widory et al., 2005)	+5.1 – +42.4			sand and gravel, subsurface alluvial formation	IF, Ww		<0.2 – 53 (mean value 30 (s.d. 13))		D
Fuhrberger Feld aquifer (Lower Saxony, Germany) (Well et al., 2012)	-2.1 – +65.5 (mean 6.9 (s.d. 11.7))	-5.0 – +33.5 (mean 1.6 (s.d. 5.9))	UA	carbonate-free sand and gravel	IF	0.0–9.6 (mean 2.4 (s.d. 2.9))	0.0 – 43.4 (mean 21.9 (s.d. 10.3))	4.1 – 6.3	D
Großenkneten aquifer (Lower Saxony, Germany) (Well et al., 2012)	-1.8 – +65 (mean +8.6 (s.d. 18.9))	-8.1 – +38 (mean +0.5 (s.d. 12.8))	UA	carbonate-free sand and gravel	IF	0.1 – 9.0 (mean 2.8 (s.d. 3.2))	0.0 – 57.6 (mean 15.2 (s.d. 18.5))	4.1 – 5.8	D
Osona region (Spain) (Vitòria et al., 2008)	+2.2 – +20.9 (mean +13)	+4.6 – +9.7 (mean +7.4)	CA	carbonate and carbonate sandstone; presence of pyrite	AM, IF		0.0 – 366 (mean 90)	>7	D

Site	$\delta^{15}\text{N}$ (‰)	$\delta^{18}\text{O}$ (‰)	Aquifer type	Aquifer material	Potential NO_3^- source	DO (mg/l)	NO_3^- (mg/l)	pH	Processes altering the $\delta^{15}\text{N}$ and $\delta^{18}\text{O}$ of NO_3^-
the alluvial aquifer of the Vibrata plain (Italy) (Di Lorenzo et al., 2012)	in summer: +4.9 – +22.8 in winter: +3.8 – +18.9	in summer: +1.3 – +11 in winter: +3.7 – +14.7	UA	gravel and sand with silty lenses	IF (NH_4^+ salts)		In summer: 0.1 – 148 (mean value 77.2); In winter: 2 – 151 (mean value 66.3)		patchy D
the Maresme groundwater (Spain) (Vitória et al., 2005)	+6.8 – +9.4	+5.1 – +10.2		sand	IF		23.5 – 48.2 (mean value 33.4)		V ⁺
the Zunyi area groundwater (China) (Li et al., 2010)	in summer: -1.8 – +20.7 (mean +7) in winter: -4.3 – +22.7 (mean +10.4)			carbonate rocks (limestone and dolomite) and clastic rocks; sulfate evaporite (gypsum) and coal occur locally	OF, IF, Ww		in summer: 0 – 90.5 in winter: 0 – 107.9	6.8 – 8.4	Mix, N
the Sichuan Basin (China) (Li et al., 2007)	well in farmland: -0.1 – +8.9 (mean value +3.7 (s.d. 2.1)) well in farmyard: mean value +9.7 (s.d. 4.7) spring: -8.3 – +6.4 (mean value - 0.2 (s.d. 3.7))		UA	redbeds and mudstone interbedded with sandstone	IF, Ww which might contain AM		well in farmland: 42.94 (s.d. 47.2) well in farmyard: 39.8 (s.d.42.1) spring: 16.4 (s.d. 13.7)		N

Site	$\delta^{15}\text{N}$ (‰)	$\delta^{18}\text{O}$ (‰)	Aquifer type	Aquifer material	Potential NO_3^- source	DO (mg/l)	NO_3^- (mg/l)	pH	Processes altering the $\delta^{15}\text{N}$ and $\delta^{18}\text{O}$ of NO_3^-
Guiyang, (China) (Liu et al., 2012)	in summer: -1.4 – +14.9 (mean 4.1) in winter: -0.1 – +15.4 (mean 7.0)	in summer: +2.8 – +18.2 (mean 10.7) in winter: +4.3 – +23.5 (mean 12.5)		carbonate rocks (limestone, dolomite) and clastic rocks (shale, sandstone); sulfate evaporite (gypsum) and coal occur locally	in summer: IF (urea, $(\text{NH}_4)_2\text{SO}_4$, N/P/K mix) in winter: IF, Ww		in summer: 0.29 – 11.7 (mean 5.0) in winter: 0 – 8.9 (mean 3.1)		suburban areas: N urbanized areas: D
the Wensum catchment (East Anglia, UK) (Wexler et al., 2011)	+6.2 (s.d. 0.6)	+0.8 (s.d. 0.5)	UA/CA	limestone	OF,IF		56.1 (s.d. 6.8)		Mix and N
Kumamoto groundwater area (Japan) (Hosono et al., 2013)	-6 – +46	-3 – +48	UA	pyroclastic and alluvial sedimentary deposits	IF, AM		0 - 73		DI and D
			CA	porous andesitic lava and pyroclastic deposits					
the Cretaceous Chalk aquifer (Cambridgeshire and Norfolk, UK) (Feast et al., 1988)	+3.6 (s.d. 1.8)	+8.5 (s.d. 2.8)	UA	limestone	IF, OF		39.2 (s.d. 14.3)	7.2 (s.d. 0.1)	N, minor D
La Pine, (Oregon, USA) (Hinkle et al., 2007)	+3.3 – +12.8 (mean 7.5)			sand	Ww, IF	<0.1 – 10.7 (mean 1.2)		6.7 – 8.2 (mean 7.4)	D
Ichikawa city (Japan) (Li et al., 2014)	+5.7		upland shallow ground water	sand	IF, OF, AM	in summer: 9.3	in summer: 76.6	6.1–6.9	N
							in winter: 5.7	in winter: 153.8	
Sacramento Valleys (USA) (Fogg et al., 1998)	+1 – +6		SCA/UA	sand and gravel	IF, AM, Ww				–
Salinas Valley (USA) (Fogg et al., 1998)	+4.1 – +5.1		SCA/UA	sand and gravel	IF, AM, Ww		32 – 74		possible D
Wexford (Ireland) (Bailey et al., 2011)	+6 – +32.4	+1.4 – +21.2	shallow ground water	greywacke, schist and massive schistose quartzites	M, IF		0 – 66.4		N,D

Site	$\delta^{15}\text{N}$ (‰)	$\delta^{18}\text{O}$ (‰)	Aquifer type	Aquifer material	Potential NO_3^- source	DO (mg/l)	NO_3^- (mg/l)	pH	Processes altering the $\delta^{15}\text{N}$ and $\delta^{18}\text{O}$ of NO_3^-
the Bure River valley (Norfolk, UK) (Feast et al., 1998)	-2.1 – +13.7	-7.01 – -8.2	UA/CA	limestone	IF		<0.1 – 95.4 (mean 18.7)		Mix, D
the Cedar River Watershed (Iowa, USA) (Gautam & Iqbal, 2010)	+0.5 – +5.4			shallow aquifer: sand and gravel deep aquifer: limestone and dolomite	IF, SON	shallow aquifer: 4.9 – 7 deep aquifer: 2.9 – 6.9	0 – 75.5 (mean 35.8)		–
Slate catchment (Ireland) (McAleer et al., 2016)	+1.9 – +6.8 (mean +3.3)	-0.5 – +3.8 (mean +0.8)	UA	slate, siltstone	IF	4.5 – 11.8 (mean 8.9)	32.8 – 51.4 (mean 35.9)		DI

1.2.1.1. Isotopic signatures of nitrate sources

The observed inflow of N into groundwater in agricultural areas can be attributed to multiple sources such as organic and inorganic fertilizers, manure, soil organic N, sewage (e.g. septic wastewater), and atmospheric precipitations. N originating from each source is characterized with distinct intervals of $^{15}\text{N}\text{-NO}_3^-$ enrichment values (Fig. 2), which can be used to determine the origin of observed NO_3^- and estimate the relative contribution of NO_3^- sources to its content in the groundwater.

In particular, it has been observed that the organic and inorganic fertilizers are characterized with different isotopic signatures, which is explained by their production processes. For example, synthetic fertilizers, such as urea or NH_4^+ and NO_3^- fertilizers, are usually produced by fixation of atmospheric N_2 which has $\delta^{15}\text{N}$ $0\pm 3\%$ (Kendall, 1998). This process only slightly fractionates the isotope composition resulting in low $\delta^{15}\text{N}$ range of inorganic fertilizers, from -4 to $+4\%$ (Sharp, 2007), -8 to $+7\%$ (Kendall, 1998) or -6 to $+6\%$ (Xue et al., 2009). However, in groundwater, this typical isotopic composition of inorganic fertilizers frequently changes because of N isotope fractionation during various physicochemical or biochemical reactions (e.g. NH_3 volatilization, nitrification or denitrification).

In line with these suggestions, further studies demonstrated that the $\delta^{15}\text{N-NO}_3$ in groundwater of cropping areas with mineral fertilizer application may be in the range of +4.5 – +8.5‰ (Choi et al., 2007) or -7 – +5‰ (Danielescu & MacQuarrie, 2013). At the same time, organic fertilizers, such as plant compost or liquid and solid animal waste, generally are characterized with higher initial $\delta^{15}\text{N}$ values and a broader range of isotopic composition (+6 to +30‰) than inorganic fertilizers. This is explained by the processes occurring in animal wastes such as excretion of isotopically light N in urine and accumulation of heavy ^{15}N isotope in the residual waste as well as volatilization of ^{15}N depleted ammonia with subsequent oxidation of the residual waste (Sharp, 2007).

In comparison to both organic and inorganic fertilizers, NO_3^- produced by nitrification of manure-N has higher $\delta^{15}\text{N-NO}_3^-$, since during its storage, treatment and application, the volatilization of NH_3 causes significant enrichment of ^{15}N in the residual NH_4^+ , while most of this NH_4^+ is subsequently oxidized to ^{15}N -enriched NO_3^- (Widory et al., 2004). Consequently, $\delta^{15}\text{N}$ values of NO_3^- originating from manure usually range between +5 to +25‰ (Xue et al., 2009), +10 to +22‰ (Bateman et al., 2005), +5 to +35‰ (Widory et al., 2005).

Soil organic-derived NO_3^- is a product of bacterial decomposition of organic matter originated from degradation of plants and animal wastes. The $\delta^{15}\text{N-NO}_3$ of soil NO_3^- may be between +3‰ and +8‰ (Kendall & Aravena, 2000). It is also particularly important to consider, in groundwater polluted by fertilizers, the possible mixing of N originating from the addition of fertilizers and N mineralized from soil organic matter which might not be taken up by crops if their demands are already satisfied (Li et al., 2007). For example, Danielescu & MacQuarrie (2013) revealed that 72% of their surface- and groundwater samples of the Trout catchment fell into the overlapping interval of +3 to +5‰. This indicates that the detected concentrations could be derived either from the use of NH_4^+ fertilizers or from the presence of soil organic-derived NO_3^- . The studies in the Cedar river basin (USA) (Gautam & Iqbal, 2014) (Table 1) also demonstrated that the $\delta^{15}\text{N-NO}_3^-$ range, between +0.45‰ and +5.35‰, was the result of the joint effect of fertilizers and soil organic Non groundwater quality. On the contrary, the isotopic signature of NO_3^- originated from animal or sewage waste is commonly less influenced

by interaction with soil N because the distribution of waste is often localized at point sources with high concentrations. In some cases, the observation of the distribution of point and non-point sources of pollution can help to identify the origin of NO_3^- more precisely.

Another significant source of NO_3^- in groundwater under agricultural lands is household sewage whose $\delta^{15}\text{N-NO}_3^-$ range vary between +4‰ and +19‰ (Xue et al., 2009). In many cases, experimental studies have revealed similar ranges of $\delta^{15}\text{N}$ for both animal manure and sewage, for instance: +3‰ – +25‰ (Lorenzo et al., 2012), +8 – +18‰ (Vitòria et al., 2008), and others. Consequently, it is often difficult to determine exactly the origin of NO_3^- in areas characterized with simultaneous occurrence of groundwater pollution from livestock manure and household wastes.

The amount of N contained in atmospheric precipitation is influenced by several factors: volatilization of NH_3 , nitrification and denitrification occurring in the soils and the impact of various anthropogenic sources. In general, the $\delta^{15}\text{N-NO}_3^-$ composition of rain is higher than that of the co-existing $\delta^{15}\text{N-NH}_4^+$ (Bedard-Haughn et al., 2003). The $\delta^{15}\text{N-NO}_3^-$ isotopic signature of rain might vary between -10‰ and +9‰ – based on various case studies (Sharp, 2007), -11.8‰ and +11.4‰ – reported for eastern Canada (Savard et. al., 2010) and -10.2 and -4.4 – reported for central China (Li et al., 2007).

This overview demonstrates that the sources of NO_3^- pollution are characterized with relatively different $\delta^{15}\text{N-NO}_3^-$ isotope ranges: rain water – from -12 to +11‰, inorganic fertilizers – from -8 to +7‰, organic fertilizers – from +6 to +30‰, soil organic matter – from +3 to +8‰, manure – from +5 to +35‰, and household sewage – from +3 to +25‰. The lowest values of $\delta^{15}\text{N-NO}_3^-$ are typical for inorganic fertilizers followed by NO_3^- derived from soil organic matter, while the highest values are usually related to the impact of manure or household wastes, both of which may overlap. However, the isotope composition of NO_3^- from different sources might be subject to considerable alterations due to fractionation processes occurring under certain biochemical or physicochemical reactions during the migration to or within the aquifer.

1.2.1.2. Isotopic effects of nitrate production/consumption processes

Previous studies showed that denitrification and nitrification alter the original $\delta^{15}\text{N-NO}_3^-$ isotopic composition of NO_3^- in groundwater under agricultural areas (Fig. 1). Isotope effects of the considered N processes are presented in terms of their enrichment factors which show isotope enrichment of a reaction product relative to that of the substrate and are determined by means of the Rayleigh equation (Mariotti et al., 1981):

$$\varepsilon = \frac{10^{-3} \delta(\text{NO}_3^-)_{\text{measured}} + 1}{10^3 \ln \frac{10^{-3} \delta(\text{NO}_3^-)_{\text{initial}} + 1}{\ln \left[\frac{C(\text{NO}_3^-)_{\text{measured}}}{C(\text{NO}_3^-)_{\text{initial}}} \right]}} \quad (7)$$

where ε is the isotopic enrichment factors for N or O, δ is the $\delta^{15}\text{N}$ and $\delta^{18}\text{O}$ values, respectively and C – NO_3^- concentration.

Denitrification has attracted most considerable research effort as it plays a significant role in the attenuation of NO_3^- pollution in the subsurface (Rivett et al., 2008). Experimental results suggest that it is a strongly fractionating process responsible for preferential conversion of the lighter isotope ^{14}N to N_2O and N_2 . Consequently, the corresponding enrichment of the residual (unreacted) NO_3^- with the heavy isotope ^{15}N is observed (Knöller et al., 2011; Fukada et al., 2003). During this process the $\delta^{15}\text{N}$ value of the initially produced NO_3^- might be enriched in comparison to N_2 or N_2O by approximately 20 – 30‰ (Clark, 2015), or 5 – 40‰ (Kendall, 1998). For example, denitrification of NO_3^- fertilizer that originally had a distinctive $\delta^{15}\text{N}$ value of +1‰ can yield residual NO_3^- with a $\delta^{15}\text{N}$ value of +15‰ which is within the range of composition expected for a NO_3^- from a manure or septic-tank source (Kendall, 1998). Among the case studies considered in this review (Table 1) the most pronounced effects of denitrification were reported for the unconfined sand and gravel aquifers of Fuhrberger Feld (Lower Saxony, Germany) and Großenkneten (Lower Saxony, Germany) (Well et al., 2012), for the Chalk aquifer (France) at the boundary between confined and unconfined zones (Mariotti et al., 1988) and for the alluvial aquifer of the Vibrata plain (Italy) (Di Lorenzo et al., 2012). These effects originate from: 1) microorganisms' activity within the pore spaces of sediments in case of Fuhrberger Feld and Großenkneten; 2) local physicochemical conditions (e.g. availability of the substrate pool

and electron donors, concentration of the electron donors) in case of the Chalk aquifer and 3) the extent of hyporheic zone (groundwater/surface water flow exchange) in case of alluvial aquifer in the Vibrata plain. However, it should be emphasized that the rate and extent of denitrification processes in the considered cases as well as other cases depend of the combination of multiple environmental factors (section 1.2.1.3) and their mutual interaction.

In contrast, nitrification reaction results in the preferential incorporation of the lighter isotopes into NO_3^- and often leads to decrease in the $\delta^{15}\text{N-NO}_3^-$ (Barnes & Raymond, 2010). In average the difference between initial $\delta^{15}\text{N-NH}_4^+$ and produced $\delta^{15}\text{N-NO}_3^-$ can reach 12 – 29‰ (Kendall & Aravena, 2000), or 5 – 35‰ (Mariotti et al., 1981). However, evidence has been also obtained that both $\delta^{15}\text{N-NH}_4^+$ and $\delta^{15}\text{N-NO}_3^-$ will increase as the NH_4^+ reservoir is converted to NO_3^- , with $\delta^{15}\text{N-NO}_3^-$ evolving toward the initial $\delta^{15}\text{N-NH}_4^+$ value (Clark, 2015). In general, it appears that the final $\delta^{15}\text{N}$ of NO_3^- derived via nitrification from manure-N would be more positive than that from fertilizer-N (Choi et al., 2003). The influence of the nitrification on the $\delta^{15}\text{N-NO}_3^-$ of groundwater was detected in the Sichuan Basin (China) (Li et al., 2007), Ichikawa city (Japan) (Li et al., 2014), shallow groundwater in Wexford (Ireland) (Baily et al., 2011), in the Cretaceous Chalk aquifer in Cambridgeshire and Norfolk, UK (Hiscock et al., 2003) and in the hydrogeological formation in Zunyi (China) (Li et al., 2010).

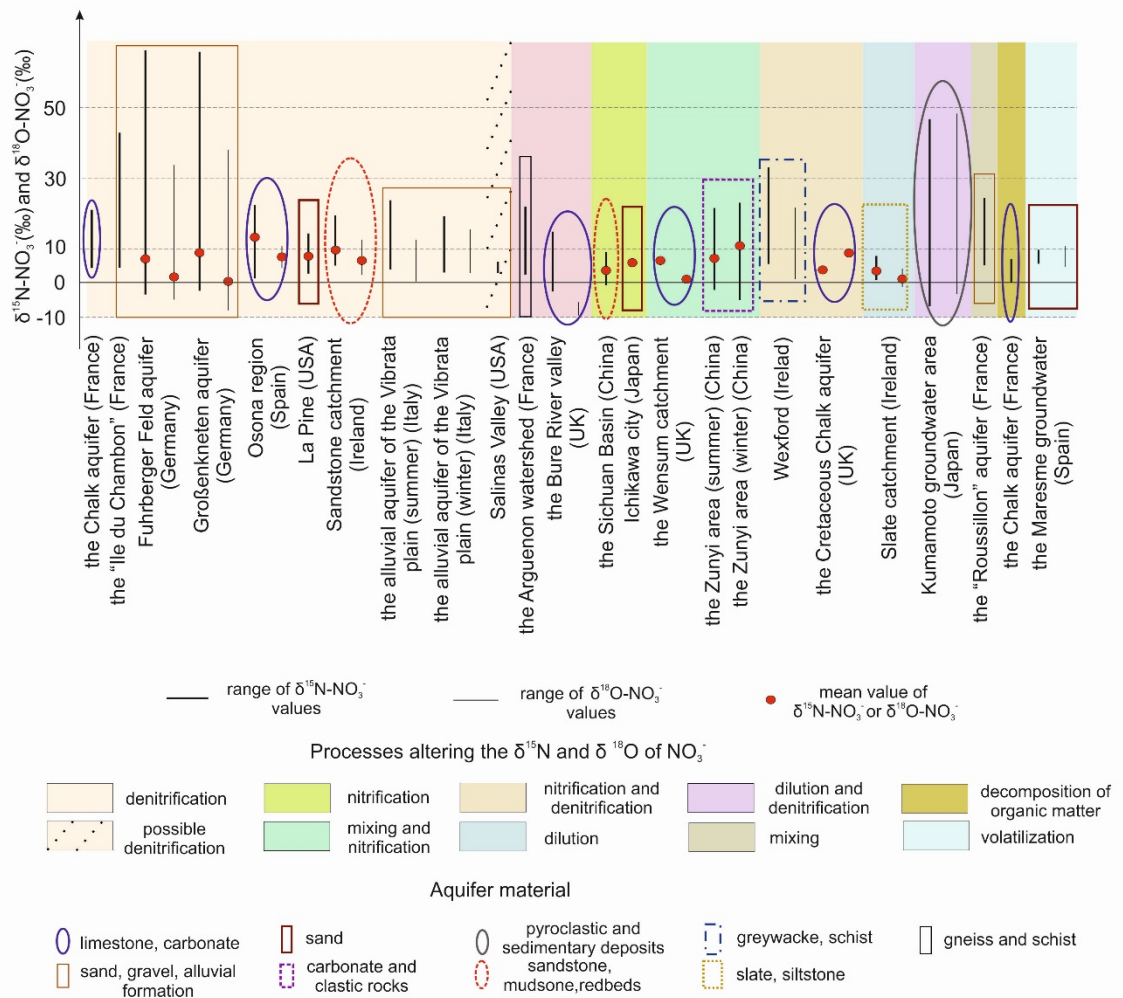


Figure 2. NO_3^- isotopic signatures in groundwater: a summary of case studies in agricultural areas.

1.2.1.3. Factors controlling nitrate production/consumption processes and their impact on $\delta^{15}\text{N-NO}_3^-$ variability

The magnitude of fractionation related to nitrification and denitrification processes is influenced by ambient conditions of hydrogeological systems where they occur, e.g. substrate concentration, availability of electron donors, concentration of dissolved oxygen, temperature, pH, residence time, etc. (Böttcher et al., 1990).

In particular, it has been demonstrated that the size of the substrate pool (the amount of the chemical species which reacts with a reagent to generate a specific product) determines the extent of fractionation by minimizing it in N-limited systems and maximizing in systems with constant and high supply of N compounds (Li et al., 2007). For example, nitrification processes will be more intensive under the presence of a large amount of NH_4^+ (e.g. due to application of artificial fertilizers), which would likely cause considerable fractionation (Kendall, 1998). However, as the NH_4^+ pool is consumed, the overall nitrification fractionation gradually decreases. It has also been revealed that excessive concentrations of NO_3^- might induce a termination of denitrification with the formation of N_2O (Rivett et al., 2008). The threshold concentrations for the occurrence of this effect appear to be case-specific, since in some cases it has been reported that even low concentrations affected the ratio between produced N_2O and N_2 . For example, an increase in the $\text{N}_2\text{O}:\text{N}_2$ ratio from 0.11 to 0.34 associated with an addition of 0–4 mg-N/l was reported by Magalha'es et al. (2003). That is why it is essential to consider the initial concentration of the substrate in order to achieve more accurate conclusions concerning the production/consumption of NO_3^- and related changes in its isotopic composition.

Availability of electron donors is mostly discussed in the context of fractionation effects caused by denitrification. In general, it is suggested that denitrification may not play an important role in increasing $\delta^{15}\text{N}$ of NO_3^- under the conditions of low contents of electron donors (Choi et al., 2003). Electrons needed for denitrification can originate from the microbial oxidation of organic C or reduced S which might be present in water as the S^{2-} state in H_2S , S^{1-} in FeS_2 , S^0 in elemental sulfur, S^{2+} in thiosulfate ($\text{S}_2\text{O}_3^{2-}$) or S^{4+} in sulfite (SO_3^{2-}), (to the S(+VI) state as sulfate) (Rivett et al., 2008). To consider the potential impact of limited availability of electron donors on isotopic composition of NO_3^- it has been proposed to monitor their concentrations throughout the periods of observation of the ^{15}N isotopic signatures. For example, the presence of DOC in waters has been used as an indicator of an available carbon source for denitrification. Moreover, concentrations of sulfate ion have also been measured to test for consistency with denitrifying environment (Kellman & Hillaire-Marcel, 2003). It should be mentioned that the amount of DOC has been shown to decrease in conjunction with an increase in sulfate

concentration. This effect is related to the reduced solubility of DOC under conditions of increased ionic strength and acidity of water (Evans et al., 2006; Clark et al., 2005).

Concentration of dissolved oxygen (DO) in hydrogeological systems can also have a crucial impact on observed NO_3^- isotopic signatures. It may determine the type of N biochemical transformations occurring, which can alternatively lead either to decrease or increase of $\delta^{15}\text{N}$ of NO_3^- . As a common rule, the low content of oxygen is associated with denitrification reactions which lead to the increase of $\delta^{15}\text{N}$ - NO_3^- . On the contrary, higher content of oxygen usually accompanies nitrification reactions which result in low $\delta^{15}\text{N}$ - NO_3^- values. From previous studies, it has become obvious that the occurrence of denitrification and nitrification processes could not be associated with clearly defined values (or narrowly constrained intervals) of DO concentrations. In particular, there is the range of DO concentration where both nitrification and denitrification can occur. For instance, denitrification cannot occur if the content of DO is above 0.2 mg/l according to Feast et al., 1998, above 2 mg/l according to Rivett et al. (2008) or above 4 mg/l according to Baily et al. (2011). At the same time, it has been reported that the rate of nitrification reactions is maximized for a range of DO concentrations between 0.3 mg/l and 4 mg/l (Stenstrom & Poduska, 1980). However, the experimental evidence is not conclusive, as in some cases it has been determined that a dissolved oxygen concentration in excess of 4.0 mg/l was required to achieve the highest nitrification rates (Stenstrom & Poduska, 1980). That is why, in order to be able to distinguish these two processes it is important to consider thoroughly the data about pH, availability of electron donors etc.

As the water temperature controls microbial activity and, consequently, DO content in groundwater, any seasonal changes could affect the $\delta^{15}\text{N}$ of NO_3^- , resulting in higher values of isotopic enrichment in the summer periods in aquifers where denitrification occurs, or lower values in groundwater influenced by nitrification activity. However, evidence about the impact of water temperature is not yet conclusive, as some reports suggested that $\delta^{15}\text{N}$ - NO_3^- values might not exhibit seasonal trends (Danielescu & MacQuarrie, 2013). So it is essential to study microbial communities and distribution of potential denitrifying genera, as this will allow to get better insight into the nature of

NO_3^- production/consumption processes and, in particular, into the impact of temperature on their dynamics. (Hernández-del Amo, 2018).

The pH range is another important factor that affects the intensity of microbiological reactions and influences the magnitude of fractionation effect. It has been reported that pH ranging between 6.5 to 8 is the optimal range for nitrification, and reaction rates are likely to be significantly decreased below pH 6.0 and above pH 8.5 (Buss et al., 2004). Denitrification processes typically occur under a pH range between 5.5 and 8, but the optimal pH is site-specific because of the effects of adaptation on the microbial ecosystems (Feast et al., 1998). Anammox activity is observed in a pH range from 6.5 to 9.3 with the optimum pH at 8 (Tomaszewski et al., 2017; Jin et al., 2012).

Furthermore, the hydrogeological structure of the area predetermines the processes of mixing of waters derived from different sources (see section 1.2.1.1 (pp. 36 – 38)) and of different age. Therefore, it also profoundly affects the dynamics of $\delta^{15}\text{N}$ isotopic signature (as demonstrated by the vast majority of considered case studies – see Table 1) (Einsiedl & Mayer., 2006). Therefore, comprehensive analysis of $\delta^{15}\text{N}\text{-NO}_3^-$ distribution in groundwater should be supported by in-depth consideration of hydrogeological features of the examined territories, for instance - the extent of confined and unconfined zones in the subsurface system, their connection and location of the recharge areas along the aquifer.

While studying variations of $\delta^{15}\text{N}\text{-NO}_3^-$ in agricultural areas, it is particularly important to consider agricultural practices and the types of adjacent land uses, as they might significantly alter the isotopic signature of NO_3^- in groundwater samples. In agricultural areas where it is common to leave crop residues on the fields over the winter period it is necessary to consider the seasonality of NO_3^- sources. Previous studies which analyzed the influx of N from inorganic fertilizers into aquifer systems under intensive row-cropping and fertilization highlighted the significance of the intermediate N cycling processes of mineralization and nitrification of soil organic matter, such as crop residue, in the overall N cycling (Savard et al., 2010). Since resulting winter and spring load of NO_3^- is attributed to slow mineralization and nitrification during soil organic matter degradation, it is hard to identify precisely the source of NO_3^- in groundwater using its

isotopic signature, since $\delta^{15}\text{N-NO}_3^-$ values are close to those typical for fertilizers. Moreover, Sebilo et al. (2013) showed that the isotopic composition of NO_3^- in groundwater might be considerably influenced by mineralization of N fertilizers incorporated into the soil organic matter pool several decades ago. Therefore, the evidence regarding the dynamics of isotopic signatures should be supported by the expert knowledge about the local agricultural practices.

To summarize, the previous studies considered in this review have demonstrated that aquifers under agricultural areas are characterized with a wide range of $\delta^{15}\text{N-NO}_3^-$ determined by the variability of N sources and N transformation processes, intensity of which is controlled by the ambient geochemical conditions and hydrogeological settings (Fig. 3).

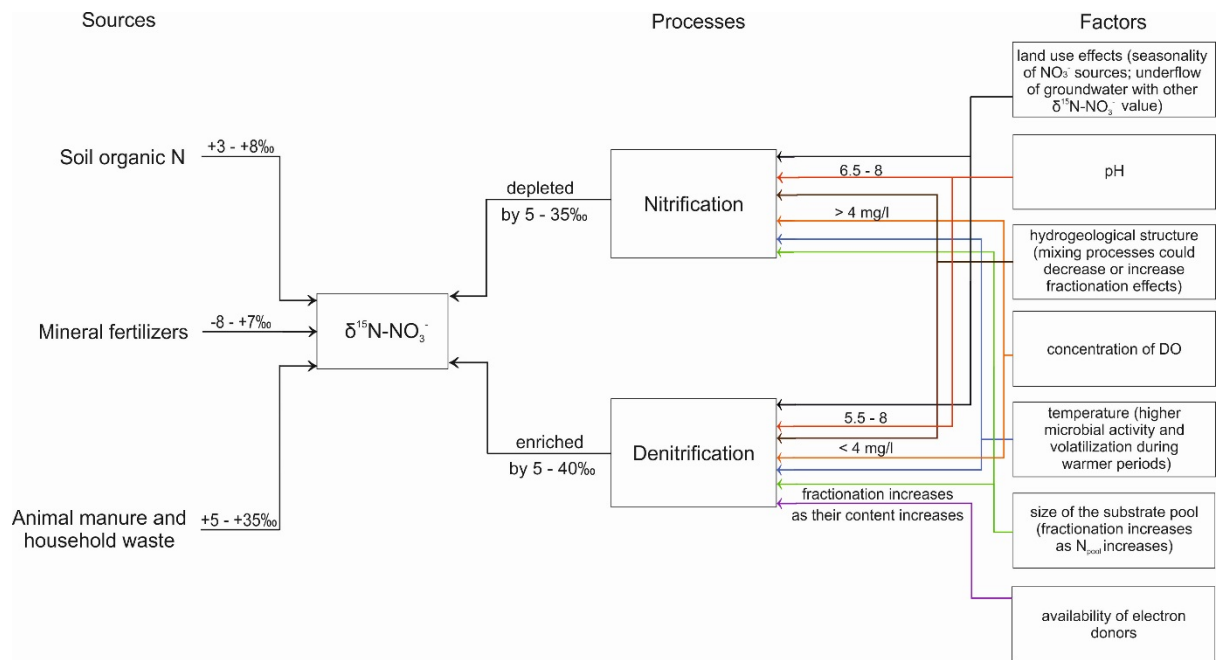


Figure 3. Sources, processes and factors that influence the $\delta^{15}\text{N-NO}_3^-$ values: summary (the following arrows connect processes with factors that have decisive effect on their dynamics and, consequently, on resulting fractionation effects: \rightarrow availability of electron donors; \rightarrow size of the substrate pool ; \rightarrow temperature; \rightarrow concentration of DO; \rightarrow hydrogeological structure; \rightarrow pH; \rightarrow land use).

In general, mineral fertilizers typically show the lowest $\delta^{15}\text{N-NO}_3^-$ values, followed by the isotopic signatures of soil-derived organic NO_3^- . The highest $\delta^{15}\text{N-NO}_3^-$ are commonly observed in animal manure or household sewage. Among the microbiological and physicochemical processes influencing isotopic composition of NO_3^- in groundwater, the highest $\delta^{15}\text{N-NO}_3^-$ values are associated with the denitrification activity. On the contrary, nitrification is responsible for the occurrence of NO_3^- with the ^{15}N isotopic signature on 5 – 35‰ lower in comparison to the ^{15}N of initial NH_4^+ . While exploring the variability of ^{15}N in groundwater systems, it is important to account for possibilities of physical mixing of water of different origins and the impact of multiple environmental parameters on the intensity of transformation processes as they might lead to change in the isotopic signature of initial N pollutants.

1.2.2. Variability of $\delta^{15}\text{N-NH}_4^+$ in groundwater

In comparison to the amount of information regarding $\delta^{15}\text{N-NO}_3^-$ in groundwater under the agricultural areas, the data about distribution of $\delta^{15}\text{N-NH}_4^+$ is less abundant. In general, conducted studies revealed that the $\delta^{15}\text{N}$ values of NH_4^+ in aquifers cover the range from -8.5‰ to +23.8‰ (Table 2), being significantly lower than the corresponding $\delta^{15}\text{N}$ values of NO_3^- (Li et al., 2010, Li et al., 2007, Hinkle et al., 2007, Liu et al., 2006).

Table 2. Analysis of NH_4^+ isotopic signatures in groundwater: an overview of case studies (Vu – volatilization of urea, N – nitrification, V – volatilization, M – mineralization of organic N, s.d. – standard deviation, bdl – below detection level).

Site	$\delta^{15}\text{N}$ (‰)	Processes altering the $\delta^{15}\text{N}$ of NH_4^+	NH_4^+ (mg/l)
the Sichuan Basin (China) (Li et al., 2007)	well in farmland: -6.7 - +5.1 mean value (-1.2 (s.d. 3)) well in farmyard: +5.4 - +23.8 (mean value +9.7 (s.d. 6.1)) Spring: mean value -8.5 (s.d. 1.5)	Vu	0.1 – 0.3
Guiyang (China) (Liu et al., 2006)	in summer: +0.04 – +1. (mean +0.64) in winter: -1.7 – +3.9 (mean +1.2)	N, V	in summer: 0.04 – 3.6 (mean 0.8) in winter: 0.04 – 18 (mean 4.1)
La Pine, (Oregon, USA) (Hinkle et al., 2007)	+2.5 – +3.9 (mean 3.5)	M	>0.02 – 38 (mean 4.3)
the Zunyi area groundwater (China) (Li et al., 2010)	-1.1 – +5.2 (mean +1.9)	N	in summer: bdl – 1.7 in winter: bdl – 1.3

1.2.2.1. Isotopic signatures of ammonium sources

Overall, fertilizers, manure and sewage effluent are the principal anthropogenic sources of the NH_4^+ in groundwater under agricultural areas. Rainwater and organic matter may also substantially contribute to NH_4^+ concentration in groundwater (Hinkle et al., 2007). The comparison of $\delta^{15}\text{N-NH}_4$ values of different pollution sources with the

isotopic signatures of groundwater samples is widely used for identification of the origin of detected NH_4^+ .

NH_4^+ fertilizers usually have $\delta^{15}\text{N}$ values of 0‰ or lower (Kendall, 1998). Available data provide the following ranges: from -1.5‰ to -0.7‰ (Wassenaar, 1995); from -7.4‰ to +3.6‰ (median value -0.6‰) (Vitòria et al., 2004); from +2.7‰ to +5.1‰ (mean value $+4.2 \pm 0.8$ ‰) (Li et al., 2007); -3.9‰ (± 0.3 ‰) (Choi et al., 2007), -0.91‰ (± 1.88 ‰) (Kendall, 1998). In general, the isotopic signature of $\delta^{15}\text{N-NH}_4^+$ is reported to be 2.5‰ lower than the isotopic signatures of $\delta^{15}\text{N-NO}_3^-$ of synthetic fertilizers.

Application of manure in agricultural fields or animal waste effluents from farms might increase the isotopic signature of $\delta^{15}\text{N-NH}_4^+$ in the groundwater located under such areas in comparison to the aquifers effected by the fertilizer use, as animal waste is characterized by higher level of $\delta^{15}\text{N}$ enrichment of NH_4^+ (Fig. 3). It appears that the higher $\delta^{15}\text{N}$ values observed in animal wastes are related to the increase in $\delta^{15}\text{N}$ by 3 – 4‰ at each successive trophic level (step in a nutritive series, or food chain, of an ecosystem). The most important factor contributing to this increase is the excretion of isotopically light urine: animal waste gets further enriched in ^{15}N by the subsequent volatilization of isotopically light NH_3 (Sharp, 2007). The initial $\delta^{15}\text{N-NH}_4^+$ values of manure may vary between +8‰ and +10‰ for pig waste (Vitoria et al., 2003) and around $+7.4\% \pm 3.8\%$ for cow waste (Maeda et. al., 2016).

NH_4^+ is also one of the major components in groundwater contamination plumes originating from septic tank effluents or wastewater release from treatment plants. In untreated sewage, the isotopic signature of $\delta^{15}\text{N-NH}_4^+$ is typically between +5‰ and +9‰ (Cole et al., 2006). The sewage effluent in Guiyang (China) showed the mean value of $\delta^{15}\text{N-NH}_4^+$ at +5.3‰ (Liu et al., 2006), and Robertson et al. (2011) detected the $\delta^{15}\text{N-NH}_4^+$ value of $+4.4\% \pm 4.6\%$ in the septic system of the Long Point campground located on the shore of Lake Erie (USA and Canada). Usually, the contamination plumes exhibit clear stratification between the differently enriched NH_4^+ species. The top of the plume is typically characterized with more enriched $\delta^{15}\text{N-NH}_4^+$ values, caused by ongoing nitrification, in comparison to the core of the plume, where NO_3^- and NH_4^+ coexist and

anammox reaction enriches both compounds, and below plume where only NO_3^- attenuated by denitrification remains (Clark, 2001).

NH_4^+ is also the most abundant N compound in rainwater which commonly exhibits negative $\delta^{15}\text{N}$ values. In particular, experimental data provided by Li et al. (2007) in the Sichuan river basin (China) showed that $\delta^{15}\text{N-NH}_4^+$ in atmospheric precipitation vary from -13.4‰ to +2.3‰ (mean value $-6.6\text{‰}\pm 4.0\text{‰}$). Isotope analyses conducted on rainwater samples from Zunyi in China, also demonstrated negative (approximately -12‰) $\delta^{15}\text{N-NH}_4^+$ values (Li et al., 2010). The inflow of NH_4^+ originating from decomposition of organic matter in sediments and soils may also influence the isotopic signature of $\delta^{15}\text{N-NH}_4^+$ in groundwater. In general, $\delta^{15}\text{N-NH}_4^+$ in soil or sediments usually differs from the isotopic composition of total organic N in such samples only by $\pm 1\text{‰}$ (Kendall, 1998). This is explained by the small magnitude of fractionation effect occurring during mineralization of organic matter. Norman et al. (2015) revealed that NH_4^+ detected in groundwater of the Nam Du area (Hanoi, Vietnam) originated from the overlaying peat which exhibited the isotopic signature of total N in the range of +2.4 to +4.1‰. In addition, Hinkle et al. (2007) (Table 2) during the studies of groundwater in La Pine (Oregon, USA) concluded that the observed groundwater NH_4^+ concentration of 38 mg/l were likely due to mineralization of organic N, with measured $\delta^{15}\text{N-NH}_4^+$ of 2.5 – 3.9‰.

To sum up, the most negative values of $\delta^{15}\text{N-NH}_4^+$ could be observed in rainwater, while the highest positive isotopic signatures are typical for animal manure and sewage. At the same time, organic matter exhibits slightly higher $\delta^{15}\text{N-NH}_4^+$ isotopic composition in comparison to synthetic fertilizers. However, the available experimental evidence also suggests that in practice the isotopic signals of various NH_4^+ sources (Fig. 3) might overlap due to the peculiarities of environmental settings in certain areas.

1.2.2.2. Isotopic effects of ammonium production/consumption processes

The existing body of research devoted to exploration of $\delta^{15}\text{N-NH}_4^+$ variability in groundwater of agricultural areas demonstrate that during the transport of contaminants within the hydrogeological system the initial $\delta^{15}\text{N}$ values of NH_4^+ pollution sources can

undergo considerable changes due to mineralization, sorption, volatilization, nitrification, anammox and dissimilatory NO_3^- reduction to NH_4^+ (DNRA). So far, significant research efforts have been devoted to estimation of fractionation effects of different processes which underlie the observed $\delta^{15}\text{N-NH}_4^+$ variability (Normann et al., 2015, Zhu et al., 2013; Jin et al., 2012; Michener & Lajtha, 2007; Böhlke et al., 2006, Buss et al., 2004).

The conducted analysis showed that mineralization or ammonification usually causes only small fractionation (nearly $\pm 1\%$) between soil organic matter and soil NH_4^+ (Sharp, 2007). According to Micheher & Lajtha (2007), the term mineralization might be used to describe the overall process of production of NO_3^- from organic matter, which usually involves several reaction steps. Under such definition, observed fractionation ranged from -35 to 0‰, depending on which step was considered as the limiting one (Micheher & Lajtha, 2007). However, the results of such observations should be used cautiously, since such large and variable range might be attributed not to the mineralization step itself, but rather to nitrification of NH_4^+ to NO_3^- .

Small isotopic fractionations have been reported for NH_4^+ sorption/desorption processes on charged surfaces of clays and other minerals. According to laboratory studies, NH_4^+ sorbed from solutions by clays commonly is enriched in ^{15}N relative to the NH_4^+ that remains in solution (Böhlke et al., 2006). These results support the findings of the research accomplished by Delwiche & Steyn (1970) which showed that ion-exchange fractionations between kaolinite and solution are in the range of 0.7 - 0.8‰. Also, Hübner (1986) showed that ion-exchange fractionations are commonly in the range of 1 to 8‰ and stated that the actual fractionation is dependent on concentration and the fractionation factor for the exchange with the clay material. According to Kendall (1998) the fractionation factor will probably vary with depth in the soil because of changes in clay composition and water chemistry. These factors might retard or intensify sorption processes leading, respectively, to enrichment or depletion of $^{15}\text{N-NH}_4^+$ in groundwater.

Volatilization is a highly fractionating process in which the produced NH_3 gas has a lower $\delta^{15}\text{N}$ value than the residual NH_4^+ . It involves several steps that cause fractionation, including: 1) equilibrium fractionation between NH_4^+ and NH_3 in solution, and between aqueous and gaseous NH_3 ; 2) kinetic fractionation caused by the diffusive

loss of ^{15}N -depleted NH_3 . In general, the overall dynamics of the process leads to the enrichment of the remaining NH_4^+ in ^{15}N on the order of 25‰ in comparison to the volatilized NH_3 . However, it is noticed that the actual fractionation could depend on the pH and temperature (Bedard-Haughn et al., 2003).

Nitrification of NH_4^+ is a two-step process which yields ^{15}N -depleted products and commonly results in a substantial increase of $\delta^{15}\text{N-NH}_4^+$ value. As was mentioned in the previous section (1.2.1.2), the oxidation of NH_4^+ to NO_3^- enriches the remaining NH_4^+ by approximately 30‰ in comparison to produced NO_3^- . In general, the total fractionation associated with nitrification depends on which step is rate determining. Because the oxidation of NO_2^- to NO_3^- is rapid in natural systems, this step is usually not considered as the rate-determining one, and most of the observed N fractionation is caused by the slower oxidation of NH_4^+ to NO_2^- (Micheher & Lajtha, 2007). The extent of fractionation during nitrification is also evidently dependent on the fraction of the substrate pool that is consumed during the process (refer to section 1.2.2.3. for further details).

Anammox or anaerobic oxidation of NH_4^+ to N_2 leads to a slight enrichment of the residual NH_4^+ by 4 – 8 ‰ (Clark, 2015; Robertson et al., 2011). The low fractionation effect of anammox process, usually observed during field studies, could probably be caused by the presence of greater reservoir of NH_4^+ sorbed on the aquifer that buffers the enrichment of $\delta^{15}\text{N}$ in the dissolved NH_4^+ in the explored cases (Clark, 2015). So far, the anammox process was detected mostly within the long pollution plumes (i.e., from several hundred meters to 1 km in length) originating from point pollution sources (septic tanks, industrial or residential effluents.). For example, Smith et al. (2015) and Böhlke et al. (2006) explored anammox activity in the contaminated groundwater plume created by land disposal of treated wastewater which appeared at the location of Cape Cod (Massachusetts, USA). Similarly, Robertson et al. (2011) explored the possibilities for occurrence of anammox conditions in a septic system plume originating from the washroom facility located on the north shore of Lake Erie (between USA and Canada).

Since it has been discovered that, under anaerobic conditions, NO_3^- may also be reduced to NH_4^+ by a process known as DNRA, it is necessary to consider its potential

impact on $\delta^{15}\text{N-NH}_4^+$ as well. In general, this process occurs under the same conditions as denitrification, but is less commonly observed in practice. While, to the best of our knowledge, the reports devoted exclusively to the investigation of the N isotope fractionation occurring during DNRA are yet not available, broader studies conducted so far have demonstrated that NH_4^+ produced by DNRA has much lower $\delta^{15}\text{N}$ than the substrate NO_3^- , which suggests an ongoing kinetic fractionation (Micheher & Lajtha, 2007).

1.2.2.3. Factors controlling ammonium production/consumption processes and their impact on $\delta^{15}\text{N-NH}_4^+$ variability

The extent of fractionation effect caused by NH_4^+ transformation processes depends on multiple environmental factors (Fig. 3) which, therefore, can substantially influence the observed dynamics of $\delta^{15}\text{N}$ values of NH_4^+ in the subsurface. Among these factors, pH, temperature and size of the substrate pool are the ones most discussed in the available research literature.

The pH parameter defines the intensity of not only microbiological reactions, but also affects the rate of volatilization: it is proved that this process is intensified under the alkaline soil pH (Witter & Lopez-Real, 1988). For this reason, the observed high rates of NH_3 volatilization are associated with the high carbonate content of soils (Bedard-Haughn et al., 2003). For example, in the unconfined High Plains aquifer (USA) NH_3 volatilization was promoted by the calcareous soils of the area (McMahon & Böhlke., 2006). At the same time, the pH values which support the development of DNRA are unclear. Some studies indicated that high rates of DNRA are associated with alkaline conditions, while the other ones revealed the negative correlation between DNRA occurrence and pH parameter (Rütting et al., 2011). As for N mineralization process, it tends to become more intensive with an increase of pH values towards more alkaline range (Curtin et al., 1998, Fu et al., 1987). At $\text{pH} < 7$, NH_4^+ is predominantly sorbed on clay surfaces, and at higher pH values it starts to be sorbed by metal oxides and oxyhydroxides (e.g. FeOOH , MnO_2) (Buss et al., 2004).

The temperature variability can also have an impact on the changes in dynamics of $\delta^{15}\text{N-NH}_4^+$ values. It should be particularly noticed that higher temperatures are also associated with the increasing rate of ongoing NH_3 volatilization, since they stimulate growth and activity of bacteria. Consequently, it can be expected that the isotopic composition of N species exhibits pronounced seasonal patterns (Bedard-Haughn et al., 2003). The optimal temperature range for mineralization is 25 - 40°, for nitrification – 15 - 35° and for anammox – 30 - 40° (Li et. al., 2014; Guntiñas et al., 2012; Shammas, 1986; Jin et al., 2012).

In addition, the extent of observed fractionation effects is assumed to be dependent on the size of the substrate pool (reservoir). Usually, in N-limited systems, fractionation associated with nitrification is comparatively small. For instance, NH_4^+ concentration in groundwater of the Sichuan basin in China (Table 2) were low (and even occasionally below the detection limit (0.05 mg/l)), suggesting minimal isotopic fractionation during nitrification in groundwater (Li et al., 2007).

Finally, it should also be noticed that the relative concentrations of NO_3^- to organic C (C/ NO_3^- ratio) control whether NO_3^- is reduced by denitrification or DNRA. In general, DNRA, which leads to the production of isotopically depleted NH_4^+ , is favored when NO_3^- is limiting, while denitrification is favored when C (electron donor) is limiting (Vidal-Gavilan et al., 2013).

The presented evidence suggests that the variability in the $\delta^{15}\text{N-NH}_4^+$ in groundwater heavily depends both on the type of pollution sources as well as on the dynamics of microbiological and physicochemical processes (Fig.4).

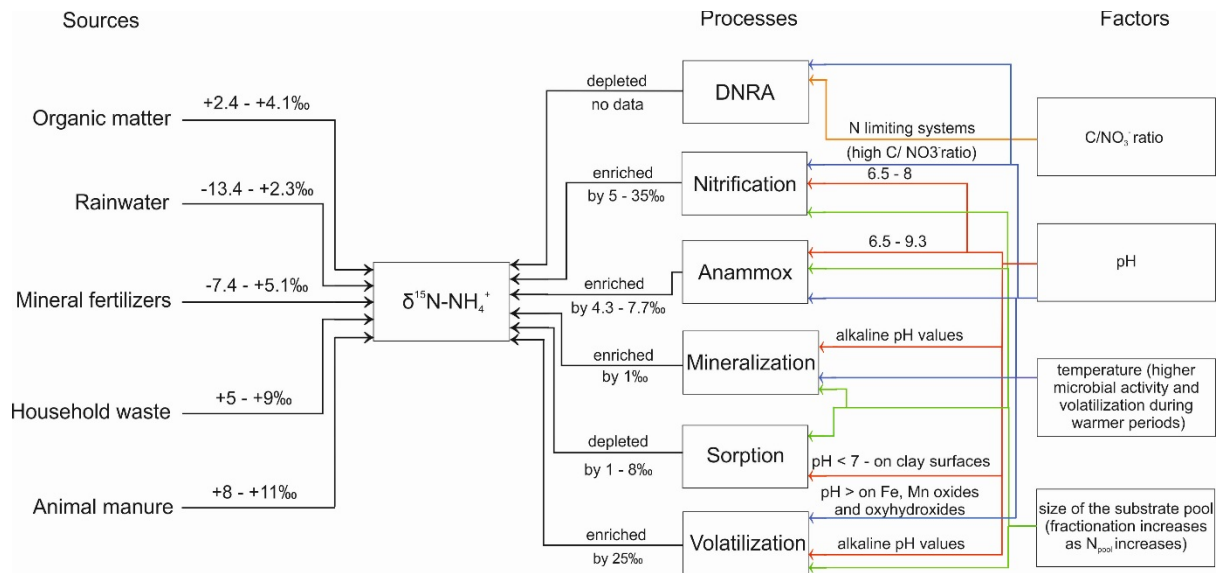


Figure 4. Sources, processes and factors that influence the $\delta^{15}\text{N-NH}_4^+$ values: summary (the following arrows connect processes with factors that have the decisive effect on their dynamics and, consequently, on resulting fractionation effects: \rightarrow C/NO₃⁻ - ratio; \rightarrow pH; \rightarrow temperature; \rightarrow size of the substrate pool).

In general, $\delta^{15}\text{N-NH}_4^+$ values in groundwater are lower and less variable in comparison to $\delta^{15}\text{N-NO}_3^-$, which is probably explained by the high sorption potential of NH_4^+ and its intensive involvement into oxidation processes. Among the pollution sources, animal wastes and household sewage contribute to the highest enrichment of NH_4^+ in groundwater with ^{15}N isotope. As for the processes resulting in isotope fractionation and respective changes in isotopic signatures of groundwater samples, it is revealed that volatilization and nitrification significantly contribute to higher accumulation of ^{15}N in the residual NH_4^+ . However, the extent of fractionation effects due to these processes may depend on the environmental conditions. On the contrary, mineralization and sorption usually show small isotopic effects. Finally, there is still not much evidence available about the quantitative alterations in the isotopic composition of NH_4^+ during DNRA (Micheher & Lajtha, 2007).

1.2.3. Variability of $\delta^{15}\text{N-N}_2\text{O}$ in groundwater

The information about the isotopic composition of $\delta^{15}\text{N-N}_2\text{O}$ in aquifers affected by agricultural activity is also scarce, as in the case of data regarding the natural abundance of $^{15}\text{N-NH}_4^+$. In general, it has been reported that the values of $\delta^{15}\text{N-N}_2\text{O}$ could vary from -55.4‰ to +89.4‰ (Table 3). So the isotopic signatures of N_2O in groundwater samples demonstrate the largest variability among different isotopic compositions of N compounds considered in this review. It appears that such wide range of observed $\delta^{15}\text{N-N}_2\text{O}$ values is related to the fact that the production of N_2O involves many reactions steps (Fig. 4) which presume diverse fractionation effects depending on chemical processes kinetics and heterogeneous conditions of the subsurface environment along the vertical and lateral groundwater flow paths. Evidently, it also reflects the impact of the diversity of isotopic signatures of the initial substrates (e.g., NO_3^- , NH_4^+) and their involvement into microbial processes. In particular, according to previous studies, $\delta^{15}\text{N}$ values of N_2O emitted from fertilized soils are predominantly negative, which is explained by ^{15}N depletion during N_2O production by nitrification and denitrification. At the same time, positive $\delta^{15}\text{N-N}_2\text{O}$ values are likely to be attributed to ongoing N_2O reduction during denitrification (Well et al., 2005). Further discussion of the factors influencing variability of $\delta^{15}\text{N-N}_2\text{O}$ in groundwater will be devoted predominantly to shifting dynamics of various hydrobiogeochemical processes that affect the isotopic composition of N_2O . The isotopic signatures of NO_3^- and NH_4^+ derived from various pollution sources have been described in more detail in the previous sections (namely, sections 1.2.1.1. and 1.2.2.1.).

Table 3. Analysis of N₂O isotopic signatures in groundwater: an overview of case studies
(D – denitrification; s. d. – standard deviation).

Site	$\delta^{15}\text{N}$ (‰)	$\delta^{18}\text{O}$ (‰)	Processes altering the $\delta^{15}\text{N}$ and $\delta^{18}\text{O}$ of N ₂ O	N ₂ O (mg/l)
Fuhrberger Feld aquifer (Lower Saxony, Germany) (Well et al., 2012)	-55.4 – +89.4 (mean -11.0 (s.d. 21.0))	+17.6 – +113.2 (mean 57.5 (s.d. 24.9))	D	0.001 – 3.7 (mean 0.08)
Großenkneten aquifer (Lower Saxony, Germany) (Well et al., 2012)	-40.5 – +11.7 (mean -9.7 (s.d. 11.2))	+32.6 – +87.6 (mean 46.1 (s.d. 13.9))	D	0.005 – 0.2 (mean 0.03)
Northwest German lowland, (Lower Saxony, Germany) (Well et al., 2005)	-41.6 – +86.1	+20.7 – +89.8	D	0.008 – 4.2
shallow groundwater under the lysimeter facility (Japan) (Minamikawa et al., 2011)	-44.7 – -16.8	+39.1 – +49.4	D	-

1.2.3.1. Isotopic effects of nitrous oxide production/consumption and transport processes

The experimental evidence suggests that changes in N₂O isotopic signatures are caused by both physical and microbial processes. It is generally assumed that the enrichment factors of microbial processes tend to be large than those related to physical

processes (Goldberg et al., 2008). Among the bacterial transformations, denitrification, nitrification and nitrifier denitrification are the processes that seem to be the most discussed in the research literature in the context of the isotopic composition of $\delta^{15}\text{N-N}_2\text{O}$ (Jurado et al., 2017, Well et al., 2012, Clough et al., 2005). As for the impact of physical processes, it appears that diffusion frequently might be responsible for the alterations of detected $\delta^{15}\text{N-N}_2\text{O}$ values.

In the denitrification pathway, N_2O is produced as well as consumed during the subsequent reduction of NO_3^- to N_2 ($\text{NO}_3^- \rightarrow \text{NO}_2^- \rightarrow \text{NO} \rightarrow \text{N}_2\text{O} \rightarrow \text{N}_2$). The $\delta^{15}\text{N}$ values of N_2O derived from denitrification depends upon the isotope fractionation during its production and consumption. N_2O originated from the reduction of NO_3^- is typically depleted in ^{15}N in comparison to the initial substrate (NO_3^-). The reduction of N_2O to N_2 results in the enrichment of the residual N_2O . It is reported that the isotope fractionation factors for N during both processes are of comparable order of magnitude (Ueda & Ogura, 1991). If N_2O is accumulated as the intermediate product of steady-state denitrification, it is observed that, its $\delta^{15}\text{N}$ value should become close to the value of the initial substrate NO_3^- . Correspondingly, significant N isotope discrimination between N_2O and NO_3^- in groundwater might suggest that a large portion of N_2O may originate from nitrification (Ueda & Ogura, 1991).

Nitrification, which is also a multistep reaction ($\text{NH}_3 / \text{NH}_4^+ \rightarrow \text{H}_2\text{N-OH} \rightarrow \text{NO}_2^- \rightarrow \text{NO}_3^-$), yields N_2O which is isotopically light in comparison to its precursors. N_2O derived during this process could be produced as a byproduct from the complete or partial direct oxidation of $\text{H}_2\text{N-OH}$ to NO or N_2O (Schmidt et al., 2004).

In addition, at low DO level, N_2O production is likely to proceed via nitrifier denitrification, i.e. NO_2^- reduction to N_2O , which yields isotopic signatures similar to bacterial denitrification (Well et al., 2012). Consequently, these two processes cannot be distinguished using solely the data regarding ^{15}N isotope natural abundance, and additional evidence is necessary (Wells et al., 2016; Zhu et al., 2013).

The isotopic composition of N_2O detected in the groundwater samples can also be significantly influenced by its upward diffusion and volatilization from shallow

groundwater to the atmosphere (Minamikawa et al., 2011). Available experimental data indicate that in the subsoil environment characterized with high diffusivity exchange with atmospheric N₂O may diminish the effects of isotopic fractionations expected from the previously described microbial processes (Goldberg et al., 2008). The rate of occurring diffusion depends mainly on the water content in the subsoil. The higher water content suggests that the time required for N₂O to diffuse from the soil profile to the surface is also increased, since diffusion of N₂O in water is approximately 4 orders of magnitude lower than in air (Clough et al., 2005). In addition, it should be highlighted that the macropores and cracks can also enhance the upward N₂O diffusion (Minamikawa et al., 2011).

To summarize, the research accomplished so far has demonstrated that both nitrification and denitrification processes are responsible for the depletion of ¹⁵N value of N₂O in comparison to its substrates (Toyoda & Yoshida, 2015; Schmidt et al., 2004; Ueda & Ogura, 1991). However, further reduction of N₂O to N₂ during denitrification leads to the enrichment of the remaining N₂O with ¹⁵N (Clark, 2015; Knöller et al., 2011). In comparison to biochemical processes occurring in aquifers, diffusion usually results in less pronounced isotopic effects. However, the distribution of the δ¹⁵N-N₂O values in groundwater cannot be comprehensively analyzed and clearly interpreted without referring to the heterogeneity of environmental factors (Fig. 4) of the studied hydrogeological systems.

1.2.3.2. Factors controlling nitrous oxide production/consumption processes and their impact on δ¹⁵N-N₂O variability

Among the factors controlling the dynamics of N₂O production/consumption processes and resulting variations in δ¹⁵N-N₂O values, the residence time, DO concentration, availability of substrate and pH are typically considered as the most decisive in the literature.

As the concentration of NO₃⁻ within a denitrifying layer diminishes with increasing residence time of groundwater, it appears, that with longer residence time, NO₃⁻ reduction to N₂ is more likely to be complete (provided there is no additional supply

of NO_3^- and a sufficient amount of electron donors), which means that the isotopic compositions of $\delta^{15}\text{N-NO}_3^-$ and $\delta^{15}\text{N-N}_2\text{O}$ become closer. At the same time, the instantaneously produced N_2O is typically depleted with respect to the NO_3^- signature (Well & Flessa, 2005).

The DO concentration significantly impacts the isotopic signatures of N_2O in groundwater, because it determines the type of dominant microbial processes in the aquifer and it also affects the completeness of their reaction steps. In particular, under anaerobic conditions, microbial nitrification is unlikely to occur and denitrification usually prevails under such conditions. In particular, it is reported that denitrification might yield the highest N_2O amounts at intermediate O_2 concentrations (below 3.15 to 4 mg/l) as most denitrifiers are facultative anaerobes (Deurer et al., 2008). That is why it is frequently reported that the NO_3^- consumption, which is associated with the formation of excess N_2 and intermediate accumulation of N_2O , increases with the depth (Well et al., 2012).

In sequential reaction processes, such as denitrification, the supply of the members of the denitrification pathways, i.e., NO_3^- , NO_2^- , NO , N_2O , N_2 , depends on the rate of previous reaction steps, except for NO_3^- which can be introduced to the system from the external sources. The availability of substrate, therefore, seems to have considerable impact on the magnitude of isotopic fractionation occurring during N_2O production/consumption processes. In particular, if NO_3^- supply is high in relation to reduction capacity of the subsurface system, substantial isotope fractionation effect occurs, whereas the effect is low or negligible in the opposite case. Overall, the same fractionation control principle appears to be relevant for the other N species subject to reduction during further stages of denitrification, namely NO_2^- , NO , and N_2O . However, for these species the situation is even more complicated, not only because their respective pool sizes depend on the rates of the previous reactions, but also because some microbes might lack enzymes for some of the reduction steps, which implies that transport within denitrifying species will be a necessary precondition for further reduction in such cases (Well et al., 2005). As a result, the isotopic signature of N_2O as an intermediate is influenced both by the kinetics of its production during NO reduction and consumption

during N₂O reduction to N₂ affected by the availability of reaction substrates on the corresponding transformation steps.

It has been found that pH values below 5.5 seem to promote accumulation of N₂O, most probably because N₂O reductase is mostly inhibited by acid conditions that enable the build-up of N₂O in the subsurface environment (Deurer et al., 2008), and the denitrification process does not proceed to the final step.

Overall, since N₂O is an intermediate product of microbial reactions, its isotopic composition is determined by the rates of previous reactions as well as biological and physicochemical conditions of the aquifer (Fig. 4). It could be summarized that production processes of N₂O (e.g., nitrification, denitrification, etc.) lead to its depletion in the $\delta^{15}\text{N}$ value, whereas consumption processes, such as reduction of N₂O to N₂, enrich it with ¹⁵N. Residence time, DO concentration, substrate availability and pH are important parameters that affect the intensity of N₂O isotope fractionation processes. The large variability of $\delta^{15}\text{N}$ value of N₂O in the groundwater (Table 3) implies that N₂O production and consumption processes in the hydrogeological system occur simultaneously. However, the isotopic fractionation effects of these processes might be diminished by the effects of upward diffusion.

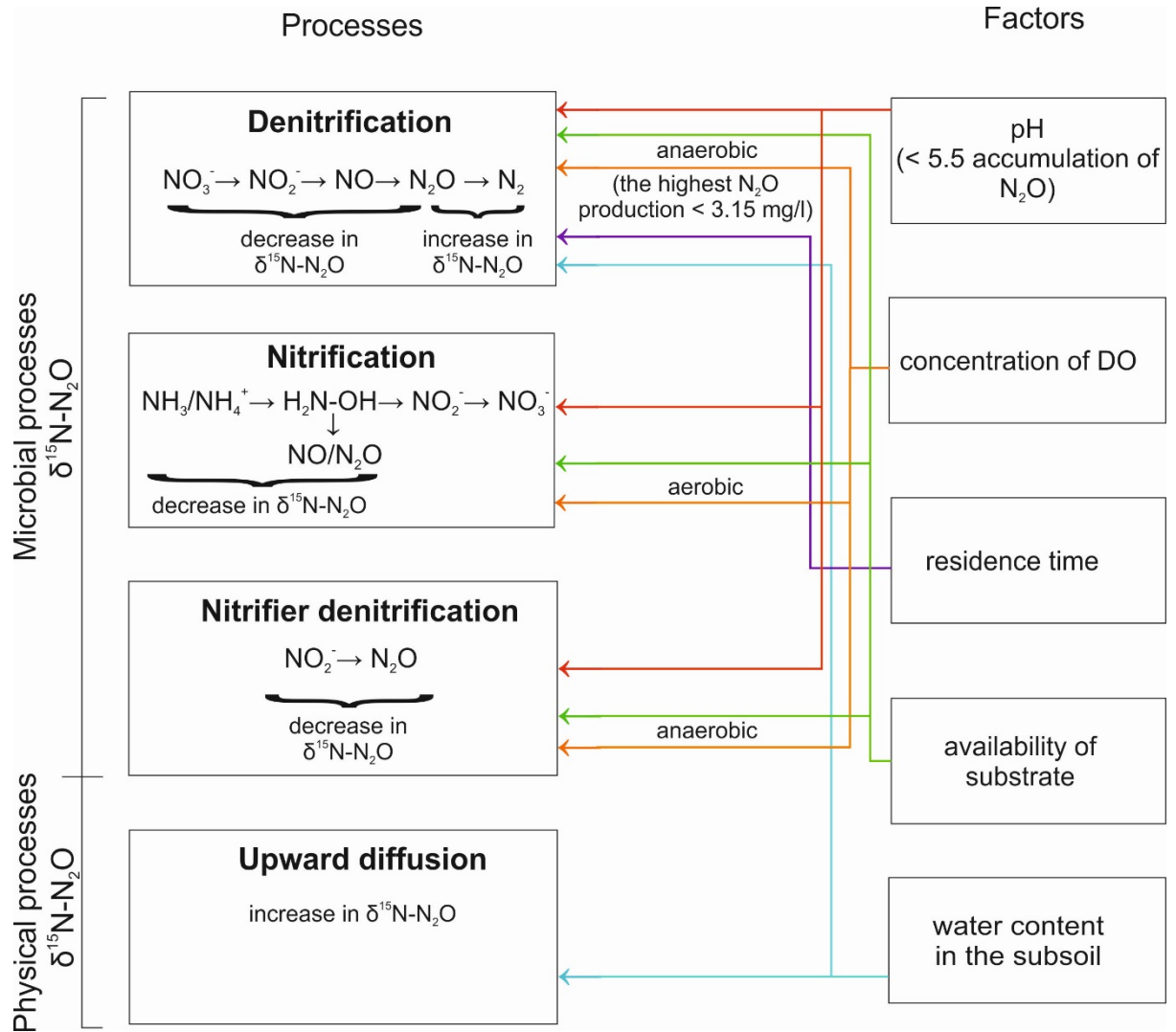


Figure 5. Sources, processes and factors that influence the $\delta^{15}\text{N-N}_2\text{O}$ values: summary (the following arrows connect processes with factors that have decisive effect on their dynamics and, consequently, on resulting fractionation effects: \rightarrow water content in the subsoil; \rightarrow availability of substrate; \rightarrow residence time; \rightarrow concentration of DO; \rightarrow pH).

1.3. Complementary investigations based on other stable isotopes

Measurements and analysis of $\delta^{15}\text{N}$ values in groundwater are commonly complemented with analysis of isotope enrichment values of other isotopes in order to address and constrain the potential ambiguity in the interpretation of $\delta^{15}\text{N}$ variation associated with overlapping of $\delta^{15}\text{N}$ isotopic signatures resulting from different sources

and processes. O, B, C, S, Sr isotopes are among the isotopes most frequently considered for such purpose (Hosono et al. 2015; Well et al., 2012; Lorenzo et al., 2012; Otero et al., 2009; Knöller et al. 2005; Widory et al., 2004, Choi et al., 2003; Böhlke & Horan, 2000). In the following section, discussion will be focused on their application to identification of N transformation processes and potential sources of N pollution, respectively.

1.3.1. Analysis of $\delta^{18}\text{O}$ values of nitrogen species in groundwater

Combined use of the $\delta^{18}\text{O}$ and $\delta^{15}\text{N}$ of NO_3^- may allow better separation of atmospheric and terrestrial NO_3^- sources, including the possible separation of different anthropogenic sources (Xue et al., 2009). In addition, oxygen isotope ratios could be used for distinguishing N_2O originating from nitrification and denitrification (Kendall, 1998). Table 1 (pp. 34 – 37) shows that the isotopic signature of $\delta^{18}\text{O}-\text{NO}_3^-$ in groundwater might vary in the range between -8.1‰ to +48‰, which reflects the variability of NO_3^- sources.

In particular, the isotopic signature $\delta^{18}\text{O}-\text{NO}_3^-$ could help to separate NO_3^- originated from the fertilizers application from NO_3^- inflow originating from other sources which deliver NO_3^- produced by nitrification of NH_4^+ or organic N. It is observed that synthetic NO_3^- fertilizers, which are derived from the atmospheric N_2 , have $\delta^{18}\text{O}$ value close to the atmospheric value of +23.5‰ (Moore et al., 2006). In particular, their isotopic composition of $\delta^{18}\text{O}-\text{NO}_3^-$ might vary from +17‰ to +25‰ (Xue et al., 2009). Meanwhile, NO_3^- from other sources tend to have lighter $\delta^{18}\text{O}$ values because the NO_3^- derived from nitrification processes incorporates only one O atom from dissolved atmospheric O_2 and the other two atoms from water (Kendall & Aravena, 2000). In general, isotopic signature of $\delta^{18}\text{O}-\text{NO}_3^-$ originated from nitrification can be calculated using the following equation (e.g. Hollocher, 1984):

$$\delta^{18}\text{O}_{\text{nitrate}} = 1/3 * \delta^{18}\text{O}_{\text{O}_2} + 2/3 * \delta^{18}\text{O}_{\text{H}_2\text{O}} \quad (8)$$

Nitrification has been associated with the $\delta^{18}\text{O}-\text{NO}_3^-$ values in a range between -2‰ to +6‰ (Liu et al., 2006; Sebilo et al., 2006; Smith et al., 2006) or approximately 0‰ (Böhlke et al., 2006). However, it should be emphasized that the isotopic composition of NO_3^- produced by nitrification depends on a range of factors which might

alter those numbers: 1) H₂O might be enriched in ¹⁸O isotope because of evaporation (Hoefs, 2015; Sharp, 2007), 2) O isotope fractionation during respiration can increase the δ¹⁸O value of soil O₂ in comparison to that of atmospheric O₂ (Mayer et al., 2001), 3) the ratio of O incorporation from H₂O and O₂ is not exactly 2:1 (e.g. more O₂ may be derived from atmospheric O₂ when NH₄⁺ is limiting) (Knöller et al., 2011; Kool et al., 2011), 4) low pH conditions might support the occurrence of another microbial process that consume atmospheric O₂ more intensively than nitrification consequently resulting in suppression of nitrification (Xue et al., 2009; Liu et al., 2006), and 5) oxygen isotope exchange of intermediates (especially NO₂) with ambient water might occur (Granger & Wankel, 2016; Casciotti et al., 2010; Kool et al., 2011).

Oxygen isotopes can also be used to trace denitrification in groundwater, as ¹⁸O and ¹⁵N become concurrently enriched in the remaining NO₃⁻ during bacterial denitrification (Petitta et al., 2009). Several studies reported constant isotope ratios that indicate enrichment of ¹⁵N relative to ¹⁸O as the evidence of denitrification occurrence: 2:1 (Kendall & Aravena, 2000), 1.5:1 (Baily et al., 2011), 2.1:1 (Aravena & Robertson, 1998) and 1.4:1 (Knöller et al., 2011; Mengis et al., 1999). During denitrification, the isotopic signature of the residual δ¹⁸O-NO₃⁻ tends to be enriched by nearly 10‰ or 8 - 18‰ in comparison to the produced N₂O (Clark, 2015; Xue et al., 2009). Therefore, N₂O that is instantaneously produced is depleted in ¹⁸O. According to Cassiotti et al. (2002), the value of δ¹⁸O is also affected by oxygen exchange with water, with the exchange ratio varying across different microbial species (Well et al., 2005).

It is also important to take into account that the isotopic expression of δ¹⁸O-NO₃⁻ in groundwater might be influenced by atmospheric precipitation. Its δ¹⁸O values can vary within an interval between +30 and +70‰ (Choi et al., 2003). Williard et al. (2001) demonstrated a seasonal variation of δ¹⁸O-NO₃⁻ in atmospheric NO₃⁻ deposition. Durka et al. (1994) and Voerkelius (1990) have associated atmospheric NO₃⁻ with values of δ¹⁸O between 52.5‰ and 73.4‰. However, usually such high values of δ¹⁸O are found in groundwater under forest ecosystems that are not undergoing significant anthropogenic impact, and are not typical for the case of arable lands (Böttcher et al., 1990).

In general, it is clear that typical $\delta^{18}\text{O}$ values of NO_3^- originated from nitrification (including $\delta^{18}\text{O}$ values of NO_3^- derived from NH_4^+ in fertilizers and precipitation, NO_3^- derived from soil N and NO_3^- derived from manure and sewage) are lower than that of NO_3^- from precipitation and NO_3^- from application of fertilizers. Denitrification is responsible for the simultaneous enrichment of the remaining NO_3^- with ^{18}O and ^{15}N isotopes which might be traced in accordance to certain constant ratios. Therefore, application of O isotopes analysis along with N isotopes measurement can help to understand better the nature of $\delta^{15}\text{N}$ variability in groundwater.

1.3.2. Boron as a tracer for identification of nitrogen sources

Boron isotopes (i.e., ^{11}B and ^{10}B) have been used to trace sewage contamination in groundwater in a range of studies (Xue et al., 2009). Since the isotopic composition of B is not affected by the denitrification process, it also can be used as an indicator of mixing processes in hydrogeological systems (Widory et al., 2004). For instance, analysis of B isotopes was used for identification of pollution sources in the Arguenon watershed, the “Roussillon” aquifer and the “Ile du Chambon” catchment (Table 1; pp. 34 – 37) in France (Widory et al., 2005).

At the unpolluted sites B originates either from mixing with seawater, or from weathering of sandstones and igneous rocks, or could be found in certain evaporates, such as borax ($\text{Na}_2\text{B}_4\text{O}_5[\text{OH}]_4 \cdot 8\text{H}_2\text{O}$) (Clark, 2015). In such context, natural B concentrations are typically only a few ppb in groundwater. However, they are significantly higher in liquid manure and septic tank effluents.

The isotopic signature of $\delta^{11}\text{B}$ of sewage reported in the literature ranges from -7.7‰ to +12.9‰ (Xue et al., 2009). Widory et al. (2004) distinguished two types of sewage: a high-B/low- NO_3^- /low- $\delta^{11}\text{B}$ type that is derived from washing powders, and a moderate-B/moderate- NO_3^- type with an isotopic signature close to animal manure (probably human excrement).

The $\delta^{11}\text{B}$ value of animal manure covers the interval from +14.5‰ to +42.5‰ (Widory et al., 2005). These values are, generally, higher than the ones reported for fertilizers whose $\delta^{11}\text{B}$ isotopic expression might fluctuate between +8‰ and +17‰.

It should be mentioned that sorption on clay minerals, iron and aluminum oxides along groundwater flow can enrich the residual B in solution with ^{11}B isotope at the pH value above 8, when the anion $\text{B}(\text{OH})_4^-$ becomes important (Clark, 2015). However, Kloppmann et al. (2009) showed that at neutral pH, B transport characterized with predominance of $\text{B}(\text{OH})_3$ is nonfractionating, and could therefore be used as a reliable tracer of source and mixing processes.

Thus, analysis of abundance of B isotopes appears to be useful in identification the sources of N contamination. The combined use of $\delta^{11}\text{B}$ and $\delta^{15}\text{N}$ values along with the data regarding concentrations of the respective compounds can help to distinguish between multiple NO_3^- sources as well as to reveal the occurrence of mixing processes. Nevertheless, during the studies the possibility of the adsorption-desorption interaction with clay and other material should be considered as it might affect B isotopic composition.

1.3.3. Analysis of carbon and sulfur isotopes in groundwater systems

It is a common practice to support the results of studies of N isotope in groundwater, which indicated the occurrence of denitrification, with additional measurement of the $\delta^{13}\text{C-DIC}$ and $\delta^{34}\text{S-SO}_4^{2-}$ values in order to identify which type of denitrification is governing the dynamics of N species (Hosono et al., 2014, Otero et al., 2009, Aravena & Robertson, 1998). This experimental approach could be employed to distinguish between two main denitrification pathways that are observed in aquifers: heterotrophic denitrification, which requires organic C source, and autotrophic denitrification, which uses zero-valent iron, ferrous ions, elemental sulfur or reduced sulfur compounds such as pyrite (FeS_2) as an electron donor (Hosono et al. 2015). While the former one generates CO_2 as one of the reaction products, the later one produces SO_4^{2-} through elemental sulfur or FeS_2 (Rivett et al., 2008).

Heterotrophic denitrification is associated with the decrease in the $\delta^{13}\text{C-DIC}$ and increase in $\delta^{15}\text{N-NO}_3^-$ values. The decrease in $\delta^{13}\text{C-DIC}$ is related to the fact that the organic source of carbon is isotopically more depleted in ^{13}C compared to that of the dissolved inorganic carbon pool (e.g. carbonate, bicarbonate). That is why the $\delta^{13}\text{C}$

values of DIC derived from organic matter are more negative than the values of DIC originated from non-organic sources (Nascimento, 1997). The values of $\delta^{13}\text{C-DIC}$ originated from organic carbon are reported to vary in the range between -29‰ to -25‰ (Aravena & Robertson, 1998). However, in the aquifer these values can be buffered by dissolution of carbonate minerals which have higher isotopic signature of C. For example, Aravena & Robertson attributed the decrease in the $\delta^{13}\text{C-DIC}$ values (from -1.9 to -8.6‰) in the groundwater system to denitrification processes, the occurrence of which was evidenced by substantial rise in $\delta^{15}\text{N-NO}_3^-$ values (from 6.4 to 58.3‰).

Autotrophic denitrification, through FeS_2 oxidation, produces SO_4^{2-} depleted in ^{34}S , since sulfur in sulphide minerals is typically characterized with smaller $\delta^{34}\text{S}$ values in comparison to that of sulfate pools in earth surface environments (Krouse & Grinenko, 1991). For instance, Otero et al. (2009) explained the detected decrease in the $\delta^{34}\text{S-SO}_4^{2-}$ values (from 10 to -20‰) accompanied by the increase in the isotopic signature signals of NO_3^- as the result of progress of autotrophic denitrification in the polluted deep aquifer in eastern Spain. Similar changes of the sulfate-sulfur isotopic composition (from +10 to -10‰) due to the impact of autotrophic denitrification in an aquifer used for drinking water production were reported by Knöller et al. 2005.

While the decline in the $\delta^{13}\text{C-DIC}$ or $\delta^{34}\text{S-SO}_4^{2-}$ values in groundwater is the sign of heterotrophic or autotrophic denitrification, respectively, their increase is usually the evidence of other bacterial processes which typically occur in the anaerobic conditions after denitrification (denitrification \rightarrow sulfate reduction \rightarrow methanogenesis) (Korom, 1992). Studying the limestone aquifer in the eastern England, Moncaster et al. (2000) detected significant enrichment of SO_4^{2-} with ^{34}S (up to +30‰) as a result of sulfate reduction. Hosono et al. (2014) related the enriched isotopic values of $^{13}\text{C-DIC}$ (+8‰) in groundwater under the Kumamoto area (Japan) to the occurrence of methanogenesis. This idea was supported by the fact that high CH_4 concentrations (up to 1 mg/l) were detected at the studied locations.

Therefore, it is obvious that additional analysis of $\delta^{13}\text{C-DIC}$ and $\delta^{34}\text{S-SO}_4^{2-}$ in groundwater can help to identify certain hydrogeochemical processes (denitrification, DNRA, sulfate reduction or methanogenesis) in the aquifers and understand their

intensity. It is especially helpful to include the measurements of these isotopes into experimental studies in the cases when the occurrence of denitrification processes is suspected, since such approach will help not only to differentiate between different types of denitrification pathways, but also reveal other bacterial processes that follow denitrification in groundwater heavily depleted in oxygen.

1.3.4. Strontium isotope as a tracer of mixing processes in subsurface environment

In contrast to N, O, B, C and S isotopes, Sr isotopes are characterized with a low biological and/or geological fractionation which make them effective tracers of transport (mixing) processes in the environment (Vilomet et al., 2001). The $^{87}\text{Sr}/^{86}\text{Sr}$ ratios in groundwater are predetermined by:

- 1) natural sources of Sr (e.g., mineral dissolution or cation exchange in soils and aquifer);
- 2) anthropogenic sources of Sr (e.g., mineral fertilizers or manure) (Widory et al., 2004; Böhlke & Horan, 2000).

During the study of groundwater in the Brittany region (France) Widory et al. (2004) detected that $^{87}\text{Sr}/^{86}\text{Sr}$ ratios of the anthropogenic sources vary from 0.7078 to 0.7145 with the lowest values corresponding to mineral fertilizers and the highest values to animal manure. However, this study showed the difficulties in distinguishing between different types of animal manure, which exhibited overlapping ranges from 0.709 to 0.712. The groundwater of the studied area showed varying $^{87}\text{Sr}/^{86}\text{Sr}$ ratios (from 0.7146 to 0.7196) suggesting the occurrence of mixing between different Sr sources, in particular Sr derived from animal manure and from water-rock interaction.

Böhlke & Horan (2000) examined the relationship between the age of groundwater and the distribution of Sr. It was revealed that higher $^{87}\text{Sr}/^{86}\text{Sr}$ ratios (0.713-0.715) are associated with younger oxic groundwater which is affected by anthropogenic activity, and the lower $^{87}\text{Sr}/^{86}\text{Sr}$ ratios (0.708-0.710) are typical for older suboxic groundwater where Sr is originated from calcareous glauconitic sediments.

To summarize, Sr isotope ratio is the useful parameter for studying mixing processes in the groundwater system, as it helps to determine the behavior of pollutants

from different sources. In general, natural sources of Sr are typically characterized with lower $^{87}\text{Sr}/^{86}\text{Sr}$ ratio compared to anthropogenic ones usually exhibiting higher values of this parameter.

1.4. Conclusions

The versatility of the stable isotope analysis method enables obtaining a comprehensive insight into transport and transformation of NO_3^- , NH_4^+ and N_2O in the subsurface: from the assessment of relative contributions of different N sources into the system (using distinctions between their respective isotopic signals) to the identification of simultaneously occurring N cycle reactions and physicochemical processes affecting the isotopic composition of N species. Such information is especially valuable for sustainable management of groundwater resources in agricultural areas typically characterized with considerable N loadings and frequently exhibiting adverse effects of N pollution.

In order to capture the dynamics of N cycling using stable isotope analyses, it is necessary to understand the ranges and causes of variability of isotopic composition of NO_3^- , NH_4^+ and N_2O in various environmental settings. This chapter summarizes the data regarding the ranges of isotopic compositions of these N species in groundwater under agricultural areas and provides information about the impact of N sources, microbiological/physicochemical processes and environmental factors on the variability of NO_3^- , NH_4^+ , N_2O isotopic signatures. It also discusses the application of additional isotopes techniques, frequently used to support the analysis of $\delta^{15}\text{N}$ values for various N compounds.

According to the reviewed literature, the isotopic signatures of NO_3^- in groundwater are characterized with the following $\delta^{15}\text{N}\text{-NO}_3^-$ isotope ranges: soil organic N – from +3 ‰ to +8 ‰, mineral fertilizers – -8 ‰ to +7 ‰, animal manure or household waste – +5 ‰ to +35 ‰. The NH_4^+ sources are characterized with the following $\delta^{15}\text{N}$ values: organic matter – +2.4 – +4.1‰, rainwater – -13.4 – +2.3‰, mineral fertilizers – -7.4 – +5.1‰, household waste – +5 – +9‰, and animal manure –

+8 – +11‰. The isotopic composition of N₂O is determined by the rates of previous reactions as well as biological and physicochemical conditions of the aquifer.

Moreover, the $\delta^{15}\text{N-NO}_3^-$ values are influenced by fractionation effects caused by denitrification ($\epsilon=5-40\text{‰}$), nitrification ($\epsilon=5-35\text{‰}$) and DNRA (range of ϵ not available in literature). As for the isotopic signature of NH_4^+ , it is also affected by nitrification and DNRA, as well as mineralization ($\epsilon=1\text{‰}$), sorption ($\epsilon=1-8\text{‰}$), anammox ($\epsilon=4.3-7.4\text{‰}$), and volatilization ($\epsilon=25\text{‰}$). $\delta^{15}\text{N-N}_2\text{O}$ values in the groundwater derive from: 1) production processes of N₂O (e.g., nitrification, denitrification, etc.) which lead to its depletion in ¹⁵N, and 2) consumption processes, such as reduction of N₂O to N₂, which enrich it with ¹⁵N. However, it should be emphasized that multiple environmental parameters regulate the extent of fractionation effects caused by the processes mentioned above, so the observed changes in isotopic composition of NO_3^- , NH_4^+ N₂O could vary.

Due to overlapping of the isotopic signatures of N sources and N cycle processes, interpretation of isotopic signatures of collected groundwater samples is not a straightforward process, and is associated with uncertainties. Moreover, the difficulty in interpretation of the results of N isotopes analyses are exacerbated by the lack of experimental data regarding variability of ¹⁵N-NH₄⁺ and ¹⁵N-N₂O. Therefore, further research is required in order to address this issue and consider the isotopic composition of NH_4^+ and N₂O in different hydrogeological contexts. In addition, during interpretation of N isotopic signatures it is important to consider thoroughly the data obtained from hydrogeological, hydrochemical and microbiological studies which might help to elucidate N transformation and transport processes occurring in the hydrogeological systems.

Though such inclusive interpretation requires extensive amount of data, it is crucial to integrate all these insights into a flexible interpretative framework for the studies N transport and transformation processes. This could help to address the limitations of stable isotope analysis method in the complicated study cases characterized with possible occurrence of overlapping isotopic signals from different N sources and simultaneous progress of different multistep reactions with a range of intermediate products in the considered aquifer.

As the analysis of distribution of $\delta^{15}\text{N}$ values observed across the aquifer should rely on precisely determined estimations of signatures of N sources and expected fractionation effects caused by N cycle processes, it is crucial to facilitate the comparative component of the research strategies employing stable isotope analysis. There is a need to systematize the experimental evidence obtained from stable isotope analysis of groundwater samples in different studies exploring the same biogeochemical processes or similar issues.

With further advancements in these areas, stable isotope analysis will allow researchers to capture more precisely the dynamics of N species transformations in the subsurface. Therefore, it will help not only to understand better the processes of attenuation of N pollution in agricultural landscapes, but also to address efficiently the emerging environmental concerns regarding estimation of the indirect effects of anthropogenic impact in such areas. In particular, this approach will yield valuable information for the studies of N_2O production/consumption in subsurface environment and its subsequent emissions on the river-atmosphere interface. Therefore, it will enhance the understanding of N_2O cycle and, correspondingly, of the global N cycle in general.

Chapter 2

This chapter is based on the following publication:

Nikolenko, O., Orban, P., Jurado, A., Morana, C., Jamin, P., Robert, T., Knöller, K., Borges, A., V., Brouyère, S. (2019). Dynamics of greenhouse gases in groundwater: hydrogeological and hydrogeochemical controls. Applied Geochemistry, 105, 31-44. <https://doi.org/10.1016/j.apgeochem.2019.04.009>

2. Dynamics of greenhouse gases in groundwater: hydrogeological and hydrogeochemical controls

2.1. Challenges in the interpretation of N dynamics in aquifers

Due to the rising concern about global climate change, significant research efforts have been devoted to the refinement of the estimates of GHGs budgets (Mosier et al., 1998; Kroeze et al., 2005; Denman et al., 2007; Battin et al., 2009, Syakila & Kroeze et al., 2011, IPCC 2013). Contributing to these research efforts, several studies have persuasively argued that it is essential to better understand and accurately quantify the contribution of groundwater affected by agricultural activities to N₂O, CO₂ and CH₄ emissions at the groundwater – surface water interface (indirect emissions) (Worrall & Lancaster, 2005; Johnson et al., 2008; Minamikawa et al., 2010; Jahangir et al., 2012; Borges et al., 2015; Jurado et al., 2018a).

So far, research studies have been mainly concentrated on: 1) obtaining better insight into the processes and factors that control the dynamics of GHGs (Clough et al., 2007; Koba et al., 2009; Macpherson, G.L., 2009; Well et al., 2012; Bunnell-Young et al., 2017) and 2) calculation of GHGs emissions from aquifers in different ecosystems with contrasting land use and hydrogeochemical conditions (Weymann et al., 2008; Butterbach-Bahl & Well, 2010; Laini et al., 2011; Vilain et al., 2012). While addressing the first question, for instance, von der Heide et al. (2007) examined the influence of land use on GHGs fluxes in the subsurface and compared the contributions of autotrophic and heterotrophic denitrification into resulting N₂O fluxes; Minamikawa et al. (2010) concentrated on the influence of different cropping systems and hydrological regimes; Jahangir et al. (2013) studied the impact of geochemical conditions (DO, Eh, pH, availability of electron donors – DOC or reduced Fe²⁺/S²⁻), hydrological activity and biological factors. While addressing the second question, Hiscock et al. (2003) compared estimates of N₂O emission based on the Intergovernmental Panel on Climate Change (IPCC) methodology and using the hydrogeological data; Jurado et al. (2018b) calculated indirect emission of GHGs from groundwater at the regional scale in Wallonia (Belgium) using the IPCC methodology.

Nevertheless, large uncertainties remain associated with quantification of groundwater fluxes of CO₂, CH₄ and N₂O and it remains a significant source of uncertainty in the global GHGs budgets (Weymann et al., 2008; Minamikawa et al., 2010; Jahangir et al., 2012). Firstly, many studies so far have focused on the GHGs production and consumption in the soil profile and calculated the estimated groundwater GHGs fluxes using the concentrations of these gases in the subsoil (Beaulieu et al., 2011). Secondly, there are difficulties related to the upscaling of point estimates of GHGs concentrations in groundwater to larger scale and longer time periods while taking into account the spatiotemporal variability of their fluxes. For example, Vilain et al. (2012) calculated annual groundwater N₂O flux in the Orgeval catchment (France) extrapolating the data obtained from 3 piezometers, which could be a rough estimate for heterogeneous landscapes considered on the broader scale. It is important to constrain and better understand the scope of uncertainties related to the upscaling procedures. That is why the studies devoted to the distribution and dynamics of GHGs in groundwater should

consider the variability in hydrogeology, hydrogeochemistry and land use across the explored area (Choi et al., 2007; Cooper et al., 2017).

This chapter presents the analysis of experimental data obtained during the regional sampling campaign conducted to improve the understanding how the interplay between hydrogeological and hydrogeochemical controls considered at the catchment scale could influence groundwater contribution into GHG emissions via rivers. It examines the distribution of GHGs in the subsurface in a Cretaceous fractured chalk aquifer extending across the border between Wallonia and Flanders in Eastern Belgium.

The regional study attempts to: 1) explore the variability of GHGs concentration along groundwater flow paths taking into account spatial changes in hydrogeochemical, hydrogeological and land management conditions; 2) identify the sources of N and C loads across the aquifer; 3) reveal the processes that govern the biogeochemistry of GHGs under different environmental settings. The obtained information will help to understand how the GHG fluxes occurring on the groundwater-river interface depend on catchment-scale dynamics of biogeochemical process of their production and consumption.

2.2. General study design

2.2.1. Study site

The studied aquifer is located in Cretaceous chalky geological formations in the eastern part of Belgium. While the southern part of the aquifer is unconfined, the northern part is confined under Tertiary clayey sediments. Subsurface flow is from the South to the North and the aquifer is mainly drained by the Geer river (Goderniaux et al., 2011). Semi-confined conditions may be observed under the Geer alluvial deposits close to the river. The piezometric map for the area (Fig. 6, p. 75) shows that groundwater discharges into the Geer River in its downstream part.

The basis of the aquifer is represented with the layer of smectite clay which is assumed to be of low hydraulic conductivity (Orban, 2010). Below the clay layer, the Houiller formation (sandstones and shales with embedded coal beds) occurs (Boulvain, 2008). The area is characterized with the presence of series of faults causing the fracturing of chalk, among which the major one is the Horion-Hozémont fault.

The aquifer is recharged by infiltration of rainfall through the overlying loess and the residual conglomerate (Orban et al., 2006). The estimated annual recharge rate is between 175 and 275 mm/y. Since the thick loess layer (up to 20 m) and unsaturated chalky zone (up to 15 m) located above the aquifer control its recharge, the resulting water fluxes at the groundwater table are smoothed, and seasonal fluctuations of hydraulic heads are attenuated, which can be more concisely observed on the multiannual scale (Brouyère et al., 2004). The recharge zone of the chalk aquifer mostly corresponds to the hydrological basin of the Geer River – tributary of the Meuse River.

The studied area is predominantly characterized with agricultural land use (nearly 65%). Agricultural activities are the largest source of the nitrate input into groundwater, followed by domestic wastewater effluents (Dautrebande & Sohler, 2004).

The chalk aquifer is one of the most exploited groundwater bodies in the Walloon Region, with about 60,000 m³ groundwater withdrawal per day, which are used, in particular, to satisfy the drinking water needs of the city of Liège and its suburbs (Orban, 2009). Groundwater is abstracted from the aquifer using 45 km of drainage galleries and pumping wells that belong to water supply companies. Groundwater consumers are divided between the following sectors: the public water sector (87%), the industrial sector (12%) and the agriculture and services (1%) (Hérivaux et al., 2013).

2.2.2. Sampling network

The sampling campaign intended to explore the distribution of GHGs within the chalk aquifer. To this end, groundwater samples from 29 wells were collected. The sampling network included existing wells across the aquifer that were selected considering hydrogeological conditions along the main groundwater flow path from the South to the North and taking into account the level of urbanization pressure (Fig. 1 of Annex). Consequently, after exploring the resulting groundwater sampling network and considering the results of previous investigations conducted within the area of the study by Hakoun et al., 2017, the selected wells were grouped into 4 zones taking into account the differences in hydrogeochemistry, hydrogeology and urbanization level (Fig. 6): 1) southern zone – unconfined conditions and the most urbanized land use; 2) central zone –

unconfined conditions and predominantly agricultural activity; 3) north-eastern zone – zone of groundwater recharge to the Geer river and predominantly agricultural land use (though sampling wells were located close to the urban areas); and 4) northern zone – confined conditions and mixed land use pattern. In total, the monitoring network included 9 pumping wells (6 of them located in the confined part of the area), 2 private wells and 18 piezometers (Fig. 6). All these sampling points are screened in the chalk aquifer, at depths varying from 16 meters to 70 meters (mean 39 meters) in the unconfined part of the aquifer in the South, and from 51 meters to 120 meters (mean 80 meters) in the confined part of the aquifer in the North. In addition, three of the sampling locations (Bovenistier, SGB and Overhaem, located in the central and north-eastern zones) are equipped with multilevel piezometers that provided the opportunity to sample groundwater at different depths (Table 5).

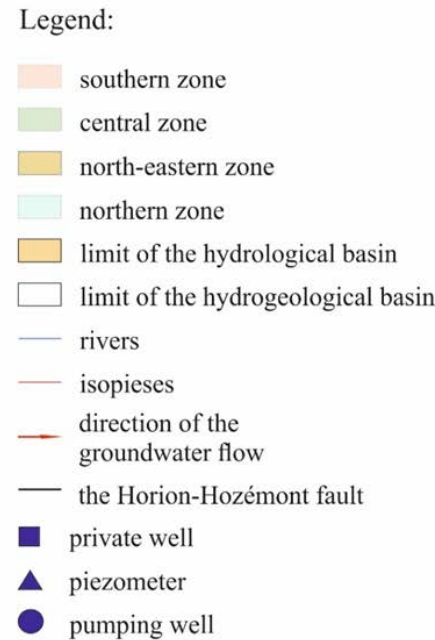
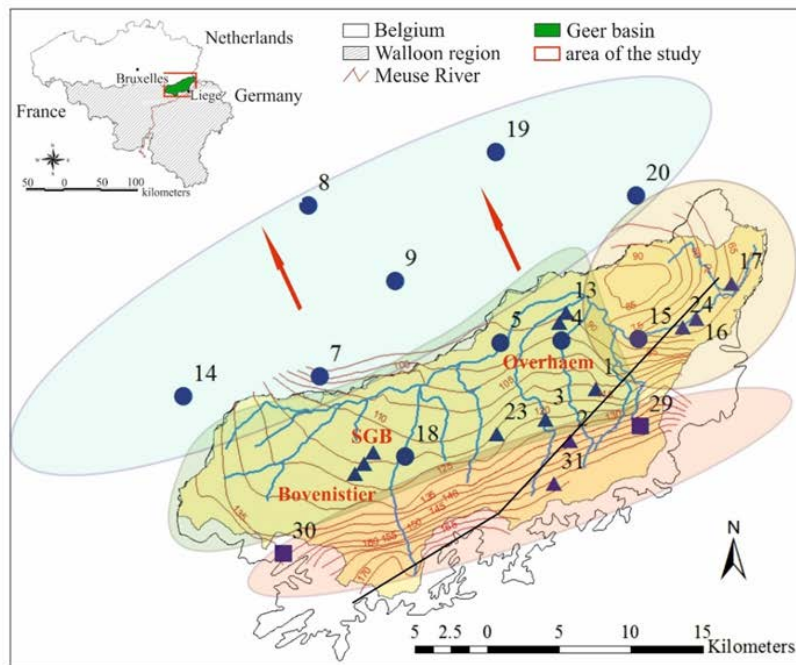


Figure 6. Map of the studied area in the Geer basin showing river network, isopieises, direction of groundwater flow and sampling points (wells and piezometers). Colors indicate different zones used to aggregate data.

2.2.3. Groundwater sampling

Groundwater sampling was accomplished between the 14th and 23rd of August 2017. Before the start of sampling, wells/piezometers were purged until stabilization of field parameters (pH, conductivity, temperature, dissolved oxygen) or by pumping three times the volume of the water present in the wellbore (including gravel pack). The samples collected in the field for the analyses of the GHGs, major and minor ions, dissolved organic carbon (DOC), metals and stable isotopes were put on the ice inside a field refrigerator and transported to the laboratory at the end of the sampling day. In addition, in-situ measurements of pH, electrical conductivity (EC, $\mu\text{S}/\text{cm}$), dissolved oxygen (DO, mg/L) and temperature ($^{\circ}\text{C}$) were conducted using a portable multimeter HQ40d (HACH), with a closed flow cell inside which the measuring probes were immersed.

Groundwater for the analyses of dissolved N_2O and CH_4 was collected into 50 mL borosilicate serum vials (two replicates per location), preserved by addition of 200 μL of saturated HgCl_2 and sealed using a butyl rubber stopper and an aluminum seal. To measure the partial pressure of CO_2 ($p\text{CO}_2$), four polypropylene syringes of 60 ml were filled. The samples for major and minor ions were stored in 180 ml polypropylene bottles preventing the contact with atmospheric oxygen. For estimation of the concentration of DOC, groundwater was filtered through 0.22 μm polyethylenesulfone filters, stored in 40 ml borosilicate vials and poisoned with 100 μl of H_3PO_4 (45%). Groundwater for the analysis of metals was filtered through a 0.45 μm polyethersulfone and microquartz fiber filter into 125 mL polypropylene vials and acidified with 1 ml of 12 N HCl for sample preservation.

Groundwater for ^{15}N and ^{18}O isotopes of N_2O was sampled into 250 mL borosilicate serum bottles (two replicates per location), preserved by addition of 400 μL of saturated HgCl_2 , sealed with a butyl stopper and crimped with an aluminum cap. For ^{15}N and ^{18}O of NO_3^- , the samples were collected into 60 ml polypropylene vials, preceded by filtration of the samples through the 0.22 μm nylon filters. For ^{34}S and ^{18}O isotopes of SO_4^{2-} , 1 L of groundwater was collected into a polyethylene bottle and stabilized with

100 ml of zinc acetate solution (3%). Groundwater samples for ^{11}B isotopes were collected into 60 ml polypropylene bottles.

2.2.4. Analytical methods

The analyses of groundwater samples for major and minor ions were performed at the Hydrogeology Laboratory of the University of Liège (Belgium). The concentrations of major (Na^+ , Mg^{2+} , K^+ , Cl^- , SO_4^{2-} and NO_3^-) and minor ions (NO_2^- and NH_4^+) were analyzed by means of aqueous phase ion chromatography via specific ion exchange resin and a conductivity detector. The concentration of Ca^{2+} and total alkalinity were measured by potentiometric titration in the laboratory.

The concentrations of dissolved N_2O and CH_4 were measured at the Chemical Oceanography Unit of the University of Liège (Belgium) with the headspace equilibration technique (25 ml of N_2 headspace in 50 ml serum bottles) and a gas chromatograph equipped with electron capture and flame ionization detectors (SRI 8610 GC-ECD-FID), as described in detail by Borges et al. (2015). The SRI 8610 GC-ECD-FID was calibrated with $\text{CH}_4:\text{CO}_2:\text{N}_2\text{O}:\text{N}_2$ mixtures (Air Liquide Belgium) of 0.2, 2.0 and 6.0 ppm N_2O and of 1, 10 and 30 ppm CH_4 . The pCO_2 was directly determined in the field using an infra-red gas analyzer (Li-Cor Li-840) by creating a headspace with ambient air in polypropylene syringes (1:1 ratio of water and air). The Li-Cor Li-840 was calibrated with a suite of $\text{CO}_2:\text{N}_2$ mixtures (Air Liquide Belgium) with mixing ratios of 388, 813, 3788 and 8300 ppm CO_2 .

The stable isotope analyses of N_2O were conducted using an off-axis cavity ringdown spectroscopy (OA-ICOS) (Los Gatos Research) instrument for the measurements of $\delta^{15}\text{N}^\alpha$, $\delta^{15}\text{N}^\beta$, $\delta^{18}\text{O}$ of N_2O at the Chemical Oceanography Unit of the University of Liège (Belgium), and the ^{15}N -site preference (SP, in ‰) was calculated as the difference between $\delta^{15}\text{N}^\alpha$ and $\delta^{15}\text{N}^\beta$ ($\delta^{15}\text{N}^\alpha - \delta^{15}\text{N}^\beta$). A 20 ml helium (He) headspace was created in the 250 ml bottles ~24h before the analysis in order to assure equilibration between gas and dissolved N_2O . Prior to the measurement of the headspace samples, the instrument was warmed and conditioned by a flow-through calibration using a standard gas mix of N_2O : synthetic air (4ppm) during ~ 30 min. This gas cylinder had been

calibrated by Tokyo Institute of Technology ($\delta^{15}\text{N}_{\text{AIR}}^{\alpha} = 0.47 \text{ ‰} \pm 0.20 \text{ ‰}$; $\delta^{15}\text{N}_{\text{AIR}}^{\beta} = 1.41 \text{ ‰} \pm 0.26 \text{ ‰}$; $\delta^{18}\text{O}_{\text{vsmow}} = 37.63 \text{ ‰} \pm 0.18 \text{ ‰}$). Headspace samples were injected into a custom-built purge and trap device (He flow : 120 ml min^{-1}) consisting of a CO_2 trap (soda lime), a water trap (magnesium perchlorate) and a stainless steel loop immersed in liquid nitrogen to trap N_2O . 5 min after sample injection, the loop was isolated from the rest of the system by switching the position of 3-way valves (Swagelok), warmed at room temperature, and connected to the instrument to inject the sample. Volume of headspace injection was adapted as function of the N_2O concentration in every sample in order to minimize any concentration-dependent effect (Wassenaar et al., 2018). Data were calibrated against standard gas mix (see above) injection following the approach of Wassenaar et al. (2018) using the purge and trap setup. The utilization of this purge and trap device helped to avoid the possible interference from CO_2 , H_2O (trapped) or CH_4 (flow through the loop) and allowed to minimize difference in gas matrix composition between different types of samples and the standard.

The isotope analyses of NO_3^- and SO_4^{2-} were carried out at the Helmholtz Center for Environmental Research (Department of Catchment Hydrology, Halle, Germany). Nitrogen ($\delta^{15}\text{N}$) and oxygen ($\delta^{18}\text{O}$) isotope analyses of NO_3^- were performed using a G-IRMS (gas isotope ratio mass spectrometer) DELTA V plus connected to a GasBench II from Thermo using the denitrifier method that converts all sampled NO_3^- to N_2O (Sigman et al., 2001; Casciotti et al., 2002). In order to determine the $\delta^{34}\text{S}$ and $\delta^{18}\text{O}$ of SO_4^{2-} , the dissolved SO_4^{2-} in groundwater samples was precipitated as BaSO_4 by adding 0.5M BaCl_2 . The $\delta^{34}\text{S}$ - SO_4^{2-} was measured after converting BaSO_4 to SO_2 using an elemental analyzer (continuous flow flash combustion technique) coupled with a G-IRMS (delta S, ThermoFinnigan, Bremen, Germany). The analysis of $\delta^{18}\text{O}$ - SO_4^{2-} on BaSO_4 was conducted by high temperature pyrolysis at $1450 \text{ }^\circ\text{C}$ in a TC/EA connected to a delta plus XL spectrometer G-IRMS (ThermoFinnigan, Bremen, Germany). The notation was expressed in terms of delta (δ) per mil relative to the international standards for all the stable isotopes (V-SMOW for $\delta^{18}\text{O}$ of NO_3^- , AIR- N_2 for $\delta^{15}\text{N}$ of NO_3^- , V-CDT for $\delta^{34}\text{S}$ of SO_4^{2-} and V-PDB for $\delta^{18}\text{O}$ of SO_4^{2-}). The reproducibility of the samples was $\pm 0.4 \text{ ‰}$ for $\delta^{15}\text{N}$; $\pm 1.6 \text{ ‰}$ for $\delta^{18}\text{O}$ of NO_3^- ; $\pm 0.3 \text{ ‰}$ for $\delta^{34}\text{S}$, and $\pm 0.5 \text{ ‰}$ for $\delta^{18}\text{O}$ of SO_4^{2-} . The isotope results represent the mean value of the true double measurements of each sample.

The concentration and stable isotope composition of DOC were analyzed at the department of Earth and Environmental Sciences of the Katholieke Universiteit Leuven. Samples analysis was carried out with an IO Analytical Aurora 1030W (persulfate oxidation) coupled to a Thermo delta V advantage IRMS as described in Morana et al. (2015). Quantification of DOC concentration and correction of its stable isotope composition was performed against IAEA-CH6 and an internally calibrated sucrose standard ($\delta^{13}\text{C} = -26.99 \text{ ‰} \pm 0.04 \text{ ‰}$). Typical reproducibility for DOC analysis was on the order of $< 5\%$.

2.2.5. Data analysis

2.2.5.1. Descriptive analysis

This study explores the distribution of GHGs concentrations in the subsurface from two perspectives: in lateral and vertical dimensions. While analyzing the lateral distribution, it attempts to demonstrate the variability of GHGs concentrations along the groundwater flow, which helps to reveal factors and processes controlling the distribution of N_2O , CO_2 and CH_4 in groundwater across four spatial zones characterized with contrasting hydrogeological and hydrogeochemical conditions. The analysis focusing on vertical dimension investigates the possible impact of variations in hydrogeochemical conditions with depth on GHGs dynamics. While exploring the distribution of GHGs concentrations in both dimensions, this chapter considers the same set of chemical and isotope parameters used to identify and characterize N and C sources and GHGs production/consumption processes (see sections 2.3.1 (pp. 81 – 83) and 2.3.2 (pp. 83 – 85)). Moreover, during the analysis of groundwater chemistry the concentrations of such major ions as Na^+ , Cl^- and SO_4^{2-} were included alongside with NO_3^- , since they are the most frequently used water pollution/anthropogenic impact indicators (Yakovlev et al., 2015).

2.2.5.2. Statistics

For the purposes of data analysis in course of this study, Kohonen's Self-Organizing Map method (SOM) was applied using the Matlab software (Vesanto et al., 2000). This approach allows projecting multidimensional data on a two-dimensional grid

and capturing complex (nonlinear) relationships between variables (Peters et al., 2007). In this study, it was used to develop maps of individual component planes and identify clusters within the obtained experimental dataset. The visual comparison of derived individual component planes provided an opportunity to reveal the statistical relationships between the analyzed variables, while k-means clustering on SOM allowed exploring the data properties in more detail, as it enables separating the dataset into different groups of similar hydrogeochemical features (Gamble & Babbar-Seben, 2012). Moreover, Pearson correlation and linear regression analyses were carried out with R software.

2.2.5.3. Isotopomer and isotope maps

Isotopomer and isotope mapping approach is used in hydrogeochemical studies to identify sources of N in the aquifer and characterize its subsurface dynamics (Koba et al., 2009; Well et al., 2012; Clagnan et al., 2018; Jurado et al., 2018b). For our study, $\delta^{15}\text{N-NO}_3^-$ (‰) versus $\delta^{18}\text{O-NO}_3^-$ (‰) and $\delta^{15}\text{N-NO}_3^-$ (‰) versus $\delta^{11}\text{B}$ (‰) isotope maps were used in order to distinguish sources of N input to the aquifer. At the same time, $\Delta\delta^{15}\text{NNO}_3^- - \text{N}_2\text{O}$ (‰) versus SP (site preference) (‰) isotopomer map, $\delta^{15}\text{N-N}_2\text{O}$ (‰ v. AIR) versus $\delta^{18}\text{O-N}_2\text{O}$ (‰ v. VSMOW) and $\delta^{34}\text{S-SO}_4^{2-}$ versus $\delta^{18}\text{O-SO}_4^{2-}$ maps were applied in order to identify the N_2O production-consumption processes.

The $\Delta\delta^{15}\text{NNO}_3^- - \text{N}_2\text{O}$ (‰) versus SP (site preference) (‰) isotopomer map was developed taking into account $\Delta\delta^{15}\text{NNO}_3^- - \text{N}_2\text{O}$ ranges for nitrification and denitrification processes proposed by Koba et al. (2009), and references therein, and SP intervals reported by Lewicka-Szczebak et al. (2017), and references therein. The second one, plotting $\Delta\delta^{15}\text{N-N}_2\text{O}$ (‰ v. AIR) versus $\delta^{18}\text{O-N}_2\text{O}$ (‰ v. VSMOW), was created considering $\delta^{18}\text{O-N}_2\text{O}$ nitrification and denitrification ranges provided by Snider et al. (2012), Snider et al. (2013) and Rosamond (2013). The $\delta^{15}\text{N-N}_2\text{O}$ values corresponding to denitrification and nitrification processes were calculated using equations proposed by Zou et al. (2014), assuming that NH_4^+ fertilizers, sewage and manure were the main sources of NO_3^- and NH_4^+ in groundwater (the ranges of the sources were taken from the literature review provided by Nikolenko et al. (2017)):

- 1) bacterial denitrification:

$$\delta^{15}N_{N_2O} = \varepsilon_{NO_3 \rightarrow N_2O} + \delta^{15}N_{NO_3} \quad (9)$$

2) bacterial nitrification:

$$\delta^{15}N_{N_2O} = \varepsilon_{NH_3 \rightarrow N_2O} + \delta^{15}N_{NH_4} \quad (10)$$

The enrichment factors (ε) for these processes were taken from previous pure culture studies: $\varepsilon_{NO_3 \rightarrow N_2O} = -45 \text{ ‰}$ to -10 ‰ (Snider et al., 2009 and references therein) for bacterial denitrification; $\varepsilon_{NH_3 \rightarrow N_2O} = -66 \text{ ‰}$ to -36.8 ‰ (Yoshida, 1988; Sutka et al., 2006; Snider et al., 2009; Li et al., 2014) for bacterial nitrification.

2.3. Variability of hydrogeochemical parameters and isotopes across the chalk aquifer

2.3.1. Lateral dimension

According to the Piper diagram, the majority of collected groundwater samples fell into the range typical for Ca – HCO₃ water type (Fig. 2 of Annex), though several points located in the southern zone corresponded to the Ca – HCO₃ – Cl type. The decrease in EC was observed from the south to the north: $980 \pm 87 \mu\text{S/cm}$ in the southern zone, $803 \pm 87 \mu\text{S/cm}$ in the central zone, $794 \pm 32 \mu\text{S/cm}$ in the north-eastern zone and $717 \pm 97 \mu\text{S/cm}$ in the northern zone. The pH values varied from 6.77 to 7.23 across the aquifer. The concentration of DOC was lower than 2 mg/L at each of the sampled locations. The variability in hydrogeochemical and isotopic composition of groundwater between four spatial zones of the area of study is summarized in Figures 3 to 8 of Annex and Table 4.

Table 4. Hydrogeochemical and isotopic composition (mean value \pm standard deviation) of groundwater in the chalk aquifer across spatial zones (see Fig. 1).

Parameter	Southern zone	Central zone	North-eastern zone	Northern zone
DO (mg/L)	6.3 \pm 2.3	9.4 \pm 0.6	5.9 \pm 2.6	1.5 \pm 2.1
NO ₃ ⁻ (mg/L)	60.7 \pm 8.9	38.8 \pm 8.1	29.1 \pm 9.0	0.2 \pm 0.4
Na ⁺ (mg/L)	30.1 \pm 12.3	12.1 \pm 2.5	14.8 \pm 3.8	11.4 \pm 3.1
Cl ⁻ (mg/L)	73.1 \pm 30.2	51.7 \pm 7.2	44.4 \pm 7.8	15.1 \pm 10.3
SO ₄ ²⁻ (mg/L)	113.9 \pm 45.9	51.7 \pm 17.5	38.5 \pm 6.9	39.4 \pm 27.1
B (μ g/L)	22.3 \pm 17.0	10.7 \pm 3.3	23.3 \pm 6.7	39.8 \pm 18.5
N ₂ O (μ g N/L)	14.6 \pm 3.2	4.9 \pm 1.5	5.2 \pm 2.1	0.07 \pm 0.08
pCO ₂ (ppm)	34032 \pm 9799	24097 \pm 3201	28552 \pm 3327	28662 \pm 4824
CH ₄ (μ g/L)	0.4 \pm 0.5	0.6 \pm 0.8	0.9 \pm 1.6	19.5 \pm 25.8
$\delta^{15}\text{N-N}_2\text{O}$ (‰)	- 14.7 \pm 3.1	- 11.9 \pm 5.6	- 10.2 \pm 5.1	not available
$\delta^{18}\text{O-N}_2\text{O}$ (‰)	+ 38.7 \pm 3.1	+ 36.9 \pm 14.4	+ 31.5 \pm 9.6	not available
$\delta^{15}\text{N-NO}_3^-$ (‰)	+ 6.5 \pm 3.5	+ 5.1 \pm 0.7	+ 6.1 \pm 1.1	not available
$\delta^{18}\text{O-NO}_3^-$ (‰)	+ 2.5 \pm 1.5	+ 0.9 \pm 3.1	-2.4 \pm 3.6	not available
$\delta^{34}\text{S-SO}_4^{2-}$ (‰)	+ 0.6 \pm 0.3	+ 0.3 \pm 0.5	- 1.7 \pm 1.5	-18.1 \pm 6.7
$\delta^{18}\text{O-SO}_4^{2-}$ (‰)	+ 3.3 \pm 2.1	+ 2.2 \pm 0.7	+ 1.9 \pm 1.3	+ 5.7 \pm 3.1
$\delta^{11}\text{B}$ (‰)	+ 28.0 \pm 20.0	+ 10.7 \pm 7.2	+ 15.1 \pm 6.8	+ 9.4 \pm 4.4
$\delta^{13}\text{C-DOC}$ (‰)	- 34.1 \pm 3.4	- 35.5 \pm 3.4	- 36.9 \pm 3.9	- 32 \pm 2.8
$\delta^2\text{H-H}_2\text{O}$ (‰)	- 49.2 \pm 1.4	- 49.4 \pm 0.7	- 50.3 \pm 0.2	- 50.1 \pm 1.6
$\delta^{18}\text{O-H}_2\text{O}$ (‰)	- 7.5 \pm 0.1	- 7.6 \pm 0.1	- 7.7 \pm 0.06	- 7.7 \pm 0.2

In general, the decrease in the concentration of major ions and GHGs was observed from the South to the North along the groundwater flow. The highest concentrations of major ions and dissolved GHGs (except CH₄) were detected in the most urbanized southern zone, and the lowest – in the confined northern zone. In the majority of groundwater samples collected from all three zones located in the unconfined part of the aquifer the concentrations of N₂O exceeded the equilibrium with ambient atmosphere

concentration (0.3 $\mu\text{gN/L}$) (Hasegawa et al., 2000). On the contrary, groundwater from the northern, confined, zone appeared to be undersaturated with respect to N_2O concentration. At the same time, the concentrations of dissolved CH_4 were higher than the equilibrium with ambient atmosphere concentration (0.05 $\mu\text{g/L}$) (Bell et al., 2017) in all of the locations, with the highest concentration detected in the northern zone. The pCO_2 did not vary significantly between the different zones, with groundwater being supersaturated with CO_2 across the whole area of the study (the atmospheric equilibrium of CO_2 is approximately 400 ppm).

Due to the low concentration of NO_3^- and N_2O in the northern zone, it was not possible to measure their isotopic signatures in the samples collected there. At the same time, the data obtained from three other zones showed that the isotopic values of N_2O varied from -18.6‰ to -3.8‰ for $\delta^{15}\text{N}$ and from $+14.7$ to $+42.6\text{‰}$ for $\delta^{18}\text{O}$. As for the isotopic signals of NO_3^- , they covered the interval from $+3.8\text{‰}$ to $+8\text{‰}$ for $\delta^{15}\text{N}$ and from -6.6‰ to $+4.7\text{‰}$. $\delta^{34}\text{S-SO}_4^{2-}$ was characterized with the most negative values in the northern zone, while southern and central zones exhibited values slightly above 0‰ . $\delta^{18}\text{O-SO}_4^{2-}$ did not change significantly between different zones and varied from approximately $+2\text{‰}$ in central and north-eastern zones to $+5.7\text{‰}$ in the northern zone. The highest values of ^{11}B were detected in the southern and north-eastern zones, while the lowest – in the northern zone. $\delta^{13}\text{C-DOC}$ values were similar across all zones, and varied in the interval from -41.8‰ to -28.8‰ . The isotopic signatures of $\delta^2\text{H-H}_2\text{O}$ (‰) and $\delta^{18}\text{O-H}_2\text{O}$ (‰) varied insignificantly between the four zones.

2.3.2. Vertical dimension

The hydrogeochemical conditions in the aquifer might also significantly vary with depth. To evaluate if this variability had an influence on the fate of GHGs in the subsurface, groundwater samples were collected from collocated piezometers screened at different depths at Bovenistier, Overhaem and SGB sites. The data about the hydrogeochemistry and isotopic composition of groundwater along the three vertical profiles are compiled in Table 5.

Table 5. Hydrogeochemical and isotopic composition of groundwater in the chalk aquifer at the Bovenistier, Overhaem and SGB sites (see Fig. 1).

Site	Name	Bovenistier			Overhaem			SGB		
	Piezometer	28	27	26	12	11	10	21	22	25
	Type	<i>shallow</i>	<i>medium</i>	<i>deep</i>	<i>shallow</i>	<i>medium</i>	<i>deep</i>	<i>shallow</i>	<i>medium</i>	<i>deep</i>
	Screen depth (m)	28 – 32	24 – 49	46 – 51	3 – 4	10 – 11	26 – 31	9 – 16	16 – 26	30 – 40
Parameters	EC ($\mu\text{S/cm}$)	955	859	564	1121	1068	909	765	752	665
	pH	7.0	7.01	7.11	7.03	7.15	7.0	7.0	7.08	7.12
	DO (mg/L)	8.8	9.5	1.8	0.3	0.1	1.3	6.1	9.3	8.7
	NO_3^- (mg/L)	60.9	51.3	4.2	23.3	36.9	11.4	43.4	38.1	27.4
	Na^+ (mg/L)	14.8	14.0	6.7	92.5	52.6	21.1	10.9	10.6	8.2
	Cl^- (mg/L)	61.6	56.5	10.5	49.6	48.3	48.2	22.7	45.2	36.8
	SO_4^{2-} (mg/L)	58.1	52.3	17.4	107.6	94.4	88.5	35.9	33.5	21.2
	B ($\mu\text{g/L}$)	11.0	9.7	12.0	21.0	33.0	9.6	20.0	8.6	8.3
	N_2O ($\mu\text{g N/L}$)	8.5	7.4	0.7	8.5	15.1	14.2	9.2	5.1	4.6
	pCO_2 (ppm)	32540	27763	16947	48614	27896	29117	34454	25148	21253
	CH_4 ($\mu\text{g/L}$)	0.09	0.17	0.19	0.21	0.19	0.39	0.59	0.19	0.60
	$\delta^{15}\text{N-N}_2\text{O}$ (‰)	- 13.7	- 15.2	NA	- 20.3	- 29.1	+ 2.0	- 24.9	- 14.5	- 6.2
	$\delta^{18}\text{O-N}_2\text{O}$ (‰)	+ 38.2	+ 32.8	NA	+ 63.1	+ 53.7	+ 50.4	+ 47.7	+ 35.7	+ 36.4
	$\delta^{15}\text{N-NO}_3^-$ (‰)	+ 6.1	+ 5.8	+ 4.5	+ 30.6	+ 10.2	+ 6.9	+ 7.7	+ 4.9	+ 4.8
	$\delta^{18}\text{O-NO}_3^-$ (‰)	- 0.2	+ 1.4	- 0.2	+ 17.4	+ 5.0	+ 4.9	+ 7.5	+ 3.1	+ 4.7
$\delta^{34}\text{S-SO}_4^{2-}$ (‰)	+ 1.2	+ 0.7	- 25.1	+ 2.5	+ 1.4	- 0.4	+ 1.5	+ 0.3	+ 3.0	
$\delta^{18}\text{O-SO}_4^{2-}$ (‰)	+ 2.5	+ 2.6	+ 5.0	+ 5.8	+ 4.6	+ 3.8	+ 5.0	+ 1.7	+ 0.9	
$\delta^{11}\text{B}$ (‰)	+ 12.0	+ 3.4	+ 0.1	+ 9.5	+ 19.0	+ 0.3	+ 29.0	+ 11.0	+ 5.4	

N_2O tended to accumulate in higher quantities in the shallow groundwater at Bovenistier and SGB sites, while at Overhaem its highest concentration was detected in the middle part of the aquifer. For all of the locations the high concentration of N_2O coincided with the high concentration of NO_3^- . The highest N_2O content (14 – 15 $\mu\text{g N/L}$)

was revealed at Overhaem, where high NO_3^- and low level of DO were detected. In all of the cases the amount of dissolved CO_2 was the highest in the shallowest part of the aquifer. In Bovenistier the concentrations of CH_4 were higher in the locations with the lower concentrations of DO, NO_3^- and SO_4^{2-} , which decreased with the depth. At Overhaem the concentration of CH_4 did not change noticeably between different depth intervals. And SGB showed the highest concentrations of CH_4 among the three studied vertical profiles, with its highest values detected at the shallowest and the deepest sampling locations. In general, in all of the groundwater samples collected from the multilevel piezometers the concentration of N_2O , CO_2 and CH_4 exceeded the equilibrium with the ambient atmosphere concentration.

As for the trends in the variation of isotopic signatures of groundwater samples along the vertical profile, no clear tendency comprising all analyzed cases was revealed, which highlights the importance of local-scale variations in the hydrogeochemical conditions and suggests that resulting isotope signatures could be influenced by simultaneous occurrence of various biogeochemical processes at different depth levels (see section 2.5.2 (pp. 99 – 100) for more details). The highest $\delta^{15}\text{N}-\text{NO}_3^-$ isotopic signatures overall were detected in groundwater samples collected from Overhaem, which was also the only site that exhibited the positive value of $\delta^{15}\text{N}-\text{N}_2\text{O}$ (detected in the deepest piezometer). The noticeably negative value of $\delta^{34}\text{S}-\text{SO}_4^{2-}$ was detected in the deepest part of the aquifer in Bovenistier, where the low concentration of N_2O did not allow to measure $\delta^{15}\text{N}-\text{N}_2\text{O}$ and $\delta^{18}\text{O}-\text{N}_2\text{O}$. $\delta^{11}\text{B}$ values increased with depths both at Bovenistier and SGB sites, though this tendency was not confirmed for the Overhaem location.

2.4. Sources of N and C loading across the aquifer

The sources of N within the aquifer were identified by analysis of isotopic signatures data, using the plots of $\delta^{15}\text{N}-\text{NO}_3^-$ versus $\delta^{18}\text{O}-\text{NO}_3^-$, $\delta^{15}\text{N}-\text{NO}_3^-$ versus $\delta^{11}\text{B}$. At the same time, the origin of C loading was determined by analyzing the findings of conducted correlation analyses. Since within the distinguished four spatial zones with contrasting environmental settings the concentration of DOC did not vary significantly, it was expected that there would be no considerable differences regarding the sources of C

compounds in the subsurface across the studied area. Therefore, the following section focuses at first on the analysis of the distribution of N sources across four spatial zones of the studied area, and afterwards considers the results of the correlation analyses elucidating origin of the C compounds in the subsurface.

The NO_3^- and B isotopic signatures of samples collected in the southern zone suggested the presence of several NO_3^- sources, including manure (locations 29 and 30 (see Fig. 6, p.75)) and NH_4^+ fertilizers or soil organic N (point 2) (Fig. 7). In addition, NO_3^- fertilizers might also be considered as the possible primary source of NO_3^- in the groundwater, since once applied they can in part be turned into soil organic N and mobilized as NO_3^- later on due to the consequent ammonification and NH_4^+ oxidation processes. The observed differences in sources of N input could be attributed to the fact that point 2 was located in close proximity to the agricultural areas.

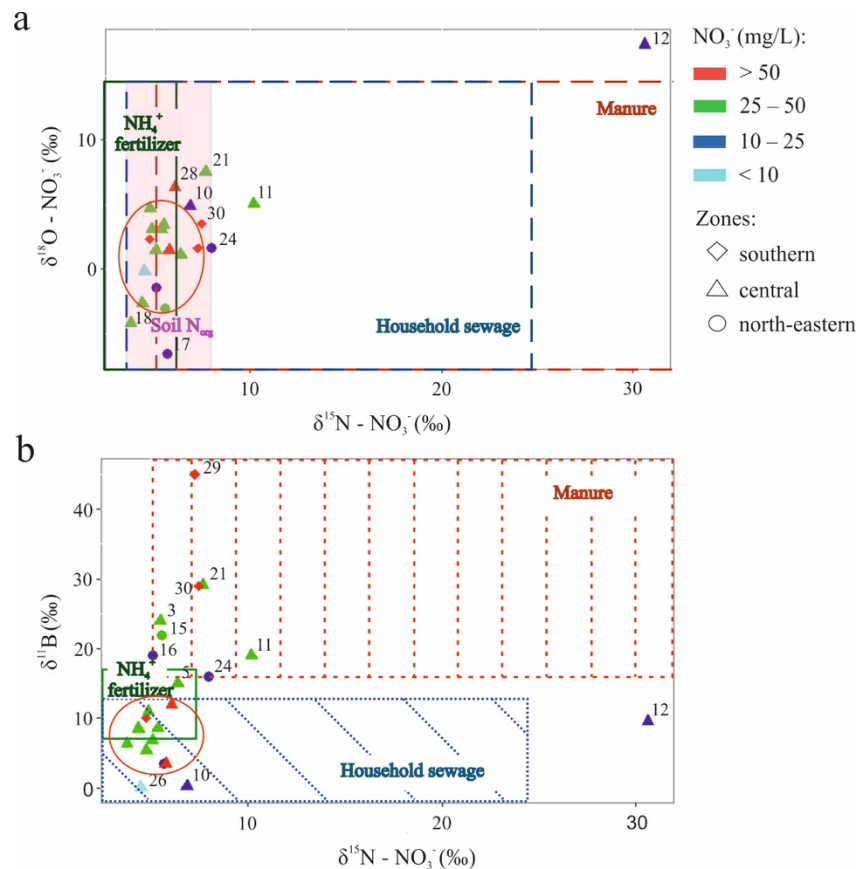


Figure 7. $\delta^{15}\text{N}$ versus $\delta^{18}\text{O}$ values of NO_3^- (a) and $\delta^{15}\text{N} - \text{NO}_3^-$ versus $\delta^{11}\text{B}$ (b) of groundwater samples. The shape of the points shows affiliation to different zones

presented in Fig. 6. Colors indicate different concentrations of NO_3^- in groundwater samples. The isotopic compositions for NO_3^- and B sources are derived from Michener & Lajtha (2008), Xue et al. (2009) and Widory et al. (2004). Areas in the red circles are zoomed and displayed in Fig. 9 of Annex.

In the central zone, NO_3^- and B isotopic signatures were in most cases close to the range typical for NH_4^+ fertilizers. According to the data, sewage did not seem to be a dominant N source, except, likely, at Bovenistier location (points 26 and 27). Isotopic signal for manure was detected at point 3. Groundwater samples collected from multilevel piezometers at Overhaem (10, 11 and 12) and SGB (21 and 25) exhibited the values which showed the simultaneous presence of two pollution sources: manure and sewage.

NO_3^- and B isotopic signatures of groundwater samples collected in the north-eastern zone suggested the presence of different types of pollution sources, namely manure (points 16, 15 and 24) and sewage (point 17).

As for the northern, confined zone of the aquifer, the concentrations of N compounds detected there were too low for analysis of N isotope composition and identification of pollution sources.

Pearson correlation *analysis* (Fig. 10 of Annex) indicated that carbonate minerals and organic matter were the principal sources of C compounds loading to subsurface system occurring across the area of study. In particular, the significant positive correlation between CO_2 and N_2O ($r = 0.446$, $p < 0.05$), CO_2 and Ca^{2+} ($r = 0.473$, $p < 0.05$), Ca^{2+} and NO_3^- ($r = 0.707$, $p < 0.05$), Ca^{2+} and N_2O ($r = 0.721$, $p < 0.05$) indicated the link between concentrations of the inorganic C and N compounds, which suggested the ongoing dissolution of carbonates following water acidification due to the production of protons during nitrification or bacterial respiration activities (Laini et al., 2011; Fitts, 2002). Though the correlation between CO_2 and DOC was non-significant ($r = 0.353$, $p > 0.05$), the strong negative correlation which was observed between the $\delta^{13}\text{C}$ -DOC and DOC ($r = -0.42$, $p < 0.05$) showed that the decomposition of organic matter occurs.

In general, the results of the isotope analyses indicated clear difference in the origin of NO_3^- , B and SO_4^{2-} between the northern zone, corresponding to the confined part of the aquifer, and three other zones, located in the unconfined part of the aquifer. Among the zones which belong to the unconfined part of the aquifer, it was the southern and north-eastern zones, which demonstrated NO_3^- and B isotopic signatures associated with manure, which might have originated as the sewage from the residential areas or leakage from septic tanks. In the central zone, NO_3^- was likely derived in the vast majority of cases from mineral fertilizers. In addition, NO_3^- might have also partly originated from NH_4^+ derived from soil mineralization processes, though the isotope signal of this source was muted by other large pollution sources. As for the sources of C in the subsurface, it was most likely derived partly from the dissolution of carbonate minerals, and partly from decomposition of organic matter.

2.5. Biogeochemistry of nitrous oxide, methane and carbon dioxide along lateral and vertical dimensions of the aquifer

2.5.1. Lateral dimension

2.5.1.1. N_2O production/consumption processes

In order to understand which processes govern the dynamics of N_2O production and consumption processes in the chalk aquifer, the experimental data were interpreted using correlation analysis along with linear regression analysis, results of examination of $\delta^{34}\text{S}\text{-SO}_4^{2-}$ versus $\delta^{18}\text{O}\text{-SO}_4^{2-}$ plot, self-organizing maps (SOMs), isotope and isotopomer maps.

The correlation analysis and linear regression were applied to the subset of data representing the sampling locations in the unconfined part of the studied aquifer (the southern, central and north-eastern zone) in order to identify the dominant processes of N production/consumption occurring in this area.

Pearson correlation analysis (Fig. 8, p. 90) revealed high positive correlation between SP and $\delta^{18}\text{O}\text{-N}_2\text{O}$ ($r = 0.7$, $p < 0.05$), while linear regression indicated positive dependency with the slope of 0.3 between these variables, which according to Ostrom et

al. (2007) (and references therein) should suggest the occurrence of incomplete denitrification in the aquifer (while the slopes close to 2.2 indicate the occurrence of N₂O reduction in the absence of N₂O production). However, the absence of correlation between $\delta^{15}\text{N-NO}_3^-$ and NO_3^- ($r = 0.25$, $p > 0.05$) and relationship between $\delta^{15}\text{N-NO}_3^-$ and $\delta^{18}\text{O-NO}_3^-$ ($Y = 5.557 + 0.1212X$, $R^2 = 0.105$) does not support the hypothesis about ongoing denitrification, because this process should lead to a strong negative correlation between $\delta^{15}\text{N-NO}_3^-$ and NO_3^- , and a slope of regression between $\delta^{15}\text{N-NO}_3^-$ and $\delta^{18}\text{O-NO}_3^-$ ranging from 0.5 to 0.8 (Aelion et al., 2009; Minet et al., 2017). Pearson analysis also indicated strong positive correlation between the concentrations of NO_3^- and N_2O ($r = 0.8$, $p < 0.5$) and between SP and N_2O ($r = 0.6$, $p < 0.05$), which also does not support the occurrence of denitrification (Ostrom et al., 2007; Jurado et al., 2017), but rather indicate ongoing nitrification. Moreover, groundwater chemistry data from the unconfined part of the aquifer demonstrated that aerobic conditions prevail across the area of study (see section 2.3.1 (pp. 81 – 83)), which also supports the idea regarding occurrence of nitrification, and inhibition of denitrification. According to Wankel et al. (2006) and McMahon and Bohlke (2006), the occurrence of nitrification can be evidenced by the existence of correlation between $\delta^{18}\text{O-NO}_3^-$ and $\delta^{18}\text{O-H}_2\text{O}$, while the absence of correlation, on the contrary, suggests ongoing denitrification. Nevertheless, as shown in Fig. 8, there was no correlation between $\delta^{18}\text{O-NO}_3^-$ and $\delta^{18}\text{O-H}_2\text{O}$ ($r = 0.1$, $p > 0.05$). Moreover, the average theoretical $\delta^{18}\text{O-NO}_3^-$ nitrification values defined from the following equation (Aelion et al., 2009):

$$\delta^{18}\text{O-NO}_3^- = 2/3(\delta^{18}\text{O-H}_2\text{O}) + 1/3(\delta^{18}\text{O-O}_2) \quad (11)$$

for the three unconfined zones of the studied aquifer (2.8 for the southern and central zones, and 2.7 for the north-eastern zone) were different from the obtained results of $\delta^{18}\text{O-NO}_3^-$ analyses (2.5 for the southern zone, 1 for the central zone and -2.4 for the north-eastern zone). However, it should be emphasized that the above equation is just a rough estimate, since isotope exchange of intermediates with water messes up the O-isotope signature (Casciotti et al., 2010).

Such mixed evidence regarding the ongoing N₂O production/consumption processes, obtained from the application of statistical analysis to the data describing

unconfined part of the aquifer, suggests that the occurrence and intensity of these processes vary throughout the aquifer across the zones with different environmental conditions.

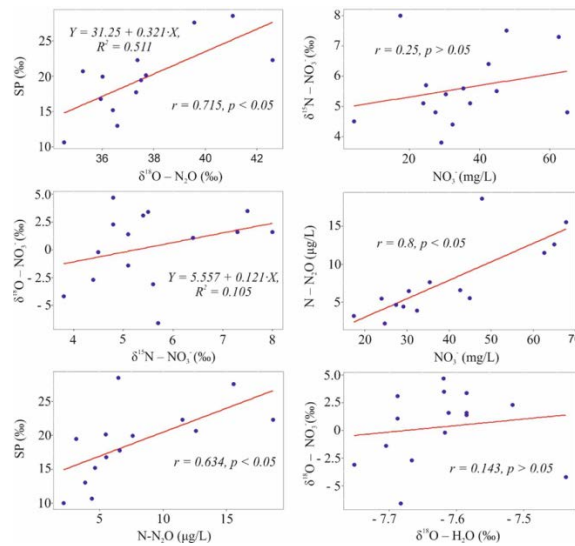


Figure 8. The results of Pearson correlation and linear regression analyses for the subset of data representing the unconfined part of the aquifer.

The values of $\delta^{34}\text{S}-\text{SO}_4^{2-}$ versus $\delta^{18}\text{O}-\text{SO}_4^{2-}$ isotopic signals were examined, since SO_4^{2-} isotope measurements are a unique tool allowing revealing the connection between denitrification and sulphide oxidation during autotrophic denitrification (Mayer, 2005). Fig. 9 shows the overlap between mineralization of organic matter and oxidation of sulphides processes in all three zones located in the unconfined part of the aquifer. However, exceptions from this trend were detected for two points in Overhaem (12 and 13), which fell into the range typical for anthropogenic sources, and one point in Bovenistier (26), which showed the values typical for sulphide oxidation. Samples from the northern zone showed SO_4^{2-} isotope values reflecting sulphide oxidation (points 7 and 9). So, the dominant process of SO_4^{2-} and, consequently, N transformation in three unconfined zones cannot be clearly identified.

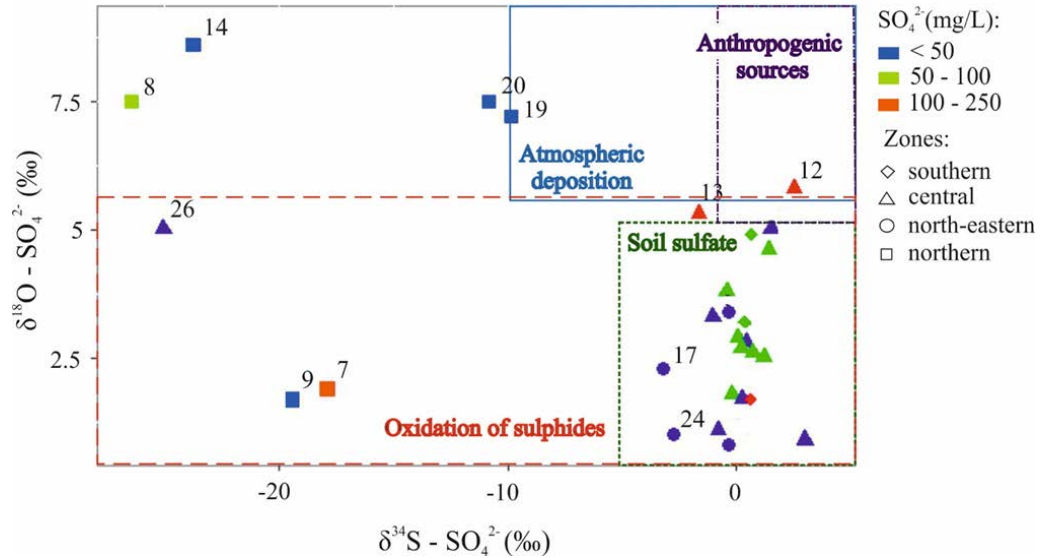


Figure 9. $\delta^{34}\text{S}$ versus $\delta^{18}\text{O}$ values of SO_4^{2-} for groundwater samples. The shape of the points shows affiliation to different zones presented in Fig. 6. Colors indicate different concentrations of SO_4^{2-} in groundwater samples. The isotopic compositions for the SO_4^{2-} sources are derived from Krouse & Mayer (2000), Mayer (2005) and Knöller et al. (2005).

Previous conclusions are supported by the examination of the component matrices resulting from the SOM application to the dataset (Fig. 10). Visual inspection reveals clear positive correlation between concentrations of Fe, Mn and CH_4 , which are negatively correlated with DO, thus indicating variations in oxido-reduction conditions across the aquifer. Results also show similar distribution patterns for N_2O and NO_3^- , suggesting nitrification as the production mechanism of N_2O in groundwater (Hiscock et al., 2003; Koba et al., 2009; Minamikawa et al., 2011). However, there is no clear relationship between N_2O and DO, which does not allow claiming that nitrification is the only production pathway for N_2O . A positive correlation is also observed between SP and $\delta^{18}\text{O}\text{-N}_2\text{O}$, which suggests the occurrence of denitrification (as N_2O reduction proceeds), which leads to the simultaneous increase of both parameters (Well et al., 2005; Well et al., 2012).

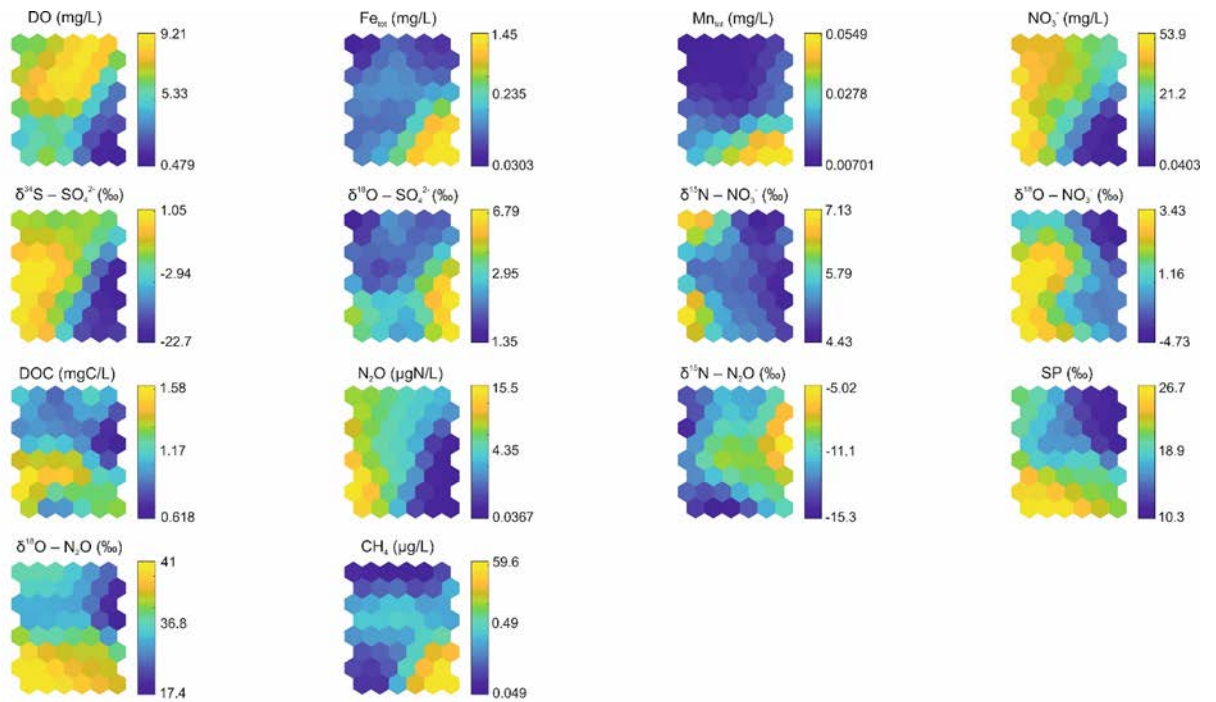


Figure 10. The component matrices derived from the application of SOM procedure.

This evidence suggests that N_2O production throughout the chalk aquifer could not be attributed unequivocally to one pathway, as none of them seems to be omnipresent and clearly dominant across the whole area under consideration. Therefore, it appears that intensity of N_2O production/consumption processes might vary spatially both in lateral and vertical dimensions (i.e. the simultaneous occurrence of nitrification in the shallower part of the aquifer and denitrification in its deeper part).

In order to obtain better understanding into the spatial variability of subsurface processes, the clustering of the dataset was conducted by means of SOM, and the isotope signatures of samples belonging to various clusters were analyzed using isotopomer maps in order to consider the probable occurrence of denitrification and nitrification.

Fig. 11 shows four different groups obtained by application of k-means clustering on SOM. The dark blue (Group 1), green (Group 2) and blue (Group 3) groups include all of the groundwater samples collected from the unconfined part of the aquifer, while yellow group (Group 4) covers all of the studied points from the northern confined zone.

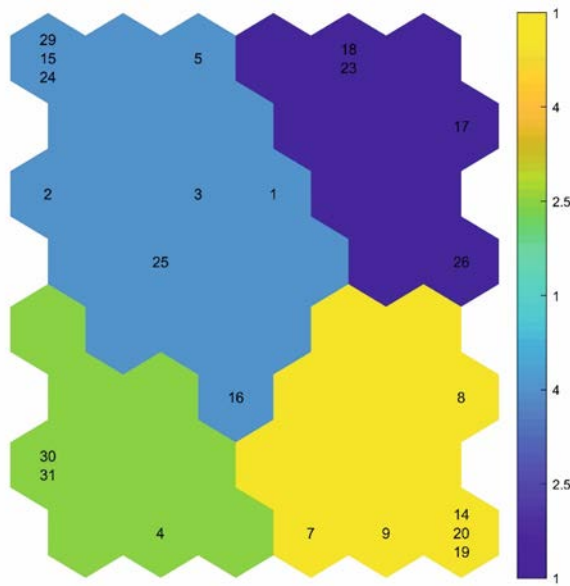


Figure 11. Clustering of the groundwater samples using SOM algorithm. Group 1 – dark blue, group 2 – green, group 3 – blue and group 4 – yellow. The numbers of sampled locations are presented within each of the group.

Group 1 includes locations in the unconfined zone which are characterized with the lowest SP (mean $11.2 \text{ ‰} \pm 1.6 \text{ ‰}$), the lowest concentration of dissolved N_2O (mean $3.5 \text{ ‰} \pm 1.2 \text{ ‰}$), high DO level (mean $8.2 \text{ mg/L} \pm 1.9 \text{ mg/L}$) and low NO_3^- (mean $28.7 \text{ mg/L} \pm 3.8 \text{ mg/L}$). Group 2 corresponds to the highest SP (mean $26.1 \text{ ‰} \pm 3.4 \text{ ‰}$), the highest concentration of N_2O (mean $13.6 \text{ ‰} \pm 6.3 \text{ ‰}$), the lowest amount of DO (mean $5.7 \text{ mg/L} \pm 2.4 \text{ mg/L}$) and the highest concentration of NO_3^- (mean $48.7 \text{ mg/L} \pm 18.7 \text{ mg/L}$). Group 3 demonstrates intermediate values of these parameters (see Table 6). Finally, Group 4 shows characteristic values for groundwater from the confined part of the aquifer, namely lowest concentrations of NO_3^- and DO (see section 2.3.1 (pp. 81 – 83) and Table 6).

Table 6. Mean hydrogeochemical parameters of the groundwater samples clusters produced by k-means clustering on SOM.

<i>Group</i>	N_2O (μg N/L)	<i>SP</i> (‰)	<i>DO</i> (mg/L)	NO_3^- (mg/L)	<i>Processes</i>
<i>Group 1</i>	3.4 ± 1.2	11.2 ± 1.6	8.2 ± 1.9	28.7 ± 3.8	nitrification and incomplete denitrification
<i>Group 2</i>	13.6 ± 6.3	26.1 ± 3.4	5.7 ± 2.4	48.7 ± 18.7	nitrification and complete denitrification
<i>Group 3</i>	6.7 ± 3.4	19.1 ± 6.7	7.2 ± 2.6	39.6 ± 16.2	nitrification and incomplete denitrification
<i>Group 4</i>	0.1 ± 0.1	not available	1.5 ± 2.1	0.2 ± 0.4	complete denitrification

The majority of SP values are lower than typical SP for hydroxylamine (NH₂OH) oxidation (nitrification) reported in previous studies. These data could support the hypothesis about the occurrence of both denitrification and nitrification processes with the following mixing of deep denitrified and shallow nitrified groundwater (which leads to the decrease in SP values produced by nitrification). To test this hypothesis, two isotopomer maps for the area of study (Fig. 12 and 13) were developed.

From the $\Delta\delta^{15}NNO_3^- - N_2O$ (‰) versus SP (‰) isotopomer map (Fig. 12), it can be concluded that the majority of data points representing the isotopic signatures of respective samples in the southern, central and north-eastern zones fall into the mixing zone between nitrification and denitrification processes. Groundwater samples from Group 1 (points 17, 23 and 18) seem to be affected the most by denitrification in comparison to other samples, which is illustrated by their closer location to the denitrification box. However, in this group the denitrification in the deeper part of the aquifer was not complete, since Group 1 was characterized with the lowest SP, and the N₂O reduction to N₂ produces SP values close to the ones caused by nitrification (Well et al., 2012). This hypothesis is also supported by the fact that the corresponding groundwater samples show high DO concentration (see Table 4, p. 82), which would not be possible if mixing with anoxic waters (< 4 mg/L) occurred.

The isotopic signatures of Group 2 (sampling points 30, 31 and 4) indicate mixing between nitrified groundwater and deep groundwater where complete denitrification occurred. The intensive denitrification processes are evidenced by the fact that all points fall outside the mixing zone (Fig. 12) and are shifted in the direction corresponding to typical N_2O reduction. In addition, the lowest DO concentration was observed in this group.

In Group 3 (see Fig. 12), all samples are slightly shifted to the right of the mixing zone, suggesting mixing between nitrified and reduced groundwater. However, compared to Group 2, N_2O reduction processes are probably less pronounced because of the high DO concentrations observed for groundwater samples from Group 3.

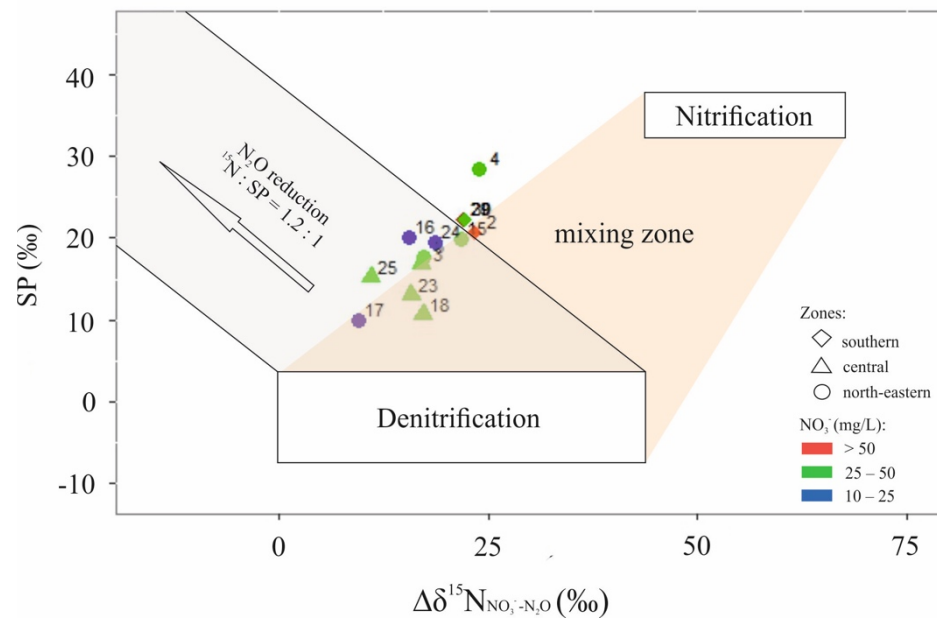


Figure 12. $\Delta\delta^{15}N_{NO_3^- - N_2O}$ versus SP (‰) isotopomer map. The shape of the points shows affiliation to different zones presented in Fig. 6. Colors indicate different concentrations of NO_3^- in groundwater samples.

The second, $\Delta\delta^{15}N - N_2O$ (‰ v. AIR) versus $\delta^{18}O - N_2O$ (‰ v. VSMOW) (Fig. 13), isotope map provides further evidence supporting the hypothesis that groundwater from the unconfined part of the aquifer is affected by both nitrification and denitrification processes. The majority of the samples fall close to the $\delta^{18}O - N_2O$ value of +35 ‰,

reported to be the boundary value between nitrification and denitrification processes (Koba et al., 2009; Li et al., 2014).

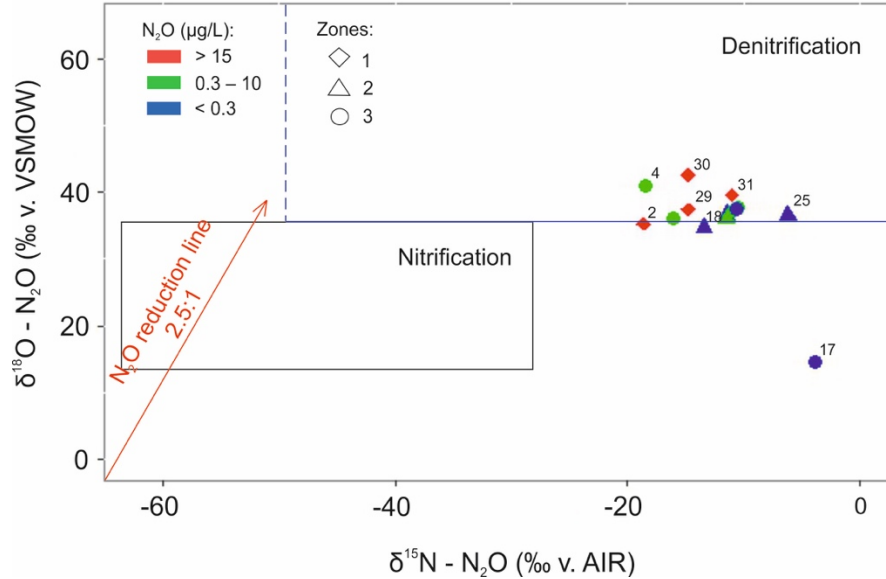


Figure 13. $\Delta\delta^{15}\text{N} - \text{N}_2\text{O}$ (‰ v. AIR) versus $\delta^{18}\text{O} - \text{N}_2\text{O}$ (‰ v. VSMOW) isotopomer map. The shape of the points shows affiliation to different zones presented in Fig. 6. Colors indicate different concentrations of NO_3^- in groundwater samples.

Finally, in the northern zone, considering the low concentrations of DO and DOC as well as the data obtained from SO_4^{2-} isotope analysis (Fig. 9), the occurrence of N_2O could possibly be attributed to autotrophic (points 9 and 7) or heterotrophic (points 8, 14, 19 and 20) denitrification.

2.5.1.2. CH_4 production/consumption processes

The chalk aquifer was characterized with high level of CH_4 accumulation despite the fact that there were detected high concentrations of DO, NO_3^- and SO_4^{2-} in the unconfined part of the aquifer, and the high concentration of SO_4^{2-} in the confined part of the aquifer (except point 14; Fig. 8 of Annex), which prohibits CH_4 production.

In the northern confined zone, characterized with low concentration of DO and negligible content of NO_3^- , the concentration of CH_4 was fifteen times higher in

comparison to three other zones. At the same time, the concentration of SO_4^{2-} , which varied from 15 mg/L to 90 mg/L within the confined area, might have prohibited CH_4 production that usually occurs under lower SO_4^{2-} concentrations (< 19 mg/L) (Whiticar, 1999, Molofsky et al., 2016). Whiticar (1999) claimed that methanogenesis using non-competitive substances (e.g. methylated amines or dimethyl sulphide) might occur in the media where SO_4^{2-} exists; however, their relative importance in CH_4 production is currently uncertain. Therefore, the high values are more likely to be explained by its thermogenic origin or presence of anaerobic microsites with favorable conditions within the aquifer.

The concentration of CH_4 in the groundwater samples from southern, central and north-eastern zones could be explained by occurrence of methanogenesis in the deeper part of the aquifer with the following mixing of deep CH_4 -enriched and shallow oxic water, which happened during the pumping activities. Moreover, the origin of CH_4 in the deeper part of the aquifer might be related to its upward migration via geological faults and fracture networks from the Houiller formations enriched in coal. This last assumption could be supported by previous investigations conducted by the Hydrogeology and Environmental Geology group of the University of Liege in 2015 which showed high accumulation of radon (28945 Bq/m^3) in the deepest part of the aquifer at Bovenistier which might be the evidence of its origin from the underlying layers. Consequently, this observation suggests the possibility of gases diffusion through the smectite clay layer which was previously considered impermeable.

In general, additional investigations are required in order to obtain better insight into the CH_4 production pathways. It will be useful to obtain data about the isotopic composition of CH_4 , $\delta^{13}\text{C-DIC}$ and microbiological community, which have been used in many studies for the identification of CH_4 origin (Teh et al., 2005; Molofsky et al., 2013; McPhillips et al., 2014; Currell et al., 2017; Iverach et al., 2017).

2.5.1.3. CO_2 production/consumption processes

Groundwater in the chalk aquifer demonstrated a tendency towards accumulation of CO_2 . It is possible to suggest four pathways of the CO_2 production in the subsurface,

namely – rhizomicrobial and root respiration, microbial decomposition of soil organic matter, denitrification and, possibly, methane generation (Kuzyakov & Larionova, 2005).

First two processes lead to the production of CO₂ in the soil and its leaching into the groundwater during the rainy periods. The occurrence of microbial decomposition was evidenced by the data obtained from SO₄²⁻ isotope analysis and parameters of water chemistry. In particular, the observed SO₄²⁻ isotope signals indicated the occurrence of mineralization processes in the subsurface, which under aerobic conditions produce SO₄²⁻ and DOC (Mayer et al., 1995; Kellman & Hillaire-Marcel, 2003). However, according to the experimental data, the studied aquifer was characterized with low concentration of DOC in groundwater, which could be the consequence of its further oxidation to CO₂ in the unsaturated or saturated zones (MacQuarrie et al., 2001). The assumption regarding occurrence of DOC decomposition was also supported by the obtained strong negative correlation between the concentration of DOC and δ¹³C-DOC.

Since it was revealed that the aquifer was characterized with suitable conditions for the occurrence of denitrification and methanogenesis processes in its deeper anoxic part, their contribution to the CO₂ production could also be considered.

However, as our study was conducted in the chalk aquifer, the amount of dissolved CO₂ in the groundwater is strongly influenced by the calcium carbonate equilibrium. CO₂, produced within or leaked to the aquifer, reacts with H₂O to form H₂CO₃, a weak acid, which stimulates the dissolution of carbonate rocks. That is why, the initially produced concentration of CO₂ will be altered by equilibration processes. In particular, saturation indexes (Text 1 of Annex) varied from 0.22 to – 0.18 (mean 0.05 ± 0.08) for calcite and from –1.25 to –0.21 (mean –0.71 ± 0.23) for dolomite, indicating that groundwater was in equilibrium with respect to the first mineral and undersaturated with respect to the second one (Table 1 of Annex) (Moore & Wade, 2013). This situation is attributed to the lower solubility of dolomite in comparison to calcite (Moore & Wade, 2013).

So, it appears that the latter two pathways of CO₂ production governed the concentration of CO₂ in the northern confined zone, while in southern, central and north-

eastern unconfined zones the presence of CO₂ was determined by the simultaneous occurrence of all processes discussed in this section.

2.5.2. Vertical dimension

2.5.2.1. N₂O production/consumption processes

According to the obtained hydrogeochemical and isotope data, nitrification and denitrification could be observed at different depths along the vertical profile of the studied aquifer. Also, these data provide evidence that mixing processes between the deep and shallow groundwater and slow infiltration of pollutants from the surface to the deeper parts of the aquifer affected the distribution of GHGs within the subsurface.

The high concentrations of DO, NO₃⁻ as well as δ¹⁵N and δ¹⁸O isotopic signatures of NO₃⁻ at two shallowest piezometers at Bovenistier 28 and 27 (Table 5, pp. 84) provided the evidence of N₂O production by nitrification processes. At the same time, the SP values of N₂O at this site were considerably lower (19.2 ‰ and 20 ‰, respectively) than SP typically reported for nitrification. The analysis of SO₄²⁻ isotopes showed that this location was the only one where obtained values of isotopic composition of the deepest groundwater (26) clearly fell into the range typical for sulphide oxidation (Fig. 9, p. 91), which might be associated with autotrophic denitrification (Jurado et al., 2018b). Such evidence suggested that the isotopic signature of N₂O of groundwater samples collected from the shallower part of the aquifer (28 and 27) was affected by both nitrification and denitrification processes (see section 2.3.2 (pp. 83 – 85)).

The anaerobic conditions and distribution of ¹⁵N and ¹⁸O isotopes of NO₃⁻ in the groundwater along vertical profile at Overhaem (10, 11 and 12) (Table 5, p. 84) suggested the occurrence of denitrification. Since the SO₄²⁻ isotopes did not indicate the occurrence of sulphide oxidation (Fig. 9, p. 91), the occurrence of heterotrophic denitrification could be a production mechanism of N₂O in this location.

The high level of DO, relatively high concentrations of NO₃⁻ (Table. 5, pp. 84), results of NO₃⁻ and SO₄²⁻ isotopes analyses (Fig. 7 and Fig. 9, pp. 86 and pp. 91, respectively) at the SGB location (21, 22 and 25) indicated the occurrence of nitrification

processes. The SP value of N_2O at the shallowest 21 piezometer was equal to almost 32 ‰, which also supported the idea about ongoing nitrification (Toyoda et al., 2017). However, the SP values of the groundwater samples collected from the deeper SGB 3 and SGB 1 piezometers were 14.1 ‰ and 15.2 ‰, respectively. Such data indicated that the production of N_2O might be the result of the simultaneous occurrence of both nitrification and denitrification or nitrifier-denitrification processes in the groundwater system at SGB site.

2.5.2.2. CH_4 production/consumption processes

The concentration of CH_4 (between 0.09 $\mu g/L$ and 0.6 $\mu g/L$) was higher than equilibrium with the atmosphere concentration in all locations across the vertical profile of the aquifer. However, no common trend in the distribution of CH_4 with depth for Bovenistier, Overhaem and SGB sampling locations was revealed.

The only site which showed the suitable conditions for the *in situ* biological production of methane was the deepest sampling point at Bovenistier (Table 5, pp. 84). As for the Overhaem and SGB, the high concentrations of NO_3^- , SO_4^- and DO (only in case of SGB) along the whole depth interval excluded the possibility of methanogenesis. Therefore, detected co-existence of CH_4 with considerable concentrations of NO_3^- , SO_4^{2-} and DO might be the evidence of its thermogenic origin and vertical migration through the system of fractures, surface contamination or methanogenesis that occur in anoxic microsites within the aquifer.

2.5.2.3. CO_2 production/consumption processes

The amount of CO_2 varied noticeably within the vertical profile of the aquifer from the lowest concentrations in deep groundwater to the highest concentrations in the shallow groundwater. Such distribution might be explained by stronger effects of rainwater on the composition of shallow groundwater and the decrease in the microbial activity with depth. In particular, it is likely that rain water washes out the CO_2 produced in the soil due to the decomposition of DOC (see section 2.5.1.3 (pp. 97 – 99)) and root respiration (Tan, 2010).

2.6. Conclusions

In this chapter the distribution of GHGs within the chalk aquifer under agricultural area was explored both across lateral and vertical dimensions. Lateral studies focused on the variability of GHGs concentrations taking into account the differences in hydrogeology, hydrogeochemistry and urbanization level across the explored region. Vertical dimension investigations attempted to elucidate the impact of heterogeneity of aquifer conditions along the depth profile on GHG concentrations.

Lateral explorations showed that among the three major GHGs it was the amount of N_2O , which exhibited the greatest cross-zonal variability between identified zones with contrasting environmental settings. The highest concentration of N_2O was detected in the unconfined aerobic part of the aquifer under most urbanized area where the concentration of NO_3^- was the highest, while the lowest N_2O content was measured in the confined anaerobic zone with the very low or almost absent NO_3^- and/or NH_4^+ concentrations in the groundwater. In the zone of groundwater discharge to the Geer River, the average concentration of N_2O was of the same magnitude as in the central zone, despite the fact that the NO_3^- content there was the lowest within the unconfined part of the aquifer. Also, in this zone the content of N_2O varied significantly between different locations, as well as the level of DO, implying that the availability of N_2O was governed by complex spatially heterogeneous pattern of different biogeochemical processes.

CH_4 revealed the high tendency towards the accumulation in groundwater. Its concentration was substantially higher in the northern confined zone in comparison to three other zones. However, even in the unconfined southern, central and north-eastern zones despite the oxic conditions and presence of electron acceptors with higher energy yield the concentration of CH_4 was, in average, approximately 13 times higher than its equilibrium atmospheric concentration.

Though the concentration of CO_2 was high in comparison to its equilibrium concentration in the ambient air, it fluctuated less in comparison to N_2O and CH_4 concentrations. CO_2 detected in the subsurface derived from root respiration or decomposition of organic matter. However, the relative uniformity of its spatial distribution is mostly attributed to the fact that in general the amount of CO_2 dissolved in

the groundwater was controlled by the process of dissolution of carbonate minerals which constitute aquifer geology.

The spatial differences in hydrogeochemical settings considerably influenced the dynamics of transformation of N and C loading in the subsurface, thus making tangible impact on the magnitude of the resulting indirect GHGs fluxes occurring on the groundwater-surface water interface. It was particularly noticeable in the case of highly volatile N₂O production/consumption processes. The production of detected N₂O could be attributed to a combination of nitrification and denitrification processes, likely occurring at different depths. However, the observed isotopic signals of N₂O demonstrated that the intensity of these processes as well as their relative contribution to the concentration of N₂O in the groundwater varied across different sampling locations.

Vertical dimension studies showed that different locations were characterized with different distribution pattern of major ions, GHGs and isotopes along the depth. However, in each of the cases they registered the shift in concentration of CO₂ (decreasing with depth in all cases considered) and significant changes in both isotope signatures and concentration level of N₂O across the depth profile. The latter observation indicated that production/consumption dynamics of N₂O was highly dependent on the hydrogeochemistry of the ambient subsurface environment. It was revealed that the variability of chemical composition of groundwater in different locations was controlled by different biogeochemical processes changing in intensity with depth.

The observed heterogeneity of biogeochemical processes leading to GHGs production/consumption in the subsurface across the aquifer show that the magnitude of occurring GHGs fluxes (especially in the case of N₂O in this study) could vary significantly due to the change in the amount of N and C inputs and distribution of their sources across different hydrogeochemical zones and in relation to groundwater flow pattern. Therefore, our study provides evidence to the assumption regarding existence of uncertainty of indirect GHGs fluxes related to upscaling of the point-derived estimations to the catchment level. In order to reduce this uncertainty, it is advised before the estimation of GHGs fluxes at the groundwater – river interface (and possible development of measures regulating their intensity) to take into account the insights

obtained from larger-scale investigations in order to identify the representative spatial zones which shape the dynamics of GHGs emissions. As demonstrated by the results of combined application of SOM-derived clustering and interpretation of isotopomer maps, combination of insights from hydrogeochemical and isotope studies is essential in this regard, as it helps to get more profound insight into the process dynamics within the underground environment where the microbiological structure and aquifer matrix might be additional factors that affect the transformation of N and C compounds.

Chapter 3

This chapter is based on the following publication:

Nikolenko, O., Brouyère, S., Goderniaux, P., Robert, T., Orban, P., Borges, A., V., Jurado, A., Duvivier, M., Morana, C. (2020). Dynamics of nitrous oxide with depth in groundwater: insights from ambient groundwater and laboratory incubation experiments (Hesbaye chalk aquifer, Belgium). Submitted to Journal of Contaminant Hydrology. (under a review)

3. Nitrification and denitrification capacity of the chalk aquifer and its effect on nitrous oxide (N₂O)

After the regional investigations, it was assumed that N₂O dynamics in the chalk aquifer is governed by both nitrification and denitrification processes. Based on that conclusion, it was decided to focus further explorations on upper and lower parts of the aquifer. Evidently they are presumably different in terms of physical-chemical and biochemical conditions, and those differences could be the reason explaining the mixed origin of N₂O. Therefore, further steps were devoted to:

- 1) obtaining better insight related to the distribution of N compounds and their isotopes with depth in the Hesbaye chalk aquifer;
- 2) the estimation of the rates of nitrification and denitrification processes.

3.1. Vertical trends in the distribution of nitrogen compounds and their isotopes

3.1.1. General study design

Two sites (Bovenistier and SGB), allowing access to different aquifer depths, were selected for the studies. Both are equipped with multilevel piezometers, which characteristics and investigated depth intervals are shown in Fig. 14. During the investigations, upper and lower groundwater layers were examined in each piezometer. For the sake of convenience in the further discussion, the sampling points (i.e., depth intervals which were sampled) are numbered from 1 to 10, as indicated in Fig. 14 along the left side of each piezometer.

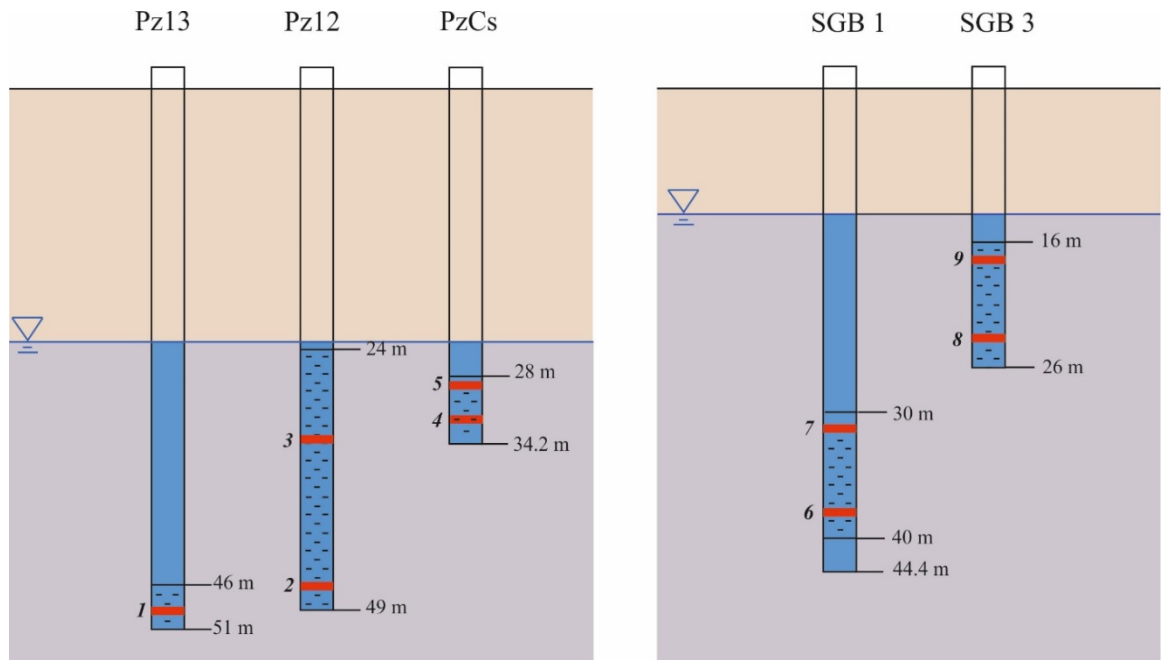


Figure 14. Piezometers and sampling depths at the Bovenistier (left) and SGB (right) sites. Sampling points are numbered from 1 to 10, as indicated in bold and italics on the left side of each piezometer. The groundwater level value is not indicated, since it was not stable between summer and winter campaigns.

Information regarding the hydrochemical conditions, concentrations of N compounds and their isotopic and isotopomer signals, used to describe the nature of N₂O dynamics, was obtained by chemical and isotope analyses of groundwater samples. Those were collected using a low-flow sampling technique during the summer (June 2019) and winter (December 2019) campaigns. Samples were collected at the end of a low flow pumping (240 ml/min) stage performed at each location until the stabilization of electrical conductivity (EC) and pH, using a Solinst bladder pump model 407 SS 1.66'' Dia. It was assumed that stabilization occurred when five consecutive measurements for EC and pH did not differ by $\pm 2\%$ and ± 0.1 units, respectively.

The results of isotopic and chemical analyses of groundwater samples consist of:

- 1) total nitrate (NO₃⁻) and boron (B) isotope maps for both SGB and Bovenistier sites;
- 2) comparative vertical distribution profiles of NO₃⁻, N₂O and N isotopes, for the summer and winter campaigns and for each of the studied sites individually.

Isotope maps help to address the question whether changes in N isotope and isotopomer values along the profiles are related to the ongoing N₂O production/consumption processes or are due to differences in the isotopic signatures of the initial substrate sources. The analysis of ¹¹B was performed only for groundwater samples collected in summer. Consequently, the conclusions regarding the origin of N in winter samples will be made both by examining NO₃⁻ isotope maps and considering the corresponding results of $\delta^{11}\text{B}$ analyses from summer samples. Comparative vertical distribution profiles are used to examine covariations between N compounds and their isotopes with depth which helps to understand N₂O dynamics in the aquifer.

3.1.2. Depth specific distribution of N compounds and their isotopes

According to the obtained results, the origin of N in groundwater samples at the Bovenistier site during the summer period (Fig. 15) was attributed to 2 major sources:

manure, the isotope signal of which was dominant at the shallowest sampling point 5 (PzCs), and NH_4^+ fertilizers identified at the deeper studied points 4 (PzCs), 3 and 2 (both in Pz12) (Fig. 15).

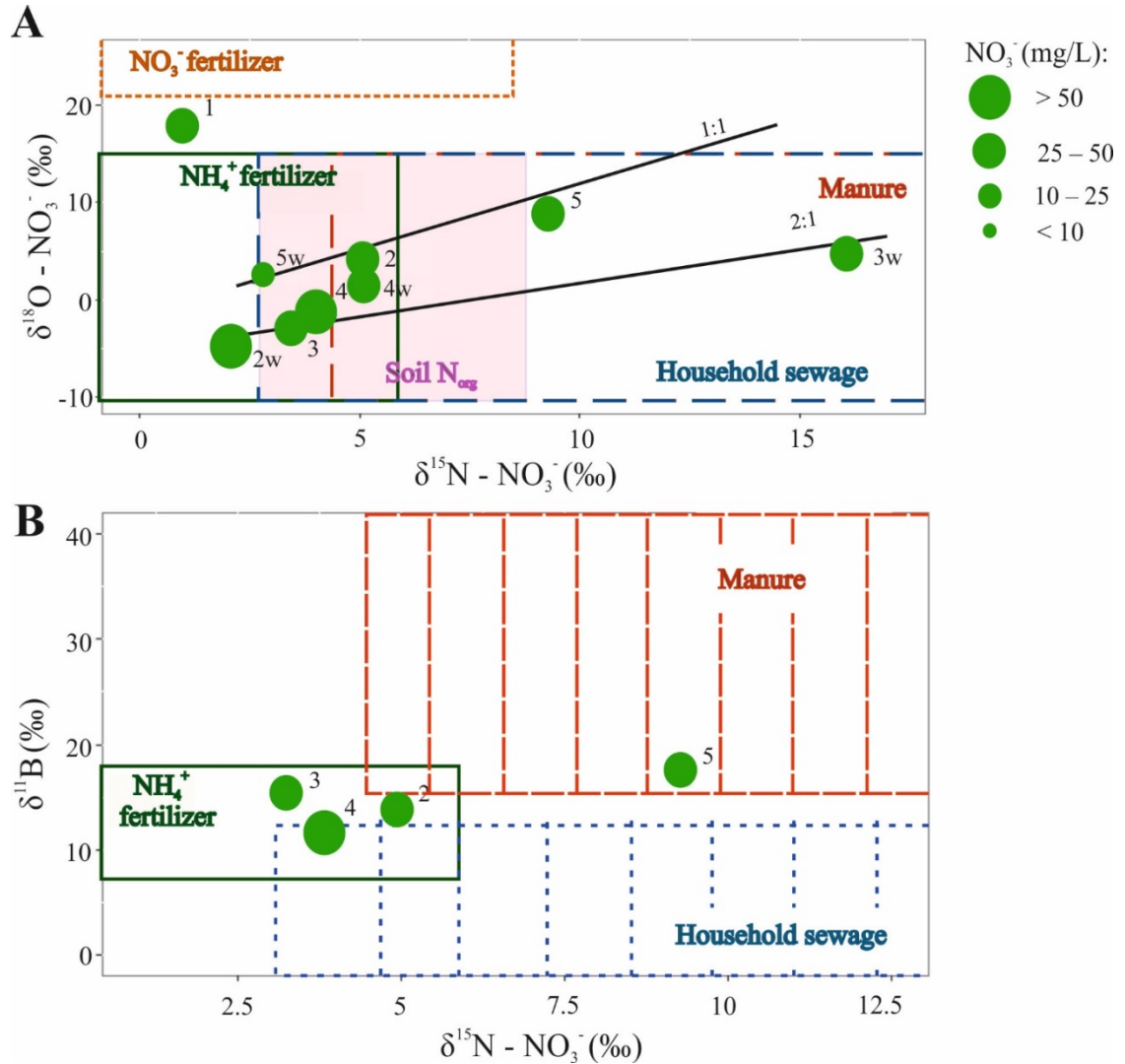


Figure 15. NO_3^- and B isotope maps of groundwater samples collected at Bovenistier site. Graph A includes the data from summer and winter and graph B includes the data from summer only. The letter “w” next to the number of sampling location means that the sample was collected in the winter. Green circles of different size indicate different concentrations of NO_3^- in groundwater samples. The ranges of isotopic compositions for NO_3^- and B sources (boxes drawn in the graphs) are derived from Michener & Lajtha

(2008), Xue et al. (2009) and Widory et al. (2004). Ratios of $\delta^{15}\text{N}$ and $\delta^{18}\text{O}$ of NO_3^- used to draw denitrification lines are taken from Koba et al., 2009.

In the absence of $\delta^{11}\text{B}$ samples for the winter campaign, it was more difficult to distinguish the N sources in this dataset. For example, sample 5_w indicates NO_3^- isotopic values typical for both fertilizers and sewage while sample 4_w exhibits NO_3^- isotopic signals typical for denitrification process as 4 and 4_w are located along the denitrifying line with a slope 1:1. As for 3_w it showed NO_3^- isotopic signature much different in comparison to summer values and typical for manure and sewage sources. At point I (Pz13) NO_3^- is detected only in the winter, and its isotope signature fall out of the ranges typically attributed to the considered N sources.

At the SGB site (Fig.16) samples 8 and 9 (SGB3) that belong to the shallower part of the aquifer show isotopic values that can be attributed to different N sources, while the samples 6 and 7 (SGB1) that belong to the deeper part of the aquifer fall in the sewage interval. During the summer campaign, samples 8 and 9 can be associated with household sewage and manure, respectively. In winter, the same samples fall into the ranges typical for household sewage and NH_4^+ fertilizers. Samples 7 show NO_3^- and B isotope values typical for both NH_4^+ fertilizers and household sewage during summer and winter periods. Sample 6_w demonstrates N isotopic signatures which can be associated with denitrification processes as 6 and 6_w fall along the denitrifying line with slope 2:1.

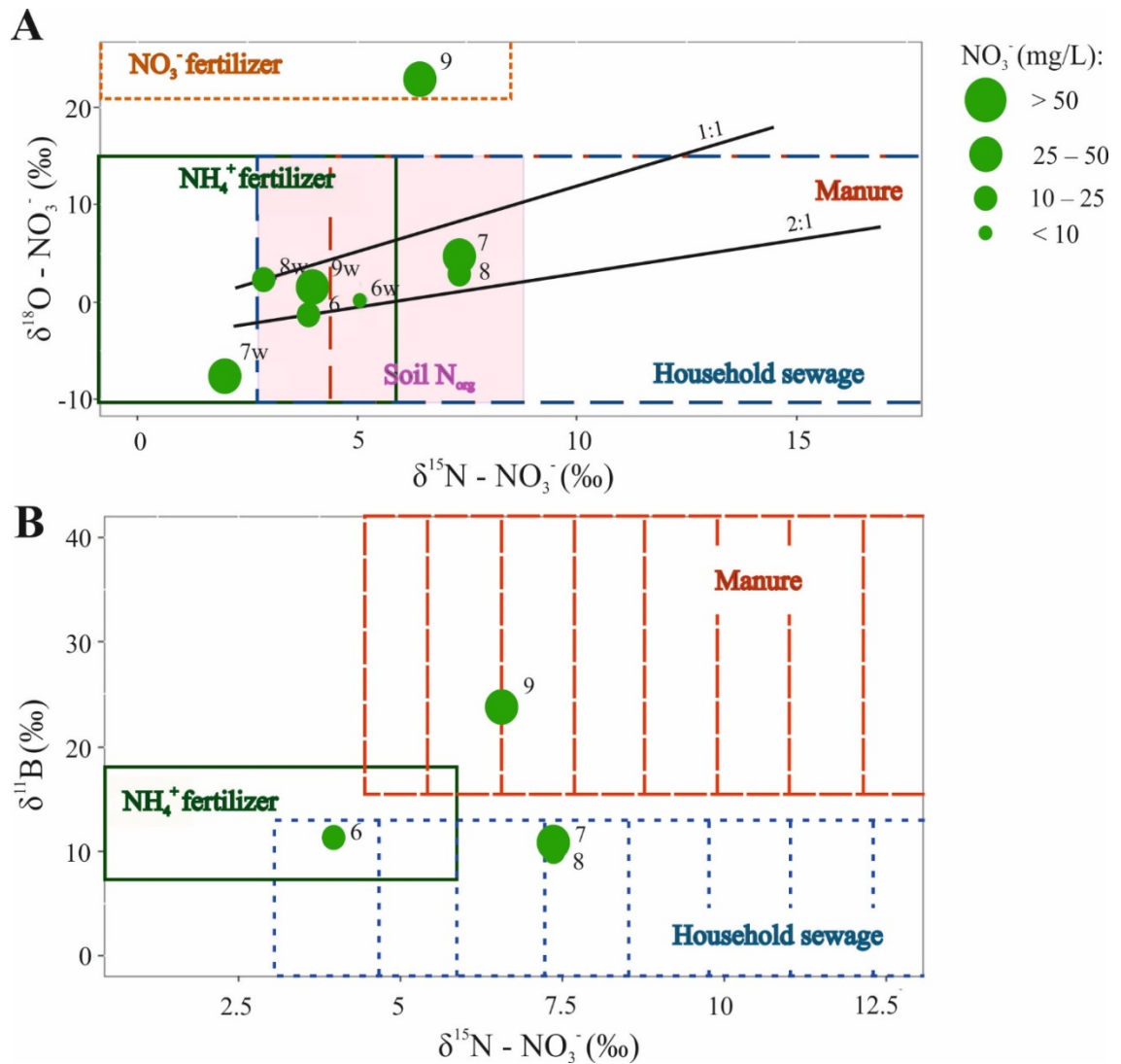


Figure 16. NO₃⁻ and B isotope maps of groundwater samples collected at SGB site. Graph A includes the data from summer and winter and graph B includes the data from summer only. The letter “w” next to the number of sampling location means that the sample was collected in the winter. Green circles of different size indicate different concentrations of NO₃⁻ in groundwater samples. The ranges of isotopic compositions for NO₃⁻ and B sources (boxes drawn in the graphs) are derived from Michener & Lajtha (2008), Xue et al. (2009) and Widory et al. (2004). Ratios of $\delta^{15}\text{N}$ and $\delta^{18}\text{O}$ of NO₃⁻ used to draw denitrification lines are taken from Koba et al., 2009.

Fig. 17 and Fig. 18 show the change in the concentration of N compounds, N isotopic signatures and DO along the vertical aquifer profile at the Bovenistier and SGB sites in summer and winter periods.

Groundwater samples from the SGB site show concentrations of N-N₂O which exceed the equilibrium with the atmosphere concentration (0.3 µg N/L) (Hasegawa et al., 2000). In winter N₂O concentrations were higher (12.6 ± 2.9 µg N/L) in comparison to the summer (8.2 ± 1.5 µgN/L). The SGB1 piezometer showed that the concentration of N-N₂O was higher in the deepest part of the piezometer (point 6 – 9.9 µg N/L and 14.5 µg N/L) than in its upper part (point 7 – 6.4 µgN/L and 11.6 µg N/L) in the summer and winter campaigns, respectively. The SGB3 piezometer did not indicate any significant difference in N-N₂O concentration with depth for the summer campaign. However, for the winter campaign the upper sampling location (sample 9) showed a concentration almost two times higher (15.5 µg N/L versus 8.6 µg N/L) compared to the deeper sampling location (sample 8).

At the SGB site the concentrations of NO₃⁻ decreased with depth, but they showed significant variations between the summer and winter sampling campaigns. The shallower sampling points 8 and 9 showed concentrations of 28.7 mg/L and 47.9 mg/L mg/L in the summer and 21.5 mg/L and 38.3 mg/L, in the winter. The deeper samples 6 and 7 showed NO₃⁻ concentrations 23.5 mg/L and 18.3 mg/L in the summer, and of 48.7 mg/L and 1.56 mg/L in the winter. The concentrations of DO were in a range between 7.0 mg/L to 9.6 mg/L, decreasing with depth during both sampling periods.

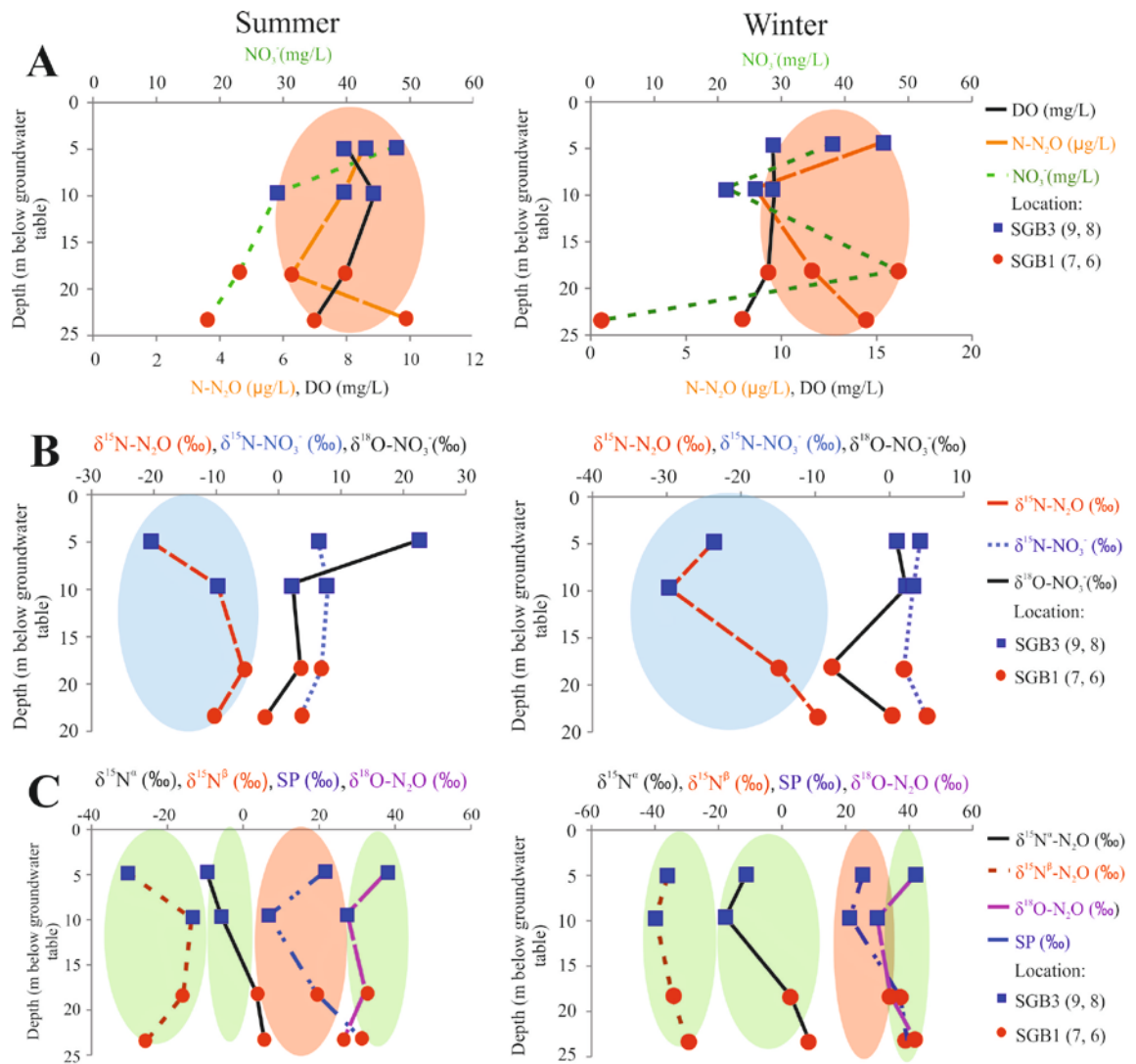


Figure 17. Vertical distribution of N compounds, their isotopes and DO at SGB site during summer and winter periods.

The SP and N-N₂O results (red circles, Fig. 17 A and C) changed in the same direction along the depth profile both in the summer and winter campaigns, with the exception of location 7 for N-N₂O. This indicates the absence of N₂O reduction processes (Ostrom et al. 2007). The similarity between N-N₂O and δ¹⁵N-N₂O evolutions (blue circle, Fig. 17 B) in the winter campaign also indicates that N₂O is not reduced. Such a similarity is not observed for the summer sampling campaign, which in this case might evidence N₂O reduction.

Moreover, data from the summer campaign show a strong covariation with depth between of $\delta^{15}\text{N-N}_2\text{O}$ and $\delta^{15}\text{N}^\beta\text{-N}_2\text{O}$ (green circle, Fig. 17 C) which suggests close dependence between these two parameters. The $\delta^{15}\text{N}^\alpha\text{-N}_2\text{O}$ enrichment increased with depth, while the $\delta^{18}\text{O-N}_2\text{O}$ (green circles, Fig. 17 C) decreased slightly.

The winter campaign data show that $\delta^{15}\text{N-N}_2\text{O}$, $\delta^{15}\text{N}^\alpha\text{-N}_2\text{O}$, $\delta^{15}\text{N}^\beta\text{-N}_2\text{O}$ and $\delta^{18}\text{O-N}_2\text{O}$ (green circles, Fig. 17 C) parameters exhibited similar vertical distribution patterns, along the vertical profile with more pronounced increase of $\delta^{15}\text{N}^\alpha\text{-N}_2\text{O}$ with depth. This observation suggests that $\delta^{15}\text{N-N}_2\text{O}$ signature might be either influenced by production processes solely or influenced to the same extent with both N_2O production and reduction processes.

All samples collected at Bovenistier showed $\text{N-N}_2\text{O}$ concentrations exceeding the equilibrium with the atmosphere. Similarly to the SGB site, the concentration of this gas was higher in the winter ($10.5 \mu\text{g N/L} \pm 1.7 \mu\text{g N/L}$) than in the summer ($8.6 \mu\text{g N/L} \pm 1.3 \mu\text{g N/L}$). For the summer campaign, samples 4 and 5 (PzCs) showed higher concentrations of $\text{N-N}_2\text{O}$ $10.16 \mu\text{g N/L}$ and $9.26 \mu\text{g N/L}$, respectively, in comparison to 3 and 2 (Pz12) where its concentrations were nearly the same (around $7 \mu\text{g N/L}$). During the winter campaign, $\text{N-N}_2\text{O}$ concentrations varied vary between $10.7 \mu\text{g N/L}$ and $12.4 \mu\text{g N/L}$ at all of the sampling points with higher concentrations observed at the bottom parts of piezometers – sampling points 4 and 2. During the winter campaign N_2O was detected at a concentration of $7.7 \mu\text{g N/L}$ at the deepest sampling location 1 (Pz13) but in the summer campaign the concentration there was below the detection limit.

During the summer campaign, the concentration of NO_3^- did not change noticeably between point 4 and 5 (PzCs) ($> 40 \text{ mg/L}$), but it varied between samples 3 and 5 (47.8 mg/L vs 37.0 mg/L) located respectively in the shallow and deep part of Pz12. During this period, NO_3^- was not detected in the sample collected at location 1 in Pz13. In the winter, the NO_3^- concentration was almost two times lower at location 5 (24.2 mg/L) than at location 4 (46.2 mg/L). At the same period, there was no significant difference in NO_3^- between locations 2 and 3 ($> 40 \text{ mg/L}$) and the concentration of NO_3^- was 47.9 mg/L at point 1 in Pz13. The concentration of DO varied from 1.5 mg/L to 9.9 mg/L .

At Bovenistier, variations with depth of N-N₂O and SP (red circles, Fig. 18 A and C) were different for both winter and summer periods. However, these differences are not significant enough to conclude on the possible occurrence of N₂O reduction. At the same time, the similarity observed between N-N₂O and $\delta^{15}\text{N-N}_2\text{O}$ (blue circle, Fig. 18 B) profiles for winter (except for the deepest sampling point at Pz12 and Pz13) indicates the absence of N₂O reduction in the shallower part of the aquifer and its occurrence in the deepest part. N₂O reduction processes at the bottom part of the aquifer are also supported by the positive value of $\delta^{15}\text{N-N}_2\text{O}$ (9.2 ‰) and the high $\delta^{18}\text{O-N}_2\text{O}$ value (66.0 ‰). During the summer campaign, differences in N-N₂O and $\delta^{15}\text{N-N}_2\text{O}$ patterns can be attributed to N₂O reduction.

Summer period shows nearly the same distributions of $\delta^{15}\text{N-N}_2\text{O}$, $\delta^{15}\text{N}^\alpha\text{-N}_2\text{O}$, $\delta^{15}\text{N}^\beta\text{-N}_2\text{O}$ and $\delta^{18}\text{O-N}_2\text{O}$ (green circles, Fig. 18 C), except the slight decrease in $\delta^{18}\text{O-N}_2\text{O}$ at the interval which corresponds to sampling locations 5 and 4.

In winter the patterns between $\delta^{15}\text{N-N}_2\text{O}$, $\delta^{15}\text{N}^\alpha\text{-N}_2\text{O}$, $\delta^{15}\text{N}^\beta\text{-N}_2\text{O}$ and $\delta^{18}\text{O-N}_2\text{O}$ (green circles, Fig. 18 C) are identical with the obvious increase at the deeper aquifer layers which corresponds to sampling point 1 (Pz13). This indicates that N₂O reduction dominates N₂O production in the deeper part of the aquifer. At the same time, N₂O production exceeds its consumption or occurs to the same extent at the upper part of the aquifer.

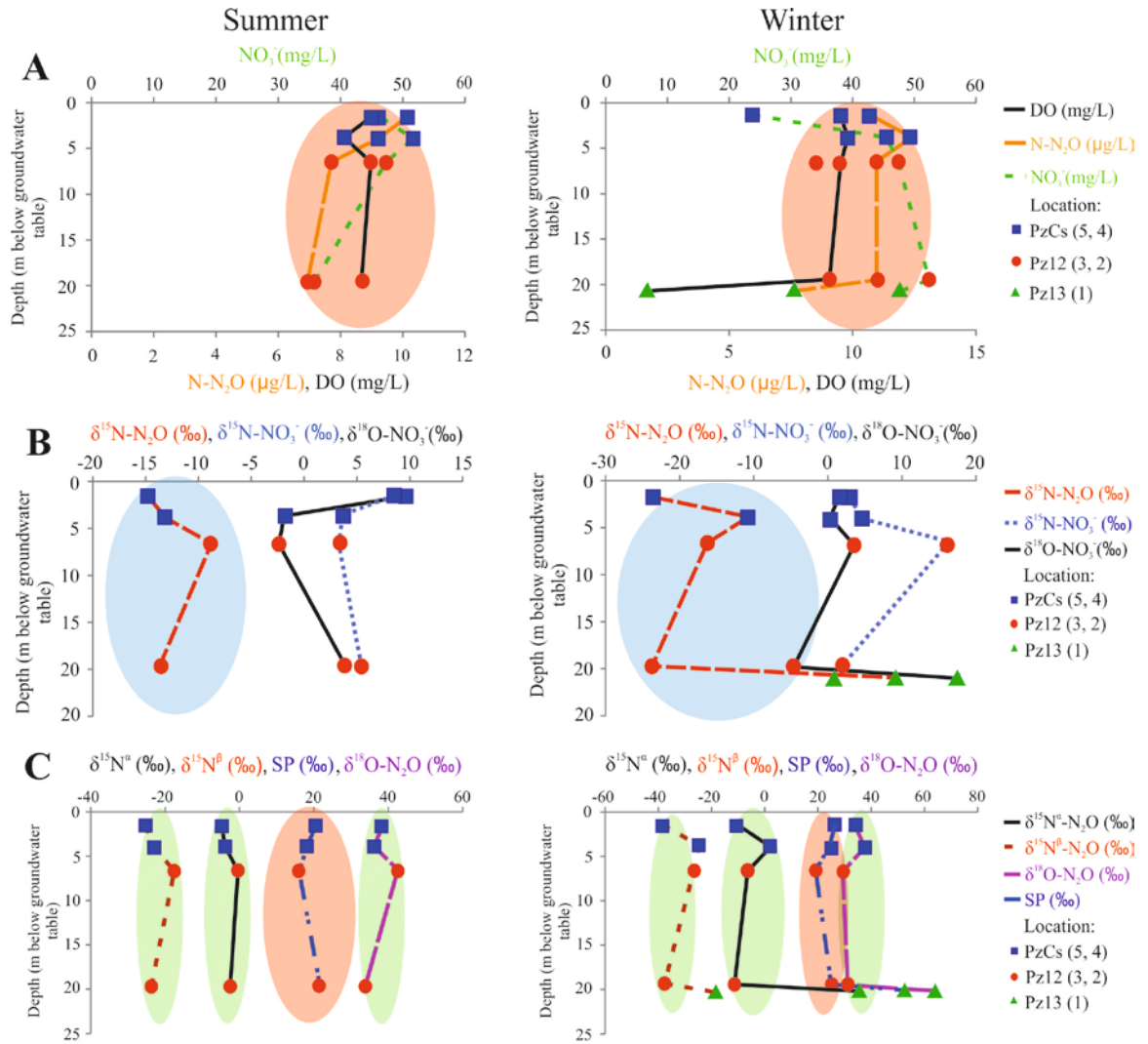


Figure 18. Vertical distribution of N compounds, their isotopes and DO at the Bovenistier site during summer and winter periods.

3.1.3. Evidence of N₂O production and consumption processes obtained from the analyses of ambient groundwater samples

According to the results, both N₂O production and consumptions processes occur in the chalk aquifer. The fact that N as an initial substrate originates from different sources at different depths complicates the distinction between nitrification and denitrification as well as between N₂O production and consumption mechanisms.

At SGB, the similarity between $\delta^{15}\text{N-N}_2\text{O}$ and $\delta^{15}\text{N}^\beta\text{-N}_2\text{O}$ in the summer campaign means that the isotopic signature of N_2O is not determined by N_2O reduction. In the winter campaign, simultaneous increase in N_2O isotopomers values (with more pronounced increase in $^{15}\text{N}^\alpha$) and $\delta^{18}\text{O-N}_2\text{O}$ at levels 7 and 6 indicates (Park et al., 2011) the occurrence of N_2O reduction processes at the bottom part of the aquifer. This is also supported by the drastic decrease in the concentration of NO_3^- at sampling point 6 in comparison to 7. The opposite patterns of NO_3^- and N_2O concentrations in the deep part of the aquifer both in summer and winter periods provide additional evidence of reduction processes (Minamikawa et al., 2011).

At Bovenistier, it could be concluded that N_2O production processes dominate over its consumption based on the similarities in the distributions of N isotopes, isotopomers, and N- N_2O concentrations along the vertical profile. Intensive N_2O consumption is revealed only in the deep part of the aquifer (Pz13) during the winter campaign. This observation is probably related to significant NO_3^- input which stimulated denitrification process and allowed to detect N_2O at measureable levels.

As a first conclusion, despite of the occurrence of aerobic conditions at SGB and Bovenistier, both production and consumption processes govern the dynamics of N_2O , with the reduction processes being more pronounced in the deeper part of the aquifer. Such conclusions are supported by the fact that there is more and more evidence of denitrifiers being capable of using both DO and NO_3^- as electron acceptors (Zhu et al., 2019). Moreover, there are studies which suggest the presence of micro anaerobic hotspots in total aerobic environments capable of supporting denitrification processes (Well et al., 2012).

3.2. Estimation of the rates of nitrification and denitrification processes

Stable isotope tracer experiments with enriched in heavy ^{15}N isotope potassium nitrate (KNO_3) and ammonium chloride (NH_4Cl) were performed to measure the intensity of denitrification and nitrification processes, respectively.

However, before deciding under which conditions (*in situ* or laboratory) tracer studies had to be conducted, it was necessary to obtain information about *in situ*

groundwater fluxes. This was required because the tracer needs to remain for sufficient amount of time in the aquifer to undergo denitrification and nitrification processes to detectable levels. However, if such fluxes are very high, it would be likely that the tracer could be transported away in the aquifer after the push phase and impossible to recover during the pull phase.

In situ field investigations consisted of:

- 1) estimation of groundwater flow rates using Finite Volume Point Dilution Technique (FVPDM). The information obtained using these measurements helped to adapt the incubation time for the following push-pull pre-test;
- 2) push-pull pretests using potassium bromide (KBr) as a conservative tracer to determine dilution effects within the aquifer.

In the end, the results showed that the in situ tracer experiments for the assessment of the magnitude of nitrification and denitrification processes might not be suitable for four (Pz12 top, PzCs, SGB3 top and SGB3 bottom) out of six locations due to the chance to obtain lower recoveries of tracers. That is why it was decided to perform lab incubation experiments. Description and results of FVPDM and push-pull studies conducted to determine the suitability of the application of tracer experiment *in situ* are described in Text 2 of Annex.

3.2.1. Laboratory tracer incubation experiment

3.2.1.1. General description

Two N stable isotope labeled experiments were conducted in order to estimate the rates of nitrification and denitrification processes in groundwater. For this purpose, groundwater was collected at different depths of the aquifer at Bovenistier and SGB sites (see sampling points on Fig. 14 section 3.1.1. (p. 105)) during the winter campaign. From each sampling point, 4 water samples of 50 mL each were collected and stored in borosilicate serum vials sealed without headspace using a butyl rubber stopper and an aluminum seal. Half of them were used for nitrification incubation experiment and another half for denitrification incubation experiment by addition of ^{15}N labeled compounds. It should be emphasized that this experiment provides the information about the potential rates of nitrification and denitrification because the addition of the ^{15}N

labeled compounds (substrates for denitrification and nitrification processes) increases their concentrations relative to its *in situ* values.

Nitrification rates were determined in headspace-free serum vials spiked with ^{15}N -labelled NH_4Cl (99 atom% ^{15}N) by measuring the changes in $\delta^{15}\text{N}\text{-NO}_3^-$ values resulting from the oxidation of the $^{15}\text{NH}_4^+$ which is a substrate for nitrification. Since the results of chemical analysis showed the ambient concentration of NH_4^+ in groundwater was below the detection limit, it was decided to amend water samples with an excess of $^{15}\text{N}\text{-NH}_4^+$ in order to reach the final concentration of ~ 2 mg/L of NH_4^+ . Similarly, denitrification rates were determined in headspace-free serum vials amended with ^{15}N -labelled KNO_3 (25 atom% ^{15}N) by observing the changes in $^{15}\text{N}\text{-N}_2\text{O}$ and $^{15}\text{N}\text{-N}_2$ isotopic signatures expecting the consumption of added isotopically enriched $^{15}\text{N}\text{-NO}_3^-$ (25 atom% ^{15}N) which is a substrate for denitrification. Considering that the background concentration of NO_3^- in groundwater vary from 0 to 52.5 mg/L (based on the results obtained from summer campaign), the amount of injected $^{15}\text{N}\text{-NO}_3^-$ was defined aiming to double the concentration of NO_3^- at each location. Amendments were made by injecting the tracer solutions through the septa of borosilicate glass vials.

The magnitudes of nitrification and denitrification processes were measured during 24 h and 48 h long experiments, respectively, each of which consisted of four time spans with 2 vials used for each time span (duplicates). The vials were incubated in the dark under 10 °C which corresponds to the mean *in situ* temperature of groundwater at the time of sampling. Both incubations started just after tracer injections. At the beginning of the incubation experiments, an addition of 200 μL of a saturated solution of HgCl_2 in two vials was performed to inhibit microbiological activity in order to have reference values of initial T_0 $^{15}\text{N}\text{-NO}_3^-$, $^{15}\text{N}\text{-N}_2\text{O}$ and $^{15}\text{N}\text{-N}_2$ isotopic values. For nitrification, further inhibitions of microbiological activity took place in 2 subsequent vials in the time course after 6 h, 12 h, 18 h and 24 h intervals. For denitrification, the intervals after which inhibition was performed in the respective vials were established at 6 h, 12 h, 24 h and 48 h.

The atom% of ^{15}N in a substrate ($^{15}\text{NH}_4^+$ or $^{15}\text{NO}_3^-$) for each experiment (a_s) was estimated considering the atom% of ^{15}N in the tracer added to the vials and in NH_4^+ or NO_3^- naturally occurring in groundwater by the following formula (Hayes, 2004):

$$a_s = (C_{bg} \times a_{bg} + C_t \times a_t) / (C_{bg} + C_t) \quad (12)$$

where C_{bg} is the background concentration of NH_4^+ or NO_3^- (nmol), C_t is the concentration of the tracer added to vials (nmol), a_{bg} is the atom% of ^{15}N in NH_4^+ or NO_3^- compounds in groundwater before the addition of a tracer, a_t is the atom% of ^{15}N in a tracer added to the vials.

The magnitude of nitrification and denitrification were estimated based on the formula provided by Hama et al. (1983) and adapted for the quantification of NO_3^- or N_2O and N_2 production rates:

$$P = \frac{C \times (a_{is} - a_0)}{t \times (a_s - a_0)} \quad (13)$$

where P is the production rate of a particular compound (nmol/L/h), C is the initial (background) concentration of this compound (nmol), a_{is} is the atom% of ^{15}N in this compound in incubated samples at the end of each incubation interval, a_0 is the atom% of ^{15}N in the studied compound at the beginning of incubation experiment (T_0) just after the addition of a tracer, a_s is the atom% of ^{15}N in a substrate for nitrification ($^{15}\text{NH}_4^+$) or denitrification ($^{15}\text{NO}_3^-$) after the addition of a tracer at the beginning of incubation and t is incubation time (h).

The concentrations of NO_3^- and N_2O were measured using the analytical procedures described in section 2.5. The ^{15}N - NO_3^- isotopes analyses was conducted using an off-axis cavity ringdown spectroscopy (OA-ICOS) (Los Gatos Research) instrument (University of Liège, Belgium) applying Cd-Azide reduction method to quantitatively converts NO_3^- to N_2O (McIlvin & Altabet, 2005; Ryabenko et al., 2009, Wassenaar et al., 2018). Groundwater dissolved gases (N_2O and N_2) from incubation samples were extracted using the headspace equilibration technique with helium (He) filling the headspace (20 ml of He headspace in 50 ml serum bottles). The ^{15}N - N_2O values were determined on a dual-inlet isotope ratio mass spectrometer (Stable Isotope Facility, UC Davis, Davis, CA) as described by Mosier and Schimel (1993). Note that only the samples from 5 locations out of 9 (Pz 13 (1), Pz12 (3 and 2) and SGB (7 and 6)) were sent for the ^{15}N - N_2O isotope analyses. The ^{15}N - N_2 was estimated by isotope ratio mass spectrometer (delta V plus, ThermoScientific) (volume injected in the mass spectrometer: 50 μL).

3.2.1.2. Evidence of N₂O production and consumption processes from laboratory incubation experiments

The results of the isotope analyses of ¹⁵N-NO₃⁻, ¹⁵N-N₂O and ¹⁵N-N₂ did not detect any considerable enrichment of respective compounds between different time spans which means that both nitrification and denitrification processes did not occur in the bottles during the incubation experiment. The maximal analytical errors of the ¹⁵N-NO₃⁻, ¹⁵N-N₂O, and ¹⁵N-N₂ analyses were ± 2 ‰, ± 0.14‰ and ± 0.1 ‰. The detection limits were: 1) for nitrification – 0.3 nmol/L/h and 2) for denitrification – 2.7 nmol/L/h for N₂ and 0.0002 nmol/L/h for N₂O.

The results show that our previous hypothesis about the simultaneous occurrence of both nitrification and denitrification processes in the aquifer might not explain the SP values of N₂O measured in groundwater samples collected during the regional and local investigations. Consequently, on the one hand the availability of N₂O in the aquifer might be explained by the infiltration of N₂O produced by nitrification and denitrification processes occurring within the other parts of the aquifer. Alternatively, there might exist a discrepancy between real aquifer conditions and laboratory experiments. In particular, in the aquifer, groundwater is in permanent contact with biofilms attached to the rocks materials, while groundwater samples collected in piezometers for incubation might not represent the real complexity of the subsurface environment. To investigate this, it would be needed to collect large volumes of groundwater to extract the available bacterial biomass and analyze it in order to determine the expression of nitrifying and denitrifying genes, which might help to obtain better insight into the qualitative diversity of biofilm biotope, since it is expected that there exists a constant flux of bacteria between biofilm and water layers.

Chapter 4

4. Microbiological evidence of nitrous oxide production/consumption processes

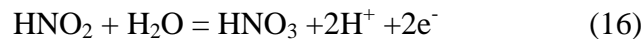
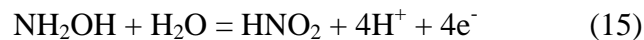
4.1. Functional gene expression as a key to understand nitrous oxide dynamics

The analysis of hydrochemical and isotope parameters during regional campaign demonstrated that the availability of N_2O in groundwater might be the consequence of the intertwining processes of nitrification and denitrification. However, based on the obtained data, it cannot be claimed unambiguously that both these processes actually occur in the aquifer. Comparison of N_2O isotopomer and isotope data only gave the information about the occurrence of N_2O consumption or production (section 3.1.3 (pp. 114 – 115)) but it was not sufficient to answer the question which processes of N production govern its dynamics (e.g. in most of the cases obtained SP values fell out of the range typical for both nitrification and denitrification processes). Also, it is not possible to reach definite conclusions regarding the completeness of these pathways and interaction between them using solely these data. For instance, it is possible that unsaturated zone might supply N compounds in different oxidation states for their further transformation to N_2O and/or N_2O by itself to the aquifer. Consequently, incomplete nitrification/denitrification or N_2O diffusion from water free zone could be responsible for the accumulation of N_2O in

groundwater, and the role of processes occurring in the aquifer itself would appear less significant. Under such scenario, the aquifers would have to be perceived as the receptor media that stores and/or transport N₂O between different environmental compartments rather than as a secondary source of GHG emissions.

Therefore, additional information about the *in situ* aquifer conditions is required in order to understand better the nature of processes in the subsurface. Since nitrification and denitrification can proceed through abiotic and biotic parts of environment, the measurements of the activity of the microorganisms that accomplish biotic N transformations might provide valuable insights into the dynamics of N₂O production/consumption. Both nitrification and denitrification can be mediated by bacteria and archaea, yet due to the time limitations of the project this study considers only the role of bacteria.

Nitrification is performed by two physiologically distinct groups of chemolithotrophic bacteria (use inorganic reduced compounds as electron sources (source of energy)): 1) the first group consists of ammonia-oxidizers (AOB) and 2) the second one is composed of nitrite-oxidizing bacteria (NOB). In the first step of nitrification AOB perform oxidation of ammonia (NH₃) to nitrite (NO₂⁻) (Equations 14 and 15), and in the second one NOB carry out oxidation of nitrite (NO₂⁻) to nitrate (NO₃⁻) (Equation 16):



In addition, there is much evidence about the existence of AOB which facilitate the complete oxidation of ammonia to nitrate (Daims et al., 2015; van Kessel et al., 2015; Koch et al., 2019).

Hydroxylamine (NH₂OH), produced at the beginning of nitrification, can be a substrate for further N₂O production in case of its incomplete oxidation. Also, under the conditions of nitrosative stress AOB use NO₂⁻ as an alternate terminal electron acceptor via nitrifier denitrification process which is accompanied by N₂O generation (Stein, 2011).

AOB can be allocated to three phylogenically different groups of the phylum Proteobacteria the gamma-, beta-, and delta-proteobacteria classes. The first group includes one genus *Nitrosococcus* represented by two described species: *Nitrosococcus oceani* and *Nitrosococcus halophilus* (Koops & Pommerening-Röser, 2001). The betaproteobacteria comprises two genera, *Nitrospira* and *Nitrosomonas*, with a total of 14 characterized species which have six distinct lineages of descent (Pommerening-Röser, 1996). Finally, the last group is defined by complete ammonia oxidizers in the bacterial genus *Nitrospira* (Daims et al., 2015; van Kessel et al., 2015). Members of *Nitrospira*, which can oxidize ammonia to nitrate on their own, belong to the most widespread clade of this diverse genus which can be phylogenetically divided into at least six lineages (Daims et al., 2016).

Nitrifiers use ammonia monooxygenase (AMO) to oxidize ammonia to hydroxylamine and hydroxylamine dehydrogenase (HAO) to transform hydroxylamine to nitrite. AMO is a multiple subunit enzyme used for the production of hydroxylamine and water (Eq. 14; page 121). It is active in the presence of oxygen (O₂), the consumption of which increases with the addition of ammonia. The structural subunits of AMO are encoded by the genes *amoA*, *amoB* and *amoC*, which belong to one operon (a functioning unit of DNA containing a cluster of genes under the control of a single promoter) (Norton et al., 2002). The *amoA* gene is commonly used as a functional marker for bacterial or archaeal ammonia oxidizers (Kim et al., 2008). In aerobic environment under the conditions of nitrosative stress AOB can activate enzymes from *nor* group to reduce nitric oxide (NO) to N₂O (Stein, 2011). Also, some studies revealed nitrite reductase encoded gene of denitrifiers in the genome sequences of nitrifying bacteria, namely *nirK*, which might be an integral component of ammonia oxidation pathway that protects bacteria from nitrite toxicity (Arp & Stein, 2003; Kozłowski et al., 2016).

Denitrifying bacteria exhibit much greater taxonomic diversity and are more widespread in different environments in comparison to other functional groups involved in the N-cycle (Geets et al., 2007). Most of them belong to various classes of Proteobacteria (Philippot, 2005). Low oxygen concentration and presence of nitrogen oxides are prevailing factors that activate denitrification system. However, regulatory

networks of denitrification are variable, since more and more strains were found to be capable of denitrifying under both aerobic and anaerobic conditions simultaneously using O_2 and NO_3^- as electron acceptors (Ward et al., 1996; Zhu et al., 2019). That is why, the capability of denitrifiers to perform complete denitrification varies and, consequently, variable amounts of intermediates (NO_2^- , NO and N_2O) may accumulate due to different environmental factors (Braker et al., 2012).

Denitrification is a cascade process of NO_3^- and NO_2^- reduction to NO, N_2O and N_2 via four enzymatic complexes: NO_3^- reductase, NO_2^- reductase, NO reductase and N_2O reductase (Fig. 19). The first step of denitrification is associated with two homologous enzymes membrane-bound (Nar) and periplasmic-bound (Nap) NO_3^- reductases. The genes coding for these enzymes (*narG* and *napA*, respectively) are also widely present in non-denitrifying bacteria, which reduces the possibility to use them to characterize the activity of denitrifiers (Wallenstein et al., 2006). Consequently, the genes coding for NO_2^- reductase are typically the first ones to be used to characterize denitrifier community (Zeng et al., 2016). NO_2^- reduction is regulated by evolutionary unrelated enzymes: a copper-containing enzyme encoded by *nirK* and a cytochrome cd 1 enzyme encoded by *nirS*, which are functionally equivalent. On the contrary to NO_3^- reductase, bacteria can have only one of these enzymes (Philippot et al., 2007). Studies show that *nirK* bearing organisms are more susceptible to environmental changes than *nirS* denitrifiers (e.g. pH, NH_4^+ and NO_3^- concentrations etc.) (Dandie et al., 2011). Further, reduction of NO to N_2O is mediated by cytochrome *c* nitric oxide reductase and quinol nitric oxide reductase encoded by *norC* and *norB* genes, respectively. The final step of denitrification pathway, reduction of N_2O to N_2 , is catalyzed by the multicopper homodimeric (formed by two identical proteins) N_2O reductase presented by *nosZ* gene. This gene is largely unique to denitrifying bacteria and its activity is the most sensitive to the concentration of oxygen, carbon-to-nitrate ratio and pH in comparison to the other denitrification genes (Cavigelli & Robertson, 2001).



Figure 19. Enzymes used in denitrification and the genes encoding them.

Despite the fact that N-cycle organisms tend to be ubiquitous in groundwater, the functional expression of their genes changes depending on NO_3^- and NH_4^+ supply, availability of C or other electron donors, oxygen concentration, temperature, pH etc. (Rivett et al., 2008; Jahangir et al., 2013; Cocco et al., 2018). The expression (transcription of DNA to RNA) of genes is encoded in their mRNA and its analysis can indicate the actual activity of microbial cells at the time of sampling. So far estimates of gene expression specific to denitrification and nitrification have been carried out mainly during laboratory incubation and microcosm experiments (Freitag & Prosser, 2009; Henderson et al., 2010; Liu et al., 2010; Van Doan et al., 2013). *In situ* field studies are less common and they are mainly focused on soils and sediments (Nogales et al., 2002; Lee et al., 2009; Pastorelli et al., 2010). It is related to the short half-life of long mRNA molecules (close to several minutes), which makes detection of functional gene abilities difficult (Härtig et al., 1999; Rauhut et al., 1999; Philippot et al., 2001). Nevertheless, the information obtained from targeting the mRNAs of nitrifying and denitrifying bacteria can be successfully used in order to reveal the active enzymatic pathways rather than observe mere indication of their presence.

This study focuses on detecting the expression of six genes which can characterize microbial nitrification and denitrification processes: *amoA*, *nirK*, *nirS*, *norB*, *norC*, *nosZ* along the vertical profile of the aquifer (Fig. 19). The following two sections describe the developed procedure for detection of genes expression and discuss the obtained results in the context of N_2O dynamics, respectively.

4.2. Developing experimental design: essential concepts

In our study the bacterial activity is measured by studying its mRNA pool. As was mentioned in the previous section, mRNA carries the coding instruction for protein formation, including enzymes that catalyze biotic reactions. Therefore, the activity of specific bacteria is determined by the presence or absence of certain enzymes in their cells. The availability of enzymes can be measured by targeting directly the specific proteins or indirectly their specific mRNAs.

mRNA is difficult to manipulate and study due to its low stability. Moreover, RNA cannot be amplified by DNA polymerase in polymerase chain reaction (PCR). That is why a DNA copy called complementary DNA (cDNA) of mRNA is required before determining expressions of certain genes. The conversion of mRNA to cDNA is conducted by reverse transcription enzymatic reaction (RT) which uses an RNA template to generate a single-stranded DNA molecule complementary to the RNA (cDNA).

Further analysis of genes requires the use of multiple copies of cDNA sequences, since each gene specific cDNA represents an extremely small fraction in total cDNA. Because each gene is tiny, it has to be amplified before it can be studied. The amplification of a specific segment of cDNA is carried out using polymerase chain reaction (PCR). PCR involves two oligonucleotide primers (short DNA molecules), typically between 18 and 24 nucleotides in length, which are complementary to targeted sequence on template.

PCR test starts with preparing solution that includes cDNA template, Taq DNA polymerase, deoxyribonucleoside triphosphates (dNTPs – the substrates for DNA polymerase), primers and magnesium ions and other salts required for the enzymatic reaction. The PCR test consists of three stages, each of which is performed at different temperatures. In the first stage called denaturation the prepared solution is heated to high degrees (around 94 °C), which leads to the separation of two strands of DNA molecules and production of two single-stranded templates. In the second stage, called annealing, test solution is cooled quickly (up to 30 ° – 60 °C), which allows the primers to bind to the template strands. One of the primers recognizes and binds to one of the target DNA

strands, and the other primer recognizes and binds to the other strand (Fig. 20 (A)). The temperature at which annealing of the primers occurs depends on the size of the primer, its nucleotide content and its affinity for the target sequence. In the last stage, called extension, the solution is heated typically to 72 °C, which is a temperature optimum for Taq DNA polymerase binding to the 3`- ends of each primer and synthesize new cDNA strand in 5` to 3` direction (Fig. 20 (A)). It should be mentioned that Taq DNA polymerase, isolated from *Thermus aquaticus* which is a hyperthermophile bacteria, is resistant to high temperatures. It can withstand the high temperature during denaturation step and remains fully active. At the end of the cycle, two new double-stranded cDNA molecules are produced for each original molecule of targeted cDNA. The whole cycle is repeated several times (usually 30 – 40 cycles in total) to allow the formation of more than 1 billion molecules of cDNA. The results of PCR reaction (PCR products) are placed on agarose gel and submitted to an electrophoresis (Fig. 20 (B)) to visualize the amount of obtained product and examine its homogeneity. If a single, discrete band is formed, it means that the produced cDNA fragment is homogeneous.

This approach allows identifying and comparing gene expression in different environmental samples, but because PCR amplification is exponential, it is important to normalize the concentration of cDNA in samples before the test, because even large differences in targeted concentration (100-fold or more) might result in the same intensity of band after 30 or 40 PCR cycles.

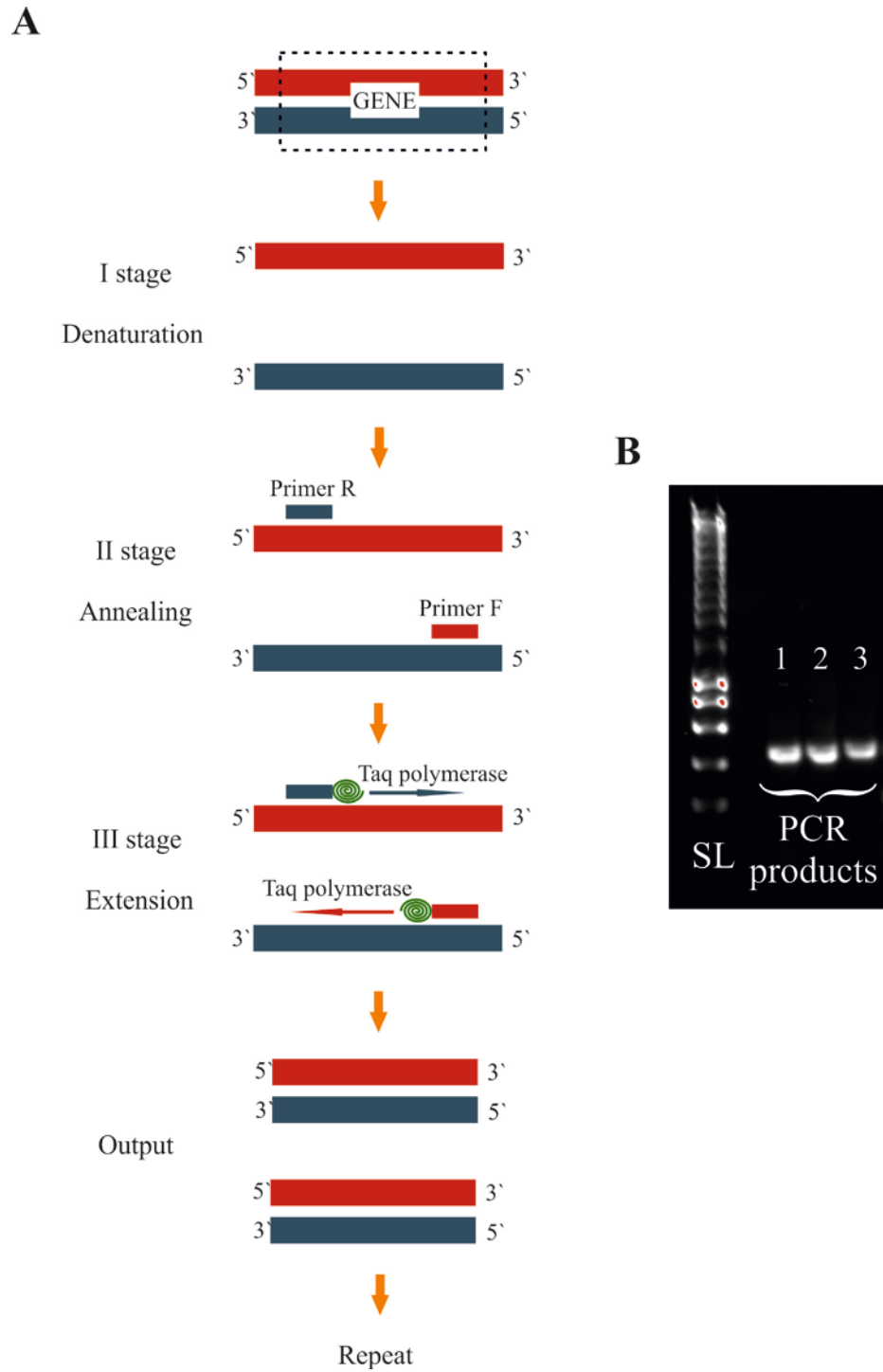


Figure 20. General scheme of ongoing PCR experiment (A) and visual presentation of its results (B): A – stages of PCR experiment; B – comparison of the location of three PCR products with a standard (Smart ladder (SL)).

Further, a DNA sequence resulting from PCR amplification must be determined in order to control that an amplified nucleotide sequence corresponds to a gene sequence initially targeted. DNA sequencing is a method used to identify the sequence of nucleotide bases (adenine (A), thymine (T), cytosine (C) and guanine (G)) in a DNA fragment. Sanger method of DNA sequencing is used for sequencing individual pieces of DNA, such as fragments required in DNA cloning or obtained using PCR. A fragment to be sequenced is replicated, and in order to know an exact composition of a DNA sequence a replication has to be brought to a pre-defined stop that allows identifying the base of the very end of this particular fragment. In order to do it, Sanger method makes use of specific (chain-terminating) nucleotides called dideoxynucleotides (ddNTPs) (Pierce, 2015). The ddNTPs are identical with dNTPs, but with one key difference: they lack a 3` - OH group (Fig. 21). In a regular nucleotide, the 3` - OH group acts as a “hook”, allowing a new nucleotide to be added to an existing chain and thus effectively allowing replication to continue. However, once a dideoxy nucleotide has been added to the DNA chain, there is no OH group available and the polymerase enzyme can no longer add normal nucleotides onto the replicated DNA fragment. The extension is stopped, and it is possible to identify the nucleotide chain terminating base at the end of the fragment. It is done by specific fluorescent dyes of a particular color depending on the base (A, T, C or G) that dideoxy nucleotide carries.

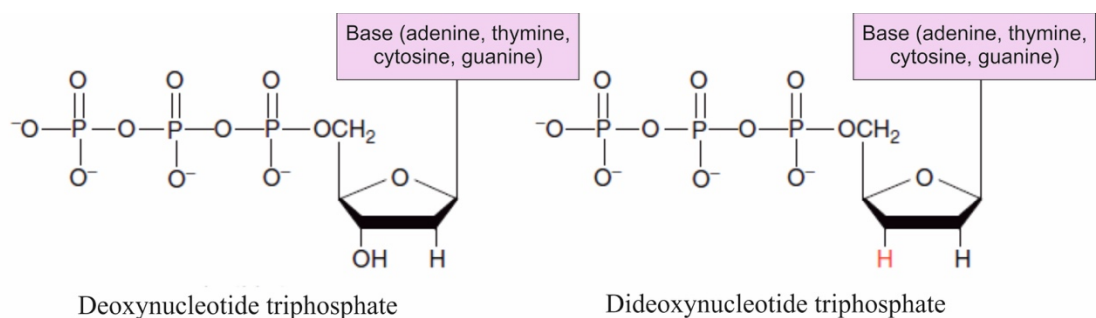


Figure 21. Structures of deoxynucleotide and dideoxynucleotide, the substances required for DNA synthesis during Sanger sequencing reaction.

Sanger sequencing results in the formation of fragments of different lengths terminated with dideoxynucleotides at the 3` ends. The replicated products are then

separated by capillary gel electrophoresis. The reaction product is injected into a long thin tube containing a gel matrix. Short fragments move quickly through the pores of the gel, while long fragments move more slowly. As each fragment crosses the end of the tube, it is illuminated by a laser, allowing the attached dye to be detected. Thus, from the colors of the dyes registered one after another on the detector, the sequence of the original piece of DNA can be built up one nucleotide per one fragment that pass under the laser. In the end, the sequence of the DNA is shown as a series of peaks in fluorescence intensity as shown in the chromatogram below (Fig. 22). The DNA sequence is read from the peaks in the chromatogram.

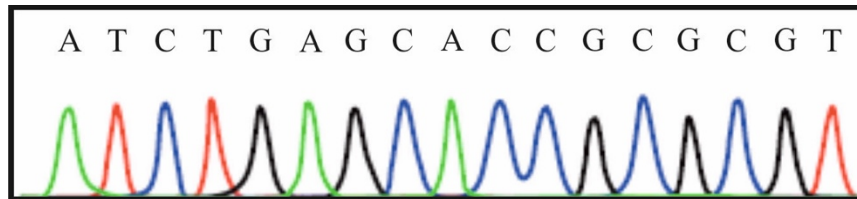


Figure 22. Scheme of computer-generated chromatogram showing obtained sequence after all fragments pass the detector.

4.3. General experimental setup

The general scheme of the experiment which was established in order to detect the activity-specific enzymes of nitrification and denitrification processes is presented on Fig. 23. Groundwater samples for analysis were obtained from different depths from piezometers located at Bovenistier and SGB sites during summer (June 2019) and winter (December 2019) sampling campaigns. Sampling depths can be seen on Fig. 14 in the section 3.1.1 on the page number 105. In total, 18 samples were subjected to the study: 9 of them collected in summer, and other 9 collected in winter (*further to distinguish between summer and winter samples winter ones are going to be indicated with an apostrophe next to them*). In summer 3L of groundwater from each sampling point were filtered through 0.45 μm pore size filters. Winter samples, 5L volume each, were filtered through 0.22 μm filter papers (the sampling procedure was adapted due to the low

biomass in summer). Filters with bacterial biomass were stored in 3 ml of RNA later at -20°C for further manipulations.

RNA and DNA extraction. RNA extraction was conducted using QIAGEN RNeasy® Mini Kit for purification of total RNA from bacteria. The manufacturer's instructions were modified by adding a mixture of phehol/chloroform/isoamylalcohol (25:24:1) during the lysis step to promote better separation of lipids and cellular debris into the organic phase leaving isolated DNA in the aqueous phase. Also, on-column DNase digestion was added to ensure the removal of residual DNA. In the final step, concentrated RNAs were diluted in 80 µL or 40 µL of RNase-free water for summer and winter samples, respectively. As for the total DNA purification, it was conducted using QIAGEN DNeasy PowerMax Soil Kit following the manufacturer's instructions.

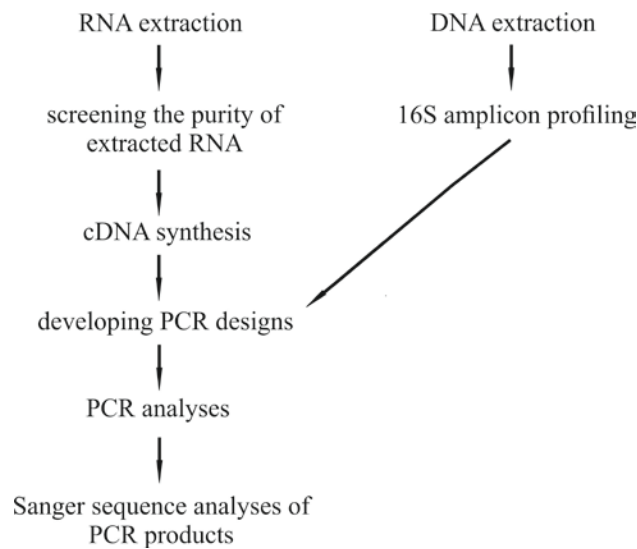


Figure 23. Flow diagrams showing steps conducted to reveal gene expression of nitrifying and denitrifying bacteria in the groundwater samples collected from piezometers screening the chalk aquifer.

The concentrations of extracted RNAs and DNAs were measured using a NanoDrop spectrophotometer (see Table 7).

Table 7. Quantities of RNA and DNA extracted from the biomass obtained from the groundwater samples collected from different depths at the Bovenistier and SGB sites during winter and summer campaigns.

Sample	Summer extraction		Winter extraction	
	Amount of RNA (ng/ μ L)	Amount of DNA (ng/ μ L)	Amount of RNA (ng/ μ L)	Amount of DNA (ng/ μ L)
1	2.5	-	7.1	3.8
2	3.8	-	3.1	4.5
3	3.0	12.3	4.5	1.1
4	3.6	8.9	2.8	1.4
5	6.8	6.7	1.0	2.4
6	13	9.3	2.7	1.9
7	4.8	-	2.2	1.6
8	3.5	-	35.8	13.4
9	59.4	53.6	1.9	1.3

Screening the purity of RNAs isolates. The quality of extracted RNAs is critical for obtaining meaningful information about gene expression from PCR tests. That is why, the purity of RNAs from residual DNA contamination was checked by amplifying 16S rDNA in the RNAs isolates using PCR. Each PCR mixture contained 2 μ L of studied RNA, 0.2 μ L of *Taq* polymerase, 2 μ L of 10 \times *Taq* buffer, 1 μ L of each primer, 1 μ L of deoxynucleoside triphosphates (dNTP), 1.6 μ L of magnesium chloride (MgCl₂), 11.2 μ L of nuclease-free water. Thermal cycling consisted of initial denaturation for 5 min at 94° C, followed by 30 cycles of denaturation at 94° C for 30 sec, annealing at 56° C for 30 sec and extension at 72° C for 1 min. The last step of PCR cycling was final extension at 72° C for 5 min. A positive control containing purified DNA from soil samples was included into PCR experiment along with a negative control (no DNA added). The PCR products were examined on 0.9% agarose gel electrophoresis (see Fig. 24). The results showed absence of DNA in all of the RNAs isolates.



Figure 24. Results of 16S rDNA amplification in groundwater samples. From left to right: a standard (Smart Ladder (SL)), from 1 to 9 groundwater samples collected in summer, 1` to 10` groundwater samples collected in winter, a positive controls (P) and a negative control (N).

In addition, purity of the RNAs was checked by examining A260/A280 ratios received during the measurement of the concentration of RNAs on NanoDrop spectrophotometer in the previous step. For all of the samples the values were ~ 2.0.

cDNA synthesis. The reaction which converts RNA to cDNA is called reverse transcription (RT). Before carrying out RT the concentrations of RNAs were normalized to 30 ng/ μ L for summer samples and to 12 ng/ μ L for winter samples. RT was conducted using QIAGEN QuantiTect[®] Reverse Transcription Kit. At first template RNAs were prepared by elimination of genomic DNAs by adding 2 μ L of gDNA Wipeout Buffer to 12 μ L of normalized RNA solutions and incubating them at 42 °C for 2 min. RT reaction master mixtures were prepared according to the instructions provided by the manufacturer and added to the template RNAs. RT reactions were performed for 30 min at 42 °C, followed by incubation for 3 min at 95 °C. Obtained cDNA were stored at -20 °C until they were used in PCR experiments.

16S Amplicon profiling. In bacteria, 16S rRNA molecules are an essential part of the ribosome (which is the machinery that converts mRNA into proteins) and are thus

ubiquitous. Moreover, its sequence is highly specific to each bacterial clade. It has been thus used for taxonomical purpose for more than 40 years. 16S amplicon profiling is a methodology combining mass amplification of specific part of the 16S rDNA from a pool of total DNA and the mass sequencing of individual amplicon using next-generation sequencer. The resulting sequencing library are then subjected to a bio-informatic treatment and analysis to give a contingency table linking sequence specific taxonomic identification to relative abundance in the sample. In summary, it allows the identification of the major bacterial populations present in any biological sample without relying on actual microbial culture and isolation.

In this study, the 16S bacterial profiles have been obtained from the total DNA extracted from both campaigns. The profiles have been used for a PICRUSt (Phylogenetic Investigation of Communities by Reconstruction of Unobserved States) analysis. In short, this software browses the bacterial genomic information available and tries to identify the populations present in our sample whose genomic content is known. From these specific populations, the program establishes the genome based theoretical metabolic content of each sample. These data have been analyzed to identify the potential (theoretical) distribution of functional genes involved in N-cycle within bacterial species present at each studied location.

Based on the obtained information the most abundant bacteria which possess targeted nitrifying and denitrifying genes were identified (Table 8). During the sequence analysis it was not possible to allocate each identified sequence to the particular bacteria species. Nevertheless, unknown sequences were related to already defined species based on BLAST (Basic Local Alignment Search Tool) similarity analysis.

Table 8. The most abundant nitrifying and denitrifying bacterial genus (species) revealed by means of 16S rRNA sequence analysis and targeted genes present in their genome (some bacteria carry several targeted genes, which explains the repeating records in the table).

Targeted gene	Bacteria genus	The number of sequence in the sample
<i>amoA</i>	<i>Nitrospira</i>	45
<i>nirK</i>	<i>Microbacterium</i>	1117
	<i>Massilia</i>	91
	<i>Undibacterium</i>	136
	<i>Cutibacterium</i>	61
	<i>Burkholderiaceae</i>	64
	<i>Gemmatimonadaceae</i>	80
	<i>Janthinobacterium</i>	39
<i>nirS</i>	<i>Dechlorosoma</i>	204
	<i>Dechloromonas</i>	148
	<i>Burkholderiaceae</i>	54
	<i>Ferribacterium</i>	58
	<i>Gallionellaceae</i>	52
<i>norB</i>	<i>Dechlorosoma</i>	204
	<i>Dechloromonas</i>	148
	<i>Massilia</i>	91
	<i>Undibacterium</i>	136
	<i>Cutibacterium</i>	61
	<i>Burkholderiaceae</i>	64
	<i>Ferribacterium</i>	58
<i>norC</i>	<i>Dechlorosoma</i>	204
	<i>Dechloromonas</i>	148
	<i>Burkholderiaceae</i>	54
	<i>Ferribacterium</i>	58

	<i>Pseudorhodobacter</i>	60
	<i>Gallionella</i>	37
<i>nosZ</i>	<i>Dechlorosoma</i>	204
	<i>Dechloromonas</i>	148
	<i>Gemmatimonadaceae</i>	80
	<i>Burkholderiaceae</i>	54
	<i>Ferribacterium</i>	58
	<i>Burkholderia-Caballeronia-Paraburkholderia</i>	47

PCR design. PCR design includes: 1) development or selection of primers suitable for targeting each studied gene; 2) identification of positive controls; 3) establishing conditions for PCRs that allow optimal amplification of gene sequences.

Primers. Nucleotide sequences of six targeted genes in bacterial species determined by 16S rRNA sequence analyses were searched in Kyoto Encyclopedia of Genes and Genomes (KEGG) database. They were used for developing the primers for PCRs.

Table 9 shows PCR primers used in this study. Primers for the amplification of *amoA* gene were taken based on the previous study (Pjevac et al., 2017). As for the primers used for targeting the denitrifying genes, it was decided to develop them based on the collected nucleotide sequences from KEGG, since there is evidence about high phylogenetic diversity of denitrifiers (Geets et al., 2007, Philippot et al., 2007). Therefore, the selected approach allowed us to be more accurate in selecting primer sequences, since only the target gene sequences extracted from genome knowledge of bacteria present in the samples were aligned to select suitable regions for primers. The sequence alignment was performed using Geneious bioinformatics software platform. Due to significant discrepancies (low level of sequence conservation) in collected gene sequences, in some cases: 1) several sets of primers targeting each gene were developed; 2) some primers were degenerated meaning that some positions of nucleotide bases contain a number of possible bases that allow to encode the consensus sequence of a population of aligned

sequences. Degenerated base symbols in biochemistry can be found in IUPAC (International Union of Pure and Applied Chemistry) notation of nucleotides (Cornish-Bowden, 1985) which provides representation for a position on a DNA sequence that can have multiple possible alternatives. These should not be confused with non-canonical bases because each particular sequence will have in fact one of the regular bases.

Table 9. Primer sets used for PCR analysis. If primers are developed in this study, third column shows entries for nucleotide sequences in KEGG used to develop them.

Gene	Primer set name	Sequence (5' – 3')	Amplicon size (bp)	Reference or Accession code in KEGG
<i>amoA</i>	1) comA 2) comB	1) F: TAYAAYTGGGTSAAAYTA R: ARATCATSGTGCTRTG 2) F: TAYTTCTGGACRTTYTA R: ARATCCARACDGTGTG	415	Pjevac et al. (2017)
<i>nirK</i>	1) nirK_2	1) F: AGTGCCCATGCTCAAAGAGA R : GTGTGGTCTGGTCGAGATG	218	HMPREF0675_3095, TIA2EST2_00450, TIA2EST36_00465, PAZ_c00990, TIB1ST10_0047, PAC1_00475
	2) nirK_3	2) F: TACACCTTCTGGACCTTC R: GATCATGCCGTACATGCC	249	ACZ75_02345, DPH57_05460, CR152_22600
	3) nirK_4	3) F: GTCGCAGCACTTCKCCGACA R: CGATGCCGCCGAGGAASACC	244	AOA12_21000, BOH66_04700
	4) nirK_5	4) F: ATGTACGGCATGATCCTG R: CTCGCCGATGATGTGGAA	255	CNX70_25620, FIQ89_14835, BZG29_25290
<i>nirS</i>	1) nirS_2	1) F: CAGGGCCGTCTGGAAAAGA R: GGAAGCGGAAGTACGGGAAA	306	Daro_3274, , Dsui_3318
	2) nirS_3	2) F: TGGACMTGATGGCSCGCT R: GCCGATCACGAACAGRTA	251	Ajs_1912, AG14_09250, Slit_1129
	3) nirS_5	3) F: AACCTGATCGACCTGTGGAT R: TSCCGGTTTCCTTCACGTT	262	Daro_3323, Dsui_2076

<i>norB</i>	1) norB_3	1) F: TTTGTTTCCTTTTCCAGACCC R: TACGACGAAAGCTACTGCC	220	HMPREF0675_5039, TIA2EST22_09670, PAZ_c20630
	2) norB_4	2) F: ATGACSSGTGTTYGCCTTCAA R: AKGATRGGCATGGYGTAG	216	EAG14_18605, Dsui_3110, Daro_3191, HYN24_04090, EJN92_21015
	3) norB_5	3) F: CCTGTGGCAGATCGGCAA R: CACGCCGCCAGCATGAA	327	Ajs_3435, C380_00925
	4) norB_6	4) F: CGTCAGCCGCACCATMCA R: ACCATGRCGATCAGRCCG	339	ACZ75_02360, DPH57_05475, EJN92_21015
<i>norC</i>	1) norC_2	1) F: GTTCCTTGCGCTGTCATTC R: GCCACGATGGCRTTCAGTT	259	HYN24_04095, Daro_3190, Dsui_3109
	2) norC_3	2) F: CGCAAATCTTYTWCGGMGG R: GSGCRAARTARGCGCCTT	161	EAG14_18600, EOK75_11550, Dsui_3109
<i>nosZ</i>	1) nosZ	1) F : TGGGGMATYACCAAYGARTC R: GVADYTYGRTGATCTTGTCGCA	196	EOK75_06080,B496 6_05785,Dtpsy_1060 ,CBP33_04725,CBP3 4_04685,CBP36_051 50,CBP35_13785,DE H84_05875,EAG14_ 13765

Positive controls. It was possible to select positive controls for *amoA* gene among available soil samples where *Nitrospira* genus was present. For this purpose the RNAs were extracted from soils using QIAGEN RNeasy PowerMicrobiome Kit followed by RT to synthesize cDNA by means of QIAGEN QuantiTect[®] Reverse Transcription Kit applying the instructions of manufacturer. Obtained cDNAs were used in PCR test together with comA and comB primer sets. Each PCR mixture contained 2 μ L of studied cDNA, 0.2 μ L of *Taq* polymerase, 2 μ L of 10 \times *Taq* buffer, 1 μ L of each primer, 1 μ L of deoxynucleoside triphosphates (dNTP), 1.6 μ L of magnesium chloride (MgCl₂), 11.2 μ L of nuclease-free water. Thermal cycling was carried out with initial denaturation for 10 min at 95° C, followed by 40 cycles of denaturation at 95° C for 30 sec, annealing at 52° C for 45 sec and extension at 72° C for 1 min. Cycling was completed by final extension at 72° C for 5 min. The results of PCR test were visualized on 0.9% agarose gel by

electrophoresis (see Fig. 25). The results showed that comB primer set is suitable for spotting *amoA* gene expression in *Nitrospira* in selected soil samples. Therefore, it was decided to use only comB group for identifying *amoA* expression in groundwater sample. Moreover, it was decided to carry out additional PCR test using comB to check if a slight increase in annealing temperature (to 54 °C) and time of electrophoresis will provide better signal of gene expression on agarose gel. Fig. 26 demonstrates the results of this experiment: indeed, the temperature change allowed achieving better output.

At the same time, it was not possible to select positive controls for any of the denitrifying genes, since all of the performed PCRs tests from available soil samples failed to detect their expression. Probably, such results are related to the fact that, as it was mentioned previously, denitrifying bacteria are a very diverse group of organisms, and the selected sets of primers was developed specifically for the bacteria communities established in groundwater of the explored aquifer. Consequently, it is likely that other sets of primers should be selected for the tested soil samples taking into consideration the nucleotide sequences of the bacteria present in them.

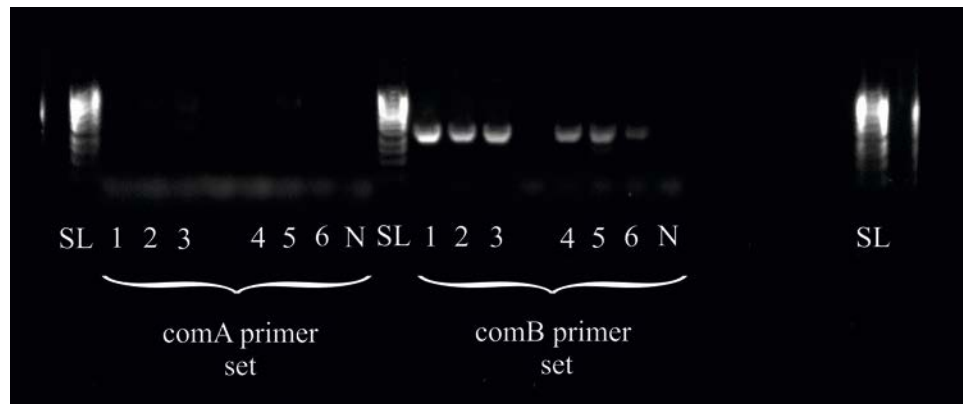


Figure 25. Results of the PCR analysis on three soil samples tested as positive controls. From left to right: a standard (Smart Ladder (SL)), soil cDNAs amplified with comA primer set (first three undiluted, followed by three diluted and negative control (N)), a standard (Smart Ladder (SL)), soil cDNAs amplified with comB primer set (first three undiluted, followed by three diluted and negative control (N)) and a standard (Smart Ladder (SL)).



Figure 26. Results of PCR analysis after the change in annealing temperature on three soil samples tested as positive controls using comB primer set. From left to right: a standard (Smart Ladder (SL)), soil cDNAs (first three undiluted, followed by three diluted) and negative control (N), a standard (Smart Ladder (SL)).

PCR conditions. For detecting of the gene expressions of nitrifying and denitrifying bacteria each PCR mixture contained the same proportions of ingredients: 2 μL of studied cDNA, 0.2 μL of *Taq* polymerase, 2 μL of $10 \times$ *Taq* buffer, 1 μL of each primer, 1 μL of deoxynucleoside triphosphates (dNTP), 1.6 μL of magnesium chloride (MgCl_2), 11.2 μL of nuclease-free water. The results of PCR experiments were examined by electrophoresis on 0.9% agarose gel. The applied conditions of thermal cycling for each gene and corresponding primer sets are summarized in Table 10. Number of cycles is related to the number of the repetitions of denaturation, annealing and extension stages.

Table 10. PCRs conditions used to detect the presence of nitrifying and denitrifying enzymes (T – temperature, t – time).

Gene	Primer set name	Initial denaturation T/t	Denaturation T/t	Annealing T/t	Extension T/t	Number of cycles	Final Extension T/t
<i>amoA</i>	comB	95°C/5min	95°C/30sec	51°C/45sec	72°C/1 min	40	72°C/5min
<i>nirK</i>	nirK_2		56°C/45sec	30			
	nirK_3		51°C/45sec	45			
	nirK_4		65°C/45sec	45			
	nirK_5		51°C/45sec	45			
<i>nirS</i>	nirS_2		57°C/45sec	30			
	nirS_3		57°C/45sec	45			
	nirS_5		56°C/45sec	45			
<i>norB</i>	norB_3		54°C/45sec	45			
	norB_4		56°C/45sec	45			
	norB_5		55°C/45sec	30			
	norB_6		57°C/45sec	45			
<i>norC</i>	norC_2		56°C/45sec	45			
	norC_3		56°C/45sec	45			
<i>nosZ</i>	nosZ		95°C/30sec	51°C/45sec		30	

Sanger sequence analysis of PCR products. The obtained PCR products were purified using Wizard® SV Genomic DNA Purification System. Some of them were purified directly from the PCR solution; however, the majority of PCR products were cut out from the agarose gel due to the occurrence of dimmers (see Annex Text 3 Figures 15 – 29). The concentrations of obtained PCR products were measured and the samples with appropriate values (excluding those exhibiting negative or unexpectedly high values) were prepared for Sanger sequencing. In particular, they were normalized in accordance with their expected amplicon size (1ng/μl for 200 – 500 bp) and sent together with the corresponding primers at the concentration of 5 μM to GIGA University of Liege (Belgium) for Sanger sequence analysis. The required volumes of PCR products and primers were 10 μl each.

4.4. Actual nitrifier and denitrifier enzymatic pathways in the aquifer

The results of PCR tests, followed by sequence analysis of the amplified products, revealed actual denitrification pathway in the studied aquifer. The following section describes the experimental results and discusses the N₂O transformations in subsurface in the investigated aquifer.

Table 11 compares the results of PCR amplification targeting the cDNA of six genes: *amoA*, *nirK*, *nirS*, *norB*, *norC* and *nosZ*, in collected groundwater samples with the results of Sanger sequencing analyses of the respective PCR products. It should be highlighted that PCR reactions were performed with all 15 developed primer sets (Table 9 (pp. 136 – 137)), however, it was not possible to obtain any amplification (or it was too slight and blurred) with 6 of them (*nirK_2*, *nirK_4*, *nirS_2*, *norB_3*, *norB_5* and *norB_6*) (more details in Annex: Text 3, Figures 15 – 29).

In the majority of cases, except *nirS_5*, *nirK_3* and *norC_2*, the produced PCR bands were blurred (occurrence of dimmers). That is why Sanger sequence analysis did not produce high quality chromatograms with defined picks which corresponds for certain nucleotides.

The nucleotide sequence of the different PCR products were compared to GenBank repository using BlastN and BlastX algorithm in order to identify the most similar sequences. The application of BLASTN allows comparing the available nucleotide sequence with the “non-redundant” nucleotide sequence database. BLASTX algorithm translates the DNA query sequence into the 6 possible amino-acid sequences and look for the nearest homolog in the Protein Database. The results of BLAST analysis showed that not all amplified nucleotide sequences corresponded to the targeted DNA (see Annex Table 6). The ones which were revealed as protein-coding for respective genes are marked with red cross in Table 11.

Table 11. Results of PCR and Sanger sequence analysis (SSA) conducted for groundwater samples collected during summer and winter campaigns at Bovenistier and SGB sites (yellow color highlights N₂O production pathway and green color – the presence of N₂O consumption mechanism). *To distinguish between summer and winter samples winter ones are indicated with an apostrophe next to them.*

Location	amoA		nirK_3		nirK_5		nirS_3		nirS_5		norB_4		norC_2		norC_3		nosZ		
	PCR	SSA	PCR	SSA	PCR	SSA	PCR	SSA	PCR	SSA	PCR	SSA	PCR	SSA	PCR	SSA	PCR	SSA	
1 (Pz13)					+	+			+	+	+	+	+					+	+
2 (Pz12 bot)	+																		
3 (Pz12 top)					+	+					+	+							
4 (PzCs bot)					+	+			+	+	+	+	+	+					
5 (PzCs top)									+										
6 (SGB1 bot)					+	+													
7 (SGB1 top)			+	+	+	+					+	+	+	+					
8 (SGB3 bot)			+	+	+	+	+		+	+	+	+	+	+	+				
9 (SGB3 top)					+	+			+	+									
1` (Pz13)	+								+	+	+	+						+	+
2` (Pz12 bot)					+				+		+	+	+	+					
3` (Pz12 top)			+	+							+	+							
4` (PzCs bot)	+				+		+		+	+	+	+				+			

5` (PzCs top)					+	+						+	+	+	+	+			
6` (SGB1 bot)					+														
7` (SGB1 top)	+				+		+					+	+					+	
8` (SGB3 bot)					+		+												
9` (SGB3 top)					+													+	

Despite the fact that it was possible to receive amplification after PCR targeting ammonia oxidizers *amoA* gene, Sanger sequence analysis did not confirm that the amplified nucleotide sequence belongs to it. As for the denitrifying genes, PCRs and Sanger sequence analysis revealed that they are expressed in the majority of studied locations, though not in all locations the sequential denitrification steps from NO_2^- to NO reduction with following production or consumption of N_2O can be confirmed. The presence of both nitrite (*nirK* and/or *nirS*) and nitric oxide (*norB* and/or *norC*) reductases were detected at locations: 3 (Pz12 top), 4 (PzCs bottom), 7 (SGB1 top), 8 (SGB3 bottom) – for summer campaign and 3 (Pz 12 top), 4 (PzCs bottom), 5 (PzCs top) – for winter campaign (Table 11). It means that at these locations N_2O production via the denitrification pathway can be suggested. N_2O production due to NO reduction could occur at location 2` (Pz 12 top), since NO reduction genes (*norB* and *norC*) were expressed there. However, it is difficult to relate N_2O production to particular process, since NO might originate from nitrification (NH_2OH oxidation) and denitrification (NO_2^- reduction) processes occurring in other parts of the aquifer. As for the N_2O consumption, the presence of active *nosZ* gene was observed only at the deepest sampled location 1 (Pz 13) for both summer and winter periods (Table 11).

So occurrence of N_2O production through denitrification pathways can be assumed for most of the studied locations at Bovenistier site. As for the SGB site, N_2O production related to denitrification might occur during summer period. N_2O consumption is sporadic and, most probably, occur only in the deepest parts of the

aquifer. Production of N₂O through ammonia oxidation pathway cannot be confirmed, since Sanger sequence analysis did not show presence of *amoA* gene in amplified PCR products.

Disentangling the N₂O production/consumption dynamics using the results of isotope/isotopomer and microbiological studies. In comparison to isotope and isotopomer studies, microbiological data helped to clarify the missing points in the interpretation of N₂O subsurface dynamics. In particular, based on isotope and hydrochemical data, obtained after vertical examination of the aquifer profile, it was possible only to understand whether the production or consumption of N₂O occurs, while the identification of the processes governing it was still not straightforward. Moreover, even such preliminary conclusions in certain cases were not fully supported by microbiological data. For instance, it was assumed that reduction of N₂O might have occurred at the deep groundwater at SGB site in winter due to the noticeable increase in $\delta^{15}\text{N}^{\alpha}\text{-N}_2\text{O}$ with depth. However, the *nosZ* gene was detected only at the deepest sampled piezometer at Bovenistier. The rest of studied points confirm N₂O production as the dominant process within the aquifer. Moreover, the expression of genes showed that incomplete denitrification (without further reduction of N₂O to N₂) has a potential to produce N₂O within the aquifer profile. This evidence show that aquifers do not only accept, store and transport GHGs but also that the processes occurring in the subsurface affect their production and/or consumption.

The results of tracer experiment, aimed to estimate the magnitude of nitrification and denitrification, partly coincide with obtained evidence of active genes abundance in the aquifer. For instance, both for the points 7 (SGB 1, top level) and 6 (SGB 1) bottom level) where N isotope measurements did not reveal denitrification activity, the actively expressed denitrifiers were also not detected.

At the same time, locations 1 (Pz 13) and 3 (Pz 12 top), which demonstrated potential for denitrification activity based on microbiological studies, did not show any change in $^{15}\text{N}\text{-N}_2\text{O}$ or $^{15}\text{N}\text{-N}_2$ during tracer experiment. It is unclear why it was not possible to detect the occurrence of denitrification by the analysis of isotopic signatures at two latter points, since the results of tracer test for location 4 (PzCs bottom) and 5

(PzCs top) which has a potential for producing N_2O based on microbiological studies, are not available. It might be the case that the experimental design developed for measuring rates of microbiological processes does not capture the complexity of subsurface media where bacteria might be attached to the surface of rocks forming biofilms next to which N transformation occurs. Another reason might be related to the nature of enzymatic reactions which increase in rate until the moment when all enzyme active sites are occupied. Afterwards, the rate of reactions levels off at much lower rate and how fast it comes back to its full extent depends on the frequency at which the enzyme-substrate complex is converted to a product along with the original enzyme. It might be the case that due to the high initial levels of NO_3^- in groundwater the available enzymatic active sites were occupied, which is a reason why it was not possible to detect denitrification activity at locations 1 and 3 within 48 hours experiment. Finally, it is also possible that the rate of denitrification is small enough, which made it difficult to be measured.

In general, it seems that even despite the high level of DO in groundwater, the mechanism triggering denitrification which lead to the production of N_2O exists in the natural aquifer conditions. It is difficult to conclude whether this is related to the occurrence of anaerobic microsites within the aquifer (suggested by many previous studies) or to the ability of bacteria to adapt or switch on protective mechanisms against certain disruptions (e.g. NO_2^-/NO toxicity). However, the SP values, which are assumed to be the most reliable evidence of the nature of N_2O transformations, do not support the incomplete denitrification (without further reduction of N_2O to N_2) as a singular process which affects N_2O availability in groundwater. Since the presence of *amoA* gene in the biomass collected from groundwater was not detected, it suggests the production of N_2O through nitrification pathway in the unsaturated zone with its following infiltration (in its dissolved form in water) and/or diffusion to the aquifer where the mixing between denitrified and nitrified N_2O occurs. However, to prove this suggestion it is important to conduct additional studies of N_2O transformation and transport within the unsaturated zone as it might be the case that under natural conditions SP values differs from the ones reported mainly based on lab design experiments. Also, it is important to make further isotope and microbiological studies including both unsaturated and saturated zone to

understand where the extent of processes has a pronounced effect on N₂O subsurface availability.

Conclusions

This study collected evidence about the dynamics of GHGs in one of the largest groundwater chalk aquifers under agricultural areas in the Walloon Region (Belgium). A series of field campaigns at regional and local scales as well as laboratory experiments were carried out in order to capture the heterogeneity of aquifer conditions which eventually affect the formation of zones suitable for accumulation of GHGs with particular focus on N₂O. In such a way, it attempted to bridge the gap between the two types of studies of N₂O dynamics in the subsurface represented in the existing body of knowledge: 1) the estimates of the emissions of GHGs in the areas of groundwater discharge without the previous rigorous examination of the potential of these selected areas to produce and release GHGs; and 2) local-scale isolated (point) measurement of the rates of GHGs production and consumption processes. The conducted research activities aimed to evaluate the potential role of aquifers affected by agricultural activities as a source of GHGs emission to the atmosphere and improve the understanding of the impact of the spatial heterogeneity of subsurface media (in both vertical and lateral dimensions) on the dynamics of N₂O production and consumption processes. Also, within the framework of this project measurement of SP values and bacterial mRNA studies were applied as the promising techniques in the field of N cycle studies in order to reveal the nature of N₂O transformations in the subsurface. The application of these experimental methods allowed to evaluate their capability and efficiency for characterization of the peculiarities of N₂O dynamics in subsurface. This information can be used in further studies aiming to model and quantify N₂O fluxes.

The data obtained during the sampling campaigns covering the studied aquifer revealed that the concentration of GHGs in groundwater varied in accordance to the change in hydrogeological conditions and the distribution of anthropogenic and natural N and C sources over the studied aquifer. In the majority of cases groundwater was oversaturated with GHGs in respect to their equilibrium atmosphere concentrations. The concentration of N₂O was the most variable among other GHGs, which is attributed to the fact that its production/consumption pathways are controlled to a large extent by microbiological metabolism the intensity of which varies under different environmental

factors (e.g. presence of enzyme activity inhibitors, availability of substrate etc.). As the amount of N_2O in the groundwater was most responsive against the spatial variations of the aquifer conditions, it becomes evident that the total flux of N_2O originating from the given aquifer is associated with high level of uncertainty, particularly in comparison to the other GHGs. The higher concentrations of N_2O were observed in the unconfined areas with denser human settlement network under which the highest concentrations of NO_3^- in groundwater were detected. On the contrary, the confined areas of the aquifer with lower levels of N input showed the lowest concentration of N_2O . Yet the overall trend remained recognizable and unchanged even under the lower N inputs: in general, N_2O concentrations increased with the rise of concentrations of N compounds. As for the concentration of CO_2 , it did not change significantly in groundwater, which might be explained by equal distribution of organic matter across the studied area and by the fact that the amount of CO_2 dissolved in the groundwater was controlled by the process of dissolution of carbonate minerals which constitute aquifer geology. Finally, the observed tendency towards the accumulation of CH_4 even in oxic subsurface conditions might be related to the presence of natural sources of this gas in the Houiller formation below the aquifer and connected with it through the fracture network.

Since agricultural activities have considerable influence on the concentration of dissolved N_2O in comparison to two other GHGs, it was decided to obtain better insight into its production and consumption pathways within the aquifer. The data obtained from isotopomer and isotope analysis of groundwater collected during the regional sampling campaign was used to build isotope maps which suggested that N_2O availability might be the result of simultaneous occurrence of both nitrification and denitrification processes within the aquifer. Direct measurement of the magnitude of respective processes within the aquifer was not possible for the majority of selected locations due to the high groundwater fluxes. The laboratory bottle incubation experiments conducted with groundwater samples in order to determine the potential rates of nitrification and denitrification did not capture the occurrence of those processes on detectable levels. Initially it appears that such outcome might be related to the fact that N_2O availability in groundwater can be determined by the nitrification and denitrification processes occurring in the unsaturated zone. Alternatively, it might be suggested that there exists a

discrepancy between the real aquifer conditions and laboratory studies which does not allow capturing the processes of N₂O production consumption occurring *in situ*. In particular, such hypothesis is supported with the following observations:

- 1) while the experiment has not detected ongoing denitrification, the only single location among the selected sampling points that exhibited the low DO level (< 1.5 mg/L) also exhibited ambient groundwater SP and $\delta^{15}\text{N-N}_2\text{O}$ values in the ranges typical for complete denitrification (with N₂O reduction);
- 2) microbiological studies detected mRNAs of denitrifiers in biomass obtained from groundwater at the locations sampled for incubation experiment, which is the evidence of active denitrifier genes present in the aquifer. In particular, at the location mentioned above the measurements of isotopomer and isotope signatures demonstrating N₂O reduction coincide with the presence of all enzymes handling denitrification, including N₂O reductase. As for the other locations, in the majority of cases the occurrence of incomplete denitrification leading to N₂O production was supported by the results of conducted mRNAs studies.

Therefore, it appears that the observed isotopic signatures of N₂O in the aquifer are indeed affected by denitrification ongoing in the aquifer, though the bacteria conducting it were not contained in sufficient quantity in the collected samples, since the majority of them might have resided in the biofilm attached to the surface of the rocks constituting the aquifer geology. Taking into account the measurements of ambient SP and $\delta^{15}\text{N-N}_2\text{O}$ values in the studied locations, it appears plausible that the size of bacterial communities as well as reaction rates between the aquifer conditions and during the laboratory experiment could have differed. Since there was no microbiological evidence of nitrification, it might be suggested that this process most probably occurs in the unsaturated zone. However, it should be pointed out that the availability of N₂O might be also governed by abiotic processes which were not considered in the framework of this research.

In the framework of this study isotopomer analysis was applied as a tool to disentangle different processes of N₂O production and consumption. It allowed collecting more information about SP ranges of N₂O under *in situ* conditions and evaluating overall role of this technique in distinguishing N transformation pathways. In most of the cases SP values varied from approximately 10 ‰ to 27 ‰ (mean 20.2 ± 5.0 (n = 25)), which falls out of the ranges reported for nitrification and denitrification processes in other field and laboratory studies. That is why it appears that mixing between those processes affects the SPs of the produced N₂O. Moreover, since high SP values (> 45 ‰) were not detected across the studied aquifer, except one location, N₂O reduction occurrence is not likely, as it is not reflected by the observed N₂O isotopic signatures. This assumption is supported by microbiological studies which demonstrated the presence of enzymatic pathways leading to N₂O production, but not towards its consumption during denitrification in the studied aquifer. The highest SP value of 54‰ was detected in the deeper part of the aquifer characterized with low concentration of DO. At this location N₂O reduction as the final step of denitrification was assumed and further supported with the presence of N₂O reduction enzyme.

While SP values typical for nitrification (from 30 ‰ to 37 ‰) were also detected in collected groundwater samples, the mRNAs studies did not reveal the presence of ammonia oxidizers in collected groundwater samples. Therefore, it might be the case that biotic nitrification which influences SP values occurs in the unsaturated zone or that abiotic nitrification producing same values of SP as biotic one takes place in the studied aquifer. To summarize, it appeared that the solitary application of SP values can provide information regarding the production or consumption of N₂O. Yet in order to identify the processes occurring *in situ* and distinguish between different pathways of N₂O dynamics it necessary to complement its findings with the study of enzyme activities.

To summarize, the results of this study showed that application of isotope/isotopomer mapping approach together with hydrochemical evidence can give the general idea about the nature of processes occurring in the subsurface. However, under the heterogeneous conditions of subsurface the values of SP and N isotope signatures are the result of mixing between continuous transformation and transport processes of N

compounds driven from different sources. The collected experimental evidence suggests that spatial heterogeneity of the aquifer conditions has pronounced impact on the observed isotopic signature. Consequently, it is difficult to make conclusions about the extent of nitrification and denitrification processes based only on the dataset of the obtained isotope and isotopomer values. Under such condition the data obtained from microbiological and *in situ* tracer experiments should be applied to trace N transport and transformation processes between different subsurface compartments (e.g. subsoil, subsoil – bedrock interface, bedrock etc.). Moreover, it is important to emphasize that microbiological findings should not be focused on the evidence of abundance of certain organisms or enzymes, which might be misleading, but rather on determining their actual activity

Perspectives

This project has shown that the simultaneous studies of bacterial activity involved into N transformations and measurements of N isotopes and isotopomers in groundwater samples can significantly improve our understanding on N subsurface dynamics. At the same time, the results obtained based on laboratory incubation N tracer experiments were inconsistent with the results obtained from the analysis of ambient groundwater samples, effectively not allowing to reach a conclusive answer regarding the role of aquifers in N₂O dynamics.

In order to precisely characterize the contribution of subsurface media to the indirect N₂O emissions, it is necessary to compare the magnitude of N transformation processes in different parts of the “soil – unsaturated zone – aquifer” system. The results of current study showed that according to SP values the concentration of N₂O in groundwater is controlled by both production and consumption processes. It is important to understand where exactly these processes take place in order to know which environmental compartment(s) (soil, unsaturated or saturated zones) is (are) contributing most to the produced indirect emissions of N₂O. Based on this information, it will be possible to compare quantitatively N₂O production in unsaturated and saturated zones with soils and to get conclusive evidence about the role of subsurface as indirect source of N₂O emission.

Furthermore, the study of the indirect emissions should be complemented with the investigations of N₂O production and consumption within the riparian zones (the interface between land and a river) and river sediments in the areas of groundwater discharge. These areas are in direct contact with both groundwater and surface water, and processes appearing there are critical in terms of the impact on N₂O concentrations and, eventually, on the emission of this greenhouse gas from aquatic systems to the atmosphere. In particular, it is important to study how the changes of the groundwater table and hydrological regime (high and low discharge) can affect N loading and N transformations within the groundwater-river system, because these changes might cause temporal variability of N₂O emissions to the atmosphere.

The understanding of the dynamics of N₂O production in subsurface should be further enriched by studying its variability in response to the changing N loading. In this regards, it will be crucial to explore the subsurface N₂O fluxes in the areas with similar hydrogeological conditions, but different sources of N input (e.g. application of NO₃⁻ or NH₄⁺ fertilizers) in order to compare which processes (NO₃⁻ or NH₄⁺ transformations) yield higher N₂O concentrations in groundwater and which impact it has on the indirect N₂O emissions.

Finally, it is essential to compare the dynamics of the N₂O fluxes occurring in the contrasting hydrological/meteorological conditions and under different agricultural management practices. The information obtained during such comparative studies can be used to refine the upscaling of point estimates of N compounds concentrations in different environmental compartments by developing the catchment-scale models of the N₂O budget. Such models should be able not only to estimate the relative contribution of different N sources to N₂O concentrations in each environmental compartment, but also to simulate the impact of different N₂O production and consumption processes on N₂O availability.

So far, the existing model allow to estimate the relative contribution of different N sources to N₂O concentrations in various environmental compartments using the isotopic signatures of those sources. However, in order to properly account for the in-situ production and consumption of N₂O in the field, further information is required regarding the dependency of the magnitude of isotope fractionation effects on different factors (e.g. concentration of substrate or electron donors, DO, residence time, pH etc.) and their combinations. For instance, in order to study the variability of isotopic fractionation effects in the laboratory conditions, it will be necessary to imitate aquifer conditions and conduct the incubation experiments with varying environmental parameters (i.e. changing nutrient supply, various pH values, t etc.) in order to measure isotopic fractionation of different N transformations. Such information will be useful for the development of more informative and accurate spatially distributed modelling approaches.

References

- Aelion, C. M., Höhener, P., Hunkeler, D., & Aravena, R. (Eds.). (2009). Environmental isotopes in biodegradation and bioremediation. CRC Press.
- Andalib, M., Nakhla, G., McIntee, E., & Zhu, J. (2011). Simultaneous denitrification and methanogenesis (SDM): Review of two decades of research. *Desalination*, 279(1-3), 1-14.
- Anderson, T. R., Groffman, P. M., Kaushal, S. S., & Walter, M. T. (2014). Shallow groundwater denitrification in riparian zones of a headwater agricultural landscape. *Journal of environmental quality*, 43(2), 732-744.
- Andersen, B. L., Bidoglio, G., Leip, A., & Rembges, D. (1998). A new method to study simultaneous methane oxidation and methane production in soils. *Global Biogeochemical Cycles*, 12(4), 587-594.
- Aravena, R., & Robertson, W. D. (1998). Use of multiple isotope tracers to evaluate denitrification in ground water: study of nitrate from a large-flux septic system plume. *Groundwater*, 36(6), 975-982.
- Arp, D. J., & Stein, L. Y. (2003). Metabolism of inorganic N compounds by ammonia-oxidizing bacteria. *Critical Reviews in Biochemistry and Molecular Biology*, 38(6), 471-495.
- Baily, A., Rock, L., Watson, C.J. & Fenton, O. (2011). Spatial and temporal variations in groundwater nitrate at an intensive dairy farm in south-east Ireland: Insights from stable isotope data. *Agric. Ecosysts. Environ.* 144, 308-318.
- Barnes, R. T., & Raymond, P. A. (2010). Land-use controls on sources and processing of nitrate in small watersheds: insights from dual isotopic analysis. *Ecological Applications*, 20(7), 1961-1978.
- Battin, T. J., Luysaert, S., Kaplan, L. A., Aufdenkampe, A. K., Richter, A., & Tranvik, L. J. (2009). The boundless carbon cycle. *Nature Geoscience*, 2(9), 598.

Beaulieu, J. J., Tank, J. L., Hamilton, S. K., Wollheim, W. M., Hall, R. O., Mulholland, P. J., ... & Dodds, W. K. (2011). Nitrous oxide emission from denitrification in stream and river networks. *Proceedings of the National Academy of Sciences*, 108(1), 214-219.

Beaumont, H. J., Lens, S. I., Reijnders, W. N., Westerhoff, H. V., & Van Spanning, R. J. (2004). Expression of nitrite reductase in *Nitrosomonas europaea* involves NsrR, a novel nitrite-sensitive transcription repressor. *Molecular microbiology*, 54(1), 148-158.

Bedard-Haughn A., A., van Groenigen J. W. & van Kessel C. (2003). Tracing ^{15}N through the landscapes: potential uses and precautions. *J. Hydrol.* 272, 175–190.

Bell, R. A., Darling, W. G., Ward, R. S., Basava-Reddi, L., Halwa, L., Manamsa, K., & Dochartaigh, B. Ó. (2017). A baseline survey of dissolved methane in aquifers of Great Britain. *Science of the Total Environment*, 601, 1803-1813.

Bernhard, A. (2012). The nitrogen cycle: Processes, players, and human impact. *Nature Education Knowledge*, 3(10), 25.

Bernstein, L., Bosch, P., Canziani, O., Chen, Z., Christ, R., & Riahi, K. (2008). *IPCC, 2007: climate change 2007: synthesis report*. IPCC.

Bedard-Haughn A., A., van Groenigen J. W. & van Kessel C. (2003). Tracing ^{15}N through the landscapes: potential uses and precautions. *J. Hydrol.* 272, 175–190.

Bock, E., Schmidt, I., Stuvén, R., Zart, D. (1986). Cell biology of nitrifying bacteria. In: Prosser, J. I. (Ed.), *Nitrification*. Special Publications of the Society of General Microbiology 20, 17-38.

De Boer, W., & Kowalchuk, G. A. (2001). Nitrification in acid soils: micro-organisms and mechanisms. *Soil Biology and Biochemistry*, 33(7), 853-866.

Borges, A. V., Darchambeau, F., Teodoru, C. R., Marwick, T. R., Tamoo, F., Geeraert, N., ... & Okuku, E. (2015). Globally significant greenhouse-gas emissions from African inland waters. *Nature Geoscience*, 8(8), 637.

Boulvain, F., & Pingot, J. L. (2008). Une introduction à la géologie de la Wallonie.

Böhlke, J. K. (2002). Groundwater recharge and agricultural contamination. *Hydrogeology Journal*, 10(1), 153-179.

Böhlke, J. K., Smith, R. L., & Miller, D. N. (2006). Ammonium transport and reaction in contaminated groundwater: Application of isotope tracers and isotope fractionation studies. *Water resources research*, 42(5).

Böttcher, J., Strebel, O., Voerkelius, S., & Schmidt, H. L. (1990). Using isotope fractionation of nitrate-nitrogen and nitrate-oxygen for evaluation of microbial denitrification in a sandy aquifer. *Journal of Hydrology*, 114(3-4), 413-424.

Braker, G., Dörsch, P., & Bakken, L. R. (2012). Genetic characterization of denitrifier communities with contrasting intrinsic functional traits. *FEMS microbiology ecology*, 79(2), 542-554.

Brandes, J. A., & Devol, A. H. (2002). A global marine-fixed nitrogen isotopic budget: Implications for Holocene nitrogen cycling. *Global Biogeochemical Cycles*, 16(4).

Bremner, J. M. (1965). Inorganic forms of nitrogen. *Methods of soil analysis. Part 2. Chemical and microbiological properties*, (methodsofsoilanb), 1179-1237.

Bremner, J. M., & Edwards, A. P. (1965). Determination and isotope-ratio analysis of different forms of nitrogen in soils: I. Apparatus and procedure for distillation and determination of ammonium. *Soil Science Society of America Journal*, 29(5), 504-507.

Brennkmeijer, C., A., M. & Röckmann, T. (1999). Mass spectrometry of the intramolecular nitrogen isotope distribution of environmental nitrous oxide using fragment-ion analysis. *Rapid Commun Mass Spectrom* 13. 2028–2033.

Brouyère, S., Dassargues, A., & Hallet, V. (2004). Migration of contaminants through the unsaturated zone overlying the Hesbaye chalky aquifer in Belgium: a field investigation. *Journal of Contaminant Hydrology*, 72(1-4), 135-164.

Brouyère, S., Battle-Aguilar, J., Goderniaux, P., & Dassargues, A. (2008). A new tracer technique for monitoring groundwater fluxes: The Finite Volume Point Dilution Method. *Journal of contaminant hydrology*, 95(3-4), 121-140.

Bunnell-Young, D., Rosen, T., Fisher, T. R., Moorshead, T., & Koslow, D. (2017). Dynamics of nitrate and methane in shallow groundwater following land use conversion from agricultural grain production to conservation easement. *Agriculture, Ecosystems & Environment*, 248, 200-214.

Burgin, A. J., & Hamilton, S. K. (2007). Have we overemphasized the role of denitrification in aquatic ecosystems? A review of nitrate removal pathways. *Frontiers in Ecology and the Environment*, 5(2), 89-96.

Buss, S. R., Herbert, A. W., Morgan, P., Thornton, S. F., & Smith, J. W. N. (2004). A review of ammonium attenuation in soil and groundwater. *Quarterly Journal of Engineering Geology and Hydrogeology*, 37(4), 347-359.

Butterbach-Bahl, K., & Well, R. (2010). Indirect emissions of nitrous oxide from nitrogen deposition and leaching of agricultural nitrogen. In *Nitrous Oxide and Climate Change*(pp. 166-193). Routledge.

Casciotti, K. L., McIlvin, M., & Buchwald, C. (2010). Oxygen isotopic exchange and fractionation during bacterial ammonia oxidation. *Limnology and Oceanography*, 55(2), 753-762.

Casciotti, K. L., Sigman, D. M., & Ward, B. B. (2003). Linking diversity and stable isotope fractionation in ammonia-oxidizing bacteria. *Geomicrobiology Journal*, 20(4), 335-353.

Casciotti, K. L., Sigman, D. M., Hastings, M. G., Böhlke, J. K., & Hilkert, A. (2002). Measurement of the oxygen isotopic composition of nitrate in seawater and freshwater using the denitrifier method. *Analytical Chemistry*, 74(19), 4905-4912.

Cavigelli, M. A., & Robertson, G. P. (2001). Role of denitrifier diversity in rates of nitrous oxide consumption in a terrestrial ecosystem. *Soil Biology and Biochemistry*, 33(3), 297-310.

Choi, W. J., Lee, S. M., & Ro, H. M. (2003). Evaluation of contamination sources of groundwater NO₃⁻ using nitrogen isotope data: a review. *Geosciences Journal*, 7(1), 81-87.

Choi, W. J., Han, G. H., Lee, S. M., Lee, G. T., Yoon, K. S., Choi, S. M., & Ro, H. M. (2007). Impact of land-use types on nitrate concentration and $\delta^{15}\text{N}$ in unconfined groundwater in rural areas of Korea. *Agriculture, ecosystems & environment*, 120(2), 259-268.

Choi, B. Y., Yun, S. T., Mayer, B., Chae, G. T., Kim, K. H., Kim, K., & Koh, Y. K. (2010). Identification of groundwater recharge sources and processes in a heterogeneous alluvial aquifer: results from multi-level monitoring of hydrochemistry and environmental isotopes in a riverside agricultural area in Korea. *Hydrological processes*, 24(3), 317-330.

Clagnan, E., Thornton, S. F., Rolfe, S. A., Tuohy, P., Peyton, D., Wells, N. S., & Fenton, O. (2018). Influence of artificial drainage system design on the nitrogen attenuation potential of gley soils: Evidence from hydrochemical and isotope studies under field-scale conditions. *Journal of Environmental Management*, 206, 1028-1038.

Clark, I. (2015). Contaminant Geochemistry and Isotopes. In *Groundwater Geochemistry and Isotopes*. Boca Raton, FL: Taylor & Francis Group, LLC

Clough, T. J., Sherlock, R. R., & Rolston, D. E. (2005). A review of the movement and fate of N₂O in the subsoil. *Nutrient Cycling in Agroecosystems*, 72(1), 3-11.

Clough, T. J., Addy, K., Kellogg, D. Q., Nowicki, B. L., Gold, A. J., & Groffman, P. M. (2007). Dynamics of nitrous oxide in groundwater at the aquatic–terrestrial interface. *Global Change Biology*, 13, 1528-1537.

Cocco, E., Bertora, C., Squartini, A., Delle Vedove, G., Berti, A., Grignani, C., ... & Morari, F. (2018). How shallow water table conditions affect N₂O emissions and associated microbial abundances under different nitrogen fertilisations. *Agriculture, Ecosystems & Environment*, 261, 1-11.

Cole, M. L., Kroeger, K. D., McClelland, J. W., & Valiela, I. (2006). Effects of watershed land use on nitrogen concentrations and δ^{15} nitrogen in groundwater. *Biogeochemistry*, 77(2), 199-215.

Cooper, R. J., Wexler, S. K., Adams, C. A., & Hiscock, K. M. (2017). Hydrogeological Controls on Regional-Scale Indirect Nitrous Oxide Emission Factors for Rivers. *Environmental Science & Technology*, 51(18), 10440-10448.

Cornish-Bowden, A. (1985). Nomenclature for incompletely specified bases in nucleic acid sequences: recommendations 1984. *Nucleic acids research*, 13(9), 3021.

Currell, M., Banfield, D., Cartwright, I., & Cendón, D. I. (2017). Geochemical indicators of the origins and evolution of methane in groundwater: Gippsland Basin, Australia. *Environmental Science and Pollution Research*, 24(15), 13168-13183.

Curtin, D., Campbell, C. A., & Jalil, A. (1998). Effects of acidity on mineralization: pH-dependence of organic matter mineralization in weakly acidic soils. *Soil Biology and Biochemistry*, 30(1), 57-64.

Daims, H., Lebedeva, E. V., Pjevac, P., Han, P., Herbold, C., Albertsen, M., ... & Kirkegaard, R. H. (2015). Complete nitrification by *Nitrospira* bacteria. *Nature*, 528(7583), 504.

Daims, Holger, Sebastian Lückner, and Michael Wagner. "A new perspective on microbes formerly known as nitrite-oxidizing bacteria." *Trends in microbiology* 24.9 (2016): 699-712.

Dandie, C. E., Wertz, S., Leclair, C. L., Goyer, C., Burton, D. L., Patten, C. L., ... & Trevors, J. T. (2011). Abundance, diversity and functional gene expression of denitrifier communities in adjacent riparian and agricultural zones. *FEMS microbiology ecology*, *77*(1), 69-82.

Danielescu, S., & MacQuarrie, K. T. (2013). Nitrogen and oxygen isotopes in nitrate in the groundwater and surface water discharge from two rural catchments: implications for nitrogen loading to coastal waters. *Biogeochemistry*, *115*(1-3), 111-127.

Dann, R., Thomas, S., Waterland, H., Flintoft, M., & Close, M. (2013). Nitrate and nitrous oxide dynamics under urine application in an alluvial gravel vadose zone. *Vadose Zone Journal*, *12*(1).

Dautrebande, S., & Sohier, C. (2004). Modélisation hydrologique des sols et des pratiques agricoles en Région wallonne (Sous-bassins de la Meuse et de l'Escaut). Faculté des Sciences Agronomiques de Gembloux, Unité d'Hydraulique Agricole.

Denman, S. E., Tomkins, N. W., & McSweeney, C. S. (2007). Quantitation and diversity analysis of ruminal methanogenic populations in response to the antimethanogenic compound bromochloromethane. *FEMS microbiology ecology*, *62*(3), 313-322.

Deurer, M., Von der Heide, C., Böttcher, J., Duijnisveld, W. H. M., Weymann, D., & Well, R. (2008). The dynamics of N₂O near the groundwater table and the transfer of N₂O into the unsaturated zone: A case study from a sandy aquifer in Germany. *Catena*, *72*(3), 362-373.

Di, H. J., & Cameron, K. C. (2002). Nitrate leaching in temperate agroecosystems: sources, factors and mitigating strategies. *Nutrient cycling in agroecosystems*, *64*(3), 237-256.

Di Lorenzo, T., Brilli, M., Del Tosto, D., Galassi, D.M.P. & Petitta, M. (2012). Nitrate source and fate at the catchment scale of the Vibrata River and aquifer (central Italy): an analysis by integrating component approaches and nitrogen isotopes. *Environ. Earth Sci.* *67*, 2383–2398.

Directive, N. (1991). Council Directive 91/676/EEC of 12 December 1991 concerning the protection of waters against pollution caused by nitrates from agricultural sources. *Official Journal L*, 375(31), 12.

Durka, W., Schulze, E. D., Gebauer, G., & Voerkelius, S. (1994). Effects of forest decline on uptake and leaching of deposited nitrate determined from (15) N and (18) O measurements. *Nature*, 372(6508), 765.

Einsiedl, F., & Mayer, B. (2006). Hydrodynamic and microbial processes controlling nitrate in a fissured-porous karst aquifer of the Franconian Alb, Southern Germany. *Environmental science & technology*, 40(21), 6697-6702.

Feast, N.A., Hiscock, K.M., Dennis, P.F. & Andrews, J.N. (1998). Nitrogen isotope hydrochemistry and denitrification within the Chalk aquifer system of north Norfolk, UK. *J. Hydrol.* 211, 233–252.

Fewtrell, L. (2004). Drinking-water nitrate, methemoglobinemia, and global burden of disease: a discussion. *Environmental health perspectives*, 1371-1374.

Fitts, C. R. (2002). *Groundwater science*. Elsevier.

Fogg, G. E., Rolston, D. E., Decker, D. L., Louie, D. T., & Grismer, M. E. (1998). Spatial variation in nitrogen isotope values beneath nitrate contamination sources. *Ground water*, 36(3), 418-426.

Foley, J. A., DeFries, R., Asner, G. P., Barford, C., Bonan, G., Carpenter, S. R., ... & Helkowski, J. H. (2005). Global consequences of land use. *science*, 309(5734), 570-574.

Freitag, T. E., & Prosser, J. I. (2009). Correlation of methane production and functional gene transcriptional activity in a peat soil. *Appl. Environ. Microbiol.*, 75(21), 6679-6687.

Fukada, T., Hiscock, K. M., Dennis, P. F., & Grischek, T. (2003). A dual isotope approach to identify denitrification in groundwater at a river-bank infiltration site. *Water Research*, 37(13), 3070-3078.

Fu, M. H., Xu, X. C., & Tabatabai, M. A. (1987). Effect of pH on nitrogen mineralization in crop-residue-treated soils. *Biology and Fertility of Soils*, 5(2), 115-119.

Gamble, A., & Babbar-Sebens, M. (2012). On the use of multivariate statistical methods for combining in-stream monitoring data and spatial analysis to characterize water quality conditions in the White River Basin, Indiana, USA. *Environmental monitoring and assessment*, 184(2), 845-875.

Gautam S. & Iqbal M.Z., (2010). Using stable isotopes of nitrogen to study its source and transformation in a heavily farmed watershed. *Environ Earth Sci.* 60, 11–20.

Geets, J., De Cooman, M., Wittebolle, L., Heylen, K., Vanparrys, B., De Vos, P., ... & Boon, N. (2007). Real-time PCR assay for the simultaneous quantification of nitrifying and denitrifying bacteria in activated sludge. *Applied microbiology and biotechnology*, 75(1), 211-221.

Goderniaux, P., Brouyere, S., Blenkinsop, S., Burton, A., Fowler, H. J., Orban, P., & Dassargues, A. (2011). Modeling climate change impacts on groundwater resources using transient stochastic climatic scenarios. *Water Resources Research*, 47(12).

Goldberg, S. D., Knorr, K. H., & Gebauer, G. (2008). N₂O concentration and isotope signature along profiles provide deeper insight into the fate of N₂O in soils. *Isotopes in environmental and health studies*, 44(4), 377-391.

Granger, J., & Wankel, S. D. (2016). Isotopic overprinting of nitrification on denitrification as a ubiquitous and unifying feature of environmental nitrogen cycling. *Proceedings of the National Academy of Sciences*, 113(42), E6391-E6400.

Hakoun, V., Orban, P., Dassargues, A., & Brouyère, S. (2017). Factors controlling spatial and temporal patterns of multiple pesticide compounds in groundwater (Hesbaye chalk aquifer, Belgium). *Environmental Pollution*, 223, 185-199.

Hallet, V. (1998). Etude de la contamination de la nappe aquifere de Hesbaye par les nitrates: hydrogéologie, hydrochimie et modélisation mathématique des écoulements et du transport en milieu saturé (Contamination of the Hesbaye aquifer by nitrates:

hydrogeology, hydrochemistry and mathematical modeling). French, PhD Thesis, University of Liege, Faculty of Sciences.

Hamilton, E. I. (1988). European community's atlas of groundwater resources: Verlag Th. Schäfer GmbH, Hannover, 1982. Price: DM196. 00 (General Survey); DM986. 00 (complete edition—nine volumes).

Hama, T., Miyazaki, T., Ogawa, Y., Iwakuma, T., Takahashi, M., Otsuki, A., & Ichimura, S. (1983). Measurement of photosynthetic production of a marine phytoplankton population using a stable ^{13}C isotope. *Marine Biology*, 73(1), 31-36.

Härtig, E., & Zumft, W. G. (1999). Kinetics of nirS expression (cytochrome c d 1 nitrite reductase) in *Pseudomonas stutzeri* during the transition from aerobic respiration to denitrification: evidence for a denitrification-specific nitrate- and nitrite-responsive regulatory system. *Journal of Bacteriology*, 181(1), 161-166.

Hasegawa, K., Hanaki, K., Matsuo, T., & Hidaka, S. (2000). Nitrous oxide from the agricultural water system contaminated with high nitrogen. *Chemosphere-Global Change Science*, 2(3), 335-345.

Hayes, J. M. (2004). An introduction to isotopic calculations. *Woods Hole Oceanographic Institution, Woods Hole, MA, 2543*.

Hernández-del Amo, E., Menció, A., Gich, F., Mas-Pla, J., & Bañeras, L. (2018). Isotope and microbiome data provide complementary information to identify natural nitrate attenuation processes in groundwater. *Science of The Total Environment*, 613, 579-591.

Henderson, S. L., Dandie, C. E., Patten, C. L., Zebarth, B. J., Burton, D. L., Trevors, J. T., & Goyer, C. (2010). Changes in denitrifier abundance, denitrification gene mRNA levels, nitrous oxide emissions, and denitrification in anoxic soil microcosms amended with glucose and plant residues. *Appl. Environ. Microbiol.*, 76(7), 2155-2164.

Hérivaux, C., Orban, P., & Brouyère, S. (2013). Is it worth protecting groundwater from diffuse pollution with agri-environmental schemes? A hydro-economic modeling approach. *Journal of environmental management*, 128, 62-74.

Hinkle, S.R., Böhlke, J.K., Duff, J.H., Morgan, D.S. & Weick, R.J. (2007). Aquifer-scale controls on the distribution of nitrate and ammonium in ground water near La Pine, Oregon, USA. *J. Hydrol.* 333, 486–503.

Hiscock, K.M., Bateman, A.S., Muhlherr, I.H., Fukada, T., Dennis, P.F. (2003). Indirect emissions of nitrous oxide from regional aquifers in the United Kingdom. *Environ. Sci. Technol.* 37 (16), 3507–3512.

Hoefs, J., & Hoefs, J. (2015). *Stable isotope geochemistry* (Seventh edition). Switzerland: springer.

Hosono, T., Tokunaga, T., Kagabu, M., Nakata, H., Orishikida, T., Lin, I.-T. & Shimada, J. (2013). The use of $\delta^{15}\text{N}$ and $\delta^{18}\text{O}$ tracers with an understanding of groundwater flow dynamics for evaluating the origins and attenuation mechanisms of nitrate pollution. *Water Res.* 47, 2661–2675.

IPCC, 2013: Climate Change 2013: The Physical Science Basis. Contribution of Working Group I to the Fifth Assessment Report of the Intergovernmental Panel on Climate Change [Stocker, T.F., D. Qin, G.-K. Plattner, M. Tignor, S.K. Allen, J. Boschung, A. Nauels, Y. Xia, V. Bex and P.M. Midgley (eds.)]. Cambridge University Press, Cambridge, United Kingdom and New York, NY, USA, 1535 pp, doi:10.1017/CBO9781107415324.

Istok, J. D. (2012). Push-pull tests for site characterization (Vol. 144). Springer Science & Business Media.

Iverach, C. P., Beckmann, S., Cendón, D. I., Manefield, M., & Kelly, B. F. (2017). Biogeochemical constraints on the origin of methane in an alluvial aquifer: evidence for the upward migration of methane from underlying coal measures. *Biogeosciences*, 14(1), 215-228.

Jamin, P., & Brouyère, S. (2018). Monitoring transient groundwater fluxes using the finite volume point dilution method. *Journal of contaminant hydrology*, 218, 10-18.

Jahangir, M. M., Khalil, M. I., Johnston, P., Cardenas, L. M., Hatch, D. J., Butler, M., ... & Richards, K. G. (2012). Denitrification potential in subsoils: a mechanism to reduce nitrate leaching to groundwater. *Agriculture, Ecosystems & Environment*, 147, 13-23.

Jahangir, M. M. R., Johnston, P., Barret, M., Khalil, M. I., Groffman, P. M., Boeckx, P., ... Richards K. G. (2013). Denitrification and indirect N₂O emissions in groundwater: hydrologic and biogeochemical influences. *Journal of Contaminant Hydrology*, 152, 70-81.

JHU AAP. (2010, July 29). *NCBI Blast Tutorial*. [Video]. YouTube. <https://www.youtube.com/watch?v=HXEpBnUbAMo&gl=BE>.

Jin, Y. H., Kawamura, A., Park, S. C., Nakagawa, N., Amaguchi, H., & Olsson, J. (2011). Spatiotemporal classification of environmental monitoring data in the Yeongsan River basin, Korea, using self-organizing maps. *Journal of Environmental Monitoring*, 13(10), 2886-2894.

Jin, R. C., Yang, G. F., Yu, J. J., & Zheng, P. (2012). The inhibition of the Anammox process: a review. *Chemical Engineering Journal*, 197, 67-79.

Johnson, M. S., Lehmann, J., Riha, S. J., Krusche, A. V., Richey, J. E., Ometto, J. P. H., & Couto, E. G. (2008). CO₂ efflux from Amazonian headwater streams represents a significant fate for deep soil respiration. *Geophysical Research Letters*, 35(17).

Jurado, A., Borges, A. V., & Brouyère, S. (2017). Dynamics and emissions of N₂O in groundwater: A review. *Science of the Total Environment*, 584, 207-218.

Jurado, A., Borges, A. V., Pujades, E., Briers, P., Nikolenko, O., Dassargues, A., & Brouyère, S. (2018a). Dynamics of greenhouse gases in the river-groundwater interface in a gaining river stretch (Triffoy catchment, Belgium). *Hydrogeology journal*, 26(8), 2739-2751.

Jurado, A., Borges, A. V., Pujades, E., Hakoun, V., Otten, J., Knöller, K., & Brouyère, S. (2018b). Occurrence of greenhouse gases in the aquifers of the Walloon Region (Belgium). *Science of the Total Environment*, 619, 1579-1588.

Kaushal, S. S., Groffman, P. M., Band, L. E., Elliott, E. M., Shields, C. A., & Kendall, C. (2011). Tracking nonpoint source nitrogen pollution in human-impacted watersheds. *Environmental science & technology*, 45(19), 8225-8232.

Kellman, L. M., & Hillaire-Marcel, C. (2003). Evaluation of nitrogen isotopes as indicators of nitrate contamination sources in an agricultural watershed. *Agriculture, ecosystems & environment*, 95(1), 87-102.

Kendall, C. (1998). Tracing nitrogen sources and cycling in catchments. In "Isotope Tracers in Catchment Hydrology", Kendall y McDonnell (eds.) 521–576.

Kendall, C., & Aravena, R. (2000). Nitrate isotopes in groundwater systems. In *Environmental tracers in subsurface hydrology* (pp. 261-297). Springer US.

Kendall, C., & Grim, E. (1990). Combustion tube method for measurement of nitrogen isotope ratios using calcium oxide for total removal of carbon dioxide and water. *Analytical Chemistry*, 62(5), 526-529.

Kellman, L. M., & Hillaire-Marcel, C. (2003). Evaluation of nitrogen isotopes as indicators of nitrate contamination sources in an agricultural watershed. *Agriculture, ecosystems & environment*, 95(1), 87-102.

Kelso, B., et al. "Dissimilatory nitrate reduction in anaerobic sediments leading to river nitrite accumulation." *Applied and Environmental Microbiology* 63.12 (1997): 4679-4685.

Keuskamp, J. A., Van Drecht, G., & Bouwman, A. F. (2012). European-scale modelling of groundwater denitrification and associated N₂O production. *Environmental pollution*, 165, 67-76.

Kim, O. S., Junier, P., Imhoff, J. F., & Witzel, K. P. (2008). Comparative analysis of ammonia monooxygenase (amoA) genes in the water column and sediment–water interface of two lakes and the Baltic Sea. *FEMS microbiology ecology*, 66(2), 367-378.

Kindler, R., Siemens, J., Kaiser, K., Walmsley, D. C., Bernhofer, C., Buchmann, ... Kaupenjohann, M. (2011). Dissolved carbon leaching from soil is a crucial component of the net ecosystem carbon balance. *Global Change Biology*, 17(2), 1167-1185.

Knowles, R. (2000). Nitrogen cycle. *Encyclopedia of microbiology*. Academic Press, San Diego.

Knöller, K., Vogt, C., Haupt, M., Feisthauer, S., & Richnow, H. H. (2011). Experimental investigation of nitrogen and oxygen isotope fractionation in nitrate and nitrite during denitrification. *Biogeochemistry*, 103(1-3), 371-384.

Knöller, K., Trettin, R., & Strauch, G. (2005). Sulphur cycling in the drinking water catchment area of Torgau–Mockritz (Germany): insights from hydrochemical and stable isotope investigations. *Hydrological Processes*, 19(17), 3445-3465.

Koba, K., Osaka, K., Tobar, Y., Toyoda, S., Ohte, N., Katsuyama, M., ... & Kim, S. J. (2009). Biogeochemistry of nitrous oxide in groundwater in a forested ecosystem elucidated by nitrous oxide isotopomer measurements. *Geochimica et Cosmochimica Acta*, 73(11), 3115-3133.

Koch, H., van Kessel, M. A., & Lüscher, S. (2019). Complete nitrification: insights into the ecophysiology of comammox *Nitrospira*. *Applied microbiology and biotechnology*, 103(1), 177-189.

Kohonen, T. (2001). Self-organizing maps, ser. Information Sciences. Berlin: Springer, 30.

Kool, D. M., Dolfing, J., Wrage, N., & Van Groenigen, J. W. (2011). Nitrifier denitrification as a distinct and significant source of nitrous oxide from soil. *Soil Biology and Biochemistry*, 43(1), 174-178.

Kool, D. M., Wrage, N., Oenema, O., Van Kessel, C., & Van Groenigen, J. W. (2011). Oxygen exchange with water alters the oxygen isotopic signature of nitrate in soil ecosystems. *Soil Biology and Biochemistry*, 43(6), 1180-1185.

Koops, H. P., & Pommerening-Röser, A. (2001). Distribution and ecophysiology of the nitrifying bacteria emphasizing cultured species. *FEMS Microbiology ecology*, 37(1), 1-9.

Korom, S. F. (1992). Natural denitrification in the saturated zone: a review. *Water resources research*, 28(6), 1657-1668.

Kozłowski, J. A., Kits, K. D., & Stein, L. Y. (2016). Comparison of nitrogen oxide metabolism among diverse ammonia-oxidizing bacteria. *Frontiers in microbiology*, 7, 1090.

Krebs, J. E., Goldstein, E. S., & Kilpatrick, S. T. (2017). *Lewin's Genes XII*. Jones & Bartlett Learning.

Krouse, H. R., & Mayer, B. (2000). Sulphur and oxygen isotopes in sulphate. In *Environmental tracers in subsurface hydrology* (pp. 195-231). Springer, Boston, MA.

Kroeze, C., Dumont, E., & Seitzinger, S. P. (2005). New estimates of global emissions of N₂O from rivers and estuaries. *Environmental Sciences*, 2(2-3), 159-165.

Kuenen, J.G. (2008). Anammox bacteria: From discovery to application. *Nature Reviews/Microbiology* 6: 320–326.

Kuzyakov, Y., & Larionova, A. A. (2005). Root and rhizomicrobial respiration: a review of approaches to estimate respiration by autotrophic and heterotrophic organisms in soil. *Journal of Plant Nutrition and Soil Science*, 168(4), 503-520. Laini, A., Bartoli, M., Castaldi, S., Viaroli, P., Capri, E., & Trevisan, M. (2011). Greenhouse gases (CO₂, CH₄ and N₂O) in lowland springs within an agricultural impacted watershed (Po River Plain, northern Italy). *Chemistry and Ecology*, 27(2), 177-187.

Laini, A., Bartoli, M., Castaldi, S., Viaroli, P., Capri, E., & Trevisan, M. (2011). Greenhouse gases (CO₂, CH₄ and N₂O) in lowland springs within an agricultural

impacted watershed (Po River Plain, northern Italy). *Chemistry and Ecology*, 27(2), 177-187.

Ledoux, E., Gomez, E., Monget, J. M., Viavattene, C., Viennot, P., Ducharme, A., ... & Mary, B. (2007). Agriculture and groundwater nitrate contamination in the Seine basin. The STICS–MODCOU modelling chain. *Science of the total environment*, 375(1), 33-47.

Lee, S. W., Im, J., DiSpirito, A. A., Bodrossy, L., Barcelona, M. J., & Semrau, J. D. (2009). Effect of nutrient and selective inhibitor amendments on methane oxidation, nitrous oxide production, and key gene presence and expression in landfill cover soils: characterization of the role of methanotrophs, nitrifiers, and denitrifiers. *Applied microbiology and biotechnology*, 85(2), 389-403.

Lewicka-Szczebak, D., Augustin, J., Giesemann, A., & Well, R. (2017). Quantifying N₂O reduction to N₂ based on N₂O isotopocules-validation with independent methods (helium incubation and ¹⁵N gas flux method). *Biogeosciences*, 14(3), 711.

Li, L., Spoelstra, J., Robertson, W. D., Schiff, S. L., & Elgood, R. J. (2014). Nitrous oxide as an indicator of nitrogen transformation in a septic system plume. *Journal of hydrology*, 519, 1882-1894.

Li, Y., Liu, Y., Wang, Y., Niu, L., Xu, X., & Tian, Y. (2014). Interactive effects of soil temperature and moisture on soil N mineralization in a *Stipa krylovii* grassland in Inner Mongolia, China. *Journal of Arid Land*, 6(5), 571-580.

Li, S., Liu, C., Lang, Y., Zhao, Z., Zhou, Z. (2010). Tracing the sources of nitrate in karstic groundwater in Zunyi, Southwest China: a combined nitrogen isotope and water chemistry approach. *Environmental Earth Sciences* 60, 1415–1423.

Li, X.D., Masuda, H., Koba, K., Zeng, H.A. (2007). Nitrogen isotope study on nitrate-contaminated groundwater in the Sichuan Basin, China. *Water Air Soil Pollut.* 178, 145–156.

Li, X., Tang, C., Han, Z., Jingqiu, P., Yingjie, C., & Chipeng, Z. (2014). Spatial and seasonal variation of dissolved nitrous oxide in wetland groundwater. *Environment and Pollution*, 3(1), 21.

Liu, C. Q., Li, S. L., Lang, Y. C., Xiao H. Y. (2006). Using $\delta^{15}\text{N}$ and $\delta^{18}\text{O}$ values to identify nitrate sources in karst ground water, Guiyang, Southwest China. *Environ. Sci. Technol.* 40, 6928–6933.

Liu, B., Mørkved, P. T., Frostegård, Å., & Bakken, L. R. (2010). Denitrification gene pools, transcription and kinetics of NO, N₂O and N₂ production as affected by soil pH. *FEMS microbiology ecology*, 72(3), 407-417.

Di Lorenzo, T., Brilli, M., Del Tosto, D., Galassi, D. M., & Petitta, M. (2012). Nitrate source and fate at the catchment scale of the Vibrata River and aquifer (central Italy): an analysis by integrating component approaches and nitrogen isotopes. *Environmental Earth Sciences*, 67(8), 2383-2398.

MacQuarrie, K. T., Sudicky, E. A., & Robertson, W. D. (2001). Multicomponent simulation of wastewater-derived nitrogen and carbon in shallow unconfined aquifers: II. Model application to a field site. *Journal of Contaminant Hydrology*, 47(1), 85-104.

Macpherson, G. L. (2009). CO₂ distribution in groundwater and the impact of groundwater extraction on the global C cycle. *Chemical Geology*, 264(1-4), 328-336.

Maeda, K., Toyoda, S., Yano, M., Hattori, S., Fukasawa, M., Nakajima, K., & Yoshida, N. (2016). Isotopically enriched ammonium shows high nitrogen transformation in the pile top zone of dairy manure compost. *Biogeosciences*, 13(4), 1341-1349.

Mariotti, A., Landreau, A., Simon, B. (1988). N isotope biogeochemistry and natural denitrification process in groundwater – application to the chalk aquifer of northern France. *Geochim Cosmochim Acta.* 52, 1869–187.

Mariotti, A., Germon, J. C., Hubert, P., Kaiser, P., Letolle, R., Tardieux, A., & Tardieux, P. (1981). Experimental determination of nitrogen kinetic isotope fractionation:

some principles; illustration for the denitrification and nitrification processes. *Plant and soil*, 62(3), 413-430.

Mayer, B., Fritz, P., Prietzel, J., & Krouse, H. R. (1995). The use of stable sulfur and oxygen isotope ratios for interpreting the mobility of sulfate in aerobic forest soils. *Applied geochemistry*, 10(2), 161-173.

Mayer, B., Bollwerk, S. M., Mansfeldt, T., Hütter, B., & Veizer, J. (2001). The oxygen isotope composition of nitrate generated by nitrification in acid forest floors. *Geochimica et Cosmochimica Acta*, 65(16), 2743-2756.

Mayer, B., Boyer, E. W., Goodale, C., Jaworski, N. A., Van Breemen, N., Howarth, R. W., ... & Van Dam, D. (2002). Sources of nitrate in rivers draining sixteen watersheds in the northeastern US: Isotopic constraints. In *The nitrogen cycle at regional to global scales* (pp. 171-197). Springer Netherlands.

Mayer, B. (2005). Assessing sources and transformations of sulphate and nitrate in the hydrosphere using isotope techniques. In *Isotopes in the Water Cycle* (pp. 67-89). Springer Netherlands.

Mayer, A., Hausfather, Z., Jones, A. D., & Silver, W. L. (2018). The potential of agricultural land management to contribute to lower global surface temperatures. *Science Advances*, 4(8), eaaq0932.

McAleer, E. B., Coxon, C. E., Richards, K. G., Jahangir, M. M. R., Grant, J., & Mellander, P. E. (2017). Groundwater nitrate reduction versus dissolved gas production: A tale of two catchments. *Science of The Total Environment*, 586, 372-389.

McIlvin, M. R., & Altabet, M. A. (2005). Chemical conversion of nitrate and nitrite to nitrous oxide for nitrogen and oxygen isotopic analysis in freshwater and seawater. *Analytical Chemistry*, 77(17), 5589-5595.

McMahon, P. B., & Böhlke, J. K. (2006). Regional patterns in the isotopic composition of natural and anthropogenic nitrate in groundwater, High Plains, USA. *Environmental science & technology*, 40(9), 2965-2970.

Michener, R. & Lajtha, K. (2007). Tracing anthropogenic inputs of nitrogen to ecosystems. In Kendall, C., Elliott, E., M. & Wankel, S., D. (Eds), *Stable Isotopes in Ecology and Environmental Science* (2nd ed.) (pp. 375-449). Carlton, Victoria: Blackwell Publishing Ltd.

Minamikawa, K., Nishimura, S., Sawamoto, T., Nakajima, Y., & Yagi, K. (2010). Annual emissions of dissolved CO₂, CH₄, and N₂O in the subsurface drainage from three cropping systems. *Global change biology*, 16(2), 796-809.

Minamikawa, K., Nishimura, S., Nakajima, Y., Osaka, K. I., Sawamoto, T., & Yagi, K. (2011). Upward diffusion of nitrous oxide produced by denitrification near shallow groundwater table in the summer: a lysimeter experiment. *Soil Science and Plant Nutrition*, 57(5), 719-732.

Minet, E. P., Goodhue, R., Meier-Augenstein, W., Kalin, R. M., Fenton, O., Richards, K. G., & Coxon, C. E. (2017). Combining stable isotopes with contamination indicators: A method for improved investigation of nitrate sources and dynamics in aquifers with mixed nitrogen inputs. *Water research*, 124, 85-96.

Molofsky, L. J., Connor, J. A., Wylie, A. S., Wagner, T., & Farhat, S. K. (2013). Evaluation of methane sources in groundwater in northeastern Pennsylvania. *Groundwater*, 51(3), 333-349.

Molofsky, L. J., Connor, J. A., McHugh, T. E., Richardson, S. D., Woroszylo, C., & Alvarez, P. J. (2016). Environmental factors associated with natural methane occurrence in the Appalachian Basin. *Groundwater*, 54(5), 656-668.

Moore, C. H., & Wade, W. J. (2013). Concepts of Sequence Stratigraphy as Applied to Carbonate Depositional Systems. In *Carbonate reservoirs: Porosity and diagenesis in a sequence stratigraphic framework* (Vol. 67). (pp.19-36). Newnes.

Moore, K. B., Ekwurzel, B., Esser, B. K., Hudson, G. B., & Moran, J. E. (2006). Sources of groundwater nitrate revealed using residence time and isotope methods. *Applied Geochemistry*, 21(6), 1016-1029.

Morana, C., Darchambeau, F., Roland, F. A. E., Borges, A. V., Muvundja, F., Kelemen, Z., ... & Bouillon, S. (2015). Biogeochemistry of a large and deep tropical lake (Lake Kivu, East Africa: insights from a stable isotope study covering an annual cycle. *Biogeosciences*, 12(16), 4953-4963.

Mosier, A., Kroeze, C., Nevison, C., Oenema, O., Seitzinger, S., & Van Cleemput, O. (1998). Closing the global N₂O budget: nitrous oxide emissions through the agricultural nitrogen cycle. *Nutrient cycling in Agroecosystems*, 52(2-3), 225-248.

Mosier, A. R., & Schimel, D. S. (1993). Nitrification and denitrification. In *Nitrogen isotope techniques* (pp. 181-208). Academic Press.

Nikolenko, O., Jurado, A., Borges, A. V., Knöller, K., & Brouyère, S. (2017). Isotopic composition of nitrogen species in groundwater under agricultural areas: A review. *Science of The Total Environment*.

Nogales, B., Timmis, K. N., Nedwell, D. B., & Osborn, A. M. (2002). Detection and diversity of expressed denitrification genes in estuarine sediments after reverse transcription-PCR amplification from mRNA. *Appl. Environ. Microbiol.*, 68(10), 5017-5025.

Norton, J. M., Alzerreca, J. J., Suwa, Y., & Klotz, M. G. (2002). Diversity of ammonia monooxygenase operon in autotrophic ammonia-oxidizing bacteria. *Archives of microbiology*, 177(2), 139-149.

Odu, C. T. I., and K. B. Adeoye. "Heterotrophic nitrification in soils—A preliminary investigation." *Soil Biology and Biochemistry* 2.1 (1970): 41-45.

Okito, A., Alves, B. R. J., Urquiaga, S., & Boddey, R. M. (2004). Isotopic fractionation during N₂ fixation by four tropical legumes. *Soil Biology and Biochemistry*, 36(7), 1179-1190.

Orban, P., J. Batlle-Aguilar, P. Goderniaux, A. Dassargues, and S. Brouyère (2006), Description of hydrogeological conditions in the Geer sub-catchment and

synthesis of available data for groundwater modelling, Deliverable R3.16, AquaTerra (Integrated Project FP6 505428).

Orban, P., Brouyère, S., Batlle-Aguilar, J., Couturier, J., Goderniaux, P., Leroy, M., ... & Dassargues, A. (2010). Regional transport modelling for nitrate trend assessment and forecasting in a chalk aquifer. *Journal of contaminant hydrology*, 118(1-2), 79-93.

Organisation of Economic Co-operation and Development. (2009). OECD environmental performance reviews of Ireland, conclusions and recommendations (pp. 2-18). Paris: Organisation of Economic Co-operation and Development.

Ostrom, N. E., Knoke, K. E., Hedin, L. O., Robertson, G. P., Smucker, A. J. M. (1998). Temporal trends in nitrogen isotopes values of nitrate leaching from an agricultural soil. *Chem. Geol.* 146, 219-227.

Ostrom, N. E., Pitt, A., Sutka, R., Ostrom, P. H., Grandy, A. S., Huizinga, K. M., & Robertson, G. P. (2007). Isotopologue effects during N₂O reduction in soils and in pure cultures of denitrifiers. *Journal of Geophysical Research: Biogeosciences*, 112(G2).

Otero, N., Torrentó, C., Soler, A., Menció, A., & Mas-Pla, J. (2009). Monitoring groundwater nitrate attenuation in a regional system coupling hydrogeology with multi-isotopic methods: the case of Plana de Vic (Osona, Spain). *Agriculture, ecosystems & environment*, 133(1), 103-113.

Park, S., Pérez, T., Boering, K. A., Trumbore, S. E., Gil, J., Marquina, S., & Tyler, S. C. (2011). Can N₂O stable isotopes and isotopomers be useful tools to characterize sources and microbial pathways of N₂O production and consumption in tropical soils?. *Global Biogeochemical Cycles*, 25(1).

Pastorelli, R., Piccolo, R., Cocco, S., & Landi, S. (2010). mRNA recovery and denitrification gene expression in clay-soil bacterial communities under different agricultural managements. *Agrochimica*, 54(3), 179-192.

Peeters, L., Bacao, R., Lobo, V., & Dassargues, A. (2007). Exploratory data analysis and clustering of multivariate spatial hydrogeological data by means of GEO3DSOM, a variant of Kohonen's Self-Organizing Map. *Hydrology and Earth System Sciences*, 11(4), 1309-1321.

Petitta, M., Fracchiolla, D., Aravena, R., & Barbieri, M. (2009). Application of isotopic and geochemical tools for the evaluation of nitrogen cycling in an agricultural basin, the Fucino Plain, Central Italy. *Journal of hydrology*, 372(1), 124-135.

Philippot, L., Mirleau, P., Mazurier, S., Siblot, S., Hartmann, A., Lemanceau, P., & Germon, J. C. (2001). Characterization and transcriptional analysis of *Pseudomonas fluorescens* denitrifying clusters containing the nar, nir, nor and nos genes. *Biochimica et Biophysica Acta (BBA)-Gene Structure and Expression*, 1517(3), 436-440.

Philippot, L., & Hallin, S. (2005). Finding the missing link between diversity and activity using denitrifying bacteria as a model functional community. *Current opinion in microbiology*, 8(3), 234-239.

Philippot, L., Hallin, S., & Schloter, M. (2007). Ecology of denitrifying prokaryotes in agricultural soil. *Advances in agronomy*, 96, 249-305.

Pierce, B. A. (2015). *Genetics essentials: Concepts and connections*. Macmillan Higher Education.

Pjevac, P., Schauburger, C., Poghosyan, L., Herbold, C. W., Van Kessel, M. A., Daebeler, A., ... & Daims, H. (2017). AmoA-targeted polymerase chain reaction primers for the specific detection and quantification of comammox Nitrospira in the environment. *Frontiers in microbiology*, 8, 1508.

Pommerening-Röser, A., Rath, G., & Koops, H. P. (1996). Phylogenetic diversity within the genus *Nitrosomonas*. *Systematic and Applied Microbiology*, 19(3), 344-351.

Rauhut, R., & Klug, G. (1999). mRNA degradation in bacteria. *FEMS microbiology reviews*, 23(3), 353-370.

Reay, D. S., Davidson, E. A., Smith, K. A., Smith, P., Melillo, J. M., Dentener, F., & Crutzen, P. J. (2012). Global agriculture and nitrous oxide emissions. *Nature climate change*, 2(6), 410-416.

Reece, R. J. (2004). *Analysis of genes and genomes* (pp. 88-95). Hoboken, NJ: John Wiley & Sons.

Ritchie, H., & Roser, M. (2020). Environmental impacts of food production. *Our World in Data*.

Rivett, M. O., Buss, S. R., Morgan, P., Smith, J. W., & Bemment, C. D. (2008). Nitrate attenuation in groundwater: a review of biogeochemical controlling processes. *Water research*, 42(16), 4215-4232.

Robertson, W. D., Moore, T. A., Spoelstra, J., Li, L., Elgood, R. J., Clark, I. D., ... & Neufeld, J. D. (2012). Natural attenuation of septic system nitrogen by anammox. *Groundwater*, 50(4), 541-553.

Rosamond, M. S. (2013). N₂O and NO₃⁻ in the Grand River: Sources, production pathways and predictability (Doctoral dissertation, Dissertation. University of Waterloo).

Robertson, G. P., & Vitousek, P. M. (2009). Nitrogen in agriculture: balancing the cost of an essential resource. *Annual Review of Environment and Resources*, 34, 97-125.

Robinson, D. (2001). $\delta^{15}\text{N}$ as an integrator of the nitrogen cycle. *Trends in Ecology & Evolution*, 16(3), 153-162.

Rütting, T., Boeckx, P., Müller, C., & Klemmedtsson, L. (2011). Assessment of the importance of dissimilatory nitrate reduction to ammonium for the terrestrial nitrogen cycle. *Biogeosciences*, 8(7), 1779-1791.

Savard, M. M., Somers, G., Smirnov, A., Paradis, D., van Bochove, E., & Liao, S. (2010). Nitrate isotopes unveil distinct seasonal N-sources and the critical role of crop residues in groundwater contamination. *Journal of hydrology*, 381(1), 134-141.

Schmidt, H. L., Werner, R. A., Yoshida, N., & Well, R. (2004). Is the isotopic composition of nitrous oxide an indicator for its origin from nitrification or denitrification? A theoretical approach from referred data and microbiological and enzyme kinetic aspects. *Rapid Communications in Mass Spectrometry*, 18(18), 2036-2040.

Schimel, J. P., & Bennett, J. (2004). Nitrogen mineralization: challenges of a changing paradigm. *Ecology*, 85(3), 591-602.

Serrano-Silva, N., Sarria-Guzmán, Y., Dendooven, L., & Luna-Guido, M. (2014). Methanogenesis and methanotrophy in soil: a review. *Pedosphere*, 24(3), 291-307.

Shammas, N. K. (1986). Interactions of temperature, pH, and biomass on the nitrification process. *Journal (Water Pollution Control Federation)*, 52-59.

Sharp, Z. (2007). Principles of Stable Isotope Geochemistry: Nitrogen. (206-219). Upper Saddle River, NJ: Pearson Prentice Hal.

Sebilo, M., Mayer, B., Nicolardot, B., Pinay, G., & Mariotti, A. (2013). Long-term fate of nitrate fertilizer in agricultural soils. *Proceedings of the National Academy of Sciences*, 110(45), 18185-18189.

Sebilo, M., Billen, G., Mayer, B., Billiou, D., Grably, M., Garnier, J., & Mariotti, A. (2006). Assessing nitrification and denitrification in the Seine River and estuary using chemical and isotopic techniques. *Ecosystems*, 9(4), 564-577.

Sigman, D. M., Casciotti, K. L., Andreani, M., Barford, C., Galanter, M. B. J. K., & Böhlke, J. K. (2001). A bacterial method for the nitrogen isotopic analysis of nitrate in seawater and freshwater. *Analytical chemistry*, 73(17), 4145-4153.

Silva, S. R., Kendall, C., Wilkison, D. H., Ziegler, A. C., Chang, C. C., & Avanzino, R. J. (2000). A new method for collection of nitrate from fresh water and the analysis of nitrogen and oxygen isotope ratios. *Journal of hydrology*, 228(1), 22-36.

Simler, R. (2009). DIAGRAMMES: Logiciel d'hydrochimie multilingue en distribution libre. *Laboratoire d'Hydrogéologie d'Avignon, France*.

- Smith, K. A. (Ed.). (2010). Nitrous oxide and climate change. Earthscan.
- Smith, R. L., Bohlke, J. K., Song, B., & Tobias, C. R. (2015). Role of anaerobic ammonium oxidation (anammox) in nitrogen removal from a freshwater aquifer. *Environmental Science & Technology*, *49*(20), 12169-12177.
- Smith, R. L., Baumgartner, L. K., Miller, D. N., Repert, D. A., & Böhlke, J. K. (2006). Assessment of nitrification potential in ground water using short term, single-well injection experiments. *Microbial Ecology*, *51*(1), 22-35.
- Smith, P., Bustamante, M., Ahammad, H., Clark, H., Dong, H., Elsiddig, E. A., ... & Masera, O. (2014). Agriculture, forestry and other land use (AFOLU). In *Climate change 2014: mitigation of climate change. Contribution of Working Group III to the Fifth Assessment Report of the Intergovernmental Panel on Climate Change* (pp. 811-922). Cambridge University Press.
- Snider, D. M., Schiff, S. L., & Spoelstra, J. (2009). $^{15}\text{N}/^{14}\text{N}$ and $^{18}\text{O}/^{16}\text{O}$ stable isotope ratios of nitrous oxide produced during denitrification in temperate forest soils. *Geochimica et Cosmochimica Acta*, *73*(4), 877-888.
- Snider, D. M., Venkiteswaran, J. J., Schiff, S. L., & Spoelstra, J. (2012). Deciphering the oxygen isotope composition of nitrous oxide produced by nitrification. *Global Change Biology*, *18*(1), 356-370.
- Snider, D. M., Venkiteswaran, J. J., Schiff, S. L., & Spoelstra, J. (2013). A new mechanistic model of $\delta^{18}\text{O}\text{-N}_2\text{O}$ formation by denitrification. *Geochimica et Cosmochimica Acta*, *112*, 102-115.
- Stein, L. Y. (2011). Surveying N_2O -producing pathways in bacteria. In *Methods in enzymology* (Vol. 486, pp. 131-152). Academic press.
- Stenstrom, M. K., & Poduska, R. A. (1980). The effect of dissolved oxygen concentration on nitrification. *Water Research*, *14*(6), 643-649.

Strebel, O. W. H. M., Duynisveld, W. H. M., & Böttcher, J. (1989). Nitrate pollution of groundwater in western Europe. *Agriculture, ecosystems & environment*, 26(3-4), 189-214.

Sutka, R. L., Ostrom, N. E., Ostrom, P. H., Gandhi, H., & Breznak, J. A. (2003). Nitrogen isotopomer site preference of N₂O produced by *Nitrosomonas europaea* and *Methylococcus capsulatus* Bath. *Rapid Communications in Mass Spectrometry*, 17(7), 738-745.

Sutka, R. L., Ostrom, N. E., Ostrom, P. H., Gandhi, H., & Breznak, J. A. (2004). Nitrogen isotopomer site preference of N₂O produced by *Nitrosomonas europaea* and *Methylococcus capsulatus* Bath. *Rapid Communications in Mass Spectrometry*, 18(12), 1411-1412.

Sutka, R. L., Ostrom, N. E., Ostrom, P. H., Breznak, J. A., Gandhi, H., Pitt, A. J., & Li, F. (2006). Distinguishing nitrous oxide production from nitrification and denitrification on the basis of isotopomer abundances. *Applied and environmental microbiology*, 72(1), 638-644.

Sutton, M. A., Howard, C. M., Erisman, J. W., Billen, G., Bleeker, A., Grennfelt, P., ... & Grizzetti, B. (Eds.). (2011). *The European nitrogen assessment: sources, effects and policy perspectives*. Cambridge University Press.

Syakila, A., & Kroeze, C. (2011). The global nitrous oxide budget revisited. *Greenhouse Gas Measurement and Management*, 1(1), 17-26.

Tanaka, N., Rye, D.M., Rye, R., Avak, H. & Yoshinari, T. (1995). High precision mass spectrometric analysis of isotopic abundance ratios in nitrous oxide by direct injection of N₂O. *Int J Mass Spectrom Ion Proc* 142,163–175.

Teh, Y. A., Silver, W. L., & Conrad, M. E. (2005). Oxygen effects on methane production and oxidation in humid tropical forest soils. *Global Change Biology*, 11(8), 1283-1297.

Tesoriero, A. J., Liebscher, H., & Cox, S. E. (2000). Mechanism and rate of denitrification in an agricultural watershed: Electron and mass balance along groundwater flow paths. *Water Resources Research*, 36(6), 1545-1559.

Tian, H., Yang, J., Xu, R., Lu, C., Canadell, J. G., Davidson, E. A., ... & Gerber, S. (2019). Global soil nitrous oxide emissions since the preindustrial era estimated by an ensemble of terrestrial biosphere models: Magnitude, attribution, and uncertainty. *Global change biology*, 25(2), 640-659.

Tomaszewski, M., Cema, G., & Ziemińska-Buczyńska, A. (2017). Influence of temperature and pH on the anammox process: A review and meta-analysis. *Chemosphere*, 182, 203-214.

Toyoda, S. & Yoshida, N. (1999). Determination of nitrogen isotopomers of nitrous oxide on a modified isotope ratio mass spectrometer. *Anal Chem*, 71, 4711-4718.

Toyoda, S., Yoshida, N., & Koba, K. (2015). Isotopocule analysis of biologically produced nitrous oxide in various environments. *Mass spectrometry reviews*.

Tubiello, F. N., Salvatore, M., Rossi, S., Ferrara, A., Fitton, N., & Smith, P. (2013). The FAOSTAT database of greenhouse gas emissions from agriculture. *Environmental Research Letters*, 8(1), 015009.

Tubiello, F. N., Salvatore, M., Ferrara, A. F., House, J., Federici, S., Rossi, S., ... & Prospero, P. (2015). The contribution of agriculture, forestry and other land use activities to global warming, 1990-2012. *Global change biology*, 21(7), 2655-2660.

Ueda, S., Ogura, N., & Wada, E. (1991). Nitrogen stable isotope ratio of groundwater N₂O. *Geophysical Research Letters*, 18(8), 1449-1452.

Van Doan, T., Lee, T. K., Shukla, S. K., Tiedje, J. M., & Park, J. (2013). Increased nitrous oxide accumulation by bioelectrochemical denitrification under autotrophic conditions: kinetics and expression of denitrification pathway genes. *Water Research*, 47(19), 7087-7097.

van Kessel, M. A., Speth, D. R., Albertsen, M., Nielsen, P. H., den Camp, H. J. O., Kartal, B., ... & Lücker, S. (2015). Complete nitrification by a single microorganism. *Nature*, 528(7583), 555-559.

Velinsky, D. J., Pennock, J. R., Sharp, J. H., Cifuentes, L. A., & Fogel, M. L. (1989). Determination of the isotopic composition of ammonium-nitrogen at the natural abundance level from estuarine waters. *Marine Chemistry*, 26(4), 351-361.

Vesanto, J., Himberg, J., Alhoniemi, E., & Parhankangas, J. (2000). SOM toolbox for Matlab 5. Helsinki University of Technology, Finland, 109.

Vidal-Gavilan, G., Folch, A., Otero, N., Solanas, A. M., & Soler, A. (2013). Isotope characterization of an *in situ* biodenitrification pilot-test in a fractured aquifer. *Applied geochemistry*, 32, 153-163.

Viers, J. H., Liptzin, D., Rosenstock, T. S., Jensen, W. B., Hollander, A. D., McNally, A., ... & Fryjoff-Hung, A. (2012). Nitrogen sources and loading to groundwater: technical report 2. *Addressing nitrate in California's drinking water with a focus on Tulare Lake Basin and Salinas Valley groundwater. Report for the State Water Resources Control Board to the Legislature, Center for Watershed Sciences, Univ. of Calif., Davis.*

Vilain, G., Garnier, J., Tallec, G., & Tournebize, J. (2012). Indirect N₂O emissions from shallow groundwater in an agricultural catchment (Seine Basin, France). *Biogeochemistry*, 111, 253-271.

Virginia, R. A., & Delwiche, C. C. (1982). Natural ¹⁵N abundance of presumed N₂-fixing and non-N₂-fixing plants from selected ecosystems. *Oecologia*, 54(3), 317-325.

Vitòria, L., Grandia, F., Soler, A. (2004a). Evolution of the chemical (NH₄) and isotopic ($\delta^{15}\text{N-NH}_4$) composition of pig manure stored in an experimental deep pit. In: International Atomic Energy Agency (Ed.), *Isotope Hydrology and Integrated Water Resources Management. Conf. Symp. Papers, Vienna*, pp. 188–189.

Vitòria, L., Otero, N., Soler, A., & Canals, À. (2004b). Fertilizer characterization: isotopic data (N, S, O, C, and Sr). *Environmental science & technology*, 38(12), 3254-3262.

Vitòria, L., Soler, A., Aravena, R. & Canals, A. (2005). Multi-isotopic approach (^{15}N , ^{13}C , ^{34}S , ^{18}O and D) for tracing agriculture contamination in groundwater (Maresme, NE Spain). In: Lichtfouse, E., Schwarzbauer, J., Robert, D. (Eds.), *Environmental Chemistry*. Springer-Verlag, Heidelberg, 43–56.

Vitòria, L., Soler, A., Canals, À. & Otero, N. (2008). Environmental isotopes (N, S, C, O, D) to determine natural attenuation process in nitrate contaminated waters: Example of Osona (NE Spain). *Applied Geochemistry* 23, 3597–3611.

Voerkelius S (1990) Isotopendiskriminierungen bei der Nitrifikation und Denitrifikation: Grundlagen und Anwendungen der Herkunfts-Zuordnung von Nitrat und Distickstoffmonoxid. PhD thesis TU Munich, Munich, 119.

von der Heide, C., Böttcher, J., Deurer, M., Weymann, D., Well, R., & Duijnsveld, W. H. M. (2008). Spatial variability of N_2O concentrations and of denitrification-related factors in the surficial groundwater of a catchment in Northern Germany. *Journal of Hydrology*, 360, 230-241.

Wallenstein, M. D., Myrold, D. D., Firestone, M., & Voytek, M. (2006). Environmental controls on denitrifying communities and denitrification rates: insights from molecular methods. *Ecological applications*, 16(6), 2143-2152.

Ward, B. B. (1996). Nitrification and denitrification: probing the nitrogen cycle in aquatic environments. *Microbial Ecology*, 32(3), 247-261.

Wassenaar, L. I. (1995). Evaluation of the origin and fate of nitrate in the Abbotsford Aquifer using the isotopes of ^{15}N and ^{18}O in NO_3^- . *Appl. Geochem.* 10, 391–405.

Wassenaar, L. I., Douence, C., Altabet, M. A., & Aggarwal, P. K. (2018). N and O isotope ($\delta^{15}\text{N}_\alpha$, $\delta^{15}\text{N}_\beta$, $\delta^{18}\text{O}$, $\delta^{17}\text{O}$) analyses of dissolved NO_3^- and NO_2^- by the

Cd-azide reduction method and N₂O laser spectrometry. *Rapid Communications in Mass Spectrometry*, 32(3), 184-194.

Welch, A. H., Plume, R. W., Frick, E. A., & Hughes, J. L. (1989). Ground-water-quality assessment of the Carson River basin, Nevada and California; analysis of available water-quality data through 1987 (No. 89-382). US Geological Survey; Books and Open-File Reports Section [distributor].

Well, R., Flessa, H., Jaradat, F., Toyoda, S. & Yoshida, N. (2005). Measurement of isotopomer signatures of N₂O in groundwater. *Journal of Geophysical Research*, 110, G02006.

Well, R., Eschenbach, W., Flessa, H., von der Heide, C. & Weymann, D. (2012). Are dual isotope and isotopomer ratios of N₂O useful indicators for N₂O turnover during denitrification in nitrate-contaminated aquifers? *Geochim. Cosmochim. Acta* 90, 265–282.

Wells, N. S., Hakoun, V., Brouyère, S., & Knöller, K. (2016). Multi-species measurements of nitrogen isotopic composition reveal the spatial constraints and biological drivers of ammonium attenuation across a highly contaminated groundwater system. *Water research*, 98, 363-375.

Wexler, S.K, Hiscock, K.M. & Dennis, P.F. (2011). Catchment-scale quantification of hyporheic denitrification using an isotopic and solute flux approach. *Environ Sci Technol.* 45, 3967–3973.

Weymann, D., Well, R., Flessa, H., von der Heide, C., Deurer, M., Meyer, K., Konrad, C., Walther, W. (2008). Groundwater N₂O emission factors of nitrate-contaminated aquifers as derived from denitrification progress and N₂O accumulation. *Biogeosciences* 5, 1215–1226.

Whiticar, M. J. (1999). Carbon and hydrogen isotope systematics of bacterial formation and oxidation of methane. *Chemical Geology*, 161(1-3), 291-314.

Widory, D., Kloppmann, W., Chery, L., Bonnin, J., Rochdi, H., & Guinamant, J. L. (2004). Nitrate in groundwater: an isotopic multi-tracer approach. *Journal of contaminant hydrology*, 72(1-4), 165-188.

Widory, D., Petelet-Giraud, E., Negrel, P., Ladouche, B. (2005). Tracking the sources of nitrate in groundwater using coupled nitrogen and boron isotopes: A synthesis. *Environmental Science and Technology*. 39(2), 539–548.

Wilcock, R. J., & Sorrell, B. K. (2008). Emissions of greenhouse gases CH₄ and N₂O from low-gradient streams in agriculturally developed catchments. *Water, air, and soil pollution*, 188(1-4), 155-170.

Witter, E., & Lopez-Real, J. (1988). Nitrogen losses during the composting of sewage sludge, and the effectiveness of clay soil, zeolite, and compost in adsorbing the volatilized ammonia. *Biological wastes*, 23(4), 279-294.

World Meteorological Organization, 2018: WMO Greenhouse Gas Bulletin (GHG Bulletin): The state of greenhouse gases in the atmosphere based on global observations through 2017.

World Health Organization. (2008). *Guidelines for drinking-water quality [electronic resource]: incorporating 1st and 2nd addenda, vol. 1, Recommendations*. World Health Organization. Widory, D., Kloppmann, W., Chery, L., Bonnin, J., Rochdi H. & Guinamant J.-L. (2004). Nitrate in groundwater: an isotopic multi-tracer approach. *Journal of Contaminant Hydrology*. 72, 165–188.

Worrall, F., & Lancaster, A. (2005). The release of CO₂ from riverwaters—the contribution of excess CO₂ from groundwater. *Biogeochemistry*, 76(2), 299-317.

Widory, D., Petelet-Giraud, E., Negrel, P., Ladouche, B. (2005). Tracking the sources of nitrate in groundwater using coupled nitrogen and boron isotopes: A synthesis. *Environmental Science and Technology*. 39(2), 539–548.

Williard, K. W., DeWalle, D. R., Edwards, P. J., & Sharpe, W. E. (2001). 18 O isotopic separation of stream nitrate sources in mid-Appalachian forested watersheds. *Journal of Hydrology*, 252(1), 174-188.

Xue, D., Botte, J., De Baets, B., Accoe, F., Nestler, A., Taylor, P., ... & Boeckx, P. (2009). Present limitations and future prospects of stable isotope methods for nitrate source identification in surface-and groundwater. *Water Research*, 43(5), 1159-1170.

Xue, Y., Song, J., Zhang, Y., Kong, F., Wen, M., & Zhang, G. (2016). Nitrate pollution and preliminary source identification of surface water in a semi-arid river basin, using isotopic and hydrochemical approaches. *Water*, 8(8), 328.

Yakovlev, V., Vystavna, Y., Diadin, D., & Vergeles, Y. (2015). Nitrates in springs and rivers of East Ukraine: Distribution, contamination and fluxes. *Applied Geochemistry*, 53, 71-78.

Yoshida N, Matsuo S. (1983). Nitrogen isotope ratio of atmospheric N₂O as a key to the global cycle of N₂O. *Geochem J* 17:231–239.

Young, C., Martin, J. B., & Hanson, G. N. (2016). Controls on nitrous oxide production in, and fluxes from a coastal aquifer in long island, NY, USA. *Journal of Marine Science and Engineering*, 4(4), 71.

Zeng, X., Hosono, T., Ohta, H., Niidome, T., Shimada, J., & Morimura, S. (2016). Comparison of microbial communities inside and outside of a denitrification hotspot in confined groundwater. *International Biodeterioration & Biodegradation*, 114, 104-109.

Zhu, X., Burger, M., Doane, T. A., & Horwath, W. R. (2013). Ammonia oxidation pathways and nitrifier denitrification are significant sources of N₂O and NO under low oxygen availability. *Proceedings of the National Academy of Sciences*, 110(16), 6328-6333.

Zhu, X., Zhao, D., Pan, Z., Zhang, W., & Ruan, X. (2019, July). Characteristics of an aerobic denitrifier isolated from unconfined aquifer. In *IOP Conference Series: Earth and Environmental Science* (Vol. 300, No. 5, p. 052009). IOP Publishing.

Zou, Y., Hirono, Y., Yanai, Y., Hattori, S., Toyoda, S., & Yoshida, N. (2014). Isotopomer analysis of nitrous oxide accumulated in soil cultivated with tea (*Camellia sinensis*) in Shizuoka, central Japan. *Soil Biology and Biochemistry*, *77*, 276-291.

Annex

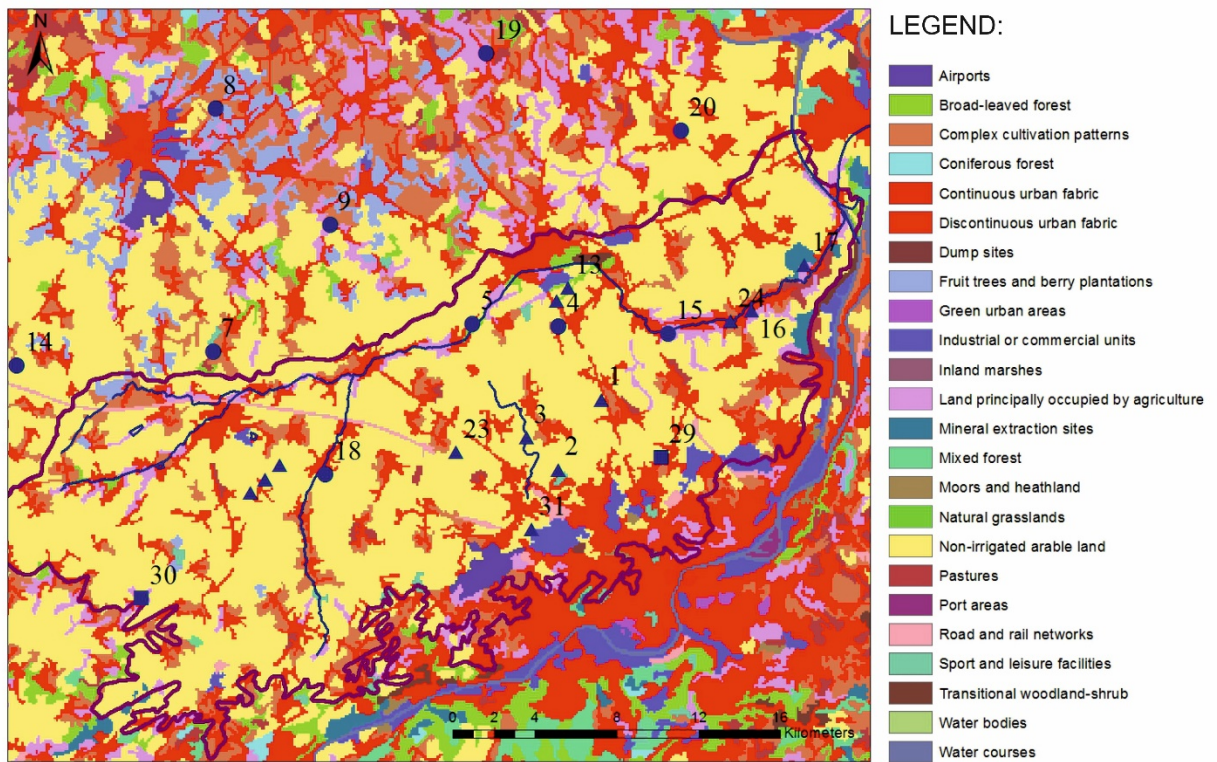


Figure 1. Land use map of the studied area.

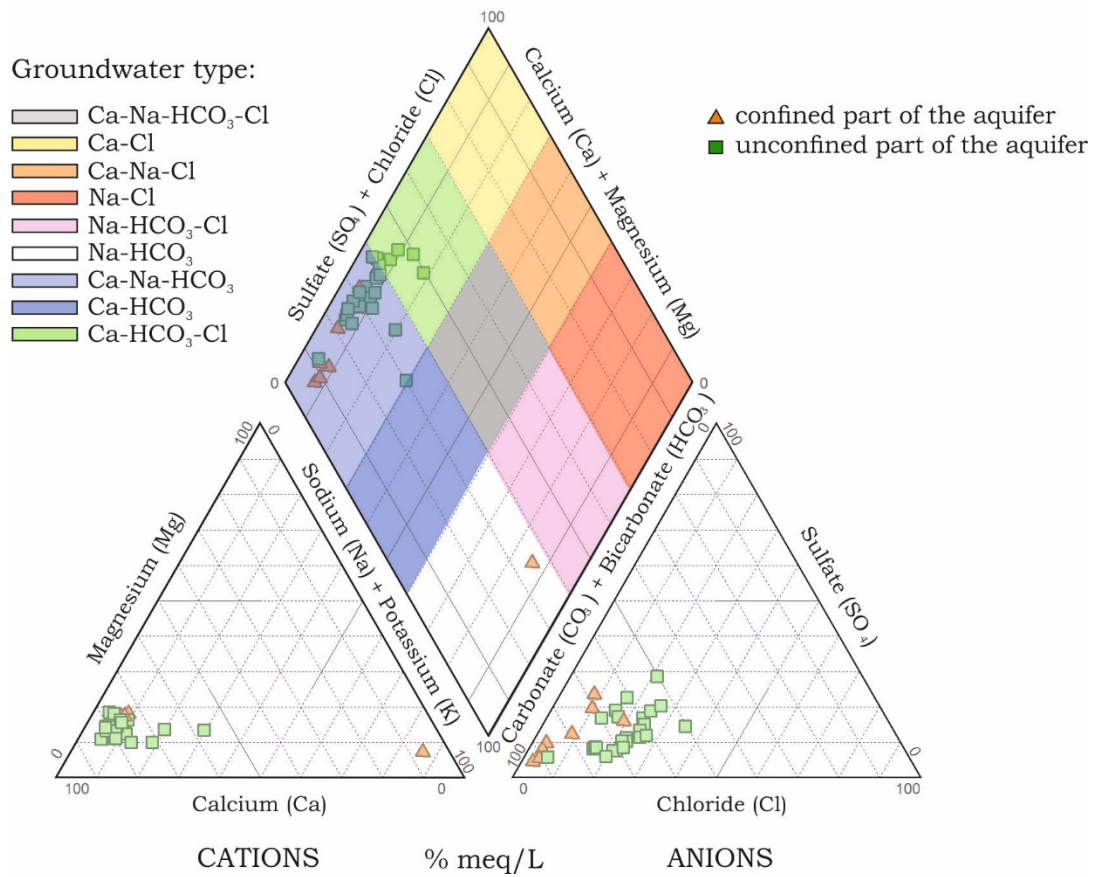


Figure 2. Piper diagram for the chalk aquifer of the Geer Basin.

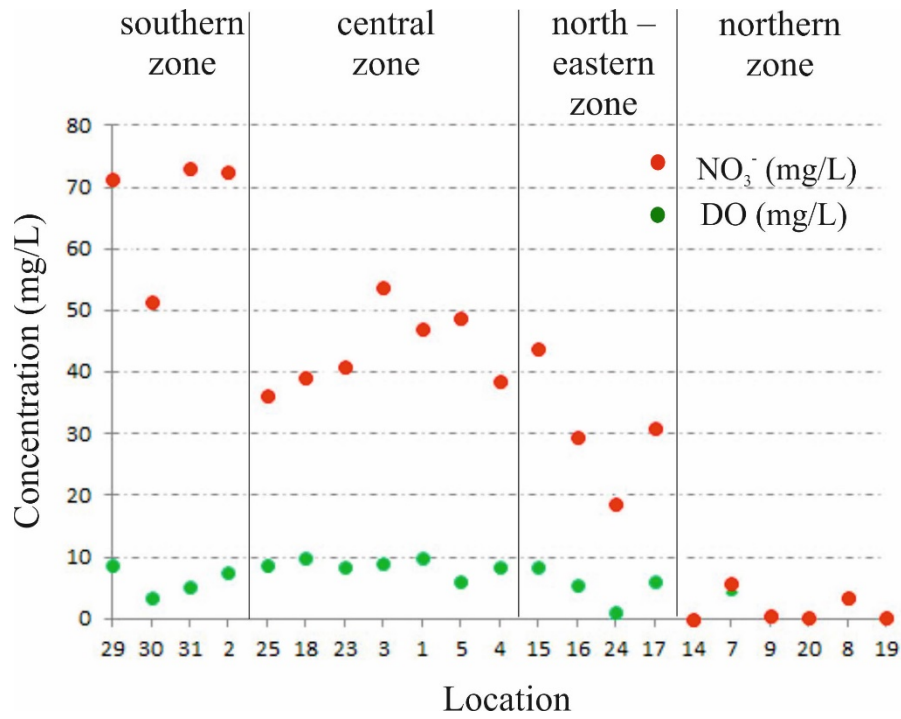


Figure 3. Distribution of nitrate (NO_3^-) and dissolved oxygen (DO) across different zones.

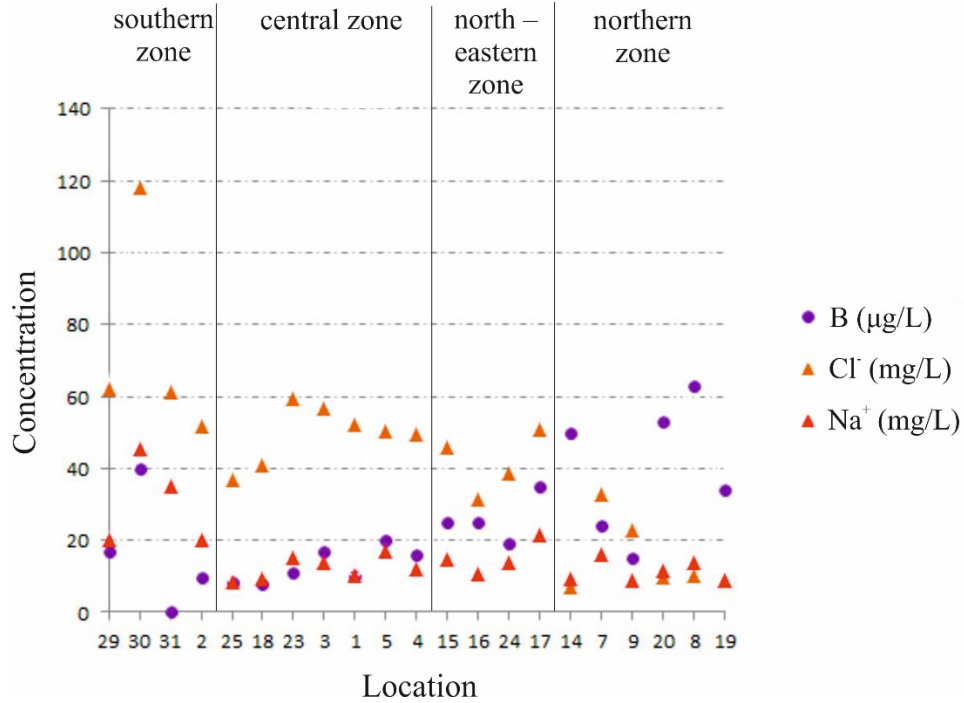


Figure 4. Distribution of B, Cl^- and Na^+ across different zones.

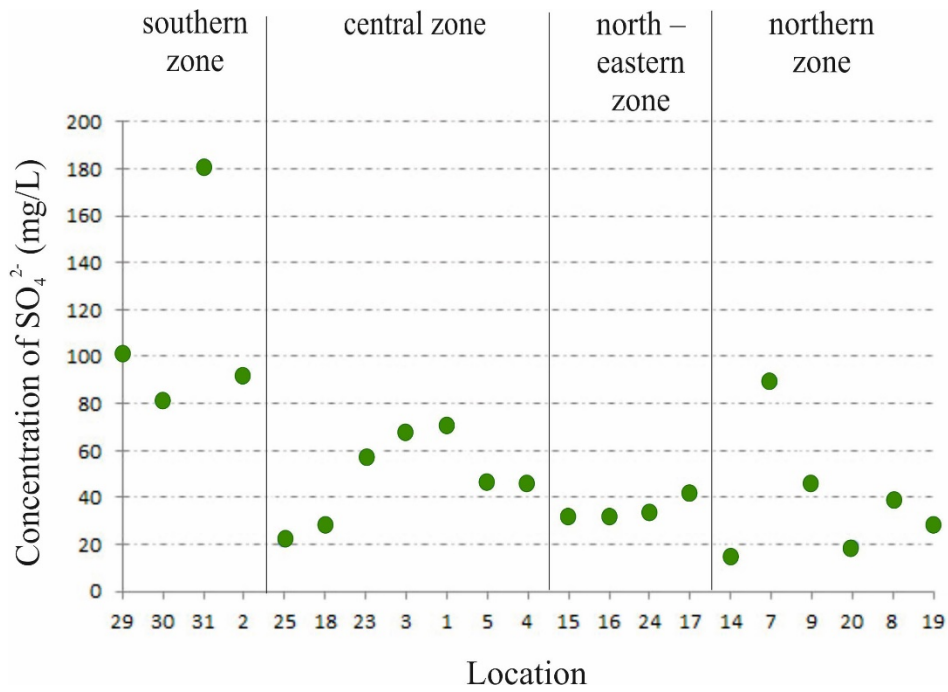


Figure 5. Distribution of SO_4^{2-} across different zones.

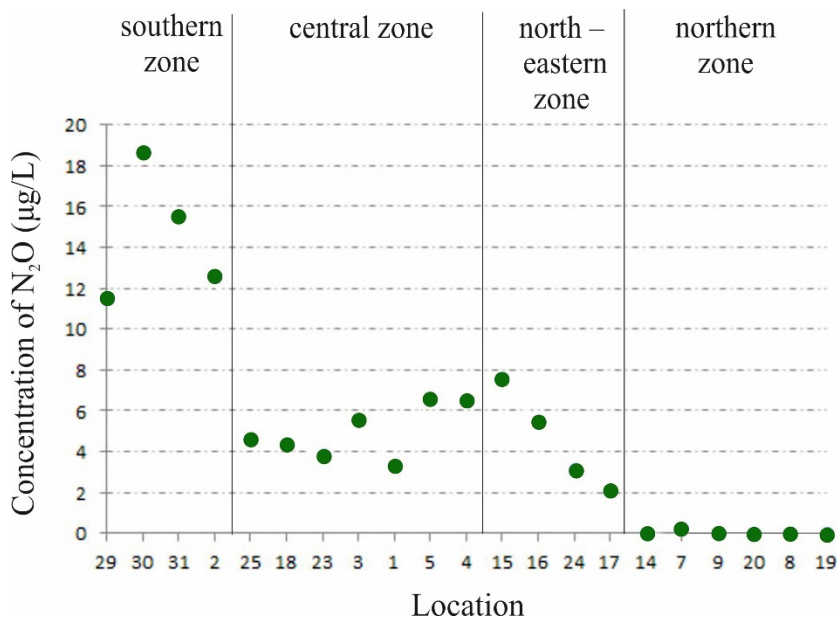


Figure 6. Distribution of N_2O across different zones.

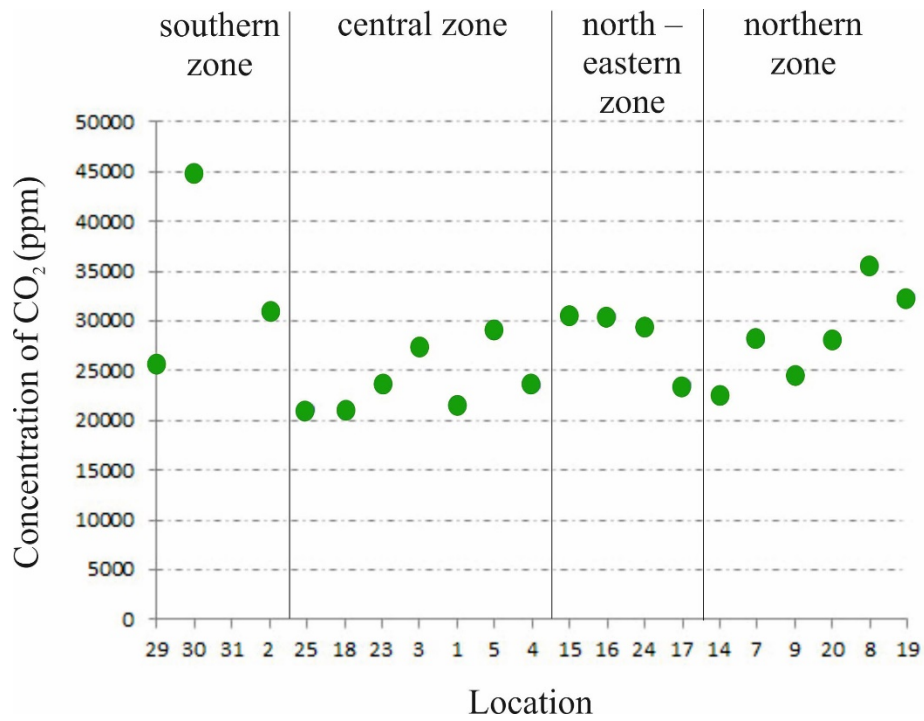


Figure 7. Distribution of CO₂ across different zone.

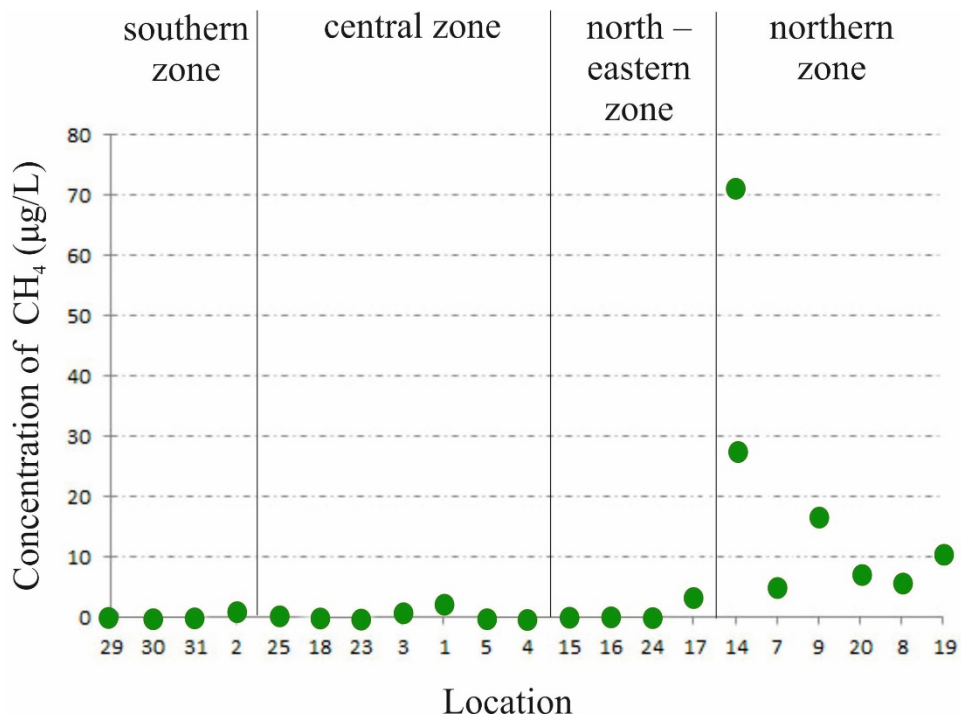


Figure 8. Distribution of CH₄ across different zones.

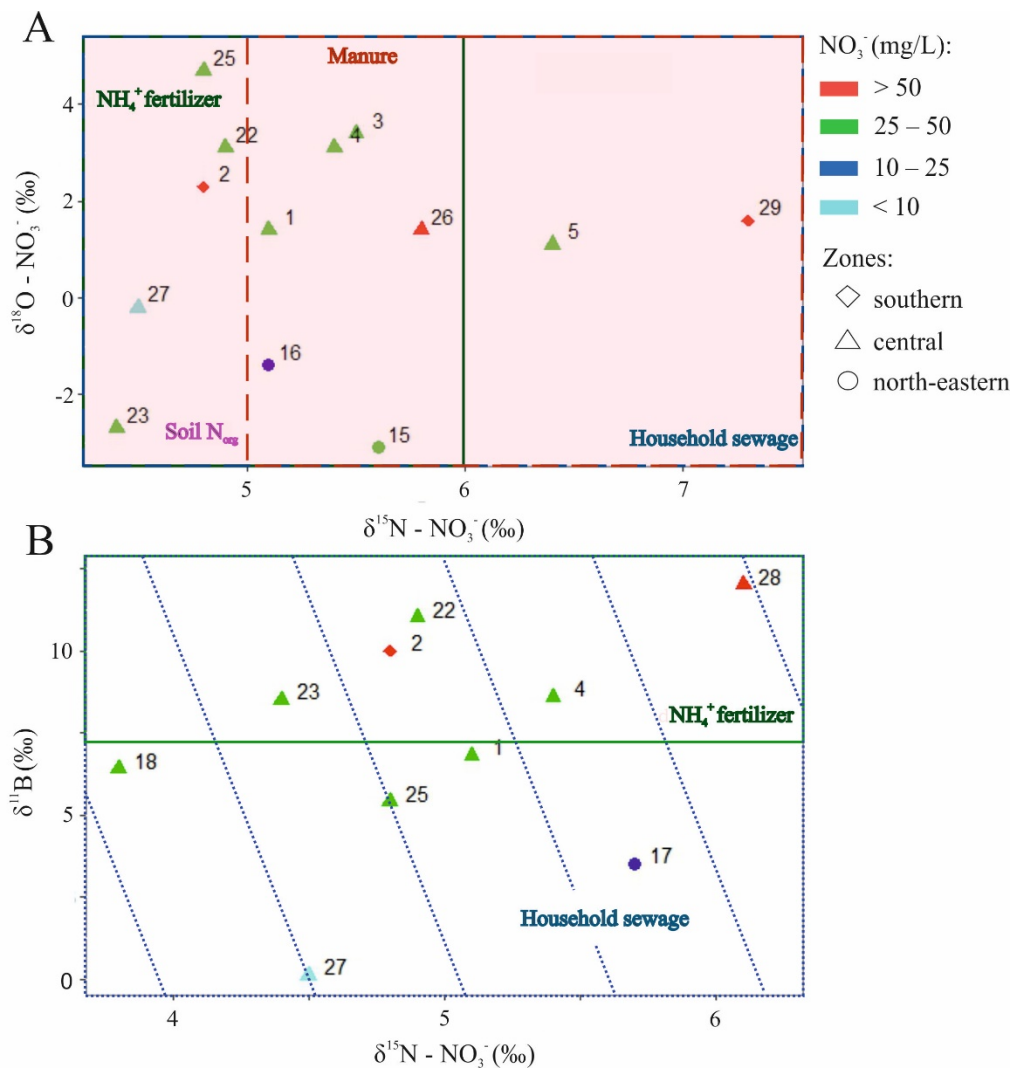


Figure 9. $\delta^{15}\text{N}$ versus $\delta^{18}\text{O}$ values of NO_3^- (A) and $\delta^{15}\text{N} - \text{NO}_3^-$ versus $\delta^{11}\text{B}$ (B) of groundwater samples. The isotopic composition for NO_3^- and B sources are derived from Michener & Lajtha (2008), Xue et al. (2009) and Widory et al. (2004).

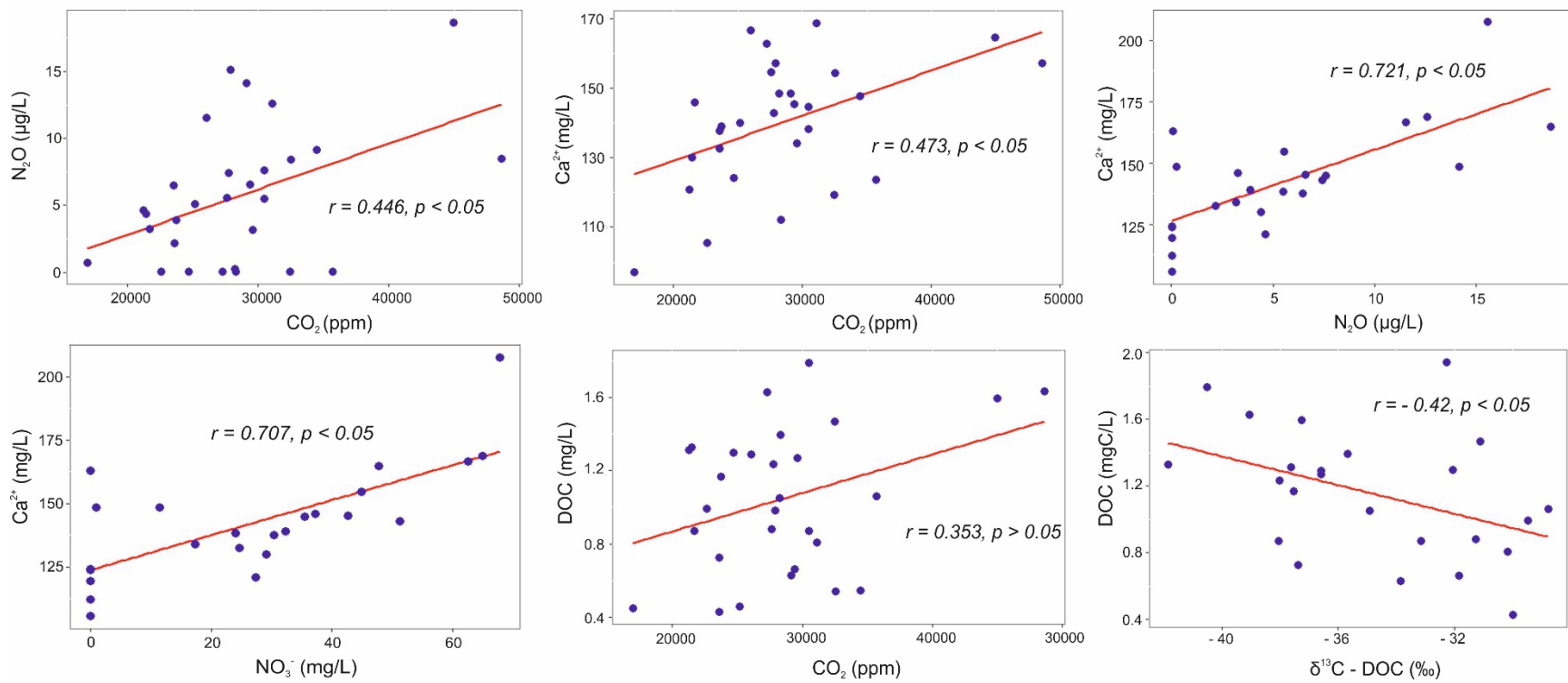


Figure 10. Pearson correlation analysis of CO₂, N₂O, NO₃⁻, Ca²⁺, DOC and δ¹³C-DOC.

Table 1. Saturation indexes.

Location	Calcite	Dolomite
29	0.05	-0.82
30	-0.18	-1.25
31	0.07	-0.8
2	-0.02	-0.92
25	0.04	-0.75
26	-0.04	-0.76
18	0.01	-0.82
23	0.05	-0.69
3	0.01	-0.84
1	0	-0.81
5	0.08	-0.62
4	0.11	-0.58
15	0.02	-0.87
16	-0.01	-0.97
24	0.06	-0.72
17	0.03	-0.79
14	0.03	-0.66
7	0.21	-0.33
9	0.13	-0.46
20	0.13	-0.42
8	0.22	-0.21
19	0.04	-0.63

Text 1. Saturation indexes.

The saturation index (SI) was calculated by comparing the chemical activities of the dissolved ions of the minerals (ion activity product, IAP) with the solubility constant of the mineral (K_{sp}) as follows:

$$SI = \log (IAP/K_{sp})$$

The SIs were estimated using Diagrammes software with the embedded PHREEQC software (University of Avignon, France) (Simler, 2009).

These indicators help to evaluate the state of equilibrium between water and minerals. If $SI < 0$, water is undersaturated and the mineral is being dissolved. If $SI > 0$, water is oversaturated and precipitation of the mineral is possible. If SI is close to 0, water is in equilibrium with respect to the given mineral. SIs values between -0.5 and 0.5 are considered to indicate equilibrium (Welch et al., 1989).

Text 2. Description and results of FVPDM and push-pull studies

1. Finite Volume Point Dilution Method (FVPDM)

1.1. General description

The Finite Volume Point Dilution Method is a single-well tracer dilution technique that allows direct measurement of a groundwater flow rate in both steady and transient states groundwater conditions (Brouyère et al., 2008; Jamin & Brouyère, 2018). It is based on continuous low-flow injection of a tracer into a tested well at a controlled injection rate and a continuous monitoring of the change in this tracer concentration in groundwater.

Brouyère et al. (2004) showed that the variation of a tracer concentration in the injection well is related to the groundwater flow in the following way:

$$C_w(t) = \frac{Q_{inj}C_{inj} - (Q_{inj}C_{inj} - (Q_{inj} + Q_t)C_{w,0})e^{-\frac{Q_{inj} + Q_t}{V_w}(t-t_0)}}{Q_{inj} + Q_t} \quad (1)$$

where Q_{inj} is the injection rate of a tracer solution (L^3/T), Q_t is the rate of water intercepted at the screen level of the well (transit flow rate) (L^3/T), C_w is the tracer concentration in the injection well at time t_0 (M/L^3), C_{inj} is the tracer concentration in the injected solution (M/L^3), $C_{w,0}$ is the tracer concentration in the injection well at time t_0 (M/L^3) and V_w is the volume of water in the injection well (L^3).

In order to determine the values of transit flow rates Q_t in the vicinity of piezometers an analytical curve showing the evolution in the tracer concentration $C_w(t)$ in groundwater have to be fitted to a real observations curve by adjusting Q_t from Equation 12. All other parameters in Equation 1 are defined based on the experimental conditions (Q_{inj} , C_{inj} , $V_w \dots$).

The transit flow rate Q_t is associated to apparent Darcy flux q_{app} through the cross-sectional area S_w (L^2) of the tested well screens. The apparent Darcy flux q_{app} (LT^{-1}) is related to the effective Darcy flux in the aquifer q_D by a flow distortion coefficient α_w that accounts for the convergence or divergence of the flow field in the vicinity of the borehole. The apparent Darcy flux $q_{D,app}$ is given by:

$$q_{D,app} = \alpha_w q_D = \frac{Q_t}{S_w} = \frac{Q_t}{2r_w e_{scr}} \quad (2)$$

where e_{scr} is the well screen length (L) and r_w the radius of the well.

FVPDM is based on the dilution of the injected tracer solution by groundwater flow passing through the well screen Q_t . The transit flow Q_t depends non-linearly on the injection flow rate Q_{inj} .

1.2. Field application

FVPDM was conducted in four piezometers at the Bovenistier site: two in Pz12, one in Pz13 and one in PzCs. These tests were dimensioned using the methodology proposed by Brouyère et al., 2008. Table 2 provides details about the depth intervals for which FVPDMs were carried out.

Table 2. Depth intervals established for FVPDM tests at the Bovenistier site.

Piezometer	Depth interval (m)
PzCs	28 – 33
Pz12 (top)	35.3 – 36.2
Pz12 (bottom)	47.5 – 48.4
Pz13	46 – 51

The scheme of field set up is presented in Brouyère et al., 2008. Uranine was used as a tracer during the tests. It was injected using a peristaltic pump to achieve controlled low flow injection rates. The constant mixing of groundwater with the injected solution was maintained by MP1 pump in order to homogenize the tracer concentration in the piezometer. The concentration of uranine was automatically measured every minute using a GGUN-FL30 fluorometer connected on the circulation loop.

1.3. Results

Fig. 11 – 14 present the results of the different FVPDM experiments and the analytical curves fitted to the observations.

Fig. 11 shows that stabilization of the tracer concentration in PzCs was reached approximately in 3.5 hours after the start of injection. The analytical curve showed the best fit with the observation curve at $Q_t = 4.14 \cdot 10^{-2} \text{ m}^3/\text{h}$, and the calculated apparent Darcy flux $q_{D, app}$ was equal to $7.33 \cdot 10^{-2} \text{ m/h}$.

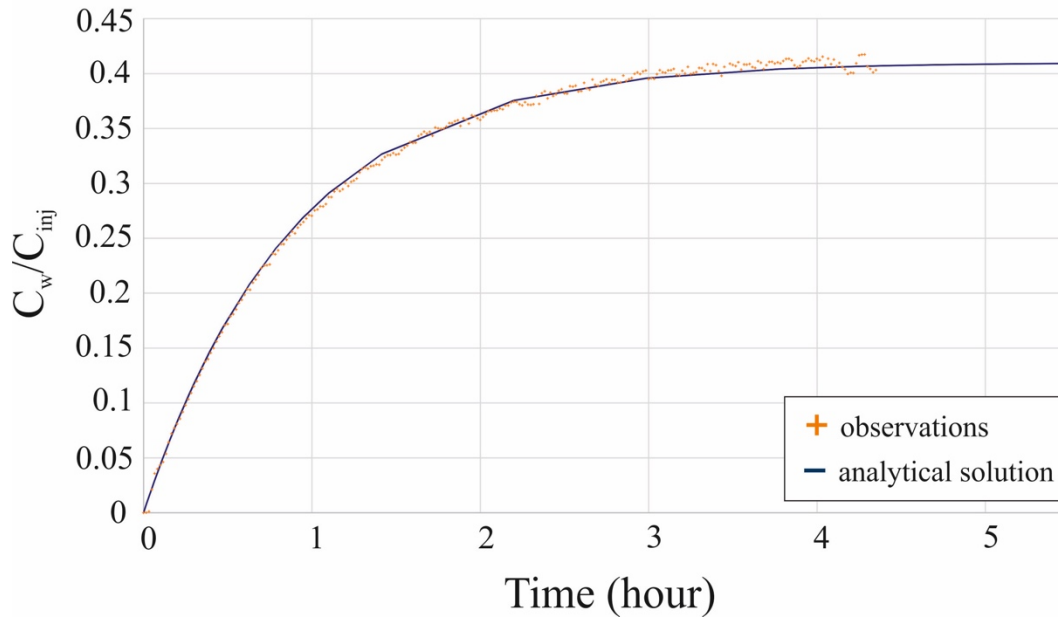


Figure 11. Evolution of the tracer concentration and fitted analytical curve for PzCs.

Fig. 12 shows the fast stabilization of tracer concentration in Pz12 (top) which is the evidence of fast transit flow rate. At this location, the FVPDM test was carried out in four stages by raising the injection rate of the tracer Q_{inj} in order to obtain more reliable estimation of the transit flow rate. The estimated transient flow rate Q_t is $0.16 \text{ m}^3/\text{h}$ and the apparent Darcy flux $q_{D, app}$ is 1.56 m/h .

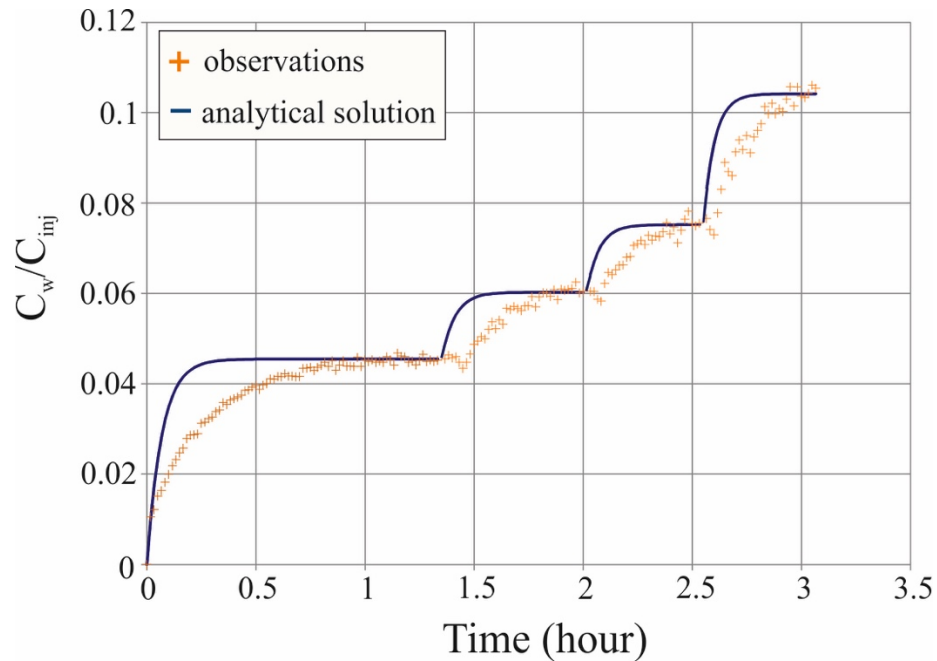


Figure 12. Evolution of the tracer concentration and fitted analytical curve for Pz12 (top).

Fig. 13 displays the adjustment of analytical curve to observations measured at Pz12 (bottom). Experiment had to be terminated after almost 8 hours since all volume of the prepared trace solution was injected into the piezometer. The concentration evolution curve did not reach stabilization because of lower than expected transient flow rate at this depth. For the purpose of this experiment, it is not necessary to reach stabilization to adjust the analytic curve to the observations as it is clear that groundwater flow rate at this location is suitable for further push – pull tracer pretest. Certainly, the obtained curve is not perfect but representative which allowed to estimate $Qt = 5.4 \cdot 10^{-3} \text{ m}^3/\text{h}$ and determine apparent Darcy flux $q_{D, app} = 5.31 \cdot 10^{-2} \text{ m/h}$.

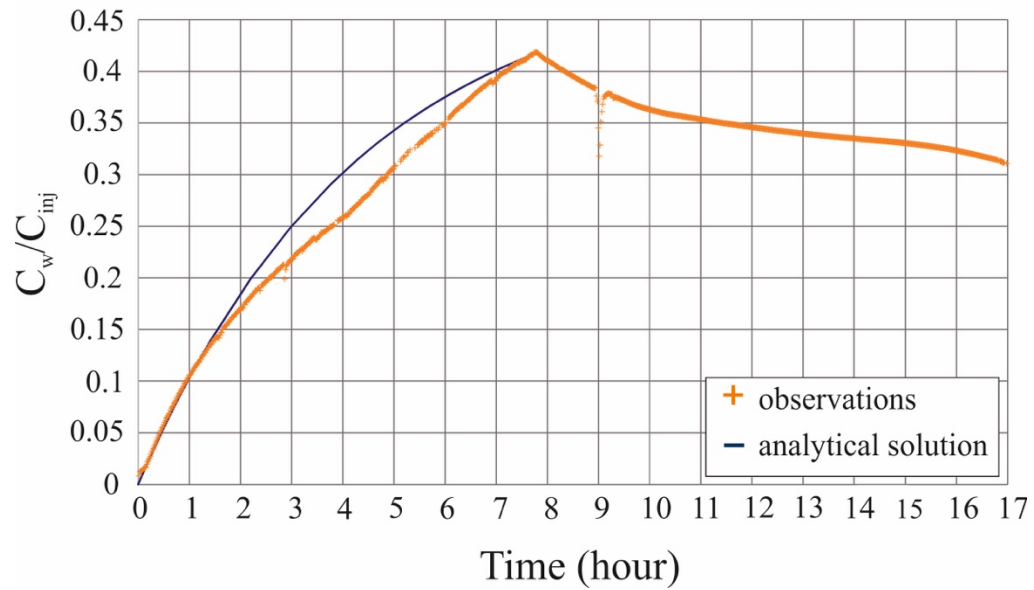


Figure 13. Evolution of the tracer concentration and fitted analytical curve for Pz12 (bottom).

Fig. 14 shows the change in the tracer concentration in Pz13 and analytical curves adjusted to observations. After around 9 hours of the experiment the concentration evolution curve did not reach stabilization. That is why, it was decided to increase the injection flow rate. As a result, two observation and two analytical curves were obtained. The best fit of the curves was achieved at $Q_t = 1.37 \cdot 10^{-2} \text{ m}^3/\text{h}$ and, consequently, apparent Darcy flux $q_{D, app}$ was equal to $3.42 \cdot 10^{-2} \text{ m/h}$.

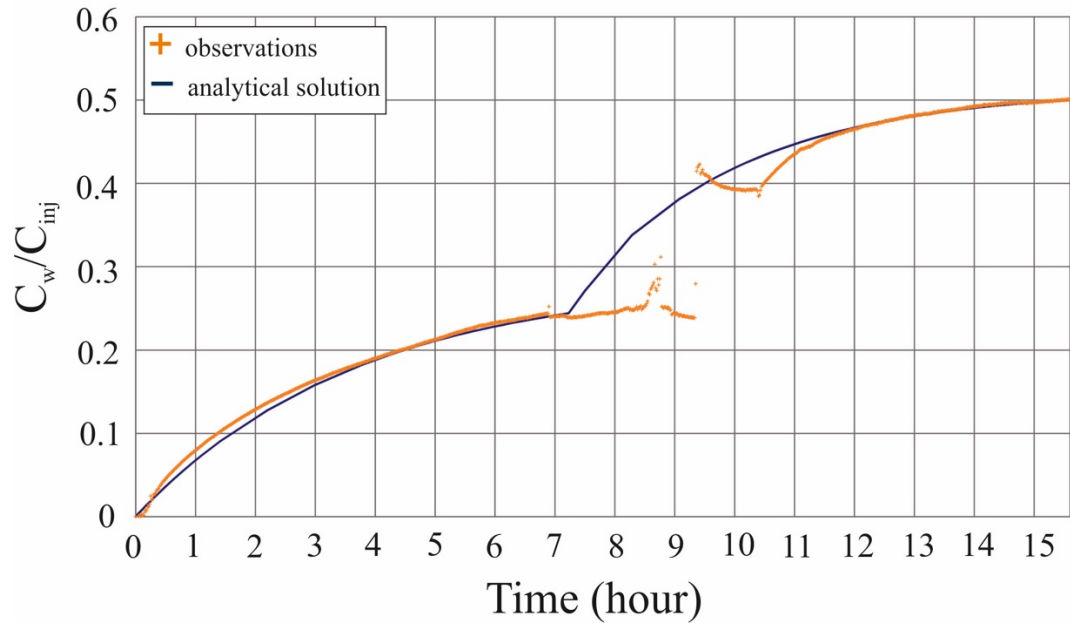


Figure 14. Evolution of the tracer concentration and fitted analytical curve for Pz13.

Table 3 summarizes the values of transit flow rate for PzCs, Pz12 (top), Pz12 (bottom) and Pz13. The highest groundwater flow rate was observed at Pz12 (top) 0.16 (m³/h) while the lowest at Pz12 (bottom) 4.19*10⁻³ (m³/h). The same magnitude of groundwater flow rate was detected at PzCs and Pz13.

Table 3. Results of FVPDM tests performed at the Bovenistier site.

Parameter	PzCs	Pz12 (top)	Pz12 (bottom)	Pz13
Q _t (m ³ /h)	4.14·10 ⁻²	0.16	5.4·10 ⁻³	1.37·10 ⁻²
q _{D, app} (m/h)	7.33·10 ⁻²	1.56	5.31·10 ⁻²	3.42·10 ⁻²
q _D (m/h)	3.66·10 ⁻²	0.78	2.65·10 ⁻²	1.71·10 ⁻²

As for the SGB site, it was not possible to conduct FVPDM tests due to its remote location.

2. Push – Pull pretest

2.1. General description

A push-pull test consists of the injection of a tracer into groundwater at a single location (e.g. a well or a piezometer) followed by its extraction from the same location after a certain period of time called incubation time. The tracer solution is prepared using groundwater previously withdrawn from the aquifer at the same location and amended with conservative and/or non-conservative tracer(s). Conservative tracers can give an insight into the physical processes of advection, dispersion, diffusion, and others, while non-conservative tracers provide information regarding sorption, cation exchange, rates of microbiological processes etc.

2.2. Field results

In situ conservative Push-Pull pretests were conducted in order to estimate the possibility to conduct *in situ* reactive tracer tests which would have been balancing high recovery of the injected tracer with sufficient time *in situ* for microbiological processes to occur at detectable levels. In particular, the duration of the “rest” periods of the following tracer tests was to be determined as the time required to obtain >50% recovery of the conservative substance. The injected solution was prepared using KBr.

At the Bovenistier site, four push-pull pretests were performed for the same piezometers and the same depth intervals as for the FVPDM tests (see Table 2, p. 197). The volume of injected solutions for each case was selected before the actual field experiments taking into account the fractured geology of the studied area and the volume of water in the “dead zone”. Incubation times were adjusted in the field taking into consideration the information about groundwater fluxes obtained from FVPDMs. The concentration of Br⁻ was selected taking into account almost negligible concentration of Br⁻ in the aquifer (mean 0.82 mg/L) and hypothesized fast groundwater fluxes. Details of the test setups are presented in the Table 4.

At the SGB site, two push-pull pretests were conducted: one at the top of SGB3 piezometer (17 – 18 meters) and another one at its bottom part (24 – 25 meters). The volume of injected tracer solution and the duration of incubation period for each case were chosen

considering the results of FVPDM but also based on the experience of the push-pull tests performed at the Bovenistier site.

After the incubation period, groundwater was pumped from the piezometers until the stabilization of electrical conductivity (EC). Stabilization usually occurred after approximately three volumes of the injected solution were pumped out. Groundwater samples were collected every five minutes for further analysis of Br recovery. The injection tracer solution was also sampled to determine the exact concentration of Br in it.

Table 4. Push-Pull test set ups for piezometers at Bovenistier and SGB sites.

Location	Incubation time (hour)	Characteristics of the injected solution		Background concentration of Br (mg/L)
		Volume (L)	Concentration of Br (mg/L)	
Pz12 top	1	300	78.38	2.63
Pz12 bottom	3	300	71.87	0.22
PzCs	3	500	70.89	0.21
Pz13 bottom	3	300	66.62	0.20
SGB3 top	1	300	72.45	0.87
SGB3 bottom	1	300	75.82	0.09

2.3. Results

Table 5 presents recovery factors of bromide (Br^-) for the different push-pull experiments performed at Bovenistier and SGB. The recovery of the tracer showed that injected tracer solutions were dispersed steadily from the screen of Pz12 bottom and Pz13 bottom with the recovery 89.03 % and 65.59%, respectively, after 3 hours of the rest period. Steady dispersion was detected for both SGB3 top (74.28 %) and SGB3 bottom (62.81%) injection points. However, the incubation time for both locations was just 1 hour, which means that its further

increase might have led to lower recovery rates of Br^- . A rapid washout of the dosing solution was observed at Pz12 top and PzCs with 14.15 % and 26.69 %, correspondingly.

Table 5. Recovery of Br^- at Bovenistier and SGB sites.

Piezometer	Recovery of Br^- (%)
Pz12 top	14.15
Pz12 bottom	89.03
PzCs	26.69
Pz13 bottom	65.59
SGB3 top	74.28
SGB3 bottom	62.81

In the end, the results showed that the *in situ* tracer experiments for the assessment of the magnitude of nitrification and denitrification processes might not be suitable for four (Pz12 top, PzCs, SGB3 top and SGB3 bottom) out of six locations due to the chance to obtain lower recoveries of tracers. That is why it was decided to perform lab incubation experiments.

Text 3. Results of PCR analyses of groundwater samples collected at Bovenistier and SGB sites during summer and winter campaigns in the framework of local scale studies of the chalk aquifer

During summer and winter campaigns groundwater samples were collected from the same locations.

Figure 15 shows the result of PCR targeting *amoA* gene in cDNA converted from total bacterial RNA collected groundwater samples. Among the summer samples it was possible to have amplification only at location 2, while winter samples showed better signals which cover points, 1', 4', 7' and two positive controls. Due to non-appropriate concentration values of PCR products only samples from 4' and 7' sites were sent for Sanger sequence analyses.

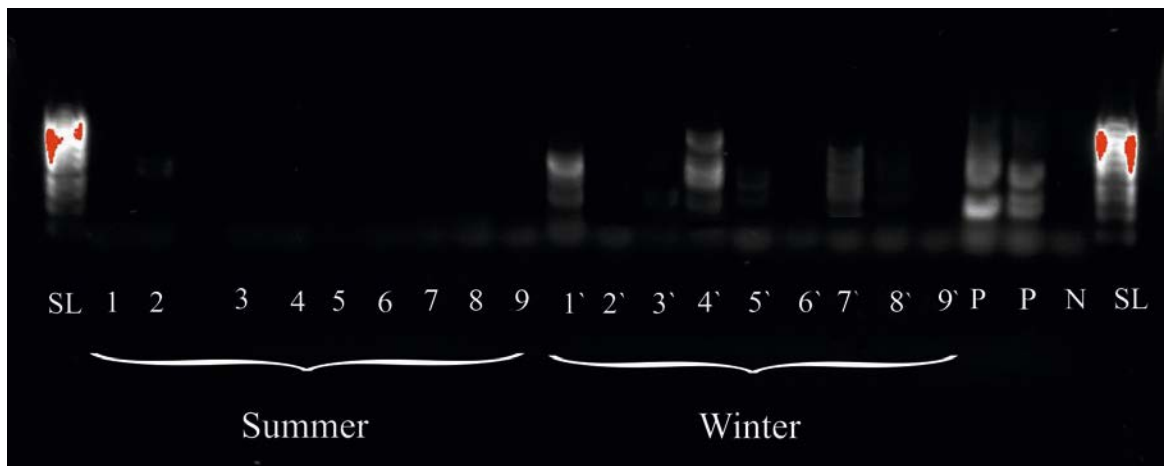


Figure 15. Results of PCR analysis aimed to reveal *amoA* gene expression in groundwater samples. From left to right: a standard (Smart Ladder (SL)), from 1 to 9 – cDNA extracted from groundwater samples collected in summer, from 1' to 9' – cDNA extracted from groundwater samples collected in winter, positive controls (P), negative control (N), and a standard (Smart Ladder (SL)).

As for the *nirK* gene, it was possible to amplify it using *nirK_3* (Figure 17) and *nirK_5* (Figure 19) primers sets while amplification did not occur with *nirK_2* (Figure 16) and *nirK_4*

(Figure 18) primer series. In particular, Figure 17 demonstrates that replication occurred at 7, 8 and 3` and Figure 19 shows signals at 1, 3, 4, 6 – 9, 2`, 4` – 9` locations.

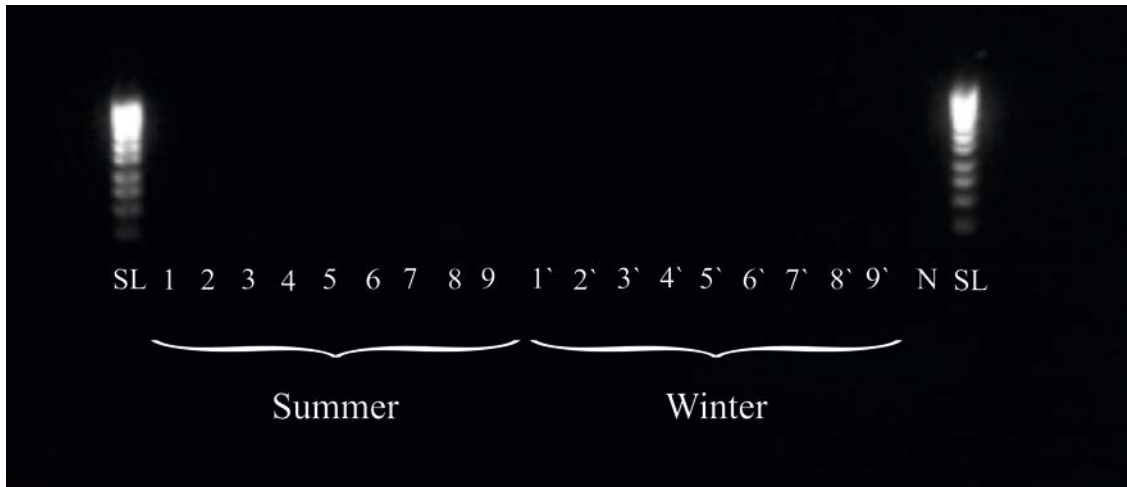


Figure 16. Results of PCR analysis aimed to reveal *nirK* gene expression in groundwater samples using *nirK_2* primer sets. From left to right: a standard (Smart Ladder (SL)), from 1 to 9 – cDNA extracted from groundwater samples collected in summer, from 1` to 9` – cDNA extracted from groundwater samples collected in winter, 20 – negative control (N), and a standard (Smart Ladder (SL)).

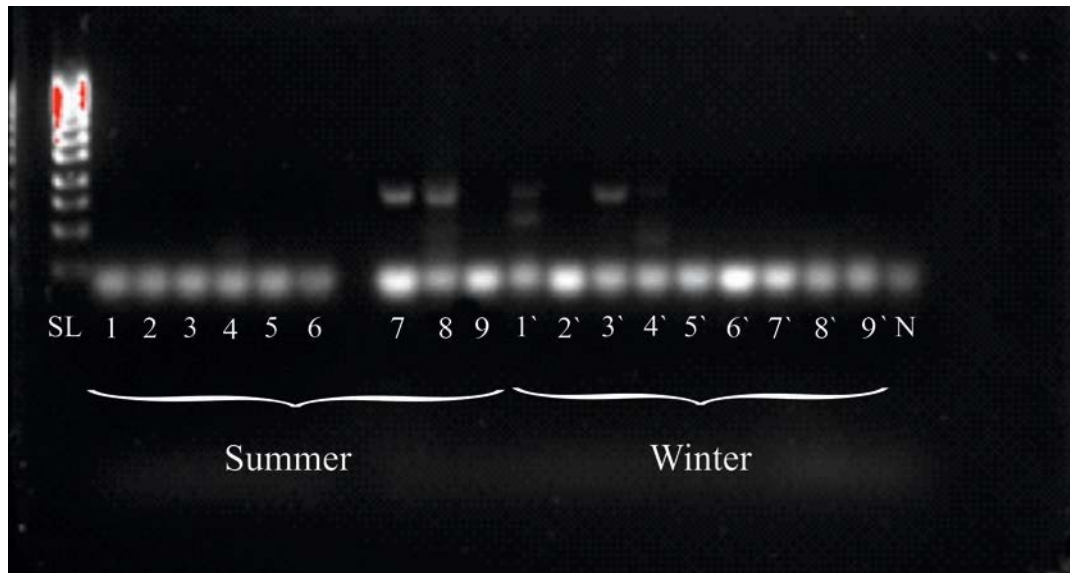


Figure 17. Results of PCR analysis aimed to reveal *nirK* gene expression in groundwater samples using *nirK_3* primer sets. From left to right: a standard (Smart Ladder (SL)), from 1 to 9 – cDNA

extracted from groundwater samples collected in summer, from 1` to 9` – cDNA extracted from groundwater samples collected in winter, negative control (N).

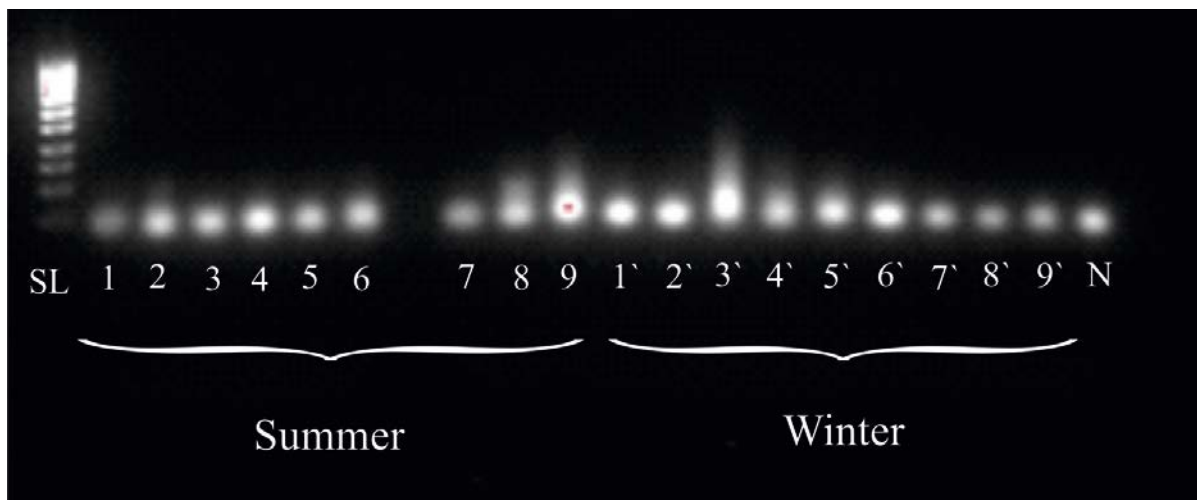


Figure 18. Results of PCR analysis aimed to reveal *nirK* gene expression in groundwater samples using *nirK_4* primer sets. From left to right: a standard (Smart Ladder (SL)), from 1 to 9 – cDNA extracted from groundwater samples collected in summer, from 1` to 9` – cDNA extracted from groundwater samples collected in winter, negative control (N).

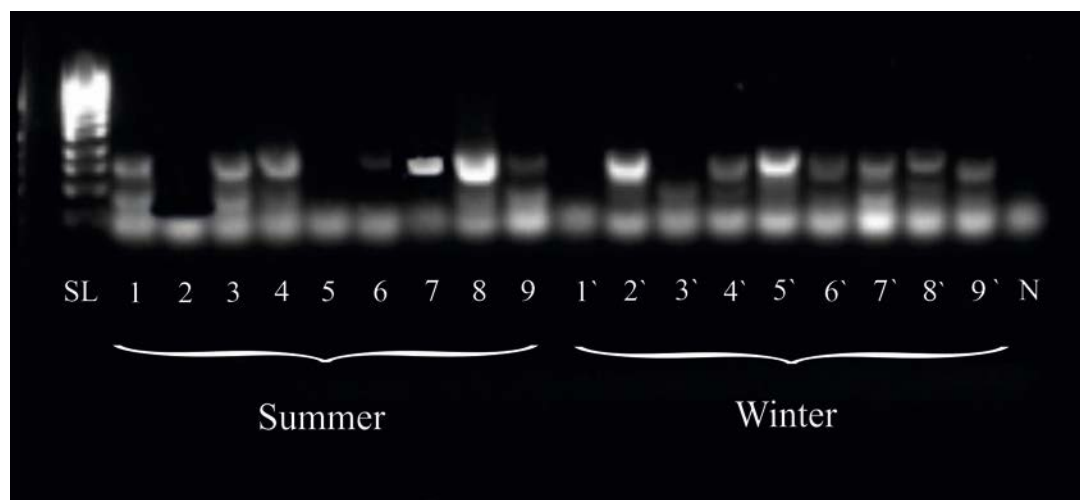


Figure 19. Results of PCR analysis aimed to reveal *nirK* gene expression in groundwater samples using *nirK_5* primer sets. From left to right: a standard (Smart Ladder (SL)), from 1 to 9 – cDNA extracted from groundwater samples collected in summer, from 1` to 9` – cDNA extracted from groundwater samples collected in winter, negative control (N).

Figures 20 – 22 display the results of PCR analysis attempting to replicate *nirS* gene using three primer series: *nirS_2*, *nirS_3* and *nirS_5*. PCR reaction with *nirS_2* primers did not show any signal (Figure 20). Amplification took place under the presence of *nirS_3* (Figure 21) and *nirS_5* (Figure 22) primers. For *nirS_3* points: 8, 4', 7' and 8' showed replication while for *nirS_5* locations: 1, 4, 5, 8, 9, 1', 2', 4' demonstrated it.

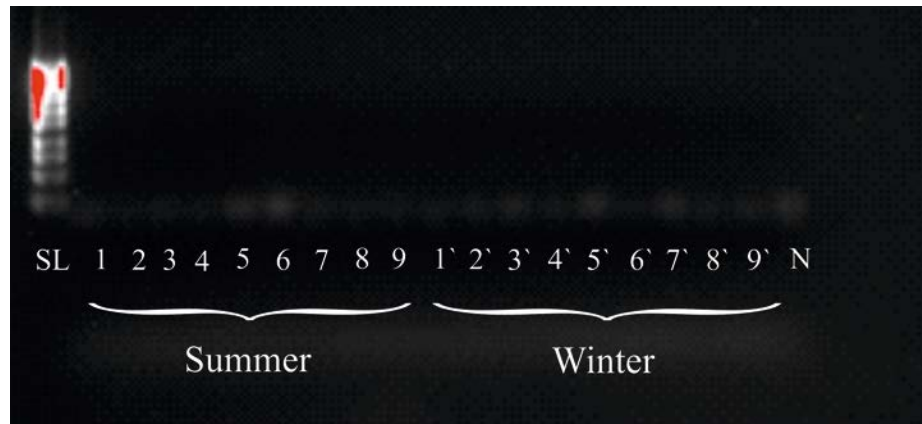


Figure 20. Results of PCR analysis aimed to reveal *nirS* gene expression in groundwater samples using *nirS_2* primer sets. From left to right: a standard (Smart Ladder (SL)), from 1 to 9 – cDNA extracted from groundwater samples collected in summer, from 1' to 9' – cDNA extracted from groundwater samples collected in winter, negative control (N).

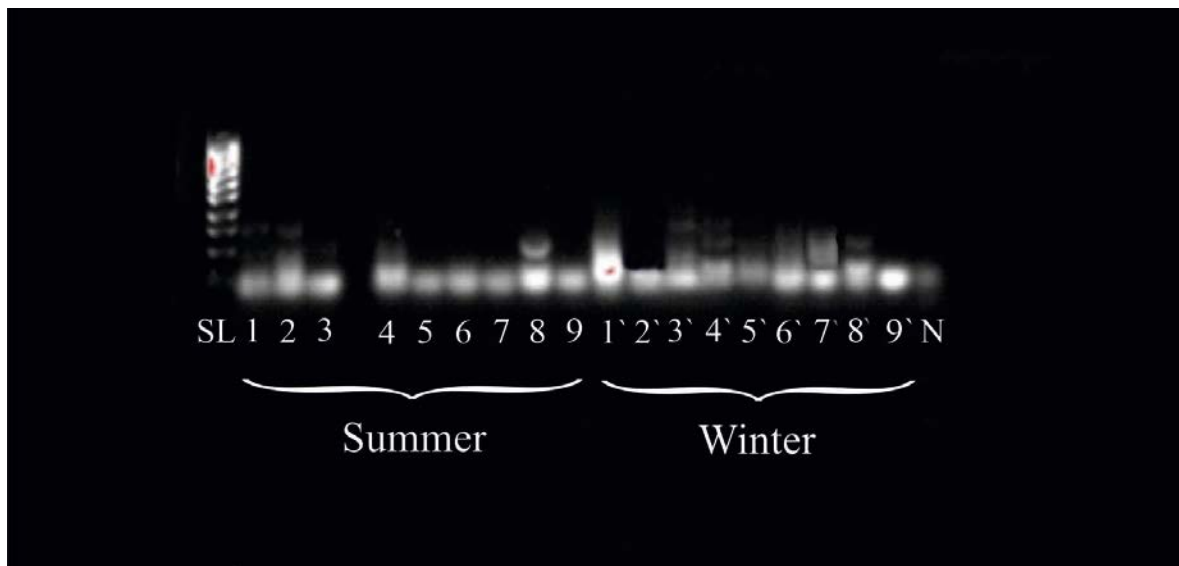


Figure 21. Results of PCR analysis aimed to reveal *nirS* gene expression in groundwater samples using *nirS_3* primer sets. From left to right: a standard (Smart Ladder (SL)), from 1 to 9

– cDNA extracted from groundwater samples collected in summer, from 1` to 9` – cDNA extracted from groundwater samples collected in winter, negative control (N).

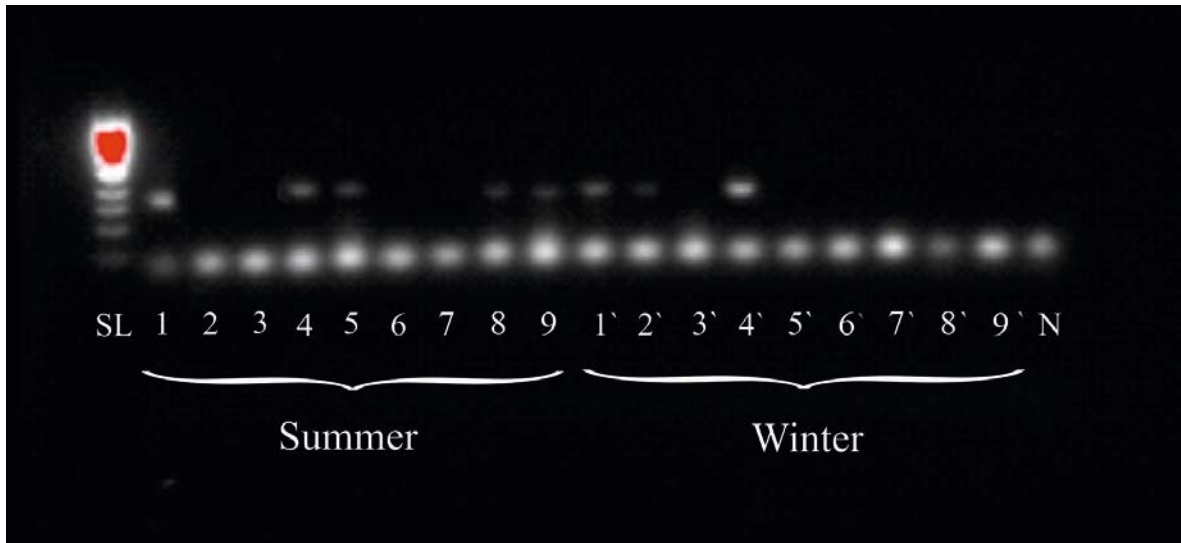


Figure 22. Results of PCR analysis aimed to reveal *nirS* gene expression in groundwater samples using *nirS*_5 primer sets. From left to right: a standard (Smart Ladder (SL)), from 1 to 9 – cDNA extracted from groundwater samples collected in summer, from 1` to 9` – cDNA extracted from groundwater samples collected in winter, negative control (N).

PCR analyses aiming to amplify *norB* genes with four primer suits: *norB*_3, *norB*_4, *norB*_5 and *norB*_6, resulted in replication only in the presence of *norB*_4 (1, 3, 4, 7, 8, 1`– 4`, 5` and 7`) (Figure 24). As for the *norB*_6 (Figure 26), it showed very slight and blurred signals so it was decided not to consider them.

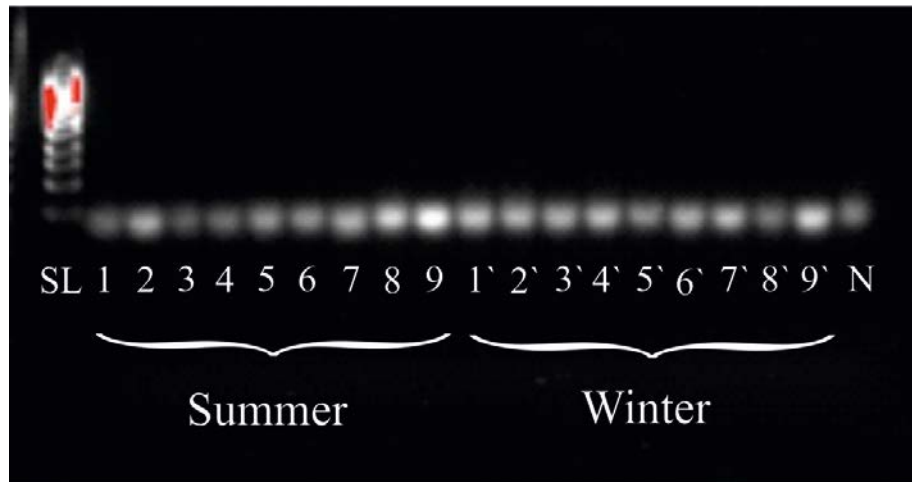


Figure 23. Results of PCR analysis aimed to reveal *norB* gene expression in groundwater samples using *norB_3* primer sets. From left to right: a standard (Smart Ladder (SL)), from 1 to 9 – cDNA extracted from groundwater samples collected in summer, from 1` to 9` – cDNA extracted from groundwater samples collected in winter, negative control (N).

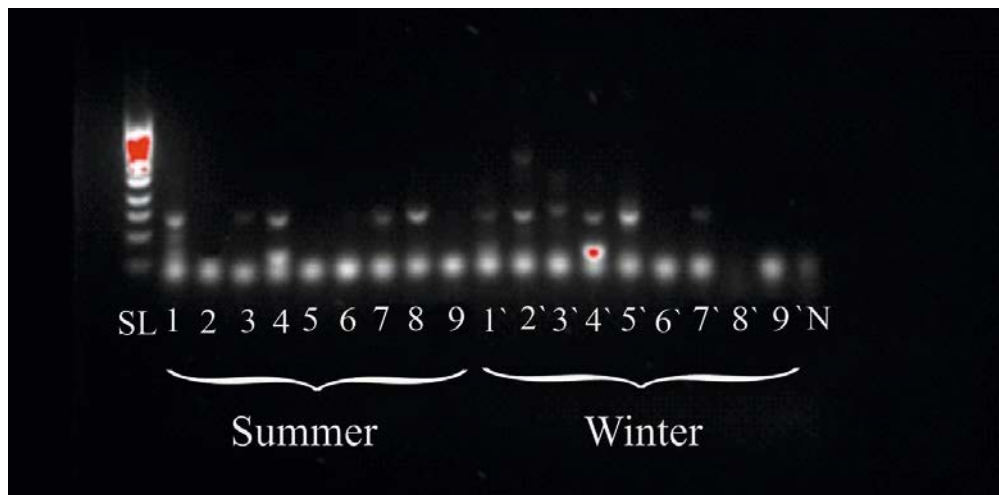


Figure 24. Results of PCR analysis aimed to reveal *norB* gene expression in groundwater samples using *norB_4* primer sets. From left to right: a standard (Smart Ladder (SL)), from 1 to 9 – cDNA extracted from groundwater samples collected in summer, from 1` to 9` – cDNA extracted from groundwater samples collected in winter, negative control (N).

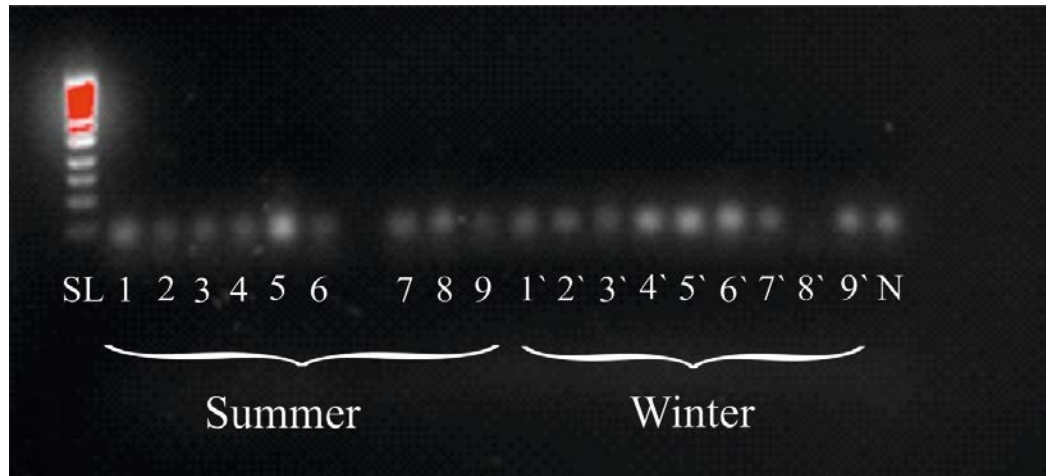


Figure 25. Results of PCR analysis aimed to reveal *norB* gene expression in groundwater samples using *norB_5* primer sets. From left to right: a standard (Smart Ladder (SL)), from 1 to 9 – cDNA extracted from groundwater samples collected in summer, from 1` to 9` – cDNA extracted from groundwater samples collected in winter, negative control (N).

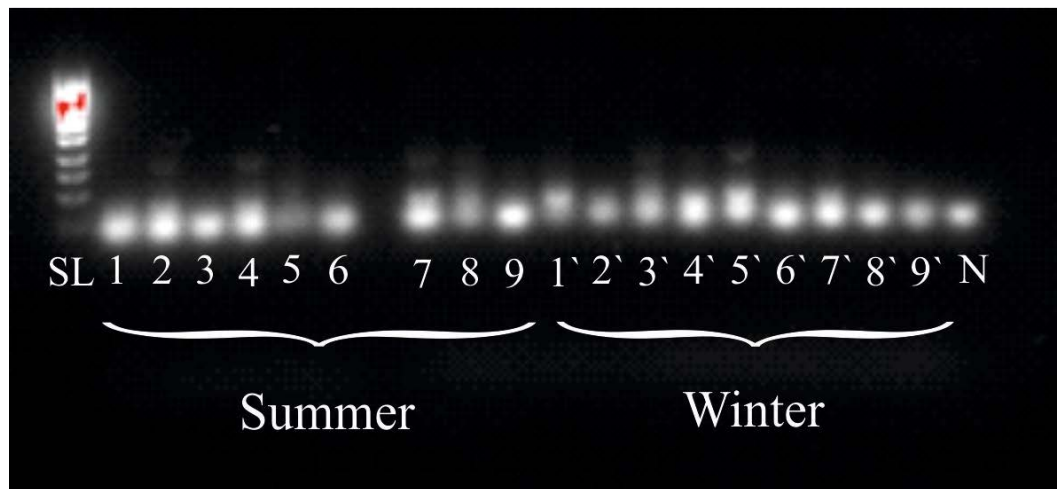


Figure 26. Results of PCR analysis aimed to reveal *norB* gene expression in groundwater samples using *norB_6* primer sets. From left to right: a standard (Smart Ladder (SL)), from 1 to 9 – cDNA extracted from groundwater samples collected in summer, from 1` to 9` – cDNA extracted from groundwater samples collected in winter, negative control (N).

As for the *norC* gene, it was replicated using two primer sets: *norC_2* and *norC_3*. Amplification occurred in both cases: *norC_2* – 1, 4, 7, 8, 2' and 5' points and *norC_3* – 8, 4', 5', 7' and 9' locations. Due to non-appropriate concentration values of PCR products at 1 point, it was not sent for Sanger sequence analyses.

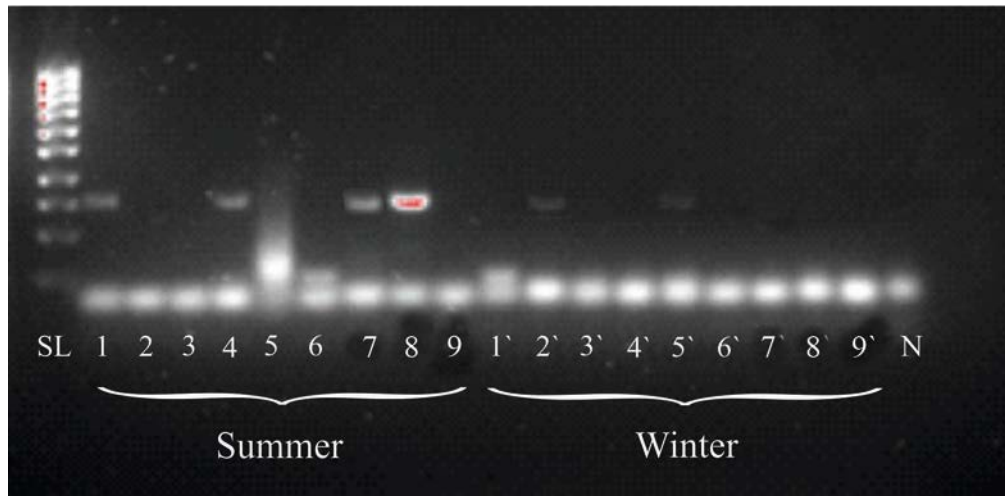


Figure 27. Results of PCR analysis aimed to reveal *norC* gene expression in groundwater samples using *norC_2* primer sets. From left to right: a standard (Smart Ladder (SL)), from 1 to 9 – cDNA extracted from groundwater samples collected in summer, from 1' to 9' – cDNA extracted from groundwater samples collected in winter, negative control (N).

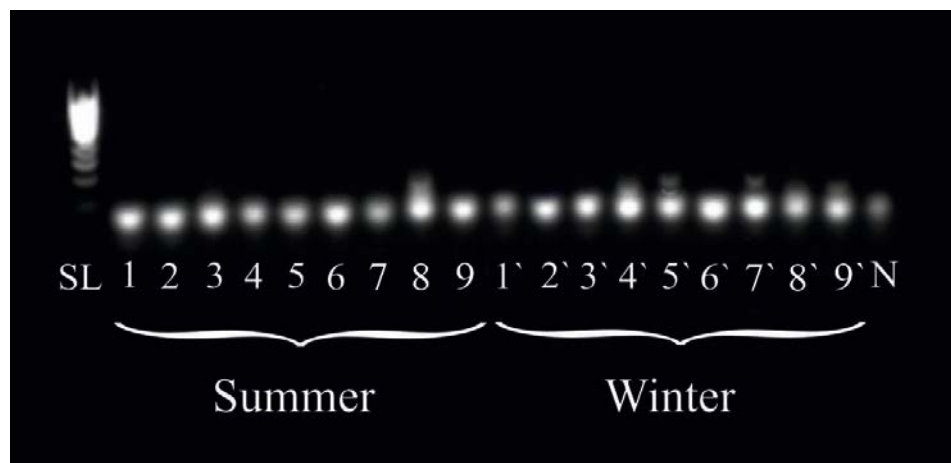


Figure 28. Results of PCR analysis aimed to reveal *norC* gene expression in groundwater samples using *norC_3* primer sets. From left to right: a standard (Smart Ladder (SL)), from 1 to 9

– cDNA extracted from groundwater samples collected in summer, from 1` to 9` – cDNA extracted from groundwater samples collected in winter, negative control (N).

As for the *nosZ* gene, it was replicated using one primer set. The replication occurred at 1 and 1`.

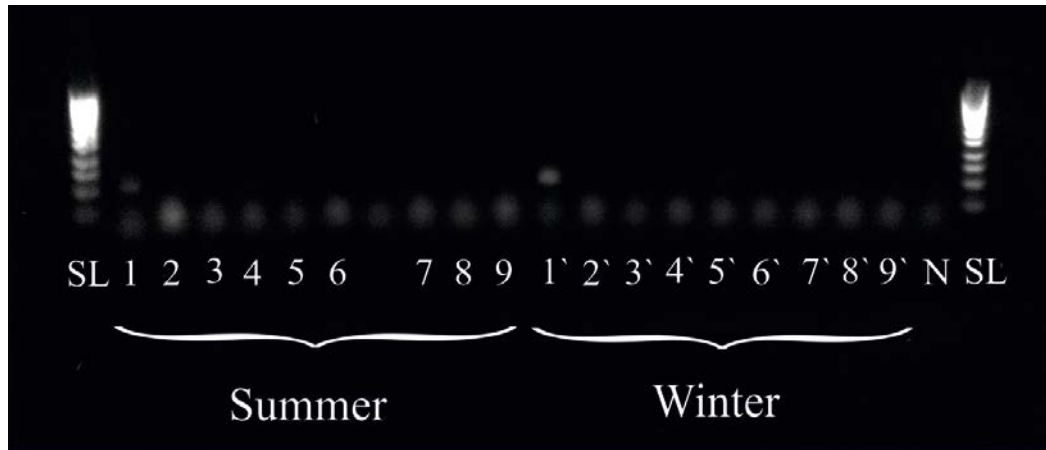


Figure 29. Results of PCR analysis aimed to detect *nosZ* gene expression in groundwater samples. From left to right: a standard (Smart Ladder (SL)), from 1 to 9 – cDNA extracted from groundwater samples collected in summer, from 1` to 9` – cDNA extracted from groundwater samples collected in winter, 19 two negative controls (N), and a standard (Smart Ladder(SL)).

Table 6. Results of BLASTX and BLASTN analysis of nucleotide sequences obtained from Sanger sequence analysis of PCR products received by carrying out a series of PCRs using several primer sets. The table provides accession codes to: 1) proteins (enzymes) which are encoded by obtained nucleotide sequences; 2) homologue nucleotide sequences which encodes studied genes. Red color highlights the locations where amplified sequences do not code for targeted protein or gene

№	Studied site	Accession code to protein (BLASTX)	Putative function	E value* (BLASTX)	Accession code to nucleotide sequence (BLASTN)	Gene	E value* (BLASTN)
Target <i>amoA</i> amplified using comB primer set							
1	4`	ELY20074.1	hypothetical protein HALTITAN_3299	1.00E-47	CP022684	non relevant	2.00E-129
2	7`	PEI34110.1	hypothetical protein CN644_18835	0.043			
Target <i>nirK</i> amplified using nirK_5 primer set							
3	1	RZA20239.1	nitrite reductase, copper-containing	6.00E-10	KF481896	nirK	2.00E-10
4	3	WP_156643355.1	nitrite reductase, copper-containing	6.00E-21	CP040871	nirk	1.00E-19
5	4	WP_146472229.1	nitrite reductase, copper-containing	9.00E-47	MN232918.1	nirK	3.00E-74
6	6	WP_117883142.1	nitrite reductase, copper-containing	2.00E-08	XM_024411336.1	nirK	0.012
7	7	WP_099790330.1	nitrite reductase,	5.00E-43	XM_024411336.1	nirK	5.00E-87

			copper-containing				
8	8	WP_083598787.1	nitrite reductase, copper-containing	3.00E-19	CP026517.1	nirK	1.00E-18
9	9	WP_045159547.1	nitrite reductase, copper-containing	9	KF481896	nirK	5.00E-84
10	2`	NA			NA		
11	4`	WP_147857635.1	MULTISPEC IES: glutamate--cysteine ligase	5.4	NA	NA	
12	5`	WP_146472229.1	nitrite reductase, copper-containing	3.00E-46	CP040871	nirK	5.00E-76
13	6`	NNE81396.1	DNA-directed RNA polymerase subunit beta'	1.00E-20	CP039690	non relevant	1.00E-57
14	7`	WP_155138164.1	DNA-directed RNA polymerase subunit beta'	4.00E-13	CP039690	non relevant	1.00E-61
15	8`	WP_099790330.1	nitrite reductase, copper-containing	4.00E-25	XM_02441133 6.1	nirK	1.00E-61
16	9`	WP_007443364.1	MULTISPEC IES: beta' subunit	1.00E-18	CP039865	non relevant	2.00E-46
Target <i>nirK</i> amplified using nirK_3 primer set							
17	7	OGX12348.1	nitrite reductase, copper-containing	3.00E-19	NA		
18	8	WP_034210261.1	nitrite reductase, copper-containing	2.00E-10	CP049872	nirK	4.00E-28
19	3`	AMS24507.1	nitrite	7.00E-32	NA		

			reductase				
Target <i>nirS</i> amplified using <i>nirS_3</i> primer set							
20	8	PJC42680.1	hypothetical protein CO040_03150	5.00E-06	NR_076925.1 Pseudoxanthomonas spadix	non relevant	2.00E-56
21	4`	PJC42680.1	hypothetical protein CO040_03150	5.00E-06	NR_076925.1 Pseudoxanthomonas spadix	non relevant	9.00E-59
22	7`	PJC42680.1	hypothetical protein CO040_03150	8.00E-07	NR_076925.1 Pseudoxanthomonas spadix	non relevant	3.00E-58
23	8`	NA			NR_076925.1 Pseudoxanthomonas spadix	non relevant	
Target <i>nirS</i> amplified using <i>nirS_5</i> primer set							
24	1	WP_169261895.1	c-type cytochrome	5.00E-25	LN997848	Nitrite reductase precursor	1.00E-52
25	4	PZU42325.1	nitrite reductase	1.00E-40	CP016278.1 Diaphorobacter polyhydroxybutyrativorans	<i>nirS</i>	6.00E-69
26	5	NA			NA		
27	8	EME68346.1	nitrite reductase precursor	6.00E-47	LN997848.1 Magnetospirillum	<i>nirS</i>	2.00E-109
28	9	KJB91632.1	nitrite reductase	8.00E-39	CP021731.1 Azoarcus	<i>nirS</i>	1.00E-55
29	1`	PZU42325.1	nitrite reductase	3.00E-38	CP001392.1 Acidovorax ebreus	<i>nirS</i>	4.00E-87
30	2`	NA			NA		
31	4`	BAE52969.1	nitrite reductase precursor	9.00E-22	AY838762.1 Thauera	<i>nirS</i>	1.00E-31
Target <i>norB</i> amplified using <i>norB_4</i> primer set							
32	1	HFL64932.1	nitric-oxide reductase large subunit	2.00E-20	CP000089.1	<i>norB</i>	5.00E-81
33	3	NA			CP014870	<i>norB</i>	

34	4	NJD25131.1	nitric-oxide reductase large subunit	2.00E-32	CP000089.1	norB	9.00E-79
35	7	NJD25131.1	nitric-oxide reductase large subunit	3.00E-35	CP003153.1	norB large subunit	
36	8	NLJ12735.1	nitric-oxide reductase large subunit	1.00E-38	Pseudomonas stutzeri	nitric oxide reductase large subunit	3.00E-69
37	1`	WP_148578267.1	cbb3-type cytochrome c oxidase subunit I	2.00E-36	CP000089	norB	1.00E-67
38	2`	RIX45183.1	nitric-oxide reductase large subunit	9.00E-11	CP000089	norB	2.00E-79
39	3`	WP_114968600.1	cbb3-type cytochrome c oxidase subunit I	3.00E-35	CP040709	nitric-oxide reductase large subunit	3.00E-48
40	4`	RIX45183.1	nitric-oxide reductase large subunit	2.00E-34	CP000089	norB	2.00E-84
41	5`	NLJ12735.1	nitric-oxide reductase large subunit	3.00E-17	MN256668	nitric oxide reductase	7.00E-55
42	7`	WP_116679084.1	DoxX family protein	8.6	NA		
Target <i>norC</i> amplified using <i>norC_2</i> primer set							
	1	NA			NA		
43	4	TXT28919.1	nitric oxide reductase subunit C	2.00E-53	CP031842.1 Dechloromonas	nitric oxide reductase subunit C	9.00E-84
44	7	TXT28919.1	nitric oxide reductase subunit C	6.00E-48	CP031842.1 Dechloromonas	nitric oxide reductase	2.00E-81

						subunit C	
45	8	TXT28919.1	nitric oxide reductase subunit C	8.00E-47	CP031842.1 Dechloromonas	nitric oxide reductase subunit C	1.00E-83
46	2`	TXT28919.1	nitric oxide reductase subunit C	2.00E-37	NA		
47	5`	TXT28919.1	nitric oxide reductase subunit C	2.00E-13	NA		
Target <i>norC</i> amplified using <i>norC_3</i> primer set							
48	8	NA			NA		
49	4`	NBQ24606.1	MBL fold metallo-hydrolase	0.58	NA		
50	5`	NA			NA		
51	7`	AQ26319.1	putative uncharacterized protein	0.002	NA		3.00E-13
52	9`	NA			NA		
Target <i>nosZ</i> amplified using <i>norC_3</i> primer set							
53	1	WP_121455022.1	nitrous-oxide reductase	3.00E-18	CP049885	nitrous-oxide reductase	6.00E-33
54	1`	NPU94037.1	nitrous-oxide reductase	4.00E-20	AP012320	nitrous-oxide reductase	2.00E-37

* E value is called expected value. Anything below 1×10^{-4} can be considered homologues or related to the query sequence (JHU AAP. (2010, July 29). *NCBI Blast Tutorial*. [Video]. YouTube. <https://www.youtube.com/watch?v=HXEpBnUbAMo&gl=BE>).